

PROGRAMA DE DOCTORADO EN INGENIERÍA AMBIENTAL CON
MENCIÓN HACIA LA EXCELENCIA

DPTO. DE CIENCIAS Y TÉCNICAS DEL AGUA Y DEL MEDIO AMBIENTE
E.T.S. DE INGENIEROS DE CAMINOS, CANALES Y PUERTOS

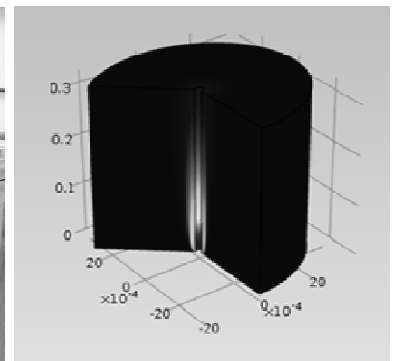
UNIVERSIDAD DE CANTABRIA



TESIS DOCTORAL

**OPTIMIZACIÓN DEL REACTOR DE BIOPELÍCULA SOPORTADA Y
OXIGENADA POR MEMBRANAS PARA EL TRATAMIENTO DE
AGUAS RESIDUALES**

**OPTIMIZATION OF THE MEMBRANE AERATED BIOFILM
REACTOR FOR WASTEWATER TREATMENT**



PATRICIA PÉREZ CALLEJA

DIRECTORES

JUAN IGNACIO TEJERO MONZÓN

ANA LORENA ESTEBAN GARCÍA

LUIS LARREA URCOLA

SANTANDER, MAYO DE 2017

Agradecimientos

Nunca agradeceré suficientemente a las personas que me han brindado su apoyo durante todo este largo, pero a su vez gratificante camino y que han hecho posible que finalmente hoy termine mi tesis doctoral.

En primer lugar, quiero dar las gracias más sinceras a mis directores, Iñaki Tejero y Ana Lorena Esteban, por la confianza depositada en mí, su sensibilidad y ánimos en momentos duros, pero sobre todo por los conocimientos brindados, por sus importantes aportes científicos y por haberme hecho crecer como investigadora.

A mi codirector Luis Larrea Urcola, por sus horas de dedicación, recomendaciones y consejos, por su paciencia, por ofrecerme sus conocimientos y por inculcarme la importancia del rigor.

Agradezco también de forma muy especial al Dr Robert Nerenberg, por su valiosa contribución en esta tesis doctoral, por su manera de trabajar, su dedicación y por la confianza depositada en mí, que han sido fundamentales para mi formación profesional. Al Dr Cristian Picioeanu, por su mente prodigiosa, sus enseñanzas, implicación y gran colaboración en esta tesis.

Al Departamento de Educación, Universidades e Investigación del Gobierno Vasco por la beca pre-doctoral que me ha permitido llevar a cabo esta tesis.

A todas las personas del Grupo de Ingeniería Ambiental, no sólo por vuestra ayuda, sino por el compañerismo, apoyo, momentos de diversión y amistad: Profesores, técnicos, doctorandos, becarios y estudiantes de máster, que merecen un agradecimiento especial por su preciada contribución en parte de este trabajo: Leti, María Herrero, Esther, Isa, Flavia, David, Nacho, Juan, Ancella, Rubén, María Castrillo, Marta, Nuria, Juanjo, Loredana, y Jose Ramón.

Una parte importante de mi etapa pre-doctoral se desarrolló fuera de la UC, en la Universidad de Navarra (CEIT, Guipúzcoa) y en la Universidad de Notre Dame (USA), que han dejado huella en mí y de las que guardo recuerdos imborrables. Agradezco a mis compañeros del CEIT por proporcionarme tan buenos momentos y hacer que el día a día fuese más grato y llevadero: Myriam, Ane, Tamara, Izaro, Jaime, y Maider. Especialmente a Carmen y a Nagore, por trabajar codo con codo conmigo, y demostrarme tanto su calidad humana como profesional. ¡Gracias por vuestra implicación y buena disposición!

De mi estancia en el grupo del Dr. Robert Nerenberg no tengo más que gratitud por la excelente acogida y amistad que me brindaron desde el día en que llegué.

Ha sido un auténtico placer trabajar con todos vosotros, por hacerme sentir como en familia, cuidada y valorada. Gracias de corazón a todas las personas que os habéis cruzado en mi camino en esta aventura americana: Callan, Sam, Andrew, Yue, Nydia, Fabrizio, J.P. Marcela, Tamara, Mauricio, Mana, Pablo, MengFei, Andrii, Stephany, Tomás, Ian, Raúl, Anurag, Jose Luís, Carlos, y Dolly. Gracias a Tina por su asesoramiento y ayuda en el laboratorio y en todo lo que estaba en su mano (también en lo que no). A mi “roommate” tan especial, Charlie, que me cuidó y mimó como a una nieta.

Mi gratitud y afecto a Agnieszka, Adam, Maryam, Elia, y Andrey por vuestra ayuda, amabilidad y amistad. Con especial mención a Elis y Ximena, que han sido como hermanas para mí, haciéndome sentir arropada y demostrándome que puedo contar y confiar en ellas en cualquier circunstancia.

Joni y Jorge, fuisteis mis anfitriones en Santander. Recuerdo como si fuese hoy el primer día en que llegué al piso, así como el último en el que nos despedimos. Fue una convivencia entrañable. Sois y seréis para mí ejemplos a seguir.

Especial mención a mis amigos de siempre, a mi cuadrilla de Vitoria, “Los Trespuenteros” por estar siempre ahí a pesar del tiempo y la distancia, por vuestro apoyo, y sobre todo, por saber siempre cómo sacarme una sonrisa. Gracias, Iñaki, Copi, Rubens, Beca, Aitor, Fer, Porti, Pablo, Erlantz, Leyre, Orozko, Marta, Ann, Bea y Ana. A Leire, Leti y Blanca, por demostrarme vuestra amistad incondicional, por estar siempre a mi lado y hacer que no decaiga.

A Diego, por su enorme curiosidad e interés mostrado durante el desarrollo de mi tesis, siempre dispuesto a estar horas escuchándome.

De forma muy especial quisiera destacar el apoyo de Marcelo Aybar, tanto en aspectos científicos como en lo personal. Gracias por tu cariño, por estar junto a mí en los buenos momentos y en los malos.

Por último quiero dedicar esta tesis a mi familia, mis tíos, primos, a Fortu, a Inma y a Bego, que siempre han estado pendientes de mí, a mi sobrina Ane, que me ha llenado de alegría en esta última etapa y por supuesto a mi madre, por creer en mí, por estar siempre a mi lado y por darme su apoyo constante y cariño infinito.

Una dedicación especial para cerrar este capítulo de agradecimientos a dos personas que viven en mi recuerdo y que de estar aún a mi lado, estarían muy contentos de presenciar los logros que voy alcanzando. Mi tío Julián y mi abuelo Paco.

Resumen

Actualmente, el proceso de fangos activos para el tratamiento de aguas residuales es uno de los más utilizados en todo el mundo. Ha demostrado su eficacia para la eliminación de carbono y nutrientes mediante el tratamiento exitoso de aguas residuales municipales e industriales. Los sistemas de biopelícula también se han utilizado durante los últimos 100 años, y aún se emplean extensamente hoy en día para el tratamiento de aguas residuales. Con el fin de mejorar las tasas de depuración, los procesos de biopelícula frecuentemente combinan la mezcla mecánica y la aireación por burbujas. Sin embargo, los métodos convencionales de aireación por burbujas son muy intensivos en cuanto a consumo energético, ya que las pérdidas de fricción a través de las tuberías, la baja solubilidad del oxígeno en el agua y la sobrepresión requerida para formar las burbujas demandan grandes cantidades de energía. Se estima que la energía necesaria para la aireación de los sistemas de fangos activos representa un 2-3% de la producción mundial de energía eléctrica. A pesar de que ha habido muchas mejoras en los difusores, las eficiencias de transferencia de oxígeno (OTE) en los sistemas de aireación por burbujas todavía se encuentran limitadas a sólo un 30-40%.

Por lo tanto, se deben encontrar tecnologías energéticamente eficientes capaces de adaptarse a normativas cada vez más estrictas y a la creciente escasez de recursos hídricos, tanto para el diseño de nuevas estaciones depuradoras de aguas residuales (EDARs), como para adaptar las instalaciones existentes aprovechando el espacio disponible.

El Reactor de Biopelícula Soportada y Oxigenada por Membranas (RBSOM) se presenta como una alternativa capaz de proporcionar un nuevo modo de aireación mucho más eficaz desde el punto de vista energético. En el RBSOM, la biopelícula activa en contacto con agua a tratar, es soportada y aireada/oxigenada por membranas permeables a gases. El oxígeno se transfiere directamente por difusión desde el interior de la membrana hacia la biopelícula sin formación de burbujas. Esta particularidad proporciona unas características excepcionales de transferencia de oxígeno, siendo posible obtener ahorros energéticos de hasta un 85% en comparación con los procesos convencionales de fangos activos. También es posible obtener sistemas mucho más compactos, ya

que la biomasa se concentra en las membranas y recibe el oxígeno directamente desde las mismas.

Las biopelículas de los RBSOM son contra-difusionales, lo cual quiere decir que los sustratos son proporcionados a la biopelícula desde direcciones opuestas. En las biopelículas contra-difusionales de los RBSOM se desarrollan estructuras de comunidades microbianas únicas, que permiten la oxidación de la demanda química de oxígeno (DQO), nitrificación y desnitrificación simultáneas.

Teniendo en cuenta este contexto, esta tesis doctoral pretende contribuir a una mejor comprensión de los procesos principales que rigen los sistemas RBSOM y también a la optimización del rendimiento de estos reactores.

Como punto de partida de este trabajo, en el **capítulo 1** se presenta una revisión bibliográfica actualizada sobre los procesos de biopelícula y la tecnología RBSOM.

En el **capítulo 2** se describen los materiales y métodos utilizados a lo largo de las diferentes etapas de experimentación y simulación.

En el **capítulo 3** se propone una nueva configuración RBSOM híbrida (RBSOMH), consistente en un reactor compacto que integra el proceso RBSOM en un reactor convencional de fangos activos. El objetivo principal del RBSOMH fue mantener la biomasa nitrificante en las membranas y lograr la desnitrificación a través de las bacterias en suspensión, con el fin de controlar el crecimiento excesivo de bacterias heterótrofas sobre la biopelícula y el espesor de la misma. Se emplearon simulaciones matemáticas con el fin de establecer las condiciones de diseño y operación óptimas del proceso RBSOMH para el tratamiento de aguas residuales urbanas.

El RBSOMH experimental consistió en un reactor de 15 L en el que se empleó un módulo de membrana plana para la transferencia de oxígeno y como soporte de la biopelícula. Se mantuvo una concentración de sólidos suspendidos en el licor mezcla (SSLM) típica de un proceso de fango activo convencional. El RBSOMH se alimentó con un agua afluyente tratando de reproducir un agua residual urbana de media-alta carga, para lo que se emplearon materias concentradas procedentes de una EDAR. La nueva configuración RBSOMH mostró un gran potencial para la eliminación de nitrógeno total (NT) a través de nitrificación y desnitrificación simultáneas. Notablemente, se obtuvo una tasa de nitrificación media de 3 gN/m²d. Este resultado es mejor que los obtenidos en estudios anteriores de RBSOMH. La concentración residual de N-NO₃ en el efluente fue esencial para mantener la distribución deseada de biomasa nitrificantes y heterótrofas. Los ensayos de tasa de producción de nitratos (TPN) y tasa de consumo de nitratos

(TCN) llevados a cabo demostraron que, como se pretendía, la mayor parte de la biomasa nitrificante se mantuvo en la biopelícula (90%) mientras que la mayoría de las bacterias desnitrificantes permanecieron en suspensión (95%). El modelo matemático desarrollado para el RBSOMH fue capaz de reproducir los resultados experimentales (con respecto a la operación continua del RBSOMH, así como a los ensayos de TPN y TCN realizados en la biomasa en suspensión y en la biopelícula). Los resultados referentes al estudio sistemático de simulaciones predijeron que en el proceso RBSOMH, los procesos de nitrificación y desnitrificación estaban en la mayoría de los casos desacoplados, siendo el área de membrana y las presiones de aire suministradas a la membrana (PAM) los parámetros principales que afectaron a las tasas de nitrificación. Ello permitió el control y optimización de forma separada de los procesos de nitrificación y desnitrificación. El estudio sistemático de simulaciones también posibilitó la definición de algunos parámetros de diseño y operación óptimos del proceso RBSOMH para diferentes tipos de membranas y requerimientos de nitrógeno en el efluente. Diferentes combinaciones de PAM y áreas de membrana permitieron obtener la concentración de amonio en el efluente deseada con el fin de maximizar las tasas de nitrificación. Se determinaron las PAM óptimas a diferentes temperaturas que permitieron cumplir con los límites de NT en el efluente establecidos por la normativa Europea para diferentes escenarios. También se obtuvieron las concentraciones de SSLM más favorables para conseguir la concentración deseada de N-NO₃ en el efluente a diferentes temperaturas.

Cuando el RBSOM es operado con el extremo de las membranas cerrado, se obtienen OTEs del 100%, lo que resulta en grandes ahorros energéticos. Sin embargo, los RBSOM con membranas cerradas son más sensibles a la retrodifusión de gases inertes, como el nitrógeno. La retrodifusión de gases reduce la tasa de transferencia de oxígeno (OTR) promedio, disminuyendo consecuentemente los flujos de eliminación de contaminantes. En el **capítulo 4**, se exploraron estrategias potenciales para mitigar el efecto perjudicial del proceso de retrodifusión en el RBSOM (alimentado con oxígeno puro) con membranas cerradas. Se planteó la hipótesis de que ventilando periódicamente el lumen de las membranas podría incrementar las OTRs y los flujos de depuración. Empleando una celda experimental y simulaciones matemáticas, este estudio demostró que los perfiles de los gases de retrodifusión en membranas de fibra hueca (MFH) sin biopelícula, se desarrollaron en una escala de tiempo relativamente larga. Por ello, con ventilaciones muy cortas del interior de las membranas se pudieron restablecer los perfiles uniformes del gas de entrada durante periodos de tiempo relativamente duraderos. Mediante simulaciones

matemáticas, se exploró sistemáticamente el efecto de los intervalos de ventilación (tiempo entre las ventilaciones) en una MFH. Para intervalos de ventilación moderados, de alrededor 30 minutos, la ventilación de los gases aumentó significativamente la OTR promedio, prácticamente sin afectar la OTE. Cuando el intervalo de ventilación fue lo suficientemente corto, en este caso de 20 minutos, la OTR promedio fue incluso mayor a la obtenida en modos de operación continuamente abiertos. La estrategia de ventilaciones periódicas se probó experimentalmente en un RBSOM con fibras cerradas, aumentando en gran medida las OTRs y tasas de depuración (llegando a alcanzar valores similares a los obtenidos en operación con extremo abierto) y alcanzando OTEs superiores al 97% (la OTE obtenida en el modo de operación abierto fue de 0.5%). Los resultados de este estudio mostraron que las ventilaciones periódicas son una estrategia prometedora que permite combinar las ventajas de los modos de operación con extremo abierto y cerrado, maximizando tanto las OTRs como las OTEs.

En el **capítulo 5**, se llevaron a cabo experimentos y simulaciones matemáticas para estudiar el efecto de biopelículas aerobias heterótrofas en la dinámica de gases de los RBSOM. Se tomó como hipótesis que el comportamiento de la retrodifusión en MFH sin biopelícula podría ser notablemente diferente que en los RBSOM. Los perfiles de retrodifusión en membranas con biopelícula se vieron afectados por dos fenómenos. En primer lugar, el consumo de oxígeno por la biopelícula afectó a los flujos de transferencia de oxígeno, lo que a su vez repercutió en los perfiles de oxígeno desarrollados a lo largo de la membrana. Se observó una mayor acumulación de nitrógeno y por tanto menores concentraciones de oxígeno a lo largo de la membrana cuando mayor era la actividad de la biopelícula. En segundo lugar, la biopelícula actuó como una barrera para la difusión del N_2 hacia el interior de la membrana. Este efecto dependió principalmente del espesor de la biopelícula y de la concentración de N_2 en el interior de la membrana. Estos efectos fueron notablemente significativos para condiciones transitorias. El tiempo requerido para alcanzar el estado estacionario del proceso de retrodifusión aumentó con los espesores de biopelícula. Estos resultados sugirieron que los efectos de la biopelícula deben ser considerados cuando se implementen estrategias de ventilación con el objetivo de minimizar los efectos negativos de la retrodifusión de gases. También se encontró que en los RBSOM con extremos cerrados y suministrados con aire, no sólo la retrodifusión de N_2 podría diluir la concentración de oxígeno dentro de la membrana, sino que también la acumulación del N_2 presente en el aire

suministrado, podría resultar en un perfil decreciente de concentración de oxígeno a lo largo de la membrana. Se simuló estrategias de ventilación para RBSOM suministrados con oxígeno puro y con aire. Los resultados alcanzados mostraron que al aplicar las estrategias de ventilación adecuadas a cada caso, se pudieron obtener presiones parciales medias de O_2 y OTRs dentro de la membrana iguales o mayores que en los RBSOM con extremo abierto, beneficiándose de altas OTEs obtenidas durante la mayor parte del ciclo, correspondiente a la fase cerrada (se lograron valores de OTE entre el 75-99%, cuando los valores de OTE para sistemas abiertos fue de 0.5-1.7%). De este modo se demostró que las estrategias de ventilación tienen el potencial de aumentar la capacidad de los RBSOM y disminuir los costes de inversión y de operación de los nuevos sistemas.

En conclusión, a partir del trabajo realizado en esta tesis se obtuvo información importante para el diseño y operación de los RBSOM. Estos reactores han demostrado ser una tecnología altamente eficaz para la eliminación de carbono y nitrógeno en aguas residuales urbanas.

Summary

Nowadays, activated sludge is one of the most widely used wastewater treatment process worldwide. It has established its efficiency for carbon and nutrient removal by successfully treating municipal and industrial wastewaters. Biofilm systems have also been used during the past 100 years, and they are still deployed extensively around the world today. To improve reaction rates, biofilm systems frequently combine mechanical mixing and bubble aeration. However, conventional bubble aeration methods are highly energy intensive, where frictional losses through the piping, low aqueous solubility of oxygen and backpressure required for blowing bubbles demand large amounts of energy. It is estimated that the energy required for aeration of activated sludge systems accounts for 2-3 % of global electrical energy production. Although there have been many improvements in the diffusers, oxygen transfer efficiencies (OTEs) in bubble aeration systems are still limited to only 30-40%.

It is therefore required to find out energy-efficient technologies capable of adapting to more strict normative and increasing scarcity of fresh water resources, both for the design of new wastewater treatment plants (WWTP) and for retrofitting existing installations by profiting available space.

Membrane aerated biofilm reactor (MABR) is presented as an alternative approach that may provide new more energy-effective aeration option. In MABR the active biofilm in contact with the water to be treated is supported on and aerated/oxygenated by a gas permeable membrane. Oxygen in the lumen is transferred into the biofilm straight by diffusion and without bubble formation. These features, give exceptional oxygen transfer characteristics, being possible to obtain energy savings up to 85% compared to conventional activated sludge processes. It is also possible to have much more compact systems as the biomass can be concentrated on the membranes and supplied with oxygen directly.

MABR biofilms are counter-diffusional, meaning substrates are supplied from opposite sides of the biofilm. The MABR supports a unique biofilm counter-diffusional microbial community structure, allowing concurrent oxidation of chemical oxygen demand (COD), nitrification, and denitrification.

Taking into account this context, this doctoral thesis aims to contribute to a better understanding of the underlying processes that govern MABR systems and also to optimize the performance of these reactors. The present work is based on experimental and model research of MABR technological process for wastewater treatment.

As a starting point of this work, an actualized literature review about biofilm processes, and MABR technology is presented in **chapter 1**.

In **chapter 2** the materials and methods used along the different experimental and modeling stages are described.

A new hybrid MABR configuration (HMABR) is proposed in **chapter 3**, consisting of a compact reactor which integrates a MABR process into a conventional completely mixed activated sludge reactor. The critical goal of the HMABR was to maintain nitrifying biomass on the membranes and achieve denitrification via suspended growth in order to control the heterotrophic attachment and avoid thick biofilms. Mathematical modeling was used as a tool to establish the optimum design and operational conditions for the HMABR process treating urban wastewater. The experimental HMABR consisted of a 15 L reactor where a flat membrane module for oxygen transfer and biofilm support was used. Bulk liquid had a mixed liquor suspended solids (MLSS) concentration typical of a conventional activated sludge process. The HMABR was fed with an influent mimicking a medium-high strength urban wastewater, for what concentrated matters proceeding from an urban WWTP were used. The new HMABR showed good potential for TN removal through simultaneous nitrification and denitrification. Remarkably, an average nitrification rate of 3 gN/m²d was achieved. This result is better than those obtained in previous HMABR studies. Effluent residual NO₃-N concentration had a crucial role to maintain the desired nitrifying and heterotrophic biomasses distribution. Performed nitrate production rate (NPR) and nitrate uptake rate (NUR) batch test results demonstrated that, as intended, most of the nitrifying biomass was in the biofilm (90%) and the majority of denitrifying bacteria remained in suspension (95%). The developed HMABR mathematical model was able to match the experimental results (with respect to continuous HMABR operation as well as NPR and NUR batch tests in suspension and in the biofilm). The results of the systematic simulation studies, predicted that in the HMABR process, nitrification was in most cases decoupled from denitrification process, being the membrane areas and the supplied membrane air pressures (MAP) the underlying parameters affecting nitrification rates. This enabled the separate control and optimization of both nitrification and denitrification processes. Systematic simulation studies also allowed defining

some optimum design and operation parameters of the HMABR process for different membrane types and effluent nitrogen requirements. Different combinations of MAPs and membrane areas allowed achieving the desired effluent ammonium concentration to maximize nitrification rates. Optimum MAPs for different operating temperatures were obtained to satisfy TN effluent standards established in European legislation for different scenarios. Most favorable MLSS concentrations for different temperatures and for achieving the desired effluent $\text{NO}_3\text{-N}$ concentrations were determined.

When MABR is operated with closed-end membranes, 100% OTEs are provided, resulting in significant energy savings. However, closed-end MABRs are more sensitive to back-diffusion of inert gases, such as nitrogen. Back-diffusion reduces the average oxygen transfer rate (OTR), consequently decreasing the average contaminant removal fluxes. In **chapter 4**, potential strategies to mitigate back-diffusion detrimental effect in closed-end MABRs (supplied with pure oxygen) were explored. It was hypothesized that periodically venting the membrane lumen would increase the OTRs and removal fluxes. Using an experimental flow cell and mathematical modeling, this study showed that back-diffusion gas profiles developed over relatively long timescales in clean hollow fiber membranes (HFM). Thus, very short ventings could re-establish uniform gas profiles for relatively long time periods. Using modeling, the effect of the venting intervals (time between ventings) was systematically explored in a HFM. At moderate venting intervals, of around 30 minutes, the venting significantly increased the average OTR without substantially impacting OTE. When the interval was short enough, in this case shorter than 20 minutes, the OTR was actually higher than for continuous open-end operation. A periodic venting strategy was experimentally assessed for a closed-end MABR greatly increasing OTRs and removal fluxes (reaching similar values to the ones obtained in open-end operation mode) and achieving OTEs higher than 97% (OTE value in open end systems was 0.5%). Results of this study showed that periodic venting is a promising strategy to combine the advantages of open-end and closed-end operation, maximizing both the OTRs and OTEs.

In **chapter 5**, experiments and modeling were used to study the effect of heterotrophic aerobic biofilms on gas dynamics in MABRs. It was hypothesized that back-diffusion behavior in clean HFMs may be significantly different than in MABRs. Gas back-diffusion profiles in biofilm supporting membranes were found to be impacted by two phenomena. First, oxygen consumption within the biofilm affected oxygen transfer fluxes, which in turn affected the O_2 profiles along the

membrane. Higher biofilm activities resulted in higher nitrogen accumulation and lower oxygen concentration profiles along the membrane length. Second, the biofilm acted as a diffusion barrier for N_2 diffusing into the membrane. This effect depended primarily on the biofilm thickness and on the N_2 concentration in the lumen. The effects were significant for transient conditions. The time required to reach back-diffusion steady-state increased with biofilm thicknesses. These results suggested that biofilm effects should be considered when using a venting approach to minimize the effects of gas back diffusion. It was also found that in closed-end air supplied MABRs, not only back-diffusion of N_2 from the bulk liquid could dilute oxygen concentration inside the membrane lumen, but also the accumulation of the N_2 present in the air gas supply could result in a decreasing oxygen concentration profile along the fiber length. Venting strategies were simulated for pure oxygen and air supplied MABRs. These results showed that applying the proper venting interval to each case, average O_2 partial pressures inside the membrane lumen and OTRs equal or higher than the open-end operation mode could be obtained, while benefiting from the high OTEs achieved during the longer closed-end cycle duration (achieving overall OTE values ranging from 75 to 99%, while reached OTE values for open-end systems was between 0.5-1.7%). Thus, venting strategies were proved to have the potential to increase the capacity of MABRs and decrease the capital and operating costs of new systems.

In conclusion, from the work performed in this thesis important information for the design and operation of MABRs was obtained. These reactors have proved to be a cost-effective technology for carbon and nitrogen removal in urban wastewaters.

List of publications

Journal Publications

International journal publications

Pérez-Calleja, P., Aybar, M., Piciooreanu, C., Esteban-García, A.L., Martin, K.J., Nerenberg, R., 2017. *Periodic venting of MABR lumen allows high removal rates and high gas-transfer efficiencies*. Water Research. Accepted 20-05-2017.

Book Chapters

Esteban-García, A.L., Díez, R., Rodríguez-Hernández, L., Lobo, A., De Florio, L., **Pérez-Calleja, P.**, Tejero, I., 2012. *Processes based on the growth of biofilms on gas permeable membranes: Biomembrane reactors*. Omil F. and Suárez S. (eds) Innovative Technologies for Urban Wastewater Treatment Plants (2nd Edition) ISBN-13: 978-84-695-3514-1, pp. 117-145.

Contributions to congresses

Pérez-Calleja, P., Zugasti, E., Díez, R., De Florio, L., Esteban-García, A.L., Tejero, I., 2012. *Procesos híbridos con biopelícula soportada y oxigenada por membranas para eliminación de nutrientes*. Meta 2012, Reunión de la Mesa Española de Tratamiento de Aguas. Almería, 4-6 octubre.

De Florio, L., Díez, R., Esteban-García, L., González-Viar, M., **Pérez-Calleja, P.**, Presmanes, D., Rodríguez L., Tejero, I., 2012. *Innovative technologies for biological wastewater treatment with enhanced oxygen transfer efficiency*. Morselli L. (ed) Atti dei seminari Tecnologie Innovative, ECOMONDO 2012, 07-10 November, Rimini Fiera, Italy. Maggioli Editore, ISBN 978-88-387-7708-0.

De Florio, L., **Pérez-Calleja, P.**, Díez, R., González-Viar, M., Esteban-García, A.L., Tejero, I., Larrea, L., 2013. *Innovative technologies for biological wastewater treatment with enhanced oxygen transfer efficiency*. In NOVEDAR Young Water Researchers Workshop. Innovative Technologies for the XXI Century WWTP and future perspectives. Santander, 28-29 March, pp. 23-26.

Pérez-Calleja, P., Esteban-García, A.L., Tejero, I., Gabaldón, C., Larrea, L., 2014. *Guidelines for the optimal operation of the Hybrid Membrane Aerated Biofilm for nitrogen removal*. Book of Abstracts of the IWA 2ndh Specialized International Conference ecoSTP2014, EcoTechnologies for Wastewater Treatment: Technical, Environmental & Economic Challenges. Verona, Italy, 23-27 June. ISBN 978-8869250002, 185-188.

Pérez-Calleja, P., Aybar, M., Picioreanu, C., Esteban-García, A.L., Nerenberg, R. 2015. *Effects of gas back-diffusion on Membrane-Aerated Biofilm Reactors (MABRs)*. Proceedings of the 3rd Water Research Conference. Shenzhen, China, 11-14 January.

Pérez-Calleja, P., Aybar; M., Picioreanu, C., Esteban-García, A.L., Nerenberg, R., 2015. *Membrane-Biofilm Reactors (MBfR) For Water Treatment: Overcoming Gas Back Diffusion Effects*. AEESP Research and Education Conference. Environmental Engineering and Science at the nexus. Yale University, Commons, New Haven, 13-16 June.

Pérez-Calleja, P., Aybar, M., Picioreanu, C., Esteban-García, A.L., Nerenberg, R., 2015. *Enhanced Operation of Membrane-Biofilm Reactor (MBfR) for Waste Water Treatment by Mitigation of Gas Back-Diffusion Effect*. WEFTEC 2015, Chicago USA.

Aybar, M., **Pérez-Calleja, P.**, Picioreanu, C., Esteban-García, A.L., Nerenberg, R., 2015. *Effects of Gas Back-diffusion on the Membrane-Biofilm Reactor (MBfR) for Water Treatment*. IWA Specialized Conference, Biofilms in drinking water systems - From treatment to tap, Arosa (Switzerland), 23-26 August.

Pérez-Calleja, P., Esteban-García, A. L., Tejero, I., Aybar, M., Larrea, L., 2016. *Guidelines for the Energy Efficient Operation of the Hybrid Membrane Aerated Biofilm Process for Nitrogen Removal*. 13th IWA Leading Edge Conference on Water and Wastewater Technologies. Jerez de la Frontera, Spain, 13-16 June.

Aybar, M., **Pérez-Calleja, P.**, Picioreanu, C., Esteban-García, A.L., Nerenberg, R., 2016. *Enhancing Energy Efficiency of Membrane Aerated Biofilm Reactors (MABRs) by Managing of Gas Back-Diffusion*. 13th IWA Leading Edge Conference on Water and Wastewater Technologies. Jerez de la Frontera, Spain, 13-16 June.

Pérez-Calleja, P., Aybar, M., Picioreanu, C., Esteban-García, A.L., Nerenberg, R., 2016. *Enhanced operation of Membrane Aerated Biofilm Reactors (MABRs) For Waste Water Treatment by Managing Gas Back-Diffusion*. 3rd IWA Specialized

International Conference: Ecotechnologies for Wastewater Treatment 2016 (ecoSTP16). Invited platform presentation. Cambridge, UK, 27-30 June.

Pérez-Calleja, P., Esteban-García, A.L., Tejero, I., Aybar, M., Larrea, L., 2016. *Mathematical Model To Describe The Behaviour Of The Hybrid Membrane Aerated Biofilm Reactor (HMABR)*. 3rd IWA Specialized International Conference Ecotechnologies for Wastewater Treatment 2016 (ecoSTP16). Poster session 3315756. Cambridge, UK, 27-30 June.

Pérez-Calleja, P., Aybar, M., Picioreanu, C., Esteban-García, A.L., Nerenberg, R., 2017. *Effect of Biofilm Development on Gas Back-Diffusion in Membrane Aerated Biofilm Reactors (MABRs)*. 24th Triennial Symposium on Advancements in Water & Wastewater. Borchardt Conference, Ann Arbor (U.S.), 21-22 February.

Pérez-Calleja, P., Esteban-García, A.L., Tejero, I., Aybar, M., Larrea, L., 2017. *Model-based Study to Optimize the Hybrid Membrane Aerated Biofilm Reactor (HMABR) for Carbon and Nitrogen Removal*. 10th International Conference on Biofilm Reactors. Dublin, Ireland, 9-12 May.

Pérez-Calleja, P., Aybar, M.; Picioreanu, C., Esteban-García, A.L., Nerenberg, R. 2017. *Periodic Venting of Membrane Aerated Biofilm Reactors (MABRs) Allows High Removal Rates and High Gas-Transfer Efficiencies*. 10th International Conference on Biofilm Reactors. Dublin, Ireland, 9-12 May.

Aybar, M., **Pérez-Calleja, P.**, Nerenberg, R., 2017. *Mechanisms of pore formation in MABR biofilms, and its effects on system performance*. 10th International Conference on Biofilm Reactors. Dublin, Ireland, 9-12 May.

Nerenberg, R., **Pérez-Calleja, P.**, Gavryliuk, A., Aybar, M., 2017. *Impact of Membrane Configuration on the Performance of Membrane-Aerated Biofilm Reactors (MABRs)*. 10th International Conference on Biofilm Reactors. Dublin, Ireland, 9-12 May.

Table of contents

List of figures.....	xix
List of tables.....	xxv
List of acronyms and symbols.....	xvii
0 INTRODUCTION	1
0.1 BACKGROUND.....	3
0.2 OBJETIVES.....	5
0.3 REFERENCES.....	5
1 STATE OF THE ART	9
SUMMARY	13
1.1 INTRODUCTION	13
1.2 WASTEWATER TREATMENT REGULATIONS.....	14
1.3 BIOFILM PROCESSES:FUNDAMENTALS AND TECHNOLOGIES	16
1.3.1 Fundamentals of biofilm systems	16
1.3.2 Biofilm process technologies.....	19
1.3.2.1 Moving Bed Biofilm Reactors: MBBR	19
1.3.2.2 Hybrid processes	22
1.3.2.3 Granular processes.....	23
1.3.2.4 Membrane Biofilm Reactors: MBfR	25
1.4 MEMBRANE AERATED BIOFILM REACTOR TECHNOLOGY: MABR	28
1.4.1 Introduction	28
1.4.2 Biofilms on gas permeable membranes.....	28
1.4.3 Oxygen transfer characteristics.....	31
1.4.4 Potential applications.....	36
1.4.5 MABR configurations and operating parameters	38
1.4.6 MABR mathematical models.....	40
1.4.7 Economical aspects	41
1.4.8 Key research and development needs	42
1.4.9 Conclusions	43
1.5 REFERENCES	44

2	<i>MATERIALS AND METHODS.....</i>	53
	SUMMARY.....	57
2.1	EXPERIMENTAL STUDY.....	57
2.1.1	Liquid phase analytical methods	58
2.1.1.1	Chemical Oxygen Demand (COD).....	58
2.1.1.2	Ammonia nitrogen (NH ₄ -N).....	60
2.1.1.3	Nitrates (NO ₃ -N).....	62
2.1.2	Solid phase analytical methods	63
2.1.2.1	Total (TSS) and Volatile Suspended Solids(VSS)	63
2.1.3	Biomass characterization	65
2.1.3.1	Batch test essays	65
2.1.3.2	Biofilm thickness determination	66
2.1.4	Dissolved oxygen profiles at membrane surface.....	67
2.2	MATHEMATICAL MODELING	68
2.2.1	HMABR mathematical model.....	68
2.2.2	Back-diffusion mathematical model for HFMs.....	72
2.2.3	Back-diffusion mathematical model for MABRs.....	74
2.3	REFERENCES.....	74
3	<i>GUIDELINES FOR THE OPTIMAL DESIGN AND OPERATION OF THE HYBRID MEMBRANE AERATED BIOFILM REACTOR (HMABR) FOR NITROGEN REMOVAL.....</i>	77
	SUMMARY.....	81
3.1	INTRODUCTION.....	82
3.2	OBJECTIVES	86
3.3	MATERIALS AND METHODS.....	86
3.3.1	Experimental study.....	86
3.3.1.1	HMABR configuration.....	86
3.3.1.2	Feed wastewater	88
3.3.1.3	Operational conditions and criteria	88
3.3.1.4	Analytical methods.....	90
3.3.1.5	Mass balances in the HMABR.....	90
3.3.1.6	Nitrification and denitrification batch tests	92
3.3.2	Simulation study.....	92
3.3.2.1	HMABR mathematical model.....	92
3.3.2.2	HMABR model calibration	97

3.3.2.3	Systematic simulation studies for the optimization of the design and operation of the HMABR process	103
3.4	RESULTS AND DISCUSSION	107
3.4.1	Experimental results.....	107
3.4.1.1	Mixed Liquor Suspended Solids (MLSS) behavior	107
3.4.1.2	Removal of soluble Chemical Oxygen Demand (COD)	108
3.4.1.3	Nitrogen removal	108
3.4.1.4	Nitrification and denitrification batch tests	114
3.4.2	Simulation results.....	115
3.4.2.1	HMABR Model calibration.....	115
3.4.2.2	Systematic simulation studies.....	118
3.5	CONCLUSIONS	128
3.5.1	Experimental study	128
3.5.2	Simulation study.....	129
3.6	REFERENCES	130
4	PERIODIC VENTING OF MABR LUMENS ALLOWS HIGH REMOVAL RATES AND HIGH OXYGEN TRANSFER EFFICIENCIES	135
	SUMMARY	139
4.1	INTRODUCTION	139
4.2	OBJECTIVES.....	141
4.3	MATERIALS AND METHODS.....	142
4.3.1	Experimental flow cell configuration	142
4.3.2	Synthetic medium for the MABRs	143
4.3.3	Analytical methods.....	144
4.3.4	DO measurements	144
4.3.5	Calculation of membrane mass transfer coefficient, K_m	145
4.3.6	Numerical model for gas back-diffusion	146
4.3.6.1	Flow and mass transport in the liquid.....	147
4.3.6.2	Flow and mass transport in the gas	148
4.4	RESULTS AND DISCUSSION	152
4.4.1	Determination of membrane mass transfer coefficient	152
4.4.2	Model evaluation	153
4.4.3	Model-based assessment of periodic venting.....	155
4.4.4	Experimental assessment of gas supply strategies on HFM with biofilm	160

List of figures

Figure	Title	Page
1-1	Different stages of biofilm development	17
1-2	Soluble (a) and particulate substrate (b) transfer from the bulk liquid to the biofilm	18
1-3	Schematic showing the principle of MBBRs in (a) aerobic reactors and (b) anoxic/anaerobic reactors	20
1-4	Plastic media used in MBBRs (without sludge return) (a) and in hybrid/IFAS processes (with sludge return) (b)	21
1-5	IFAS process versus conventional activated sludge process	22
1-6	Activated sludge from a wastewater treatment plant (a) and aerobic granular sludge cultivated in a laboratory scale reactor (b) and in a pilot plant (c)	24
1-7	Schematic of mass transport into a membrane attached biofilm	26
1-8	Theoretical zoning of a thick biofilm on (a) conventional co-diffusional biofilm and (b) membrane aerated counter-diffusional biofilm	29
1-9	Typical behavior of hollow-fiber membranes pressurized with pure O ₂	34
1-10	Comparison of head losses between conventional bubble aeration and MABR systems	35
1-11	Evolution in wastewater aeration technology	36
2-1	Set up for batch essays in the biofilm covered membrane (a) and in suspended biomass (b)	66
2-2	Biofilm thickness measurement using a microsensor tip and a stereomicroscope	67
2-3	Detail of a flow-cell port used for DO measurement with a microsensor controlled by a micromanipulator	68
2-4	Logical structure of AQUASIM systems consisting of four subsystems	69
2-5	Typical screenshot of AQUASIM software	71
2-6	Schematic representation of the general methodology for model calibration	71
2-7	Typical screenshot of COMSOL software	72
2-8	Fluid flow and mass transport phenomena considered in back-diffusion model	73

Figure	Title	Page
3-1	Biofilm in a MABR with nitrifying and heterotrophic biomass, which can lead to substrate transfer limitations due to overgrowth of heterotrophs; (b) Biofilm in a HMABR, with nitrifying biomass in the biofilm, limiting heterotrophic attachment by maintaining high suspended solids and low bulk BOD concentrations	84
3-2	Diagram of different interactions between colloids, flocs and biofilm in the Extended MCB model	85
3-3	Conceptual structure of the HMABR model	86
3-4	(a) Schematics of the HMABR and (b) an image of the experimental pilot plant	87
3-5	Nitrogen mass balance for this study	91
3-6	Fractionations of influent soluble COD (a) and particulate COD (b) in the HMABR model	100
3-7	Flow chart of the iterative step-wise procedure for the HMABR mathematical model calibration	102
3-8	Schematics of the optimization process methodology during the systematic simulation studies	104
3-9	Evolution of MLSS concentration over time	108
3-10	Evolution of influent sCOD (black squares) and t COD (black triangles) concentrations and effluent (open squares) sCOD concentrations	
3-11	Performance of the HMABR over 145 days of operation. (a) Influent (closed diamonds, average black dashed line) and effluent (open diamonds, average gray dashed line) $\text{NH}_4\text{-N}$ concentrations and nitrification rates per unit of membrane area (closed circles, continuous line); (b) total available (closed triangles, average black dashed line) and effluent (open triangles, average gray dashed line) $\text{NO}_3\text{-N}$ concentrations, and volumetric denitrification rates (closed circles, continuous line)	109
3-12	Relation between effluent $\text{NO}_3\text{-N}$ (open triangles) and sCOD (open squares) concentrations (a) and nitrification rates (black circles) (b)	113
3-13	Model predicted particulate (a) and dissolved (b) species profiles within the biofilm	118
3-14	MAP required for different membrane areas in order to achieve effluent ammonium concentration of around 4 mg/L, at 12°C	119
3-15	Particulate (a) and dissolved species (b) biofilm profiles for a membrane area of 120000 m ² and a MAP of 140 kPa	121
3-16	Particulate (a) and dissolved species (b) biofilm profiles for a membrane area of 180000 m ² and a MAP of 8 kPa	122

Figure	Title	Page
3-17	Design optimization plot that allow determining the HMABR process optimum design HRT for achieving the desired effluent nitrate and bulk MLSS concentrations, for a constant supplied MAP of 40 kPa and a membrane area of 150000 m ²	123
3-18	MAP required at different temperatures (12, 16 and 20°C) in order to accomplish with effluent ammonium concentration criterion (NH ₄ -N≈4 mg/L), for a total membrane area of 150000 m ²	126
3-19	Operation optimization plots for determining the optimum MLSS concentration to be maintained depending on the temperature and the desired effluent NO ₃ -N concentrations for a total membrane area of 150000 m ² , and HRTs of 2.5 hours	127
4-1	Schematic showing differences between hollow-fiber membranes at steady-state in: (a) closed-end operation, and (b) open-end operation	141
4-2	(a) Schematic of flow cell. Oxygen-free water from a reservoir was pumped into the square-section glass tube with a hollow-fiber membrane supplied with O ₂ in the middle. (b) Detail of a flow-cell port used for DO measurement with a microsensor controlled by a micromanipulator	143
4-3	(a) Schematic representation (not at scale) of the experimental co-current aeration system with a single HFM inside a square-section flow cell filled with liquid. (b) Model representation including a 2-D axisymmetric liquid domain connected via the membrane wall with a 1-D gas domain	147
4-4	A representative profile of measured dissolved oxygen concentration through the mass transfer boundary layer in the liquid adjacent to the membrane	152
4-5	Experimental and model-simulated dissolved oxygen (DO) profiles at the membrane surface for the experimental HFM flow cell	154
4-6	Simulated O ₂ partial pressures in the lumen, averaged along the entire membrane length for different operation regimes: (i) transient (solid line) and time-averaged (dotted line) during three venting cycles, (ii) steady state closed end (short-dashed gray line), and (iii) steady state open end (long-dashed gray line)	156
4-7	Comparison of simulated (a) oxygen transfer rates (OTR) and (b) oxyge transfer efficiencies (OTE) for open operation, closed operation, and intermittent opening. Venting mode was tested for venting intervals (time between ventings) ranging from 1 to 30 min, with 20 seconds open phases	157

Figure	Title	Page
4-8	Oxygen partial pressure profiles along the membrane length for open-end (thick black line) and closed-end (thick gray line) steady state conditions, and time-averaged for transient conditions from open- to closed-end (thin black lines)	158
4-9	Biofilm thickness development along the membrane length in normally operated open-end MABR-1 (a) and closed-end MABR-2 (b). Experimental DO profiles at membrane surface for open-end MABR-1 (c) and closed-end MABR-2 (d)	161
4-10	Experimentally observed COD removal fluxes in MABR-1 (triangles) and MABR-2 (squares) plotted against time. Circles enclosed in the black rectangle represent COD removal fluxes for the closed-end MABR-2 when a venting strategy of 20s open and 20 min closed was implemented	162
4-11	Biofilm thicknesses along the fiber length of MABR-2 just prior to initiating the venting cycles, and after eight days of periodic venting. Venting provides a much more uniform biofilm thickness	163
5-1	Schematic showing differences between hollow-fiber membranes with biofilm in: (a) closed-end operation, and (b) open-end operation	175
5-2	(a) Schematic representation (not at scale) of the experimental aeration system with a single HFM supporting a biofilm inside a square-section flow cell filled with liquid; (b) Model representation including a 2-D axisymmetric liquid domain connected via the membrane wall with a 1-D gas domain	179
5-3	Experimental (open dots) and model-predicted (continuous line) dissolved oxygen (DO) profiles at membrane surface for heterotrophic MABRs and for a HFM flow cell. (a) DO steady state profiles for a HFM flow cell without biofilm and for a 180 μm biofilm MABR after closing the end of the membrane; (b) DO concentrations over time when transitioning from an open-end to a closed-end operation for a HFM with no biofilm and for a 700 μm biofilm MABR, and a bulk liquid Ac concentrations of 10 mg/L.	185
5-4	(a) Model-simulated DO profiles at membrane surface for a closed-end HFM without biofilm (dashed line), and a closed-end MABR with 700 μm biofilm (continuous black line); (b) Diffusive fluxes of O_2 along the membrane in the HFM without biofilm (dashed lines) and in the 700 μm biofilm MABR (continuous line)	187
5-5	(a) Model-simulated gas velocity profiles inside the lumen gas for the closed-end HFM without biofilm (dashed line), and for	188

Figure	Title	Page
	the closed-end MABR (continuous black line); (b) Simulations of partial pressures for O ₂ and N ₂ in the closed-end HFM (dashed lines) and in the MABR (continuous line)	
5-6	Model-simulated steady-state DO profiles for MABRs with biofilm thicknesses of 1300, 700 and 300 μm, for a bulk liquid Ac concentration of 20 mg/L (a), and 320 mg /L (b). Using pure oxygen at an inlet relative pressure of 0.05 atm and $u_{in}=27$ mm/s	190
5-7	DO concentrations over time when transitioning from an open-end to a closed-end operation for a HFM with no biofilm and MABRs with 1300, 700 and 300 μm biofilm thicknesses for a bulk liquid Ac concentration of 20 mg/L (a) and 320 mg/L (b)	192
5-8	Comparison of simulated (a) average O ₂ partial pressures (PO_{2ave}) and (b) oxygen transfer efficiencies (OTE) for open operation, closed operation, and intermittent opening. Venting mode was tested for venting intervals (time between ventings) ranging from 1 to 30 min, with 20 seconds open phases	194
5-9	(a) Model-simulated DO profiles at membrane surface for a closed-end air supplied 700 μm MABR. Using air at an inlet relative pressure of 1.68 atm and $u_{in}=5$ mm/s; (b) Diffusive fluxes of N ₂ and O ₂ out of the membrane (negative values); (c) Simulations of partial pressures for O ₂ and N ₂ along the membrane	197
5-10	Comparison of simulated average O ₂ partial pressures inside the membrane lumen for a 700-μm biofilm air supplied MABR operated in open-end mode (dashed lines) and with venting intervals (continuous black line)	198
S-7	The Hagen-Poiseuille relationship for slightly compressible fluids and observed flows for a broad range of pressures, ranging from 0.07 (1 psi) to 0.68 (10 psi) atm	228

List of tables

Table	Title	Page
1-1	Summary of MABR configurations investigated	40
2-1	Specific data for the COD determination method used in Chapter 3	59
3-1	Operational conditions during the experimental campaign	90
3-2	HMABR model operational parameters	96
3-3	Summary of fitting parameters adopted during the HMABR model calibration process	103
3-4	Summary of design and operation parameters values during the optimization plots	107
3-5	Adjusted values for the fitting parameters in the HMABR model	116
3-6	Summary of experimental and model predicted continuous and batch test results of the HMABR	116
3-7	Example of obtained X_A concentrations in the biofilm and in suspension, for a membrane area of 150000 m ² , MLSS concentration of 3500 mg/L and HRT of 2, 2.5 and 3 hours	120
3-8	Comparison of two examples (membrane area = 150000 m ² and HRT = 2.5 h) where target effluent ammonium concentration was and was not fulfilled	120
3-9	Examples of different HRTs and MLSS combinations that resulted in a similar effluent residual NO ₃ -N concentrations	122
3-10	Example of the effect of HRTs in the resulting suspended X_H biomasses and effluent residual NO ₃ -N concentrations. Data shown correspond with MLSS isoline of 3500 mg/L	124
3-11	Summary of SRT values obtained for each HRT and MLSS combination represented in Figure 3-17	124
3-12	Example of obtained effluent X_S and S_S concentrations for MLSS isoline of 3500 mg/L	125
3-13	Example of variations in X_S and X_I concentrations for different MLSS at T ^a =20°C	127
4-1	Back-diffusion model parameters	150
4-2	Required membrane areas and oxygen fluxes for closed-end, open-end, and venting modes. Areas and fluxes are normalized by the closed-end value	160
5-1	Biofilm back-diffusion model parameters	181
S-1	Kinetic parameters used in the HMABR mathematical model	222

Table	Title	Page
S-2	Stoichiometric parameters used in the HMABR mathematical model	223
S-3	Matrixes of the process rate equations for the HMABR mathematical model	224
S-4	Stoichiometric matrix of the HMABR mathematical model	225
S-5	Kinetics of the interaction between suspended flocs and colloids	227
S-6	Physical and fitting parameters of the HMABR mathematical model	227

List of acronyms and symbols

A	Surface area	m^2
Ac	Acetate	-
Anammox	Anaerobic Ammonium Oxidation	-
APHA	American Public Health Association	-
ASM2d	Activated Sludge Model n° 2	-
AS	Activated Sludge	-
BF	Biofilm	-
BOD	Biochemical Oxygen Demand	$mg L^{-1}$
BOD/N	Biochemical Oxygen Demand to Nitrogen ratio	$Kg BOD Kg N^{-1}$
C/N	Carbon to Nitrogen ratio	$Kg COD Kg N^{-1}$
CAS	Conventional Activated Sludge	-
COD	Chemical Oxygen Demand	-
D	Diffusion coefficient	$m^2 d^{-1}$
DMP	Dimethylphenol	-
DNR	Denitrification Rate	$g N m^{-3} d^{-1}$
DO	Dissolved oxygen	$mg L^{-1}$
e	Efficiency	%
EAWAG	Swiss Federal Institute of Aquatic Science	-
EPA	US Environmental Protection Agency	-
EPS	Extracellular Polymeric Substances	-
FAS	Ferrous Ammonium Sulphate	-
h	Depth	m
HF	Hollow Fiber	-
HFM	Hollow Fiber Membrane	-
HMABR	Hybrid Membrane Aerated Biofilm Reactor	-
H	Henry's coefficient	$mol(aq) mol(g)^{-1}$
HRT	Hydraulic Retention Time	h
IFAS	Integrate Fixed Activated Sludge	-
ISO	International Organization for Standardization	-
J	Flux	$g m^{-2} d^{-1}$
K	Mass transfer coefficient	$m d^{-1}$
$K_{AT,BXi}$	Attachment coefficient of particulate compounds	$m d^{-1}$
$K_{AT,F}$	Attachment coefficient from colloids to flocs	d^{-1}
K_C	Colloids saturation coefficient	$gX_{i,C} gX_{i,F}^{-1}$
$K_{DE,B}$	Biofilm detachment coefficient	d^{-1}

K_{DET,F}	Detachment coefficient from flocs to colloids	d ⁻¹
K_S	Half saturation coefficient	mg L ⁻¹
LDL	Liquid Diffusion Layer	μm
L_F	Biofilm thickness	μm
L_m	Membrane length	-
MAB	Membrane Aerated Biofilm	-
MABR	Membrane Aerated Biofilm Reactor	-
MAP	Membrane Air Pressure	atm
MBBR	Moving Bed Biofilm Reactor	-
MBfR	Membrane Biofilm Reactor	-
MCB	Mixed-Culture Biofilm model	-
MLSS	Mixed Liquor Suspended Solids	mg L ⁻¹
MLTSS	Mixed Liquor Total Suspended Solids	mg L ⁻¹
MLVSS	Mixed Liquor Volatile Suspended Solids	mg L ⁻¹
MSA	Membrane Specific Area	m ⁻¹
NH₄⁺-N	Ammonia nitrogen concentration	mg L ⁻¹
NO₃⁻-N	Nitrate nitrogen concentration	mg L ⁻¹
NPR	Nitrate Production Rate	gN m ⁻³ d ⁻¹
NUR	Nitrate Uptake Rate	gN m ⁻³ d ⁻¹
OTE	Oxygen Transfer Efficiency	%
OTR	Oxygen Transfer Rate	mg O ₂ m ⁻² s ⁻¹
p	Pressure	atm
pCOD	Particulate COD	g COD m ⁻³
p.e.	Population equivalent	-
PVC	Polyvinylchloride	-
P_w	Power requirement	kW
Q_{in}	Influent Flow Rate	L d ⁻¹
q_{max}	Maximum specific utilization rate	d ⁻¹
Q_R	Recycle rate	% Q _{in}
Q_w	Wastage Flow Rate	L d ⁻¹
R	Ideal gas constant	m ³ atm mol ⁻¹ K ⁻¹
RBC	Rotating Biofilm Contactor	-
R_m	Membrane outer radius	μm
R_{m,i}	Membrane inner radius	μm
S	Soluble compounds	mg L ⁻¹
sbCOD	Slowly biodegradable COD	g COD m ⁻³
SBR	Sequencing Batch Reactor	-
sCOD	Soluble Chemical Oxygen Demand	g COD m ⁻³
SDN	Specific Denitrification Rate	gN gMVLSS ⁻¹ d ⁻¹

S_I	Inert soluble COD	g COD m ⁻³
S_L	Slowly biodegradable soluble COD	g COD m ⁻³
S_S	Readily biodegradable soluble COD	g COD m ⁻³
SNR	Specific Nitrification Rate	gN m ⁻² d ⁻¹
SRT	Solids Retention Time	d
T	Temperature	°C, K
t_c	Interval between ventings	min
t_{COD}	Total Chemical Oxygen Demand	mg L ⁻¹
TF	Tricking Filter	-
TN	Total Nitrogen	mg L ⁻¹
t_o	Venting open-end duration	s
TSS	Total Suspended Solids	mg L ⁻¹
u	Velocity	mm s ⁻¹
UASB	Upflow Anaerobic Sludge Blanket	-
UNICEF	United Nations International Children's Emergency Fund	-
USEPA	United States Environmental Protection Agency	-
VFA	Volatile Fatty Acids	mg L ⁻¹
VOC	Volatile Organic Compounds	-
V_R	Reactor Volume	m ³
VSS	Volatile suspended solids	mg L ⁻¹
w	Air mass flow rate	Kg s ⁻¹
WHO	World Health Organization	-
WWTP	Waste Water Treatment Plant	-
X	Particulate compounds	g COD m ⁻³
X_A	Autotrophic bacteria	g COD m ⁻³
X_H	Heterotrophic bacteria	g COD m ⁻³
X_I	Inert Particulate COD	g COD m ⁻³
X_S	Slowly biodegradable particulate COD	g COD m ⁻³
Y	Biomass yield	gVSS g BOD ⁻¹
μ	Dynamic Viscosity	Pa s
Δh_{fric}	Frictional losses	-
ΔP	Pressure losses	-
ρ	Density	Kg m ⁻³
θ	Biofilm liquid volumetric fraction	-

Chapter 0

Introduction

0.1 BACKGROUND

Wastewater treatment faces the task of responding to the ever-increasing stringent regulations on discharge limits, and the challenge of reducing its energy consumption and improving its sustainability. Spain in particular has some specific problems, such as water scarcity or the limited capacity of their WWTPs due to growing municipalities and massive displacements of people (seasonal in many cases), frequently not being able to meet the effluent standards for nutrient removal. Therefore, there is a clear driving force towards the development of innovative technologies for new wastewater treatment plants (WWTPs) or the retrofitting of existing ones, better adapted to current and future regulatory, economic and environmental requirements.

The activated sludge process has been widely applied for carbon, nitrogen and phosphorous removal. However, because of the low oxygen aqueous solubility, continuous aeration is required to avoid oxygen depletion in aerobic processes. The most widespread method of aeration, gas bubbling, requires large amounts of energy and can strip volatile organic compounds and greenhouse gases from the water. The search for more energy efficient treatment systems has become fundamental for the eco sustainability of WWTPs.

Membrane Aerated Biofilm Reactors (MABRs) are gaining in importance since they are able to achieve high oxygen transfer efficiencies (OTEs) resulting in significant energy savings, up to 85% compared to conventional activated sludge processes (Aybar et al., 2014). In the MABR, the active biofilm is supported on and aerated by a gas permeable membrane. The membrane's lumen can be pressurized with a gas (air or oxygen), which diffuses through the membrane wall straight to the biofilm attached at the membrane's outer surface without bubble formation.

MABR biofilms are counter-diffusional, meaning that substrates are supplied from opposite sides of the biofilm (Nerenberg, 2016). The MABR also supports a unique counter-diffusive microbial community structure, allowing concurrent oxidation of chemical oxygen demand (COD), nitrification and denitrification (Timberlake et al., 1988; Hibiya et al., 2003; Semmens et al., 2003; Terada et al., 2003; Jácome et al., 2006; Matsumoto et al., 2007; Downing and Nerenberg, 2008; Syron and Casey, 2008), therefore providing a smaller reactor footprint. Several commercial applications are in development, but very few full-scale applications exist.

Despite the many advantages of the MABR process, it presents some limitations.

On the one hand it is necessary to control the excessive biofilm thickness, which has been observed to be thicker than in conventional biofilms due to overgrowth of heterotrophs (Casey et al., 2000). Thick biofilms increase the mass transfer limitation resulting in decreased removal ability. On the other hand, despite satisfactory nitrogen removal results have been obtained in MABR pilot studies using synthetic wastewater (Semmens et al., 2003; Stricker et al., 2011), the potential for application with real urban wastewater can be limited, because the relatively low availability of readily biodegradable substrate can hamper the growth of enough denitrifying biomass in the biofilm.

Several methods for biofilm management have been tested. Most studies combined high shear and gas sparging (Celmer et al., 2008; Pankhania et al., 1999; Semmens et al., 2003). Nevertheless, maintaining an optimal biofilm thickness through these methods is challenging, as detachment is a complex process that varies with biofilm age, type and environmental conditions (Liu and Tay, 2001).

MABRs can be operated in closed end or open end mode. The closed end mode allows 100% OTEs (Brindle et al., 1998; Pankhania et al., 1999; Hibiya et al., 2003; Terada et al., 2003; Syron and Casey, 2008; Martin and Nerenberg, 2012), but the gas supplying membranes can suffer from gas back-diffusion, where N_2 and other dissolved gases diffuse into the membrane lumen, leading to lower average oxygen transfer rates (OTRs) compared to open end operation.

The mechanisms of gas transfer using hollow-fiber membranes have been extensively studied, and several researchers have explored ways to improve OTRs of gas supplying membranes (Ahmed and Semmens, 1992; Matsuda et al., 1999; Ahmed et al., 2004). However, few studies have tried to concurrently improve the OTR and OTE. Furthermore, most back-diffusion studies have neglected the effects of biofilms growing on the membranes, even though they are an integral part of the process.

Previous researches on MABR are encouraging but there is a need for a deeper investigation in order to understand the potential capabilities of the MABR process.

This Doctoral Thesis arises in order to contribute to generate new knowledge in the field of the emerging MABR technology for wastewater treatment, focusing on overcoming some of the main limitations and optimizing the process.

0.2 OBJECTIVES OF THE STUDY

In this work lab-scale and bench-scale experiments were combined with modeling in order to provide a complementary knowledge to the MABR process. Strategies to overcome biofilm thickness limitation for achieving TN removal in a single MABR reactor treating urban wastewater, and to minimize the detrimental effect of back-diffusion, were addressed.

In this context, the objectives of this study were:

1. Performance evaluation of a hybrid MABR (HMABR). Experimental definition of the criteria for the optimal HMABR operation and biomasses distribution. Development and validation of a simulation model of the process. Establish the optimum design and operation conditions of the HMABR process for treating urban raw wastewater through systematic simulation studies.
2. Systematically study the back-diffusion effect in hollow-fiber membranes through experimentation and modeling. Explore gas supply strategies as a means to maximize OTEs and OTRs of MABRs.
3. Explore the impact of biofilms on gas dynamics in pure oxygen and air supplied MABRs, in order to improve gas supply strategies to mitigate gas back-diffusion detrimental effects.

0.3 REFERENCES

Ahmed, T., Semmens, M.J., 1992. The Use of Independently Sealed Microporous Hollow Fiber Membranes for Oxygenation of Water - Model Development. *J. Memb. Sci.* 69, 11–20.

Ahmed, T., Semmens, M.J., Voss, M.A., 2004. Oxygen transfer characteristics of hollow-fiber, composite membranes. *Adv. Environ. Res.* 8, 637–646.

Aybar, M., Pizarro, G., Boltz, J.P., Downing, L., Nerenberg, R., 2014. Energy-efficient wastewater treatment via the air-based, hybrid membrane biofilm reactor (hybrid MfBR). *Water Sci. Technol.* 69, 1735–1741.

Brindle, K., Stephenson, T., Semmens, M.J., 1998. Nitrification and oxygen utilisation in a membrane aeration bioreactor. *J. Memb. Sci.* 144, 197–209.

- Casey, E., Glennon, B., Hamer, G., 2000. Biofilm development in a membrane-aerated biofilm reactor: Effect of flow velocity on performance. *Biotechnol. Bioeng.* 67, 476–486.
- Celmer, D., Oleszkiewicz, J.A., Cicek, N., 2008. Impact of shear force on the biofilm structure and performance of a membrane biofilm reactor for tertiary hydrogen-driven denitrification of municipal wastewater. *Water Res.* 42, 3057–3065.
- Downing L.S. and Nerenberg R., 2008. Total nitrogen removal in a hybrid, membrane-aerated activated sludge process. *Water Res.* 42 (14), 3697–3708.
- Hibiya, K., Terada, A., Tsuneda, S., Hirata, A., 2003. Simultaneous nitrification and denitrification by controlling vertical and horizontal microenvironment in a membrane-aerated biofilm reactor. *J. Biotechnol.* 100, 23–32.
- Jácome, A., Molina, J., Suarez, J., Tejero, I., 2006. Simultaneous removal of organic matter and nitrogen compounds in autoaerated biofilms. *J. Environ. Eng.* 132, 1255–1263.
- Liu, Y., Tay, J.H., 2001. Strategy for minimization of excess sludge production from the activated sludge process. *Biotechnol. Adv.* 19, 97–107.
- Martin, K.J., Nerenberg, R., 2012. The membrane biofilm reactor (MBfR) for water and wastewater treatment: principles, applications, and recent developments. *Bioresour. Technol.* 122, 83–94.
- Matsuda, N., Nakamura, M., Sakai, K., Kuwana, K., Tahara, K., 1999. Theoretical and experimental evaluation for blood pressure drop and oxygen transfer rate in outside blood flow membrane oxygenator. *J. Chem. Eng. Japan* 32, 752–759.
- Matsumoto, S., Terada, A., Aoi, Y., Tsuneda, S., Alpkvist, E., Picioreanu, C., van Loosdrecht, M.C.M., 2007. Experimental and simulation analysis of community structure of nitrifying bacteria in a membrane-aerated biofilm. *Water Sci. Technol.* 55, 283–290.
- Nerenberg, R., 2016. The membrane-biofilm reactor (MBfR) as a counter-diffusional biofilm process. *Curr. Opin. Biotechnol.* 38, 131–136.
- Pankhania, M., Brindle, K., Stephenson, T., 1999. Membrane aeration bioreactors for wastewater treatment: completely mixed and plug-flow operation. *Chem. Eng. J.* 73, 131–136.
- Semmens, M.J., Dahm, K., Shanahan, J., Christianson, A., 2003. COD and nitrogen removal by biofilms growing on gas permeable membranes. *Water Res.* 37, 4343–4350.

Stricker, A.E., Lossing, H., Gibson, J.H., Hong, Y., Urbanic, J.C., 2011. Pilot scale testing of a new configuration of the membrane aerated biofilm reactor (MABR) to treat high-strength industrial sewage. *Water Environ. Res.* 83, 3–14.

Syron, E., Casey, E., 2008. Membrane-aerated biofilms for high rate biotreatment: performance appraisal, engineering principles, scale-up, and development requirements. *Env. Sci Technol.* 42, 1833–1844.

Terada, A., Hibiya, K., Nagai, J., Tsuneda, S., Hirata, A., 2003. Nitrogen removal characteristics and biofilm analysis of a membrane-aerated biofilm reactor applicable to high-strength nitrogenous wastewater treatment. *J. Biosci. Bioeng.* 95, 170–178.

Timberlake, D.L., Strand, S.E., Williamson, K.J., 1988. Combined aerobic heterotrophic oxidation, nitrification and denitrification in a permeable-support biofilm. *Water Res.* 22, 1513–1517.

Chapter 1

State of the art¹

¹ Part of section 1.4 of this chapter has been published as:

Esteban-García, A.L., Díez, R., Rodríguez-Hernández, L., Lobo, A., De Florio, L., **Pérez-Calleja, P.**, Tejero, I., 2012. *Processes based on the growth of biofilms on gas permeable membranes: Biomembrane reactors*. Omil F. and Suárez S. (eds) Innovative Technologies for Urban Wastewater Treatment Plants (2nd Edition) ISBN-13: 978-84-695-3514-1, pp. 117-145.

OUTLINE

SUMMARY.....	13
1.1 INTRODUCTION.....	13
1.2 WASTEWATER TREATMENT REGULATIONS.....	14
1.3 BIOFILM PROCESSES: FUNDAMENTALS AND TECHNOLOGIES	16
1.3.1 Fundamentals of biofilm systems	16
1.3.2 Biofilm process technologies	19
1.3.2.1 Moving Bed Biofilm Reactors: MBBR.....	19
1.3.2.2 Hybrid processes (suspended – biofilm biomass)	22
1.3.2.3 Granular processes	23
1.3.2.4 Membrane Biofilm Reactors: MBfR	25
1.4 MEMBRANE AERATED BIOFILM REACTOR TECHNOLOGY: MABR	28
1.4.1 Introduction	28
1.4.2 Biofilms on gas permeable membranes	28
1.4.3 Oxygen transfer characteristics	31
1.4.4 Potential applications	36
1.4.5 MABR configurations and operating parameters	38
1.4.6 MABRs models.....	40
1.4.7 Economical aspects.....	41
1.4.8 Key research and development needs	42
1.4.9 Conclusions	43
1.5 REFERENCES.....	44

SUMMARY

In this chapter, starting with a brief summary of the requirements for wastewater treatment, an overview of the research literature on biofilm processes and on membrane aerated biofilm reactor (MABR) technology is provided. Firstly, the fundamentals and some innovative biofilm processes technologies are described, focusing on membrane biofilm reactors (MBfRs). These processes use gas permeable membranes to deliver a gaseous substrate by diffusion to a biofilm naturally forming on the membrane's outer surface. This technology provides a more effective alternative to supply dissolved gases to microorganisms than conventional processes. This chapter also reviews the MABR technology, in which this thesis is focused on, providing fundamentals, main applications, economical aspects and key research needs underlying this technology. Among the factors affecting the MABR operation, special interest in managing biofilm thickness and back-diffusion detrimental effects are shown.

1.1 INTRODUCTION

Wastewater treatment is crucial as there is a scarcity of natural water resources and a higher demand for clean water supply. Furthermore, huge volumes of wastewater being sent back to the natural water resources, such as rivers and the sea, will affect the source water quality. Moreover, in the near future, many facilities should be updated to fulfill more stringent environmental requirements. The need of implementing wastewater treatment systems is even more evident in developing countries as it has been evidenced by UNICEF and WHO (2012), who reported that in 2010 only half of the population (56%) living in developing regions used improved sanitation facilities.

Biological treatment processes are based on the use of active biomass or organisms to degrade the contaminants present in wastewater. Biomass present as a fixed film attached to some form of support medium have been called biofilm processes (BF), and the biomass dispersed in suspension within the bulk liquid have been called activated sludge processes (AS).

The AS wastewater treatment process was invented by Andern and Lockett in 1914. Due to its supposed operation simplicity and high quality effluents, the AS has been the most commonly used process employed in urban wastewater treatment plants (WWTP) for organic matter, nitrogen and phosphorous removal.

However, AS current applications have been regarded as inefficient by some researchers. The issue of compact wastewater treatment system is gaining an elevated concern internationally particularly in densely populated regions where there is a higher strain on the environment which results in high demand on waste abatement. Both the cost and availability of land combined with implementation of secondary treatment standards, sets demands for WWTP that have a small footprint, produce an effluent of high standard and also comply with waste minimization (Leiknes and Ødegaard, 2001).

Innovative BF technologies, with either fixed or suspended support, which offer alternatives for compact treatment plant designs and more effective treatment system than AS processes, have emerged in the last years. In this way, these novel biofilm technologies are able to fulfill the increasingly stringent effluent requirements demanded nowadays.

1.2 WASTEWATER TREATMENT REGULATIONS

At the present time, in response to the problems of water scarcity, there is a trend towards more stringent laws to protect against water pollution. In this context, the European Urban Waste Water Treatment Directive (Council Directive 91/271/EEC) requires that Member States ensure that agglomerations (towns, cities, settlements) larger than 2000 people equivalent (p.e.) properly collect and treat their urban wastewater. However, it does not involve any duty to municipalities lower than said population. On the other hand, to achieve the good ecological status of water bodies required by the European Directive 2000/60/EU (Water Framework Directive) an appropriate treatment of the wastewater is needed, including the one generated by small agglomerations (Molinos-Senante et al., 2011). Untreated wastewater can be contaminated with harmful bacteria and viruses and thus presents a risk to public health. It also contains nutrients, such as nitrogen and phosphorous, which can damage freshwaters and the marine environment by promoting excessive growth of algae that chokes other life, a process known as eutrophication.

Council Directive 91/271/EEC regarding urban wastewater treatment was transposed to the Spanish legal system via Act 11/1995 and Royal Decree 509/1996. Royal Decree 509/1996 establishes norms applicable to urban wastewater treatment and laid out the minimum requirements that must be met. To these effects, it fixes concentration values and reduction percentages (it allows

a choice between the two) for three parameters, biochemical oxygen demand (BOD), chemical oxygen demand (COD), and total suspended solids (TSS), for discharges from secondary treatment facilities or facilities of an equivalent process. Nevertheless, discharge authorizations can impose stricter requirements when necessary in order to ensure that the recipient water meets quality objectives set in current regulations. For discharges from treatment facilities in sensitive zones, Royal Decree 509/1996 also allows the choice between concentration values and reduction percentages which are fixed in this case for five substances (in addition to the three previously mentioned it also applies to phosphorous and nitrogen). In any case, stricter requirements can be imposed if necessary to ensure that quality objectives are met.

In Spain, as in the rest of the European Union (EU) Countries, when Council Directive 91/271/EEC concerning urban wastewater came into effect, there was a considerable increase in the construction of treatment plants and the obtaining of good quality treated effluent (Iglesias and Ortega de Miguel, 2008). However, the Court of Justice of the EU ruled on 14 April 2011, that Spain violated EU law by not adequately collecting and treating the urban wastewater discharged by 37 agglomerations (towns, cities, settlements). Six years later, this matter remains unaddressed in 17 agglomerations (out of the 37 covered by the judgment) corresponding to 1400000 people. In addition, more than 16 years after the deadline of 31 December 2000 for the implementation of the applicable EU rules (Council Directive 91/271/EEC), the perspective for full compliance in all these agglomerations is still unclear.

Consequently, the current problems of water scarcity and implementation of EU regulations in Spain, have made it necessary to adapt and update an important part of existing facilities as well as to promote suitable wastewater treatment processes.

Therefore, taking into account the need of water availability and to contribute to improve the treatment trains applied, this Thesis focuses on innovative membrane aerated biofilm reactors (MABRs) that may be employed for this purpose.

1.3 BIOFILM PROCESSES: FUNDAMENTALS AND TECHNOLOGIES

1.3.1 Fundamentals of biofilm systems

Removal of contaminants (organic matter and nutrients) in wastewater treatment systems can be carried out by suspended biomass within the bulk liquid (AS processes) or by biomass attached to a support media (BF processes).

Most microorganisms (predominantly bacteria) can colonize the surface of an inert support becoming attached and forming biomass-aggregates or biofilms. The ability of a cell to attach to a support/surface is controlled by environmental factors (nutrient concentrations, temperature, pH), genetic factors (presence of genes encoding motility functions, environmental sensors) and adhesiveness factors (specific surface proteins and appendages) (Costerton et al., 1995; O'Toole et al., 2000).

Thus, biofilms consist in a group of simple cells or micro-colonies embedded in a matrix of biological origin and attached to a surface through extracellular polymeric substances (EPS) (Wuertz et al., 2008). The microbial community of a biofilm commonly contains many different species of bacteria, each influencing each other's gene expression and growth.

The basic steps for biofilm development can be summarized in the following stages, and are represented in Figure 1-1:

- 1) Initial attachment, where bacteria adhere to a solid surface by inducing weak, reversible bonds called van der Waals forces.
- 2) Irreversible attachment, cell adhesion molecules (proteins in their surfaces that bind other cells) permanently anchor the bacteria to the surface.
- 3) Maturation I, biofilm grows due to cell division and recruitment of other bacteria and particulate matter. Cells begin to build the matrix, composed primarily by polysaccharides, that holds the biofilm together.
- 4) Maturation II, the EPS matrix fully encases all the cells, as the biofilm continues to thicken and grow, taking on a more complex morphology.
- 5) Detachment and sloughing, where individual cells or pieces of biofilm are broken down and released to the bulk liquid. This detachment can be triggered by environmental factors like shear forces in the bulk liquid or substrate concentrations.

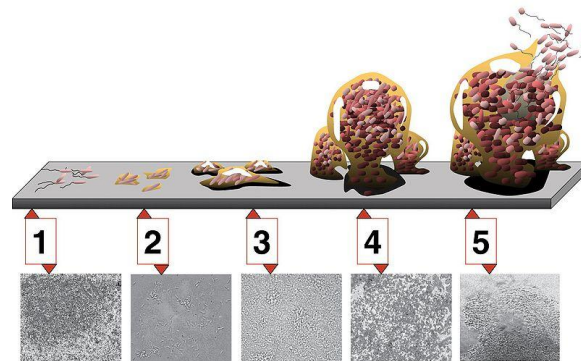


Figure 1-1 Different stages of biofilm development (credit: Monroe, 2007).

The biofilm will reach a steady-state density concentration and thickness that depends on the balance between the described growth and detachment processes.

Although the basic metabolic processes for removing carbon and nutrients are the same for BF and AS systems, there are some inherent differences that provide several advantages and some challenges for the application of biofilm systems. These main differences are based in the way of retaining biomass in the reactors and substrate transport processes.

In AS systems, the microorganisms responsible for wastewater treatment are kept in suspension and aerated. The separation of suspended biomass and effluent through settling is necessary, and a recycle is used for returning the separated biomass back to the reactor and maintaining sufficient MLSS concentration (typically around 3000-4000 mg/L).

Unlike AS processes, biological performance in BF systems does not depend on the biomass separation and recycle steps because the active biomass is continuously retained in the reactor (without the need of intermediate pumping). The solids concentration leaving the reactor with the effluent is at least an order of magnitude lower in concentration than in activated sludge processes. As a result, BF processes are compatible with a variety of different separation techniques, not only conventional settlers.

Suspended biomass in AS systems is comprised of small biological flocs and theoretically, all dissolved wastewater substrate is available to all cells. In BF systems, substrates must diffuse initially through a layer of stagnant water (liquid diffusion layer, LDL) and later through the biofilm layers to become available (Figure 1-2 a). Thus, mass transfer of soluble substrates and/or electron acceptors can become in a limiting factor for the biofilm inner layers (van Loosdrecht and

Heijnen, 1993). Therefore, overall removal fluxes in biofilm systems depend on mass transfer velocities and in substrate concentrations within the biofilm. This implies the need to maintain a higher bulk liquid DO concentration than in a conventional activated sludge process, in which a concentration of around 2 mg/L is sufficient.

Besides mass transport of particulate components from the bulk liquid to the biofilm is more complex, requiring a previous attachment and a subsequent diffusion (Okabe et al., 1998), which is in turn much slower than diffusion of soluble compounds (Figure 1-2 b).

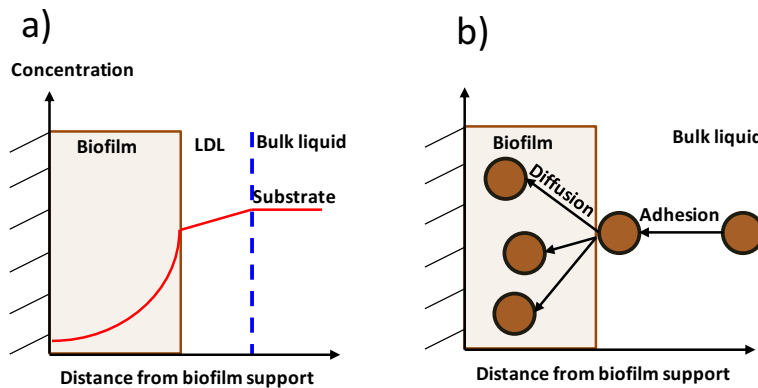


Figure 1-2 Soluble (a) and particulate substrate (b) transfer from the bulk liquid to the biofilm.

These mass transport phenomena can lead to varying environmental conditions and kinetic characteristics within the biofilm. In this way a mature biofilm may have aerobic, anoxic and anaerobic processes occurring, where the limiting substrate will change through the depth of the biofilm.

Some advantages associated with BF reactors in comparison with AS processes include: reduced operating and energy costs, higher biomass concentration per reactor volume (resulting in smaller and more compact reactors), higher mean cell retention time, increased protection from harmful conditions or substances (i.e. temperature variations or toxicity shock loads) improving the operational stability, higher biodegradation rates (due to higher active biomass), extensive microbial diversity, enhanced cell-to-cell communication and genetic exchange, minimized need for settling capacity, and greater efficiency to degrade recalcitrant (Esteban-García, 2009; Verma et al., 2006). Apart from that, biofilm systems versatility allows the technology to be applied in a variety of reactors geometries, making this

technology well suited for retrofitting installations in order to upgrade existing plants.

Some general drawbacks associated with BF systems are: potential clogging of the system as a result of inadequate screening, excessive biofilm growth, which could plug the media system, inadequate mixing or short-circuiting, resulting in inefficient use of the media, and greater complexity for controlling the present biomass (Water Environment Federation, 2010).

1.3.2 Biofilm process technologies

Within biofilm treatment processes two main groups can be differentiated, depending if the wastewater flows through the support media (fixed-support systems), or on the contrary, if the support media moves within the wastewater to be treated (moving-support systems). In addition, hybrid systems, which combine suspended biomass and fixed biomass, can be distinguished. Among the hybrid processes, there are those with the support medium mechanically mixed and with the structured support inserted in the aeration tank.

There is a wide range of biofilm systems that have been applied to wastewater treatment. Conventionally, tricking filters (TFs), rotating biological contactors (RBC), fluidized beds, and sand filters, among others, have been used in biological wastewater treatment for several decades. These processes are however fairly complicated because of the need of periodic back-washing or fluidization (Rusten et al., 1995). Thus, currently much focus is on moving bed biofilm reactors (MBBRs), integrated fixed-film activated sludge processes (IFAS), granular processes and membrane biofilm reactors (MBfRs) (Boltz et al., 2017).

1.3.2.1 Moving Bed Biofilm Reactors: MBBR

The MBBR process was developed in Norway in the late 1980s by the Norwegian company AnoxKaldnes AS in cooperation with a water treatment research group at NTNU/SINTEF. In the last 20 years, MBBR has been established as a simple-yet-robust, flexible and compact technology for wastewater treatment (Jenkins and Sanders, 2012).

MBBR systems use submerged free-moving plastic carriers on which biomass attaches and grows and can be used for carbon oxidation, nitrification, denitrification, and deammonification (Rusten et al., 2006; McQuarrie and Boltz, 2011). MBBRs are designed to meet a wide range of effluent quality standards,

including stringent nutrient limits and are also applicable to a wide range of wastewater flows ranging from 10000 to 150000 m³/d (Barkman, 2010). Whereas static biofilms have relatively low specific surface areas, biofilm carriers dramatically increase the reactor specific surface area, decreasing mass-transfer limitations and allowing high-rate applications with compact reactors.

In aerobic processes, biofilm carrier movement is caused by the agitation set up by the air, while in anoxic and anaerobic processes a mixer keeps the carriers moving (Figure 3-3). A screen is provided at the outfall end of the reactor to keep media from passing out of the reactor.

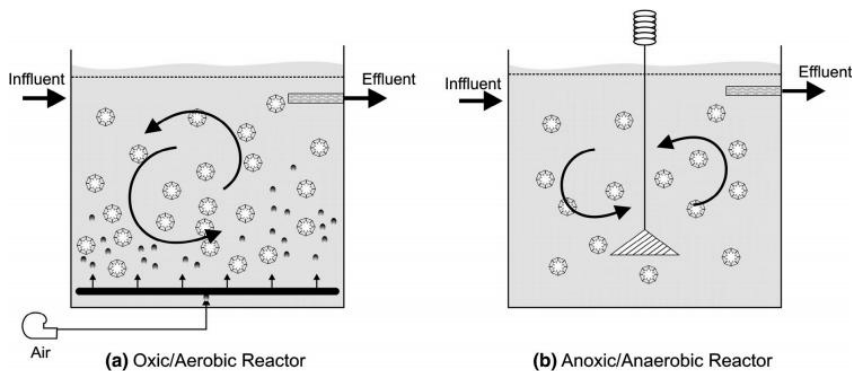


Figure 1-3 Schematic showing the principle of MBBRs in (a) aerobic reactors and (b) anoxic/anaerobic reactors (source of images: Barwal and Chaudhary, 2014).

Due to the mixing turbulence and the erosion caused by frequent collision between carrier elements, they are automatically self-washed, maintaining thinner and more evenly distributed biofilms over the carrier surfaces, as compared with other fixed-film processes (Ødegaard, 2006). The detached biomass (excess sludge with 300-500 mg TSS/L) must be later separated in a secondary clarifier.

There are different types of biofilm carriers available having different shapes and sizes (specific area (SA): 500-1000 m² m⁻³), with a density slightly less than water (approximately 0.95 g cm⁻³) so that they can be kept in suspension with minimum mixing energy (Ødegaard, 2006). The high specific area of the carrier media allows very high biofilm concentrations in a small reactor volume which controls the system performance. One important advantage of the MBBR is that the filling fraction of biofilm carriers in the reactor may be subject to preferences. One can use almost any reactor shape and choose different operating loads in a given reactor volume, simply by choice of carrier filling. Filling fractions up to 70% are

recommended in order to allow the carriers to move freely in suspension (Rusten et al., 2006).

Globally, there are more than 1200 full-scale, operating MBBRs having a capacity of 200 population equivalent (p.e.) or greater. MBBRs having a capacity less than 200 p.e. are numbered more than 7000 globally (Boltz et al., 2017).

The MBBR have the advantages of both biofilm and activated sludge systems. It is a continuously operating, non-cloggable biofilm reactor with no need for backwashing, low head-loss, high specific biofilm surface area, high organic loading rates, and short hydraulic retention times (HRT) (Rusten et al., 1998). Unfortunately, in these systems the production of filamentous bacteria and poorly settling biomass often hinder solids separation in secondary settler operations. According to Ødegaard (2000) settleability of biosolids remains the largest challenge in MBBRs design.

The free-floating carriers have been applied in both MBBR and combined hybrid/IFAS configurations. The MBBR process differs from hybrid/IFAS in that there is no return of activated sludge (Figure 1-4 a); thus, the MBBR is a pure fixed-film process and not a hybrid, and the biomass retention in the system is limited to biofilms retained on the support medium. The hybrid/IFAS process does have a return sludge and maintains MLSS concentrations that are typical of a conventional activated sludge process (Figure 1-4 b). This type of process will be discussed further in next section.

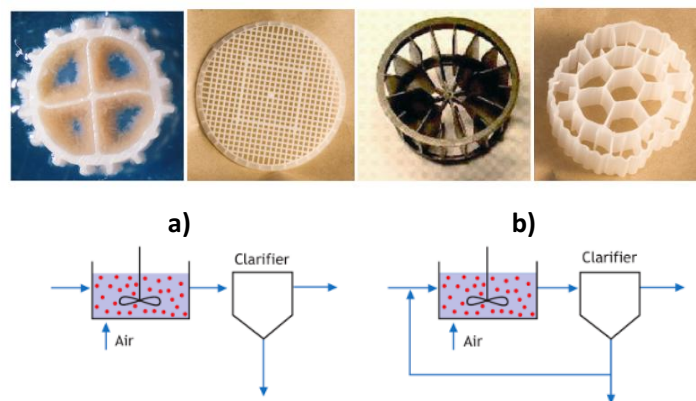


Figure 1-4 Plastic media used in MBBRs (without sludge return) (a) and in hybrid/IFAS processes (with sludge return) (b) (source of images: Henze et al., 2008).

1.3.2.2 Hybrid processes (suspended – biofilm biomass)

The word hybrid can describe any type of treatment process that combines the features of several different technologies. The focus of this chapter on hybrid processes is on integrated fixed-film activated sludge (IFAS) process, which combines fixed-biofilm and conventional suspended-growth activated treatment processes. The basic intent of an IFAS process is to provide additional biomass within the reactor volume of an activated sludge process, for the purpose of increasing the capacity of the system or upgrading its performance, as illustrated in Figure 1-5. The effective mixed liquor suspended solids (MLSS) concentration can essentially be doubled by using media in IFAS processes.

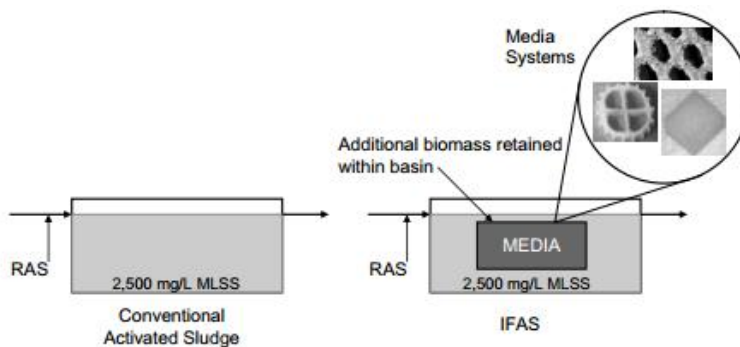


Figure 1-5 IFAS process versus conventional activated sludge process (source of images: Water Environment Federation, 2010).

Because the biomass is fixed on a media system, the MLSS concentrations are not increased, and the performance of the downstream final clarifiers is not negatively affected by an increase in the solids loading rate. In fact, in many cases, clarifier performance is improved by a reduction in the sludge volume index (SVI), as a result of the fixed film growth. Therefore, the IFAS process typically has been considered as an upgrade option in existing treatment plants that must incorporate nutrient removal. The media, and the biomass it supports, allows the aerobic treatment processes to be completed within a reduced volume and thus allows a portion of the existing tank volume to be converted to an anoxic zone or to incorporate an anaerobic zone for biologically enhanced phosphorus removal. Increased capacity is also possible, because the clarifiers are not subjected to the increased mixed-liquor concentration, although there would be hydraulic limits to an increase in capacity. Thus, IFAS offers a practical and often cost-effective approach to upgrade treatment facilities that are located on tight sites and must improve their level of performance.

Biofilm packing material has to be selected in a way that it will not be clogged by the suspended activated sludge in the reactor. Packing material includes suspended media (as in MBBR) or fixed packing material including plastic strings, structured PVC packing, or submerged rotating biological contactors (Tchobanoglous et al., 2003).

Some of the general advantages of hybrid/IFAS processes include the following: ability to phase-in additional capacity or improve performance by adding more media, additional biomass for treatment without increasing the solids loading in final clarifiers, higher rate treatment processes possible, thus allowing greater treatment in a smaller space, improved settling characteristics, reduced sludge production, simultaneous nitrification and denitrification, and improved recovery from process upsets. Disadvantages of IFAS systems include: potential odor (when tank dewatered), additional operating appurtenances, need to recollect media, and increased head loss associated with media retention screens (Water Environment Federation, 2010).

1.3.2.3 Granular processes

A significant, relatively new development within fixed-film technologies is the use of granular sludge reactors, in which naturally formed sludge granules behave similarly to suspended-media biofilms. Granular biofilms are microbial aggregates (which grow without support medium) that occur under specific reactor conditions, and can be managed to achieve cost-effective solutions to water remediation. Granules have excellent settling properties, similar to carriers. Therefore, granular sludge systems can be considered a type of suspended carrier (Nicolella et al., 2000).

The first patent for a granular process was granted by Heijnen and van Loosdrecht (1998) and since then, this technology has been systematically tested in order to solve technical challenges and scale-up considerations. The key features of this type of microbial forms are: 1) high biomass retention thus improving volumetric contaminant removal capacity, 2) substrates such as oxygen, carbon and nitrogen, must overcome the mass transfer resistance imposed by the granule structure to be consumed, and 3) due to the mass transfer resistance, a growth gradient also exist within the aggregate. In multispecies granules, this would enhance the creation of micro-niches where different microorganism would co-exist (i.e. nitrifiers, heterotrophs, methanogens, etc.).

Granular biofilms possess higher surface areas in comparison to static biofilms (Nicoletta et al., 2000). A large surface area means more exposed biofilm surface to dissolved substrates, thus higher removal fluxes are expected for granular biofilms.

The morphology, density, and size of granular sludge is, like in biofilm systems, directly influenced by shear forces and corresponding detachment in the reactor (van Loosdrecht et al., 1995), affecting both the conversion rate and the particle sedimentation rate. This issue is one of the main design criteria to optimize the overall performance of granular based reactors.

Granulation has been observed both in aerobic and in anaerobic reactors where the formation of larger and faster settling microbial aggregates provides an ecological advantage when the reactor is operated in a way where smaller flocs are washed out of the system. Upflow anaerobic sludge blanket reactors (UASB) are a widely used technology to achieve granulation under anaerobic conditions. One approach that is commonly used for aerobic granulation is to operate a sequencing batch reactor with very short settling times (Henze et al., 2008). Depending on the reactor operation, the size of granules can range from a few hundred micrometers up to a few millimeters (Figure 1-6) (Liu and Tay, 2002).

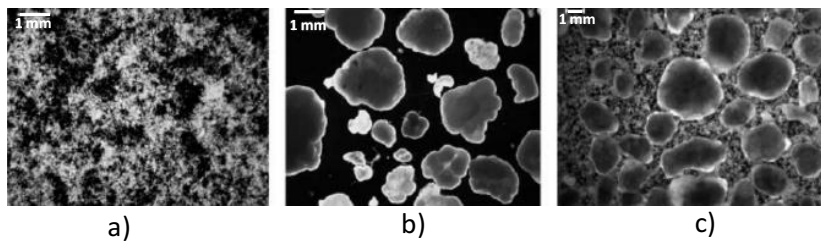


Figure 1-6 Activated sludge from a wastewater treatment plant (a) and aerobic granular sludge cultivated in a laboratory scale reactor (b) and in a pilot plant (c) (source of images: de Kreuk et al., 2007).

Aerobic granular sludge that is formed by slow growing bacteria is more stable than when fast growing bacteria are present (van Loosdrecht et al., 1995). Therefore use of (slow growing) phosphate accumulating organisms to convert the COD instead of (fast growing) normal heterotrophic bacteria will stabilize the system and makes such systems easier to operate (de Kreuk and van Loosdrecht, 2004). This aerobic granular sludge process is currently developed for nutrient removal in municipal wastewater treatment systems.

At present, more than 25 WWTPs are operating or under construction around the world, using aerobic granular biomass processes to remove nutrients from

municipal wastewaters. A commercially available aerobic sludge process to treat primary effluents is named NEREDA™. This process maintains a constant liquid/biomass volume and considers filling, settling, decanting and aeration steps. Effluents from these reactors can achieve total nitrogen and phosphorous concentrations lower than 5 and 1 g/m³ respectively. Another approach is to use a cyclone or screens for retention of granular biomass. Granules have also been used for partial nitrification/anammox (PN/A) systems of high ammonia-nitrogen concentration streams in processes such as ANAMMOX™ and DEMON™ (Boltz et al., 2017). Adav et al., (2008) proposed some research lines to continue exploring this technology in the future. For example, the use of thermophilic aerobic granules that have shown advantages in the waste production and degradation rates; combining granule processes with membrane bioreactors which showed good membrane permeability with aerobic granules; and genetically engineered granules for specific contaminant degradation.

1.3.2.4 Membrane Biofilm Reactors: MBfR

Certain dissolved gases, serve as electron donors or acceptors for microbial treatment processes. For example, dissolved oxygen is used by aerobic microorganisms to oxidize COD and ammonium; hydrogen drives the microbial reduction of oxidized contaminants and halogenated organics; and methane supports the cometabolic oxidation of a wide range of organic compounds (Martin and Nerenberg, 2012). Despite the versatility and efficiency of many gaseous substrates, their low aqueous solubility limits their practical use. In activated sludge processes the oxygen low solubility bottleneck is solved by continuously bubbling air to avoid oxygen depletion, requiring large amounts of energy and allowing the stripping of volatile organic compounds (VOCs) and greenhouse gases. Furthermore, this approach is infeasible for more expensive or dangerous gases, such as hydrogen or methane. A more effective means of supplying dissolved gases to microorganisms is through gas permeable membranes.

Membranes have long been used for gas separation and gas transfer to liquids. In the late 1980s, researchers found that these same membranes could deliver a gaseous substrate by diffusion to a biofilm naturally forming on the membrane's outer surface (Timberlake et al., 1988; Lee and Rittmann, 2000; Syron and Casey, 2008a) (Figure 1-7). When used to deliver air or oxygen, the process is often called as membrane aerated biofilm reactor (MABR) (Brindle and Stephenson, 1996; Casey et al., 1999), but more generally can be called as membrane biofilm reactors

MBfRs (Rittman, 2006). The focus of this thesis is on MABRs, so this specific application within MBfR technology will be further discussed in the next section.

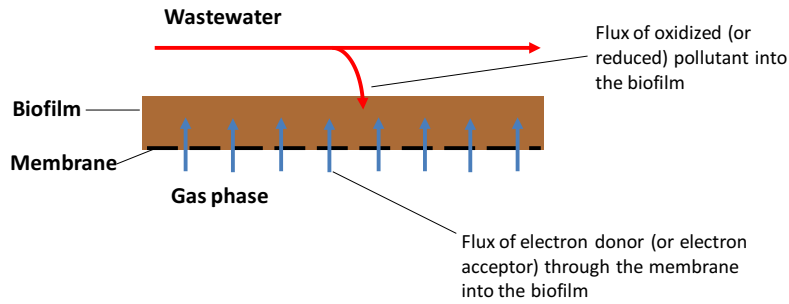


Figure 1-7 Schematic of mass transport into a membrane attached biofilm.

Hollow-fiber (HF) membranes are commonly used in MBfRs because, with outside diameters as small as 0.1 mm, they can provide high specific surface areas. Membrane sheets are also used. Microporous membranes (i.e. polypropylene membranes) typically provide much higher gas transfer rates than dense materials as gas molecules diffuse much more quickly through dry pores than through liquid-filled pores (Yang and Cussler, 1986). Hydrophobic materials (i.e. silicone membranes) are used to prevent the pores from wetting. Smaller pore sizes allow higher transmembrane pressures without gas bubbling, and a membrane with a thin, dense layer can also discourage bubbling. Unlike membrane bioreactors (MBRs), where the membranes act as filters, the MBfR pores simply convey gas and therefore do not become fouled with solids or bacteria.

When HF membranes are used, they often are collected into a gas supplying manifold at one end, while the opposite end may be open or sealed. Sealed ends are typically used when supplying gases are toxic, flammable, or expensive. Sealed end processes are highly efficient, as 100% of the gas supplied to the MBfR passes into the biofilm. The gas flux to the biofilm can be modulated by controlling the gas-supply pressure.

The MBfR biofilms behave differently than conventional biofilms due to the counter-diffusional delivery of substrates. For conventional co-diffusional biofilms, both the electron donor and acceptor concentrations are greatest at the outer edge of the biofilm (near the bulk liquid) where the biological activity is highest. For counter-diffusional biofilms one substrate (either donor or acceptor) enters the biofilm from the bulk liquid, while the other diffuses from the attachment surface

(i.e. the membrane). Unlike co-diffusional biofilms, the highest activity will be located in any location within the biofilm depth, depending on substrates concentration. Consequently, knowledge of the dissolved gas concentration dynamics within the biofilm is crucial for understanding its behavior (Martin and Nerenberg, 2012).

Several important features distinguish gas transfer in the MBfR from that in conventional biofilms:

- In conventional biofilms, the dissolved gas must diffuse through the LDL in order to penetrate the biofilm. In an MBfR, no LDL exists between the gas-supplying membrane and the biofilm.
- The LDL, located at the outer edge of the biofilm, helps to resist the loss of gas to the bulk liquid, enhancing the gas utilization efficiencies.
- Gas transfer flux can be controlled through the adjustment of gas supply pressure.
- The gas flux is self-regulating, in that biochemical demand for dissolved gases increases the concentration gradient in the biofilm, which thereby increases the driving force for gas supply.

MBfR biofilms can exhibit greater protection from toxic shocks or inhibitory compounds since they maintain high activity in the inner portions of the biofilm (Syron et al., 2009). Counter diffusional biofilms also supports unique microbial niches that in the case of MABRs allow for simultaneous removal of COD and nitrogen from wastewater (Downing and Nerenberg, 2008a; Semmens et al., 2003). Hydrogen-based MBfRs have been studied for the reduction of nitrate (Ergas and Reuss, 2001; Lee and Rittmann, 2002) and other oxidized contaminants in drinking water (Nerenberg and Rittmann, 2004). Pilot-scale tests have been conducted with MBfRs for nitrate and perchlorate from groundwater (Adham et al., 2004), showing high removals. Several researchers have used methane-based MBfRs to co-metabolically degrade trichloroethylene (Grimberg et al., 2000).

Key advances include insights into the microbial community structure of MBfRs, applying the MBfR to novel contaminants, providing a better understanding of biofilm morphology and its effects on MBfR behavior, and the development of methane-based MBfR applications. These advances are likely to further the development of the MBfR for environmental applications, such as energy-efficient wastewater treatment and advanced water treatment.

Despite the many advantages of the MBfR process, more research is needed to determine the optimal membrane materials, diameter, packing density, and bulk

liquid mixing strategy. A key need is for effective management of biofilm growth, as excessive growth reduces reactor efficiency.

1.4 MEMBRANE AERATED BIOFILM REACTOR TECHNOLOGY: MABR

1.4.1 Introduction

The membrane aerated biofilm reactor (MABR) is based on gas-permeable membranes that deliver pure oxygen or air to biofilms naturally forming on the membrane outer surface (Nerenberg, 2016). The concept of MABR was proposed to comply with two different research needs. On the one hand, experts in membrane technology were making efforts to develop the potential of membranes for bubbleless membrane aeration of activated sludge (Weiss et al., 1996). But they found out that a biological fouling formed on the surface of the membrane, greatly increased the resistance to gas transfer consuming the oxygen even before it could reach the bulk liquid. Timberlake et al., (1988) were the first to transform this disadvantage into a possibility to exploit the activity of such a biofilm. On the other hand, some researchers working on biofilm processes for wastewater treatment were searching for better support materials, therefore studying the behavior of biofilms growing on membranes, either supplied with oxygen (Eguía, 1991; Eguía et al., 1993) or air (Vidart et al., 1993).

In recent years, given the water quality and increasing need for cost-effective, sustainable processes, the MABR has received an intense interest in the research community. Also several companies have developed commercial MABRs applications, including Oxymem, GE, Emefcy, and BioGill, spurring further interest.

The use of membranes as a mean to transfer oxygen to the microorganisms and the way the different substrates penetrates in a biofilm, attached to a gas-permeable membrane, configure the most important features of a MABR: unique biofilm stratification and exceptional oxygen transfer characteristics.

1.4.2 Biofilms on gas permeable membranes

MABRs (and MBfRs) behave differently than conventional biofilms, as counter-diffusional biofilms form on the membrane surface. With co-diffusional biofilms, the most metabolic active region is typically the exterior, near the bulk liquid, where the electron donor and acceptor concentrations are at their highest

concentrations (Figure 1-8 a). Depending on the relative concentrations of oxygen and substrate in the internal layers of the biofilm, the anaerobic degradation, nitrification, or anaerobic digestion of the biofilm will take place. In MABR counter-diffusional biofilms, by contrast, the dissolved oxygen diffuses into the biofilm from the membrane, while the substrate to be degraded diffuses from the bulk liquid (from the opposite side) (Figure 1-8 b). Thus, the most active zone is typically located inside the biofilm. This counter diffusion of donor and acceptor leads to unique behavior, including three key differences: development of unique microbial community structures, greater sensitivity to biofilm accumulation, and reduced susceptibility to liquid diffusion layer (LDL) resistance (Nerenberg, 2016).

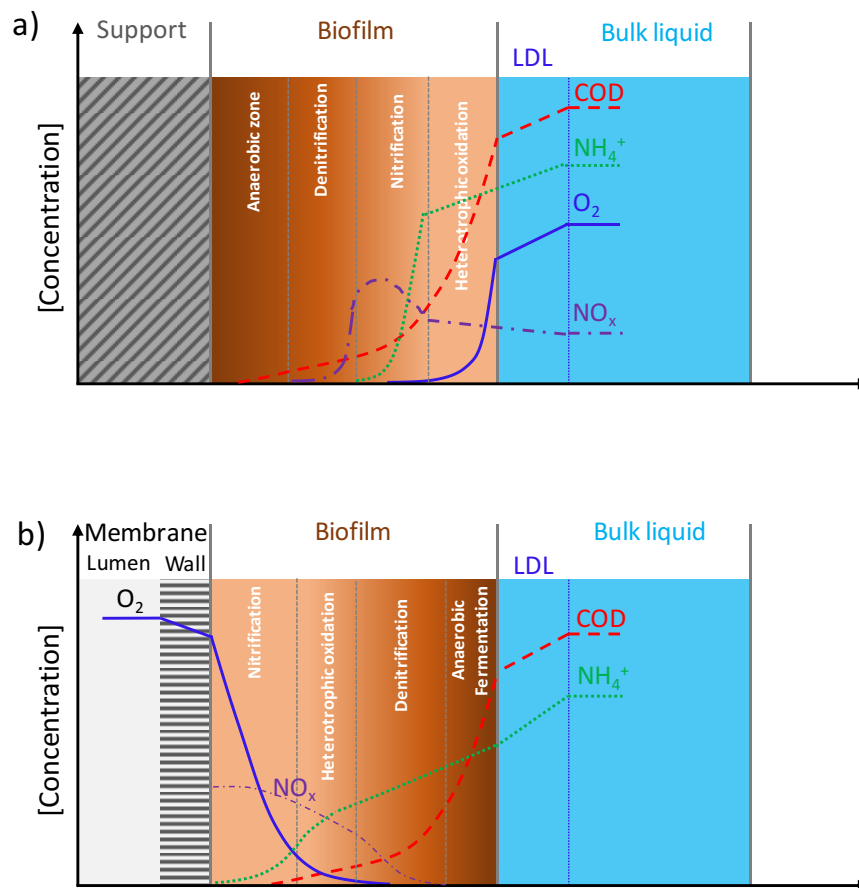


Figure 1-8 Theoretical zoning of a thick biofilm on (a) conventional co-diffusional biofilm and (b) membrane aerated counter-diffusional biofilm.

Development of unique microbial community structures

In a membrane aerated biofilm (MAB), nitrifying microorganisms will tend to grow near the membrane, where oxygen concentration is high, concentration of organic carbonaceous material may be low (because of the oxidation occurring in the external layers) and ammoniacal nitrogen may be available. In the intermediate layers reached by the dissolved oxygen, there may be a high availability of carbon to be used by heterotrophic organisms for the detriment of the nitrifying organisms. If the oxygen is depleted before reaching the biofilm-water interface, closer to the bulk liquid, there will be a zone with supply of nitrates from inside the biofilm and supply of carbon from outside, thus producing the anoxic ideal conditions for denitrification. Finally, if the thickness of the biofilm allows for it and the bulk liquid is anoxic, suitable conditions for the development of anaerobic bacteria could be produced in the more external layer (Esteban et al., 2012) (Figure 1-8 b). Thus, simultaneous organic carbon removal, nitrification and denitrification are possible in a MABR (Timberlake et al., 1988; Osa et al., 1997; Terada et al., 2003; Semmens et al., 2003; Downing and Nerenberg, 2008a). This theoretical stratification has been confirmed through modeling (Semmens and Essila, 2001; Shanahan and Semmens, 2004) and by the use of electronic microscopy, bacterial community identification and microelectrodes profiling (De Beer and Schramm, 1999; Walter et al., 2005; Downing and Nerenberg, 2008a).

Greater sensitivity to biofilm accumulation

In conventional biofilms, the initial contaminant transformation fluxes are low, due to low biofilm thicknesses. The fluxes then increase as the biofilm thickness increases, until the biofilm growth is balanced by decay and detachment. In counter-diffusional biofilms, fluxes increase up to a point, but then decrease as the thickness increase further. This is because the donor and acceptor counter diffusion. The biofilm interior has low activity due to limitation of one substrate, while the exterior has low rates due to limitation of the other (Nerenberg, 2006). Thus, careful management of biofilm accumulation is needed to maintain high fluxes (Martin and Nerenberg, 2012).

Lower susceptibility to LDL resistance

In a conventional biofilm, the LDL limits the substrate fluxes into the biofilm. As the biofilm thickness and flux increase, the LDL provides mass transfer resistance and limits further biofilm growth. Higher bulk substrate concentrations are needed to overcome the LDL resistance. By contrast, in a counter-diffusional biofilm, the LDL provides a barrier to loss of the internal substrate to the bulk liquid (Nerenberg,

2006). Thus, as long as substrate from the bulk is present at non-rate limiting concentrations, the LDL will not limit, and may actually enhance, microbial activity (Martin and Nerenberg, 2012).

1.4.3 Oxygen transfer characteristics

There are two main characteristics associated with the use of membranes to transfer oxygen to a biomass attached on its surface: flexibility in oxygen delivery and potential for energy savings. Both are explained below.

Flexibility in oxygen delivery

Considering that gas and liquid phases are physically separated, membrane gas transfer allows for a better control in gas transfer rate than conventional aeration. The rate of oxygen transfer is given by Equation 1.

$$J_{O_2} = A \cdot K \cdot (C^* - C) \quad \text{Eq. 1-1}$$

where:

J_{O_2} = rate of oxygen transfer (g s^{-1})

K = mass transfer coefficient (m s^{-1})

A = bubbles/fiber surface area (m^2)

C^* = water phase concentration at equilibrium with the oxygen pressure inside the bubble/fiber (g m^{-3})

C = concentration of oxygen in water (g m^{-3})

The improvement in oxygen delivery control is given by the following features:

- In a membrane, the mass transfer coefficient only depends on membrane characteristics and oxygen diffusivity, whereas for bubble oxygenation we have to take into consideration the liquid hydrodynamics (which determines the LDL thickness).
- Surface area is constant in membrane-based aeration (it is the membrane surface itself), whilst for bubbles it is sensitive to atmospheric and hydrostatic factors.

- In membranes, it is possible to select the kind of gas (air or pure oxygen) and adjust the feed pressure (in closed-end configurations), which provides a high flexibility in design and response to variations in oxygen demand.

Energy savings

It is estimated that the cost of aeration in a wastewater treatment plant can account for 50-90% of the total energy costs (WPCF, 1988). Therefore, numerous efforts have been made to optimize aeration in order to minimize the operational costs of treatment. MABRs have a great potential for energy savings. Studies suggest that the MABR can be up to 85% more energy efficient than conventional activated sludge process (Aybar et al., 2014; Syron et al., 2015). Two reasons affect the reduction in energy consumption: high oxygen utilization efficiencies and low head losses compared to conventional activated sludge treatment. These are briefly explained in the next two subsections.

Oxygen transfer efficiency (OTE)

In the MABR process some steps in oxygen transfer from bulk gas to bacteria, such as the solubilization of oxygen in water and the overcoming of LDL resistance are avoided, improving the overall oxygen transfer efficiency (OTE). As a result, oxygen transfer rate (OTR) can be very high. In a MABR, no LDL exists between the gas supplying membrane and the biofilm. The LDL, located at the outer edge of the biofilm, helps to resist the loss of gas to the bulk liquid, thus contributing to higher oxygen utilization efficiencies (Martin and Nerenberg, 2012). OTEs up to 100 % can be obtained in closed-end operated MABRs, as all the oxygen supplied to the membranes is delivered to the biofilm (Syron and Casey, 2008a; Martin and Nerenberg, 2012). In conventional bubble aeration (Metcalf and Eddy, 2003), oxygen transfer rates are rather lower, ranging from 12 to 37 % (for a depth of 4.5 m).

One of the restrictions in bubble aeration OTR is the maximum value of C^* (see Eq. 1-1), around 8 and 40 mg/l when air or oxygen gas is used, respectively. Membrane transfer allows for the increase of gas pressure and hence C^* and OTRs.

An interesting point, highlighted by several authors, is that the observed OTR becomes usually much higher in the presence versus the absence of biofilm (Casey et al., 2000; Osa et al., 1997; Jácome et al., 2006; Shanahan and Semmens, 2006). This result is not obvious, as the biofilm substitute the LDL and imposes a diffusional resistance. An explanation could be that biochemical demand for

dissolved oxygen increases the concentration gradient in the biofilm, which thereby increases the driving force for oxygen supply. This phenomenon, can overcome in certain conditions, the increase in mass transfer resistance caused by the biofilm itself (Semmens and Essila, 2001). Other authors justify it by the presence of convective transport despite diffusive transport in some zones of the biofilm, either by the formation of channels (Emanuelsson and Livingston, 2004; De Beer et al., 1997) or by chemotaxis, the turbulence created by motile organisms inside the biofilm (“biologically enhanced oxygen transfer”, Jácome et al., 2006).

In addition, the mode of gas supply can lead to special behavior. Gas can be supplied via HF membranes, which can be operated in closed-end mode, where the distal end of the membrane is sealed, or in open-end mode, where the distal end is open and the supply gas is continuously vented. Closed-ends are required for combustible or expensive gases (i.e. H_2 , CH_4 , or O_2). As mentioned above, closed-end membranes can allow up to 100% in OTEs. However, close ended membranes typically suffer from gas back-diffusion, where N_2 and other dissolved gases diffuse back into the membrane lumen diluting the supply gas (Schaffer et al., 1960; Ahmed and Semmens, 1992). These gases concentrate at the distal end of the membrane, decreasing its effectiveness and leading to lower average OTRs (Figure 1-9) compared to open-end operation. Another disadvantage is that water vapour may also accumulate and condense at the distal ends of close ended membranes (Côte et al., 1988; Côte et al., 1989; Fang et al., 2004).

To minimize the deadening effect, HF membranes can be operated with open ends, allowing a relatively high gas velocity through the membrane. When the advective mass transfer into the membrane is high relative to mass transfer across the membrane, the gas concentration remains relatively constant along the membrane, allowing for high OTRs along the entire membrane (Figure 1-9 b). Open ended operation, however, has several disadvantages. Some gas is vented from the membrane and lost. This can be a concern with expensive gases, or where stripping of dissolved volatile compounds is to be avoided. Also, greater frictional pressure losses occur within the membrane. Finally, the increased gas flow leads to greater energy requirements. Gas profiles and velocities for closed and open-end operation are illustrated schematically in Figure 1-9.

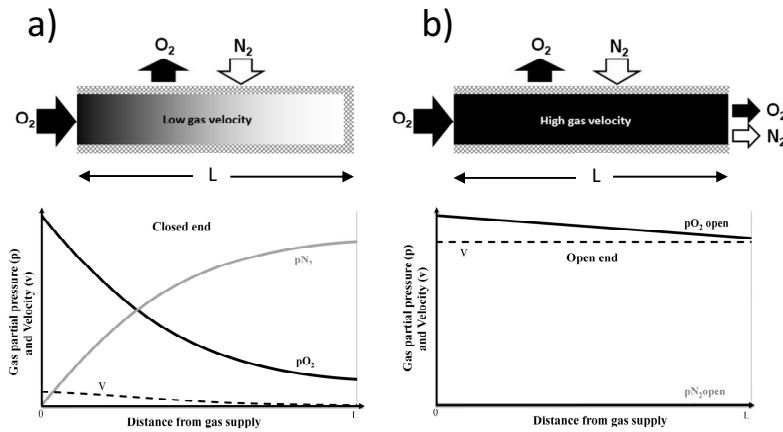


Figure 1-9 Typical behavior of HF membranes pressurized with pure O₂ transferring to liquid containing dissolved N₂ in: (a) Open-end operation, and (b) closed-end operation.

In Figure 1-9 the top panels show a schematic of the membrane, while the lower panels show typical oxygen and nitrogen partial pressures (PO₂ and PN₂) and gas velocities (v) along the length of the membranes.

Head losses

Head losses (ΔP) are highly reduced in MABR (Esteban-García et al., 2012). In conventional bubble aeration, frictional losses (Δh_{fric}) through the piping, hydrostatic pressure of the water and backpressure required to blow bubbles through the diffuser device must be taken into account. The tank depth (h) is the main parameter affecting the head losses, which have an order of magnitude of meters. Conventional bubble aeration typically suffers energy losses of 65-80%. In a MABR, it is required only the sufficient pressure to overcome the frictional losses (Δh_{fric}) across the fiber length, which have an order of magnitude of centimeters (Figure 1-10). If the reactor works in a flow-through mode, a simple blower can be used instead of a compressor (Semmens, 2008).

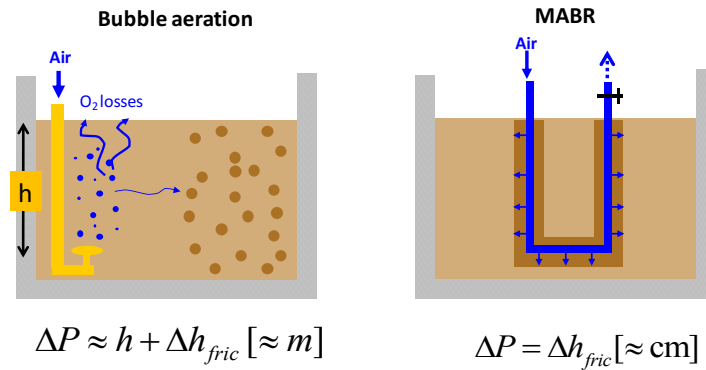


Figure 1-10 Comparison of head losses between conventional bubble aeration and MABR systems.

To estimate aeration costs for a conventional activated sludge (CAS) compared to a MABR, the following considerations must be analyzed. First, the power requirement of a blower can be calculated as in Equation 1- 2 (Tchobanoglous et al., 2003):

$$P_w = \frac{wRT}{29.7ne} \left[\left(\frac{p_2}{p_1} \right)^{0.283} - 1 \right] \quad \text{Eq. 1-2}$$

where:

P_w = power requirement of the blower [kW]

w = weight of air flow [kg s^{-1}]

R = gas constant for air [$8.314 \text{ kJ kmol}^{-1} \text{ K}^{-1}$]

T = absolute inlet temperature [K]

p_1 = absolute inlet pressure [atm]

p_2 = absolute outlet pressure [atm] (inlet + head loss)

$n = 0.283$ (for air)

e = blower efficiency (usual range 0.70 - 0.90)

The weight of air flow is equal to the required air flow divided by the oxygen transfer efficiency (OTE) of the aeration system.

In CAS, the tank depth is the main parameter affecting the amount of required energy: the more depth means an increased OTE, but on the other side, the head loss increases too.

In a MABR the power requirement is reduced by acting in two terms: as it has already been stated, OTE can be highly improved (diminishing w) and, on the other side, head losses (and so the term p_2) are significantly reduced (Esteban-García et al., 2012). Thus, it can be concluded that the MABR is the latest evolution of wastewater aeration technology (Figure 1-11).



Figure 1-11 Evolution in wastewater aeration technology (adapted from www. emefcy.com).

1.4.4 Potential applications

Some of the advantages of MABRs have been exploited in the following applications, classified according to the pollutant type.

High oxygen demanding wastewaters

In conventional biofilms, the low solubility of oxygen in water and diffusional limitations restrict the available OTR. The possibility of using pure oxygen in MABR,

coupled to the high OTE achievable, offers a potential of applying MABR as an aerobic technology for high strength or high rate wastewater treatment (a niche not normally associated with biofilm reactors) (Brindle et al., 1999). Another approach consists of introducing membranes in anaerobic reactors, with the objective of nitrifying and enhancing COD removal in the biofilm (Kappell et al., 2005).

Nutrients removal

Two MABR characteristics make them interesting for nitrogen removal: the possibility of simultaneous nitrification, denitrification and COD removal in a single biofilm, and their ability to create an appropriate environment for nitrifying bacteria (protecting them from shock loads, toxics and detachment inside the biofilm, and lowering carbon concentration to be able to compete with heterotrophs). Different strategies for nitrogen removal have been applied:

- Concurrent COD oxidation and total nitrogen removal (nitrification and denitrification) when oxygen is supplied via membrane and ammonia and COD via the bulk liquid (Figure 1-8 b). (Timberlake et al., 1988; Pankhania et al., 1994; Semmens et al., 2003; Downing and Nerenberg, 2008a).
- Decoupled nitrification and denitrification: systems utilizing biofilm on the membrane for nitrification and suspended biomass (hybrid system, Downing and Nerenberg, 2008b) or plastic media (Landes et al., 2011) for organic removal and denitrification.
- Autotrophic aerobic nitrification, for the treatment of wastewaters with very low C/N ratios, considering ammonium as a high oxygen demanding substrate (Brindle et al., 1998; Suzuki et al., 2000; Lackner et al., 2008; Pellicer-Nàcher et al., 2010).
- Aerobic nitrification in one reactor and autotrophic denitrification in a second reactor with a membrane delivering H_2 to the attached biofilm (Shin et al., 2005).
- Anaerobic ammonia oxidation, where ammonium and nitrite serve as donor and acceptor for specialized anammox bacteria. Nitrification is fostered in the aerobic inner regions of the biofilm near the membrane interface, while anaerobic, ammonia oxidation occurs on the outer edges of the biofilm (Terada et al., 2007). Pellicer-Nàcher et al., (2010) found that sequential aeration in a MABR enhances nitrite formation and improves anammox activity.

Biological phosphorus removal has also been attempted. In one configuration (Castillo et al., 1999), a sequential batch reactor was fed alternatively with O₂ (to provide aerobic-anoxic conditions for phosphate accumulation and nitrification-denitrification) and N₂ (to shift to anaerobic conditions for the phosphate release). Another approach, also in sequential batch mode, was to use nitrifying biofilm on permeable membranes and denitrifying polyphosphate-accumulating organisms in the bulk liquid (Terada et al., 2006).

Emerging applications for MABRs

The MABR is a viable option for specialized contaminant removal due to its ability to support slow-growing, xenobiotic-degrading bacteria. Researchers have used the MABR to treat organic xenobiotics such as benzene, toluene, ethylbenzene, and xylene compounds, chlorinated solvents, and chlorophenols (Syron and Casey, 2008a). Li et al., (2008) achieved concurrent nitrification, denitrification, and acetonitrile degradation, and recently researchers have tested the degradation of pharmaceuticals (Kim et al., 2010).

Other interesting, potential applications include the use of MABRs as the base for microbial fuel cells (Butler and Nerenberg, 2010) and the oxidation of unwanted sulfide to elemental sulfur (Sahinkaya et al., 2011).

1.4.5 MABR configurations and operating parameters

Multiple configurations have been investigated in MABR references (the most frequent are summarized in Table 1-1). Most experiments have been carried out with hollow or tubular fiber due to their versatility, ability to provide high specific surface areas, and superior biomass retention (Martin and Nerenberg, 2012).

MABRs have been tested using microporous, dense, and composite membranes with outer diameters ranging from less than 100 µm to more than one centimeter. Microporous membranes provide the highest gas transfer rates, since diffusion through gas-filled pores is significantly greater than through dense materials. However, microporous membranes must be operated at lower intramembrane gas pressures to avoid bubbling and the consequent loss of gas and biofilm. Porous materials are also more susceptible to clogging or wetting (Semmens, 2005). Dense membranes remain free of clogging or wetting problems and their higher diffusive resistance can be overcome by higher intramembrane gas pressures. The relatively high permeability of silicone has made it a popular dense membrane choice (Casey et al., 1999; Wang et al., 2009).

Composite (essentially microporous membranes with a thin dense layer) membranes promote high gas transfer and maintain a high bubble-point (high pressures can be applied). This is achieved through the addition of a thin, dense layer to a microporous membrane layer. The dense layer may be “sandwiched” between porous membrane layers, as in Mitsubishi Rayon MHF200 fiber (Ahmed et al., 2004). Unfortunately, composite membranes tend to be notably more expensive than conventional membranes.

Recently, some membranes have been specifically designed for MABR applications. Like GE water (Canada) Oxymem (Ireland) and Emefcy (Israel). Both GE and Oxymem have chosen to use dense (non-porous) membranes. GE developed their Zeelung product, which consist in polymethylpentane HF membranes, with an outer diameter of 50-70 μm and a very thin membrane wall of 5-20 μm , distributed longitudinally around the circumference of a yarn-based reinforcing cord. Multiple cords are potted into top and bottom headers to create a module. OxyMem have developed a polydimethylsiloxane membrane for use in their MABR, with an outer diameter of around 500 μm and a wall thickness of 100 μm . The membranes are vertically arranged in their commercial modules in bunches of 400. Both Zeelung and OxyMem technologies target retrofitting existing plants (centralized treatment plants). A decentralized wastewater treatment based in MABR technology has been developed by Emefcy company: The Spiral Aerobic Biofilm Reactor. This technology uses a spirally wound sleeve with an internal air-side spacer, through which low pressure air is blown, and an external water side spacer between wraps of the spiral. The spiral is submerged in a tank, to which wastewater is fed continuously and effluent is discharged by overflow.

Gas supply strategy is a very important feature in MABR operation. Pure oxygen (more expensive but more efficient too) or air (cheap but less efficient) can be supplied. The selected gas has also influence on intra-membrane oxygen concentration, an important factor in MABR behavior.

Gas supply modes are closed-end, open-end (flow-through) and auto-aerated. As explained above (in oxygen transfer characteristics section), in closed-end mode, maximum OTE can be achieved but problems with the accumulation of gases produced by back-diffusion effect and water condensation may appear. Just the opposite occurs in open-end MABRs. Intermediate solutions must be developed to maximize both OTEs and OTRs (such as periodic gas venting or controlled open-end). Finally, an auto-aerated MABR have also been evaluated (Osa et al., 1997; Jácome et al., 2006). In this configuration, both ends of the hollow fiber

membranes are connected with the atmospheric air, so oxygen passive transport along and across the fiber occur spontaneously.

Table 1-1 Summary of MABR configurations investigated (adapted from Esteban-García et al., 2012).

Membrane	Gas supply	Hydraulic flux
<i>Material</i>	<i>Type</i>	<i>Mode</i>
Microporous	Pure oxygen	Completely mixed
Dense	Air	Plug flow
Composite	<i>Mode</i>	Sequential batch
<i>Geometry</i>	Closed or sealed-end	
Flat sheet	Open or flow-through	
Tubular	Autoaerated	
Hollow fiber		
Sheets of stitched hollow fibers		
<i>Configuration</i>		
Plate and frame		
Spiral wound		
Fiber bundle		

1.4.6 MABR mathematical models

Considering the complexity associated with MABRs operation, a few models of permeable-supported biofilms have been developed (Semmens and Essila, 2001; Matsumoto et al., 2007; Downing and Nerenberg, 2008b; Shanahan and Semmens, 2015). These models confirm the theoretical stratification proposed in Figure 1-8.

Some modeling efforts have also being made as a tool to select the most appropriate configuration (Casey, 2007; Syron and Casey, 2008b).

Finally, considering that intramembrane gas composition also affects the biofilm behavior, implementing the gas dynamics in the models is also needed. Gas-back diffusion has been studied previously for clean, membranes (Ahmed and Semmens, 1992; Fang et al., 2004), but little has been done for biofilm supporting membranes. Further research is needed to explore the effect of biofilms on back-diffusion in closed-end membranes, as well as the effects of partially opened membranes or transient effects of opening and closing membranes. Optimal gas supply strategies should be explored for these approaches.

1.4.7 Economical aspects

When comparing MABR to conventional technologies, three potential sources of costs savings must be considered:

- Reduction in space requirement: COD removal, nitrification and denitrification can occur in the same tank in a MABR in contrast to CAS. Besides, biofilm systems can sustain very high biomass concentration, which can be fed by the high oxygen transfer capacity of membranes.
- Less sludge processing and disposal costs: it is expected that MABR systems produces less excess sludge than CAS.
- Energy cost savings in aeration: as stated in previous section, this is one of the main characteristics of a MABR, and the most important factor in costs savings.

On the other side, membrane price is the major cost item in MABR systems.

Casey et al., (2008) took these conditions into account for a 10000 m³/d urban wastewater treatment plant. They compared CAS and MABR from an economical point of view, concluding that especially membrane and electricity costs, too, were the critical parameters in defining their relative feasibility. In this example, MABR was economically advantageous with membrane costs below 40 €/m² and electricity costs higher than 0.1 €/kWh. Aybar et al., (2014) predicted energy and cost savings obtained by replacing fine-bubble diffusers in CAS with air-supplying, hollow fiber membrane modules. Results showed reductions in power requirements as high as 86%. The decrease mainly resulted from the dramatically lower air flows for the MABR, resulting from its higher OTEs. Savings up to 180 €/1000 m³ of treated water were predicted. In this study, costs savings were also highly sensitive to the costs of the membrane modules and electrical power, as well as to the membrane life. To demonstrate the low energy treatment capacity of the MABR, OxyMem demonstration plants have been installed and tested in several WWTP. Results derived from these case studies showed that when a WWTP with a size of 10000 PE and flow capacity of 1500 m³/day was taken as an example, OxyMem MABR delivered supreme water quality by taking up only 104m² in comparison to 375m² footprint required to have a CAS plant operating with a similar treatment capacity. According to the operational costs of the municipal 10000 PE WWTP, OxyMem MABR required only a fifth of the energy used by the CAS installation. This resulted, taken into account price of the energy set at 0.1 €/kWh, savings of 14000 € per year. Footprint and energy consumption comparison for a 50% additional capacity by upgrading with CAS or retrofitting with OxyMem

MABR for a 10000 PE WWTP, showed that OxyMem MABR required no reactor footprint and resulted in 7049 € savings per year.

Not only commercial membrane costs are decreasing now, but new specialty membranes designed for MABR applications (i.e. Zeelung, OxyMem) are expected to cost significantly less. This, together with increases in energy costs, will continue to make the MABR a more attractive and cost-effective technology.

1.4.8 Key research and development needs

Past studies have clearly shown that the MABR offers valuable advantages over conventional biofilm and activated sludge processes. However concerns over performance consistency and cost effectiveness are especially important.

To perform consistently the MABR must maintain active biofilms that cover the membranes without fouling. This means keeping the biofilm around its optimum thicknesses. As biomass control is challenging, an appropriate regime of mechanical shear or gas sparging for detachment or the combination of MABR technology with AS may be adequate. The effect of biofilm detachment on microbial community structure is a topic that has great implication for multispecies MABRs and should be studied in greater depth together with biofilm mechanical properties.

As for cost effectiveness, membrane capital costs and durability are by far the largest concerns (Martin and Nerenberg, 2012). Research must continue addressing the ideal membrane material and design for specific applications, not only in terms of performance, but also with regards to cost-effectiveness and manufacturing feasibility.

Regarding membrane performance, gas back-diffusion needs to be studied in greater depth. There have been few investigations for clean membranes despite its potential impact in MABR performance. Furthermore, there are no systematic studies of gas-back diffusion in membranes supporting a biofilm. This is especially complex, as gas back-diffusion affects biofilm activity, and biofilm activity impacts gases profiles along the membranes. Strategies to mitigate the back-diffusion detrimental effect should be addressed.

1.4.9 Conclusions

Processes based on the growth of biofilms on gas permeable membranes have shown promising potential for a number of wastewater treatment applications. Membrane aerated biofilm reactors (MABRs), in particular, exhibit two important features: unique biofilm stratification and exceptional oxygen transfer characteristics. The areas where MABR can find greatest application are nitrogen removal, high-rate treatment, high-strength COD removal and treatment of VOCs.

Moreover, the MABR technology is approaching maturity and is now available at commercial scale. A surge in research, both fundamental and applied, has been seen globally in recent years. This is leading to a better understanding of the special behavior of the MABR, as well as new applications. More basic applied research on the membranes life expectancy and costs will improve the MABR technology as a means of providing a cost-effective, sustainable solution for water and wastewater treatment.

The basis of the research presented in this Thesis, is to provide a more thorough understanding of MABR technologies, addressing some of the MABR performance main limitations like: the proper control of biofilm thickness for total nitrogen removal, maintaining optimum biomass distribution by a hybrid membrane aerated biofilm reactor (HMABR) (Chapter 3); gas back-diffusion detrimental effects by exploring gas supply strategies to maximize both OTEs and OTRs in MABRs (Chapter 4) and understand the biofilm effect in back-diffusion process to optimize the potential strategies that will enhance MABR operation (Chapter 5).

1.5 REFERENCES

- Adav, S. S., Lee, D. J., Show, K. Y., Tay, J. H., 2008. Aerobic granular sludge: Recent advances. *Biotechnol. Adv.* 26, 411-423.
- Adham, S., Gillogly, T., Nerenberg, R., Lehman, G., Rittmann, B. E., 2004. Membrane Biofilm Reactor Process for Nitrate and Perchlorate Removal. *Water Res. Found.* Denver, Colorado.
- Ahmed, T., Semmens, M.J., 1992. The Use of Independently Sealed Microporous Hollow Fiber Membranes for Oxygenation of Water - Model Development. *J. Memb. Sci.* 69, 11–20.
- Andern, E., Lockett, W.T., 1994. Microorganisms for Waste Treatment. *J.Soc. Chem. Ind.* 33, 1122-1124.
- Aybar, M., Pizarro, G., Boltz, J.P., Downing, L., Nerenberg, R., 2014. Energy-efficient wastewater treatment via the air-based, hybrid membrane biofilm reactor (hybrid MfBR). *Water Sci. Technol.* 69, 1735–1741.
- Barkman, E., 2010. Moving bed bioreactor technology for secondary treatment of wastewater. Moltoni Infra Tech Pty. Ltd., Perth.
- Barwal, A., Chaudhary, R., 2014. To study the performance of biocarriers in moving bed biofilm reactor (MBBR) technology and kinetics of biofilm for retrofitting the existing aerobic treatment systems: A review. *Rev. Environ. Sci. and Biotechnol.* 13, 285-299.
- Bishop, P. L., Zhang, T. C., and Fu, Y. C., 1995. Effect of biofilm structure, microbial distribution and mass distribution on biodegradation processes. *Water Sci. Technol.* 31, 197–203.
- Boltz, J. P., Smets, B. F., Rittmann, B. E., van Loosdrecht, M. C. M., Morgenroth, E., Daigger, G. T., 2017. From biofilm ecology to reactors: a focused review. *Water Sci. Technol.* 75, 1753-1760.
- Brindle, K., Stephenson, T., 1996. The Application of Membrane Biological Reactors for the Treatment of Wastewaters. *Biotechnol. Bioeng.* 49, 601–610.
- Brindle, K., Stephenson, T., Semmens, M.J., 1998. Nitrification and oxygen utilisation in a membrane aeration bioreactor. *J. Memb. Sci.* 144, 197–209.
- Brindle, K., Stephenson, T., Semmens, M.J., 1999. Pilot-plant treatment of a high-strength brewery wastewater using a membrane-aeration bioreactor. *Water Environ. Res.* 71, 1197–1204.

- Butler, C.S., Nerenberg, R., 2010. Performance and microbial ecology of air-cathode microbial fuel cells with layered electrode assemblies. *Appl. Microbiol. Biotechnol.* 86, 1399–1408.
- Casey, E., Glennon, B., Hamer, G., 1999. Review of Membrane Aerated Biofilm Reactors. *Resour. Conserv. Recycl.* 27, 203–215.
- Casey, E., Glennon, B., Hamer, G., 2000. Biofilm development in a membrane-aerated biofilm reactor: Effect of flow velocity on performance. *Biotechnol. Bioeng.* 67, 476–486.
- Casey E., 2007. Simulation studies of process scale membrane aerated biofilm reactor configurations. Proceedings of the 4th International Water Association Membranes Conference. 15-17 of May. Harrogate, UK.
- Casey E., Syron, E., Shanahan, J., Semmens, M., 2008. Comparative economic analysis of full scale MABR configurations. North American Membrane Research Conference, University of Massachusetts, Amherst, USA.
- Castillo, P., 1999. Biological Phosphorus Removal Using a Biofilm membrane reactor: Operation at High Organic Loading Rates. *Water Sci. Technol.* 40, 321-329.
- Costerton, J.W., Lewandowski, Z., Caldwell, D.E., Korber, D.R., Lappin-Scott, H.M., 1995. Microbial biofilms. *Annu. Rev. Microbiol.* 49, 711–45.
- De Beer, D., Schramm, A., Santegoeds, C.M., Kuhl, M., 1997. A nitrite microsensor for profiling environmental biofilms. *Appl. Environ. Microbiol.* 63, 973–977.
- De Beer, D., Schramm, A., 1999. Micro-environments and mass transfer phenomena in biofilms studied with microsensors. *Water Sci. Technol.* 39, 173–178.
- de Kreuk, M.K., van Loosdrecht, M.C.M., 2004. Selection of slow growing organisms as a means for improving aerobic granular sludge stability. *Water Sci. Technol.* 49, 9–17.
- de Kreuk, M.K., Kishida, N., van Loosdrecht, M.C.M., 2007. Aerobic granular sludge-state of the art. *Water Sci. Technol.* 55, 75–81.
- Downing, L.S., Nerenberg, R., 2008a. Effect of bulk liquid BOD concentration on activity and microbial community structure of a nitrifying, membrane-aerated biofilm. *Appl. Microbiol. Biotechnol.* 81, 153–162.
- Downing, L.S., Nerenberg, R., 2008b. Total nitrogen removal in a hybrid, membrane-aerated activated sludge process. *Water Res.* 42, 3697–3708.

Eguía, E. 1991. Desarrollo de la biopelícula en medio soporte permeable. Doctoral Thesis. University of Cantabria. Santander.

Eguía, E., Vidart, T., Jácome, A., Tejero, I., 1993. Application of a permeable support biofilm reactor (PSBR) to ships. VI-th Congress of the International Maritime Association of the Mediterranean (IMAM). Varna. Bulgaria. 191-196.

Emanuelsson, E.A.C., Livingston, A.G., 2004. Overcoming oxygen limitations in membrane-attached biofilms - Investigation of flux and diffusivity in an anoxic biofilm. *Water Res.* 38, 1530–1541.

Ergas, S. J., Reuss, A. F., 2001. Hydrogenotrophic Denitrification of Drinking Water Using a Hollow Fibre Membrane Bioreactor. *J. Water Supply Res. Technol- AQUA.* 50, 161–171.

Esteban-García, A.L., 2009. Modelización de reactores de biopelícula soportada y oxigenada por membranas (RBSOM) para la depuración de aguas residuales. Doctoral Thesis. University of Cantabria. Santander.

Esteban-García, A.L., Díez, R., Rodríguez, L., Lobo, A., De Florio, L., Pérez-Calleja, P., Tejero, I. 2012. Processes based on the growth of biofilms on gas permeable membranes: Biomembrane reactors. In *Innovative Technologies for Urban Wastewater Treatment Plants (2nd Edition)*, Editors Omil F. and Suárez S., Santiago de Compostela. 117-145. ISBN-13: 9788469339923.

Fang, Y., Clapp, L.W., Hozalski, R.M., Novak, P.J., Semmens, M.J., 2004. Membrane gas transfer under conditions of creeping flow: modeling gas composition effects. *Water Res.* 38, 2489–2498.

Grimberg, S. J., Rury, M. J., Jimenez, K. M., Zander, A. K., 2000. Trinitrophenol Treatment in a Hollow Fiber Membrane Biofilm Reactor. *Water Sci. Technol.* 41, 235–238.

Heijnen, J., van Loosdrecht, M.C.M., 1998. Method for acquiring grain-shaped growth of a microorganism in a reactor. *Biofutur.* 183, 50.

Henze, M., Van Loosdrecht, M.C.M., Ekama, G.A., Brdjanovic, D., 2008. *Biological wastewater treatment : principles, modelling and design.* IWA publishing, London.

Iglesias Esteban, R., Ortega de Miguel, E., 2008. Present and future of wastewater reuse in Spain. *Desalination* 218, 105–119.

Jácome, A., Molina, J., Suarez, J., Tejero, I., 2006. Simultaneous removal of organic matter and nitrogen compounds in autoaerated biofilms. *J. Environ. Eng.* 132, 1255–1263.

Jenkins, A. M., Sanders, D., 2012. Introduction to fixed-film bio-reactors for decentralized wastewater treatment. Contech, Engineered Solutions. Available in: <http://www.conteches.com/knowledge-center/pdh-article-series/introduction-to-fixed-film-bio-reactors.aspx>.

Kappell, A.S., Semmens, M.J., Novak, P.J., Lapara, T.M., 2005. Novel application of oxygen-transferring membranes to improve anaerobic wastewater treatment. *Biotechnol. Bioeng.* 89, 373–380.

Kim, J., Song, I., Lee, S., Kim, P., Oh, H., Park, J., Choung, Y., 2010. Decomposition of pharmaceuticals (sulfamethazine and sulfathiazole) using oxygen-based membrane biofilm reactor. *Desalination* 250, 751–756.

Lackner, S., Terada, A., Smets, B.F., 2008. Heterotrophic activity compromises autotrophic nitrogen removal in membrane-aerated biofilms: Results of a modeling study. *Water Res.* 42, 1102–1112.

Landes, N.C., Jackson, W.A., Morse, A.N., 2011. Limitations Encountered for the Treatment of a Low C:N Waste Using a Modified Membrane-Aerated Biofilm Reactor. *Water Environ. Res.* 83, 128–139.

Lee, K. C., Rittmann, B. E., 2000. A Novel Hollow-Fiber Membrane Biofilm Reactor for Autohydrogenotrophic Denitrification of Drinking Water. *Water Sci. Technol.* 41, 219–226.

Lee, K. C., Rittmann, B. E., 2002. Applying a Novel Autohydrogenotrophic Hollow-Fiber Membrane Biofilm Reactor for Denitrification of Drinking Water. *Water Res.* 36, 2040–2052.

Leiknes, T., Ødegaard, H. 2001. Moving bed biofilm membrane reactor (MBB-MR): characteristics and potentials of a hybrid process design for compact wastewater treatment plants. *Proceedings, Engineering with Membranes, Granada, Spain 2001*

Li, T., Liu, J., Bai, R., 2008. Membrane aerated biofilm reactors: a brief current review. *Recent Pat. Biotechnol.* 2, 88–93.

Liu, Y., Tay, J. H., 2002. The essential role of hydrodynamic shear force in the formation of biofilm and granular sludge. *Water Res.* 36, 1653-1665.

Martin, K.J., Nerenberg, R., 2012. The membrane biofilm reactor (MBfR) for water and wastewater treatment: Principles, applications, and recent developments. *Bioresour. Technol.* 122, 83-94.

Matsumoto, S., Terada, A., Aoi, Y., Tsuneda, S., Alpkvist, E., Picioreanu, C., van Loosdrecht, M.C.M., 2007. Experimental and simulation analysis of community

structure of nitrifying bacteria in a membrane-aerated biofilm. *Water Sci. Technol.* 55, 283–290.

McQuarrie, J. P., Boltz, J. P., 2011. Moving bed biofilm reactor technology: Process applications, design, and performance. *Water Environ. Res.* 83, 560–575.

Molinos-Senante, M., Hernández-Sancho, F., Sala-Garrido, R., 2011. Assessing disproportionate costs to achieve good ecological status of water bodies in a Mediterranean river basin. *J. Environ. Monit.* 13, 2091–101.

Monroe, D., 2007. Looking for chinks in the armor of bacterial biofilms. *PLoS Biol.* 5, 307.

Nerenberg, R., Rittmann, B. E., 2004. Reduction of Oxidized Water Contaminants with a Hydrogen-Based, Hollow-Fiber Membrane Biofilm Reactor. *Water Sci. Technol.* 49, 223–230.

Nerenberg, R., 2016. The membrane-biofilm reactor (MBfR) as a counter-diffusional biofilm process. *Curr. Opin. Biotechnol.* 38, 131–136.

Nicolella, C., van Loosdrecht, M. C. M., Heijnen, S. J., 2000. Particle-Based Biofilm Reactor Technology. *Trends Biotechnol.* 18, 312–320.

O’Toole, G. A., Kaplan, H., and Kolter, R., 2000. Biofilm formation as microbial development. *Annu. Rev. Microbiol.* 54, 49–79.

Ødegaard, H., 2000. Advanced compact wastewater treatment based on coagulation and moving bed biofilm processes. *Water Sci. Technol.* 42, 33–48.

Ødegaard, H., 2006. Innovations in wastewater treatment: The moving bed biofilm process. *Water Sci. Technol.* 53, 17–33.

Okabe, S., Kuroda, H., Watanabe, Y., 1998. Significance of biofilm structure on transport of inert particulates into biofilms. *Water Sci. Technol.* 38, 163–170.

Osa J.J., Eguía E., Vidart T., Jácome A., Lorda I., Amieva J.J., Tejero, I., 1997. Wastewater treatment with biofilm membrane reactors. En: NIGEL. J. HORAN (ed) *Advanced Wastewater Treatment Processes*. University of Leeds. 11-17. ISBN: 0-8522270-2-9.

Pankhania, M., Stephenson, T., Semmens, M.J., 1994. Hollow fibre bioreactor for wastewater treatment using bubbleless membrane aeration. *Water Res.* 28, 2233–2236.

Pellicer-Nàcher, C., Sun, S., Lackner, S., Terada, A., Schreiber, F., Zhou, Q., Smets, B.F., 2010. Sequential aeration of membrane-aerated biofilm reactors for high-rate

autotrophic nitrogen removal: Experimental demonstration. *Environ. Sci. Technol.* 44, 7628–7634.

Rittmann, B. E., 1996. Environmental biotechnology. *Current Opinion in Biotechnol.* 7, 357–365.

Rittman, B.E., 2006. The membrane biofilm reactor: The natural partnership of membranes and biofilm. *Water Sci. Technol.* 53, 219–225.

Rusten, B., Hem, L. J., Ødegaard, H., 1995. Nitrification of municipal wastewater in moving-bed biofilm reactors. *Water Environ. Res.* 67, 75–86.

Rusten B., McCoy M., Proctor R., Siljudalen J. G., 1998. The innovative moving bed biofilm reactor/solids contact re-aeration process for secondary treatment of municipal wastewater. *Water Environ. Res.* 70, 1083–1089.

Rusten, B., Eikebrokk, B., Ulgenes, Y., Lygren, E., 2006. Design and operations of the kaldnes moving bed biofilm reactors. *Aquac. Eng.* 34, 322–331.

Sahinkaya, E., Hasar, H., Kaksonen, A.H., Rittmann, B.E., 2011. Performance of a sulfide-oxidizing, sulfur-producing membrane biofilm reactor treating sulfide-containing bioreactor effluent. *Environ. Sci. Technol.* 45, 4080–4087.

Schaffer, R.B., Ludzack, F.J., Ettinger, M.B.C.F. publication date S., 1960. Sewage Treatment by Oxygenation through Permeable Plastic Films. *J. Water Pollut. Control Fed.* 32, 939–941.

Semmens M.J. and Essila N.J. 2001. Modeling biofilms on gas-permeable supports: flux limitations. *J. Environ. Eng. ASCE.* 127, 126-133.

Semmens, M. J., Dahm, K., Shanahan, J., Christianson, A., 2003. COD and Nitrogen Removal by Biofilms Growing on Gas Permeable Membranes. *Water Resour.* 37, 4343–4350.

Semmens, M.J., 2008. Alternative MBR configurations: using membranes for gas transfer. *Desalination* 231, 236–242.

Shanahan, J.W., Semmens, M.J., 2004. Multipopulation model of membrane-aerated biofilms. *Environ. Sci. Technol.* 38, 3176–3183.

Shanahan, J.W., Semmens, M.J., 2006. Influence of a nitrifying biofilm on local oxygen fluxes across a micro-porous flat sheet membrane. *J. Memb. Sci.* 277, 65–74.

- Shanahan, J.W., Semmens, M.J., 2015. Alkalinity and pH effects on nitrification in a membrane aerated bioreactor: An experimental and model analysis. *Water Res.* 74, 10–22.
- Shin, J.H., Sang, B.I., Chung, Y.C., Choung, Y.K., 2005. The removal of nitrogen using an autotrophic hybrid hollow-fiber membrane biofilm reactor. *Desalination* 183, 447–454.
- Suzuki, Y., Hatano, N., Ito, S., Ikeda, H., 2000. Performance of nitrogen removal and biofilm structure of porous gas permeable membrane reactor. *Water Sci. Technol.* 41, 211–217.
- Syron, E., Casey, E., 2008a. Membrane-Aerated Biofilms for High Rate Biotreatment: Performance Appraisal, Engineering Principles, and Development Requirements. *Environ. Sci. Technol.* 42, 1833–1844.
- Syron, E., Casey, E., 2008b. Model-based comparative performance analysis of membrane aerated biofilm reactor configurations. *Biotechnol. Bioeng.* 99, 1361–1373
- Syron, E., Kelly, H., Casey, E., 2009. Studies on the effect of concentration of a self-inhibitory substrate on biofilm reaction rate under co-diffusion and counter-diffusion configurations. *J. Membr. Sci.* 335, 76–82.
- Syron, E., Semmens, M.J., Casey, E., 2015. Performance analysis of a pilot-scale membrane aerated biofilm reactor for the treatment of landfill leachate. *Chem. Eng. J.* 273, 120–129.
- Tchobanoglous, G., Burton, F.L., Stensel, H.D., 2003. *Wastewater engineering : treatment and reuse*. Metcalf-Eddy, 4th ed. McGraw-Hill, Boston.
- Terada, A., Hibiya, K., Nagai, J., Tsuneda, S., Hirata, A., 2003. Nitrogen removal characteristics and biofilm analysis of a membrane-aerated biofilm reactor applicable to high-strength nitrogenous wastewater treatment. *J. Biosci. Bioeng.* 95, 170–178.
- Terada, A., Yamamoto, T., Igarashi, R., Tsuneda, S., Hirata, A., 2006. Feasibility of a membrane-aerated biofilm reactor to achieve controllable nitrification. *Biochem. Eng. J.* 28, 123–130.
- Terada, A., Lackner, S., Tsuneda, S., Smets, B.F., 2007. Redox-stratification controlled biofilm (ReSCoBi) for completely autotrophic nitrogen removal: The effect of co- versus counter-diffusion on reactor performance. *Biotechnol. Bioeng.* 97, 40–51.

- Timberlake, D., Strand, S., Williamson, K., 1988. Combined Aerobic Heterotrophic Oxidation, Nitrification and Denitrification in a Permeable-Support Biofilm. *Water Res.* 22, 1513–1517.
- van Benthum, W. A. J., Garrido, J. M., Mathijssen, J. P. M., Sunde, J., van Loosdrecht, M. C. M. and Heijnen, J. J. 1997. Nitrogen removal in an intermittently aerated biofilm airlift suspension reactor. *J. Environ. Eng.* 124, 239-248.
- Van Loosdrecht, M. C. M., Heijnen, S. J., 1993. Biofilm bioreactors for waste-water treatment. *Trends in Biotechnol.* 11, 117–121.
- Van Loosdrecht, M. C. M., Eikelboom, D., Gjaltema, A., Mulder, A., Tjihuis, L., Heijnen, J. J., 1995. Biofilm structures. *Water Sci. Technol.* 32, 35–43.
- Verma, M., Brar, S. K., Blais, J. F., Tyagi, R. D., Surampalli, R. Y., 2006. Aerobic biofiltration processes. *Advances in wastewater treatment. Pract. Period. Hazardous, Toxic, Radioact. Waste Manag.* 10, 264–276
- Vidart, T., Eguía, E., Jácome, A., Tejero, I., 1993. Biofilm process with a support permeable to gasses using air. *Proceedings of Second IWAQ International conference on biofilm reactors. Paris, 29, September-1 October.* 921-923.
- Walter, B., Haase, C., Rübiger, N., 2005. Combined nitrification/denitrification in a membrane reactor. *Water Res.* 39, 2781–2788.
- Wang, R., Terada, A., Lackner, S., Smets, B.F., Henze, M., Xia, S., Zhao, J., 2009. Nitritation performance and biofilm development of co- and counter-diffusion biofilm reactors: Modeling and experimental comparison. *Water Res.* 43, 2699–2709.
- Water Environment Federation, W., 2010. *Biofilm Reactors*, MOP 35 ed. McGraw-Hill, New York etc.
- Water Pollution Control Federation and ASCE. 1988. *Aeration. Manual of Practice FD-13.* ASCE Manuals and Reports on Engineering Practice nº 68. Alexandria, Va.: WPCF and ASCE. ISBN: 0-87262-673-3.
- Weiss, P.T., Oakley, B.T., Gulliver, J.S., Semmens, M.J., 1996. Bubbleless fiber aerator for surface waters. *Jour. Environ. Eng.* Vol. 122, 631–639.
- Who, Unicef, 2012. *Progress on Drinking Water and Sanitation: 2012, Update.* Available from <http://www.unicef.org/media/files/JMPreport2012.pdf> (2012)

Wuertz, S., Bishop, P., Wilderer, P. A., 2008. Biofilms in Wastewater Treatment: An Interdisciplinary Approach. Water and Wastewater Practitioner Series: STOWA Report, 424.

Yang, M. C., Cussler, E. L., 1986. Designing Hollow-Fiber Contactors. AIChE J. 32, 1910–1916.

Chapter 2

Materials & methods

OUTLINE

SUMMARY.....	57
2.1 EXPERIMENTAL STUDY.....	57
2.1.1 Liquid phase analytical methods	58
2.1.1.1 Chemical Organic Demand (COD).....	58
2.1.1.2 Ammonia nitrogen (NH ₄ -N)	60
2.1.1.3 Nitrates (NO ₃ -N).....	62
2.1.2 Solid phase analytical methods	63
2.1.2.1 Total (TSS) and Volatile Suspended Solids (VSS).....	63
2.1.3 Biomass characterization.....	65
2.1.3.1 Batch test essays.....	65
2.1.3.2 Biofilm thickness determination.....	66
2.1.4 Dissolved oxygen profiles at membrane surface.....	67
2.2 MATHEMATICAL MODELING	68
2.2.1 HMABR mathematical model	68
2.2.2 Back-diffusion mathematical model for HFMs.....	72
2.2.3 Back-diffusion mathematical model for MABRs.....	74
2.3 REFERENCES.....	74

SUMMARY

The specific materials and methods for defining guidelines for the optimal design and operation of the hybrid membrane aerated biofilm reactor (HMABR), addressing gas-supply strategies that allows high removal rates and high gas transfer efficiencies in a MABR, and evaluating how biofilms affect gas dynamics in MABRs, are reported in Chapters 3, 4 and 5 respectively. All those experimental and modeling methodologies are gathered in this chapter aiming to provide an overall overview of the materials and methods used in this Thesis in a self-combined document, including:

- Methodology used in the experimental phases:
 - Conventional chemical parameters used to characterize the liquid phase, such as COD, forms of nitrogen, etc.
 - Parameters to characterize the solid phases, such as total and volatile suspended solids (TSS and VSS) and biofilm thickness.
 - Techniques for the characterization of the biomass present in the experimental setup, applied to biofilm and suspended biomass.
 - Methodology applied for measuring gas-back diffusion steady state and transient profiles with microsensors.
- General methodology corresponding to mathematical modeling performed in this Thesis:
 - HMABR mathematical model.
 - Back-diffusion mathematical model for hollow fiber membranes (HFM).
 - Back-diffusion mathematical model for MABRs.

Part of the information and figures presented in this chapter are reported again in each specific chapter.

2.1 EXPERIMENTAL STUDY

The experimental set-up of this research thesis was carried out in two configurations. The work presented in chapter 3 was conducted in a bench-scale pilot plant placed at CEIT (University of Navarra, Gipuzkoa, Spain) during a pre-doctoral stage. Chapters 4 and 5 refer to lab-scale reactors, located in the

Environmental Biotechnology Laboratory at University of Notre Dame (UND, Indiana, USA).

The features of the pilot plants used in every part of the work are described in the corresponding chapters.

2.1.1 Liquid phase analytical methods

Different methods were employed during the experimental period for the determination of the conventional parameters of wastewater and sludge. For soluble fraction analysis, samples were previously filtered with a pore size of 0.45 μm in order to remove suspended solids.

2.1.1.1 Chemical Oxygen Demand (COD)

The Chemical Oxygen Demand (COD) is defined as the amount of oxygen required to oxidise the organic matter present in a liquid sample (in this case wastewater) using a strong chemical oxidant (potassium dichromate) in an acid medium.

In the experimentation carried out in chapter 3, the total and soluble Chemical Oxygen Demand (tCOD and sCOD) were determined according to open reflux method 5220 B of the Standard Methods for the Examination of Water and Wastewater (APHA, 2005). During experimentations corresponding to Chapters 4 and 5, COD concentrations were measured using a colorimetric method (Low Range, Hach, Loveland, Colorado), which is USEPA approved for wastewater analyses, and follows the Standard Method 5220 D (APHA, 2005). The difference between total COD and soluble (filtrated) COD is that tCOD is determined using the raw sample, while for sCOD determination, the sample is previously filtered through filters (nitrocellulose-fiber Whatman, Millipore or similar) with a pore size of 0.45 μm .

COD measurement based on open reflux method 5220 B:

Silver sulphate is used as catalyst to improve the oxidation of some organic compounds. After digestion, the remaining unreduced $\text{K}_2\text{Cr}_2\text{O}_7$ is titrated with ferrous ammonium sulphate to determine the amount of $\text{K}_2\text{Cr}_2\text{O}_7$ consumed, being the amount of oxidisable matter calculated in terms of oxygen equivalent.

During the experimental period corresponding to Chapter 3, a modification of method 5220 B (APHA, 2005) was used for COD determination. The modifications that were made with respect to the original method corresponded to the

temperature value (220°C instead of 150°C) as well as the digestion time (10 min instead of 2 hours). The rest of the modifications have been included in Table 2-1.

Table 2-1 Specific data for the COD determination method used in Chapter 3

	Concentration (N)	Volume (mL)
Potassium dichromate solution	0.25	10
Ferrous ammonium sulphate titrant	0.10	
Sulfuric acid + silver sulphate reagent		30
Sample		20

Reagents:

$K_2Cr_2O_7$ digestion solution: 12.25 g of $K_2Cr_2O_7$ (previously dried at 105 °C for 2 hours) are dissolved in a small volume of distilled water. Then, 28 mL of concentrated H_2SO_4 are added. Once cooled, the solution is stirred and 40 g of $HgSO_4$, dissolved in 700 mL of distilled water, are added. The solution is cooled to room temperature and, finally, diluted to 1000 mL.

$H_2SO_4 + Ag_2SO_4$ reagent: 25.3 g of Ag_2SO_4 are added to 2.5 L of concentrated H_2SO_4 . The solution must stand 2 days to dissolve before use.

Ferriin indicator solution: 1.485 g of $C_{18}H_8N_2 \cdot H_2O$ (phenanthroline monohydrate) and 0.695 g of $FeSO_4 \cdot 7H_2O$ are dissolved in 100 mL of distilled water.

Standard ferrous ammonium sulphate titrant (FAS): 39.2 g of $Fe(NH_4)(SO)_2 \cdot 6H_2O$ are dissolved in distilled water. Then, 20 mL of concentrated H_2SO_4 are added and, finally, the solution is cooled and diluted to 1000 mL.

Procedure

The sample (20 mL) was placed in a refluxing tube. 10 mL of digestion solution and 30 mL of sulphuric acid reagent were added in each tube. Then, tubes were introduced in a digester at 220°C. Tubes were removed from the digester 10 minutes after the solutions started to boil. A blank sample using distilled water was refluxed in the same way. This blank acted as "reference", representing the COD of the distilled water. After the digestion period, the mixture was diluted to about twice its volume with distilled water and cooled to room temperature. 2-3 drops of ferriin indicator were added, and the solution was titrated under rapid stirring with FAS titrant (to determine the amount of $K_2Cr_2O_7$ consumed). The end-point is a sharp colour change from blue-green to reddish brown. The COD concentration was calculated with Equation 2-1:

$$COD = \frac{(A - B) \cdot M \cdot 8000}{V_{sample}} \quad \text{Eq. 2-1}$$

Where:

COD: Chemical Oxygen Demand (mg O₂ L⁻¹);

A: mL of FAS consumed by the blank;

B: mL of FAS consumed by the sample;

M: Molarity of FAS and;

V_{sample}: mL of sample used;

8000: Conversion factor.

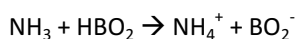
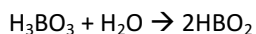
COD measurement according to colorimetric method (5220 C):

During experimentations performed in Chapters 4 and 5, COD was determined using a colorimetric method (Hach, Low Range). This method is based in the same principle as the one described above. The sample (2mL) was heated for 2 hours with sulphuric acid and a strong oxidizing agent (potassium dichromate) in a block digester preheated to 150 °C. Silver is a catalyst, and mercury is used to complex chloride interferences. During digestion, oxidizable organic compounds react, reducing the dichromate ion (Cr₂O₇²⁻) to green chromic ion (Cr³⁺). The amount of Cr⁶⁺ that remained was determined by photometric measurements using a Hach colorimeter (Hach DR/890) at a wavelength of 420 nm. In the same way as in previous described method, a reagent blank was also measured as a reference, subtracting its value from the results of each performed test. Results in mg/L COD were defined as the milligrams of O₂ consumed per liter of sample.

2.1.1.2 Ammonia nitrogen (NH₄-N)

In Chapter 3, ammonia was determined through titrimetric method 4500-NH₃-C (APHA, 2005) after distillation in a Büchi B-315 Distillation Unit.

The method is based in an acidic valoration of a weak base (NH₃) using a strong acid solution (H₂SO₄). A distillation step is required through which ammonia is trapped with boric acid according to reaction:



Reagents

NaOH 8N solution: 320 g NaOH are dissolved in 1000 mL of distilled water

H₃BO₃ solution (4%): 40 g H₃BO₄ are dissolved in a small distilled water volume. Heat is applied to favour the dissolution. Finally, the solution is diluted to 1000 mL of distilled water.

H₂SO₄ 0.02N solution: commercially prepared solution was used.

Indicator (*shiro-tashiro*) pH 4.4-5.8: 50 mL of methyl red indicator (0.2%) and 20 mL of methylene blue (0.2%) are mixed.

Procedure

The sample was buffered at pH 9.5 using sodium hydroxide to decrease hydrolysis of cyanates and organic nitrogen compounds. Then, the sample was distilled at a rate of 6 to 10 mL/min. During this step the ammonia gas formed was removed by distillation. The ammonia gas was then absorbed in a boric acid solution (containing 5-6 drops of the indicator) where it was converted back to ammonium. The distillation removes the ammonia from the sample and leaves substances which may interfere with the analysis behind.

After distillation using boric acid as absorbent solution, ammonia in the distillate was determined by titration with a 0.02N H₂SO₄ solution. At the end point of the titration, the colour of the sample turns to a pale lavender colour. The amount of sulphuric acid used for the colour change is proportional to the amount of ammonium in the sample. A blank titration with distilled water was carried out to apply the necessary corrections to the results. The result is presented as mg NH₄-N L⁻¹ according to Equation 2-2:

$$NH_4-N = \frac{A \cdot N \cdot 14000}{V_{sample}} \quad \text{Eq. 2-2}$$

Where:

NH₄-N: Ammonia nitrogen (mg NH₄-N L⁻¹);

A: mL of H₂SO₄ titrated for the sample;

N: Normality of the acid used for titration;

V_{sample} : mL of sample used;

1400: Conversion factor.

2.1.1.3 Nitrates ($\text{NO}_3\text{-N}$)

Nitrate concentration in wastewater (in Chapter 3) was determined through sodium salicylate method (APHA, 2005), and using chemical test kits (Spectroquant) which is a developed method according to approved USEPA or ISO standards.

Nitrate measurement according to sodium salicylate method:

The method is based on the formation, under acid conditions and heat, of nitronium ions (NO_2^+), which react with salicylate, under alkaline conditions, to form mostly a nitrobenzoic compound of yellow color, allowing for its spectrophotometric detection.

Reagents

Sodium hydroxide solution: The solution is prepared by dissolving 400 g of NaOH in 600 mL of distilled water. 60 g of sodium and potassium tartrate are added to the solution. Then, the solution is transferred into a 1000 mL volumetric flask, and the volume is made with distilled water.

Sodium salicylate solution: 0.5 g of sodium salicylate are dissolved into 100 mL of distilled water.

$\text{NO}_3\text{-N}$ standard solution (100 ppm): 1 mL of chloroform is added to 0.7220 g of potassium nitrate (KNO_3) (previously desiccated at 100°C during 2 h). Then it is dissolved into 1000 mL distilled water.

$\text{NO}_3\text{-N}$ standard solution (10 ppm): 10 mL of $\text{NO}_3\text{-N}$ 100 ppm standard are diluted to 100 mL of distilled water.

Procedure:

A calibration curve was prepared with the nitrate standards, indicating that Lambert-Beer's linearity for the method was 7 mg $\text{NO}_3\text{-N/L}$. Thus, samples estimated to have higher nitrates concentration required to be previously diluted.

An aliquot of previously filtered 5 mL sample was pipetted into a 100 mL beaker. 5 mL of distilled water and 1 mL of the salicylate solution were added. The solution was evaporated to dryness in an oven at 80°C . Then, 2 mL of concentrated sulfuric acid was added. The solution was allowed to stand for 10 minutes,

swirling occasionally to ensure dissolution of all solids. When cold, 15 mL of distilled water were added and swirled to mix. 15 mL containing sodium hydroxide and sodium and potassium tartrate were added. The yellowish color was developed and after 10 minutes, the solution was transferred to the cell of the spectrophotometer (Ultraviolet Spectrophotometer Lambda 3B) and absorbances were measured at 420 nm wavelength. A blank solution, containing all reagents without the sample, and the calibration solutions were treated in the same manner.

Nitrate determination using Spectroquant kits:

Under sulphuric and phosphoric solution the nitrate ions form with 2,6-dimethylphenol (DMP) the 4-nitro-2,6-dimethylphenol compound which is determined photometrically.

Contents of reagent set:

Reagent R1: Contains sulphuric acid 51-80% and phosphoric acid 25-50%.

Reagent R2: Contains 2-propanol 20-50%.

Procedure

4 mL, of R1, 0.5 mL of filtered sample, and 0.5 mL of R2 were placed into a test tube. The solution was mixed by shaking gently. After 10 minutes, the contents of the test tubes were poured into cuvettes and nitrate concentration was determined spectrophotometrically (Spectroquant Nova 60 Merck).

2.1.2 Solid phase analytical methods

2.1.2.1 Total (TSS) and Volatile Suspended Solids (VSS)

Total or Mixed Liquor Suspended Solids (TSS, MLSS) and Volatile or Mixed Liquor Volatile Suspended Solids (VSS, MLVSS) are solids that refer to matter suspended or dissolved in water or wastewater. Both parameters were measured according to the analytical methods 2540D and 2450E of Standard Methods (APHA, 2005).

Procedure:

For MLSS determination, a well-mixed sample is filtered through a weight standard glass-fiber filter disk (Millipore, AP 47 mm of diameter, 1.5 μm of pore size or other filter that gives demonstrably equivalent results) and the residue retained in the filter is dried for two hours to a constant weight at 103-105°C. The weight of the filter and the dried residue is determined and used to calculate the TSS in mg L^{-1} .

$$TSS = (A - B) \cdot 1000/V \quad \text{Eq. 2-3}$$

Where:

TSS: total suspended solids (mg L^{-1});

A: weight of the filter + dried residue (mg);

B: weight of the filter (mg);

V: sample volume (mL).

VSS is determined by the combustion of the MLSS filter in a furnace at a temperature of 550 °C for one hour. The remaining solids (weighted after cooling first in air and after in desiccator) represent the fixed total, dissolved, or suspended solids, while the weight lost on ignition corresponds to the volatile solids. This determination offers a rough approximation of the amount of organic matter present in the solid fraction of wastewater, activated sludge and industrial wastes.

VSS concentration is calculated as follows:

$$VSS = (A - B) \cdot 1000/V \quad \text{Eq. 2-4}$$

$$FS = (B - C) \cdot 1000/V \quad \text{Eq. 2-5}$$

Where:

VSS: volatile suspended solids (mg L^{-1});

FS: fixed solids (mg L^{-1});

A: weight of residue + filter before ignition (mg);

B: weight of residue + filter after ignition (mg);

C: weight of filter (mg).

2.1.3 Biomass characterization

2.1.3.1 Batch test essays

During the experimentation carried out in Chapter 3, nitrate production rate (NPR) and nitrate uptake rate (NUR) batch tests were carried out under no substrate and electron acceptor limiting conditions, in order to evaluate the activity and distribution of biomasses in both, biofilm and suspended phases.

With respect to NPR batch tests in the biofilm, the bulk liquid containing the suspended biomass was extracted from the hybrid membrane aerated biofilm reactor (HMABR). Then, the reactor containing the biofilm covered membrane was filled with settled effluent (Figure 2-1 a). In case of NPR batch tests in suspended biomass, 1 L of HMABR mixed liquor was introduced in a container provided with an air diffuser and a magnetic stirrer (Figure 2-1 b). In order to ensure aerobic conditions in both, biofilm and suspended biomass NPR batch tests, the bulk liquid was oxygenated using an air diffuser, maintaining a bulk liquid DO concentration of 8-9 mg/L (in case of biofilm NPR batch test, the membrane was also pressurized with the operational relative air pressure of 0.07 atm). A solution of ammonium chloride was added so that the initial ammonium concentration in the bulk liquid was around 30 mg/L. A sodium bicarbonate buffer solution was also added to maintain a pH value around 7-8 during the test duration. The essay consisted in taking samples from the bulk liquid every 60 minutes, and measure nitrate concentrations in order to see its linear variation over time. The nitrate concentration rising slope, will correspond with the NPR for each biofilm or suspended biomass test.

Regarding NUR batch tests, biofilm and suspended biomasses were separated in the same way as described for NPR batch essays. In order to guarantee anoxic conditions in both biofilm and suspended biomasses, nitrogen gas was continuously sparged within the bulk liquid, and in case of biofilm NUR batch test, the membrane lumen was also pressurized with nitrogen. Acetate substrate as a carbon source and nitrate, using a potassium nitrate solution, were spiked at the beginning of the essay in order to obtain 100 mg/L of COD and 30 mg/L of $\text{NO}_3\text{-N}$ concentrations. In this case, samples from the bulk liquid were taken every 20 minutes and the decrease in nitrate concentrations was measured, which slope relative to the time was the NUR.

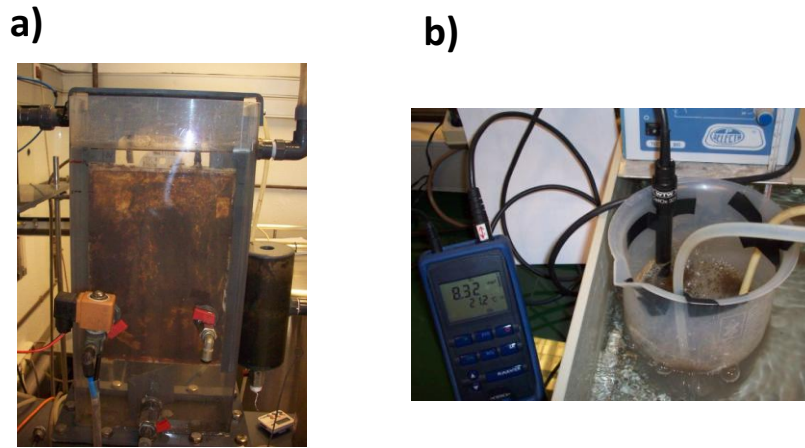


Figure 2-1 Set up for batch essays in the biofilm covered membrane (a) and in suspended biomass (b).

2.1.3.2 Biofilm thickness determination

Biofilm thicknesses in experimental set ups corresponding to Chapters 4 and 5, were measured using a microsensor by attaching it to a motorized micromanipulator with a vertical resolution of 0.010 mm. The microsensor tip was first positioned at membrane surface (Figure 2-2). Then, the tip was raised with the computer-controlled motor until the tip reached the outer edge of the biofilm, which was checked visually by microscopy. The distance was measured and recorded by SensorTrace Suit software (Unisense). Biofilm image acquisition was also performed in all seven flow-cell ports after four weeks of operation. Image processing for each measurement was followed by statistical evaluation of the results.

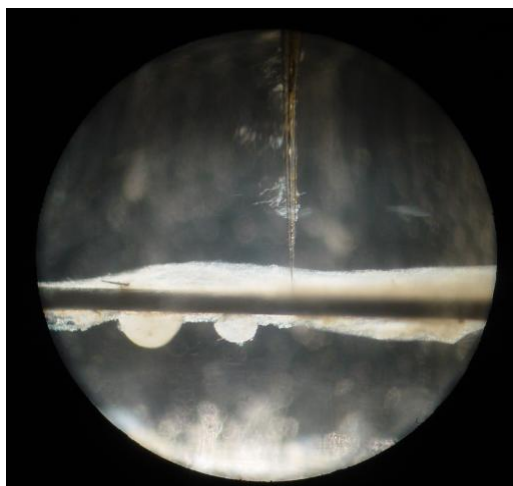


Figure 2-2 Biofilm thickness measurement using a microsensor tip and a stereomicroscope.

2.1.4 Dissolved oxygen profiles at membrane surface

The analyses described in this section were only conducted in the lab-scale MABRs at University of Notre Dame (see chapters 4 and 5). In order to evaluate back-diffusion gas profiles developed in a closed-end hollow fiber membrane (HFM), dissolved oxygen (DO) concentrations along the membrane surface (with and without biofilm) were measured.

Clark-type oxygen microsensors (Unisense A/S, Denmark) with a 10 μm tip diameter were used to measure DO concentrations. The microelectrode movement was controlled with a micro-manipulator (Model MM33-2, Unisense A/S). The use of microsensors consists in an invasive method that can slightly affect the results. However, considering that the tip was only 10 μm diameter and was immersed in a much thicker boundary layer, the microsensors would be expected to have a minimal impact on the DO concentration. Hydrodynamic measurements made by Hondzo et al., (2005), using a similar DO microsensor diameters and Reynolds number as used in this study, concluded that the disturbance of the flow by microsensors stem was minimal.

Longitudinal profiles of DO at the HFM surface were collected from the seven ports of the flow-cells once the system reached the steady state, typically two hours after closing the membrane. For each port, transversal DO profiles were collected starting from the HFM surface, across the liquid diffusion layer (LDL) or the biofilm, and into the bulk. The transversal DO measurements were collected

at 20- μm intervals, and typically reached a distance of around 1000 μm from the membrane surface. Profiles were collected at least in triplicate. For transient conditions, DO was measured continuously at the membrane surface, for one of the intermediate ports, during the shift from open-end to closed-end operation.

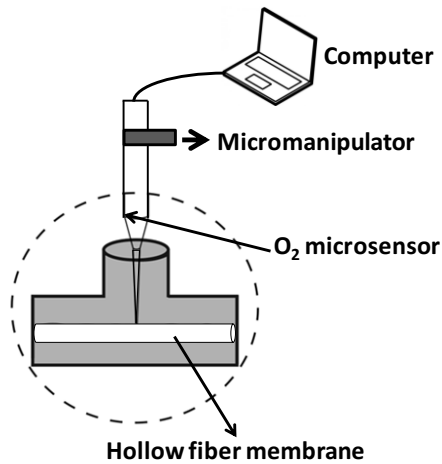


Figure 2-3 Detail of a flow-cell port used for DO measurement with a microsensor controlled by a micromanipulator.

2.2 MATHEMATICAL MODELING

In this Thesis mathematical modeling has been performed to (a) define optimum design and operation parameters of the HMABR process for different scenarios; (b) systematically explore periodic venting of hollow-fiber membranes (HFM) as a means to maximize the oxygen transfer efficiencies (OTE) and oxygen transfer rates (OTR) of MABRs; and (c) explore the impact of biofilm on back-diffusion process in air and pure oxygen supplied MABRs, aiming to minimize the detrimental effects of gas back diffusion.

2.2.1 HMABR mathematical model

The model was used as a tool to establish the optimum design and operation conditions for the HMABR process treating urban wastewater through systematic simulation studies.

The proposed HMABR process configuration, integrated a MABR process into a conventional completely mixed activated sludge reactor. The model which included biochemical, physical transport, and gas transfer submodels was

implemented in AQUASIM 2.1 simulation platform developed by EAWAG (Reichert, 1994). In AQUASIM a model consists of a system of ordinary and/or partial differential equations and algebraic equations, which deterministically describes the behaviour of a given set of state variables. The differential equations for water flow and substance transport can be selected by the choice of environmental compartments, which can be connected to each other by links (Reichert, 1998). As represented in Figure 2-4, a model structure in AQUASIM comprises four main subsystems: variables, processes, compartments and links that need to be defined by the program user.

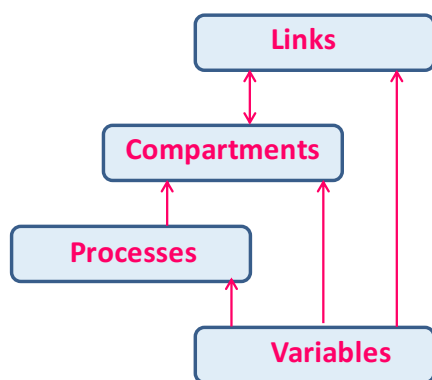


Figure 2-4 Logical structure of AQUASIM systems consisting of four subsystems (Source: Reichert, 1994).

Kinetics and stoichiometries taking place both in the sludge and in the biofilm were based on Activated Sludge Model n° 2 (ASM2d) (Henze et al., 2000). An extension of the ASM2d model proposed by Larrea et al., (2002), where the slowly biodegradable COD was divided into soluble (S_L) and particulate fractions (X_S) was also considered. Typical values for the kinetic and stoichiometric parameters were mostly adopted from ASM2d (Henze et al., 2000).

For the physical transport model, the one-dimensional mixed culture biofilm (MCB) model (Wanner and Reichert, 1996) was used. Besides, an extension of the MCB model (Extended MCB model) developed at CEIT (Albizuri et al., 2009) was implemented. According to the Extended MCB model, colloids were incorporated in the state variables of particulate components, leading to three different states for such components: colloids ($X_{i,C}$), flocs ($X_{i,F}$) and biofilm.

With respect to the gas transfer model, a gas permeable membrane supplied oxygen at the biofilm base while organic carbon and ammonia nitrogen were supplied from the bulk liquid. Oxygen flux (J_{O_2}) from the gas phase to the biofilm through the gas permeable membrane was given by the following equation:

$$J_{O_2} = AK_m \left(C_{O_2,g} / H_{O_2} - C_{O_2} \right) \quad \text{Eq. 2-6}$$

Where

J_{O_2} : Oxygen flux from the membrane to the biofilm ($\text{g O}_2 \text{ d}^{-1}$)

$C_{O_2,g}$: Concentration of oxygen in the membrane on gas side (g m^{-3})

C_{O_2} : Concentration of oxygen in the membrane on biofilm side (g m^{-3})

A : Biofilm surface (m^2)

K_m : Membrane oxygen mass transfer coefficient (m d^{-1})

H_{O_2} : Henry's coefficient for oxygen (non-dimensional)

The biofilm and the bulk liquid were modelled in AQUASIM as a biofilm reactor compartment, which consisted of a reactor with a completely mixed bulk water volume and a biofilm growing on a gas transferring membrane surface. The interior of the membrane was modelled as a completely mixed air filled compartment and the wall of the membrane permeable to oxygen as a diffusive link connected to the biofilm base. In this type of links there is no water flow and a conversion factor is used that allows for the description of phase transitions, like oxygen exchange between gas and liquid-biofilm phases (see Equation 2-6). Water flow, external recirculation and wastage flow were simulated using advective links.

As an example, in Figure 2-5 a typical screenshot of AQUASIM simulation platform is shown:

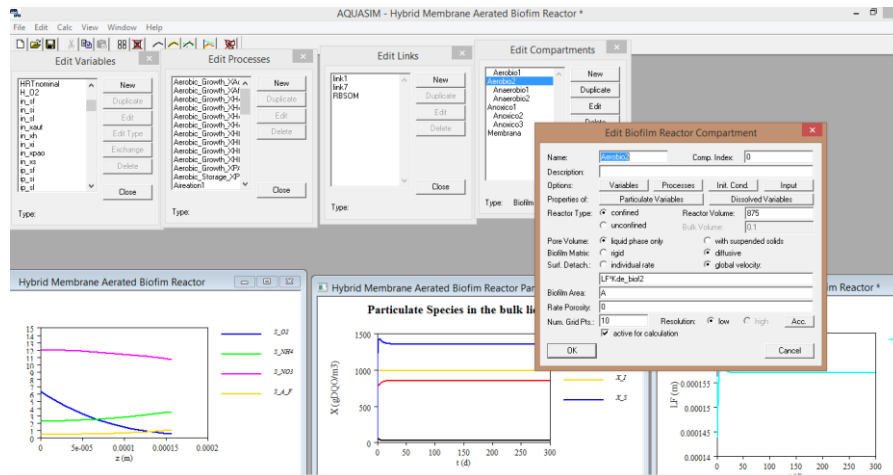


Figure 2-5 Typical screenshot of AQUASIM software.

The first step in the general model calibration methodology consisted on selecting, among the overall available information, those model parameters to be adopted from literature, and those parameters to be adjusted (fitting parameters) (Figure 2-6). Once fitting and adopted parameters were selected, as a second step in the general calibration methodology, simulations were run until simulation and experimental results matched.

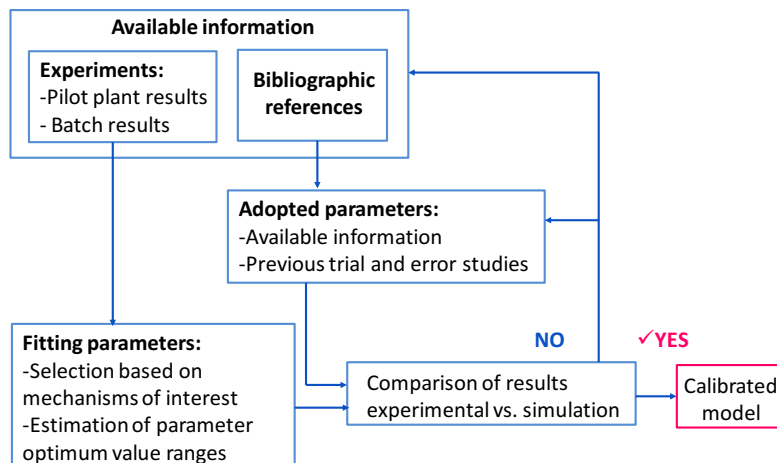


Figure 2-6 Schematic representation of the general methodology for model calibration.

2.2.2 Back-diffusion mathematical model for HFMs

This model was used to explore strategies to improve oxygen transfer efficiencies (OTE) and oxygen transfer rates (OTR) in HFM applications (i.e. MABR).

For that purpose, a mathematical model for gas back-diffusion was developed addressing both steady-state and transient conditions. It was tested and calibrated with experimental measurements, then applied to predict the behavior of gas dynamics for a board range of conditions.

The model included O_2 supply from the HFM lumen, and assumed that the bulk liquid was in equilibrium with 1 atm of N_2 . However, the resulting trends are applicable to other gases as well. The model was implemented with the finite-element simulation platform COMSOL Multiphysics (COMSOL 4.4, Comsol Inc., Burlington, MA, www.comsol.com).

A typical screenshot of COMSOL simulation platform is shown as an example in Figure 2-7:

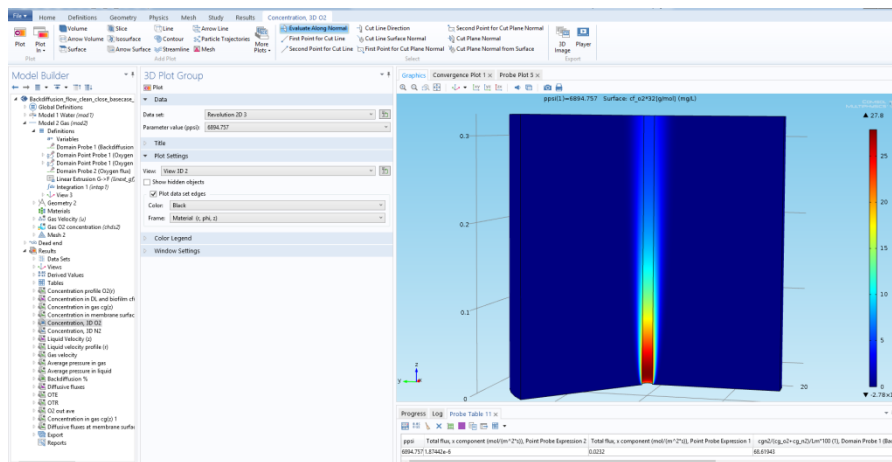
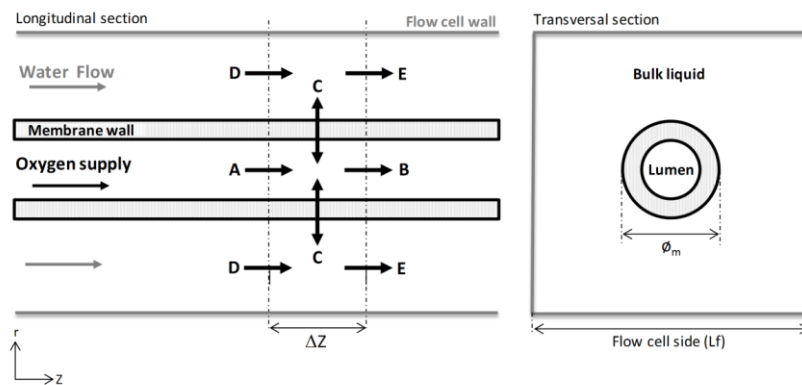


Figure 2-7 Typical screenshot of COMSOL software.

The numerical model included fluid flow and mass transport of O_2 and N_2 , both in the liquid surrounding the HFM and in the lumen gas (Figure 2-8). For the flow and mass transport in the liquid phase, a two-dimensional (2-D) axisymmetric geometry was set along the axis of the membrane lumen (direction z) with radial gradients along direction r . The 2-D model implies an annular cross-section for the flow (the radius of a circle with the same area as the square cross-section). This

model was coupled with a one-dimensional (1-D) domain for gas flow and mass transport in the membrane lumen (assuming no radial gradients in the lumen).



Gas transport in lumen and across membrane

A: Advective flow and axial diffusion In

B: Advective flow and axial diffusion Out

C: O₂ and N₂ fluxes In and Out

Gas transport in liquid

D: Advective flow and diffusion In

E: Advective flow and diffusion Out

Figure 2-8 Fluid flow and mass transport phenomena considered in the back-diffusion model. The model assesses a single hollow-fiber membrane inside a square-section flow cell. Water flows between the membrane and the flow cell wall, and the membrane is supplied with pure oxygen. Δz is an element of flow cell, including the membrane. Schematic is not to scale.

The fluid regime in the flow cell was determined by solution of the two-dimensional Navier-Stokes equation. The mass balances for the gases in the membrane lumen were adapted from Ahmed and Semmens (1992), being the mass transfer from the membrane wall into the liquid determined by Fick's first law of diffusion. In open end systems, the gas velocity in the lumen of the membrane was estimated using the Hagen-Poiseuille expression for slightly compressible fluids. Key differences with previous models included allowing dissolved gas concentrations to vary along the length of the membrane due to upstream gas transfer, accounting for frictional pressure losses in the membrane, considering transient conditions, and explicitly incorporating the membrane mass transfer coefficient (K_m).

Predicted DO concentrations at the surface of the fiber were directly compared with experimental measures in both steady and transient states. Several model

parameters were fixed from experimental conditions, such as: O₂ diffusivity in the membrane, water velocity, membrane length and radius, dissolved nitrogen concentration, oxygen gas in the influent water, and oxygen gas pressures in the membrane inlet and outlet. Other parameters were obtained from literature.

2.2.3 Back-diffusion mathematical model for MABRs

This model was used to explore the impact of biofilm on gas back-diffusion process in air and pure oxygen supplied MABRs, as a means to minimize the detrimental effects of gas back-diffusion and maximize both OTEs and OTRs.

This model was constructed by implementing a biofilm domain in the previously described back-diffusion mathematical model for HFMs. Thus, in addition to considering fluid flow and mass transport in the liquid and gas phases, it also considered mass transport and reaction inside the biofilm. Mass transport of O₂, N₂, and acetate (Ac) in the biofilm were determined by Fick's law. Biomass activity followed dual Monod kinetics (Rittmann and McCarty, 2001) as concentrations of O₂ and Ac can be simultaneously limited in counter-diffusional biofilms. Since the back-diffusion process time scale is in the order of seconds to minutes (as it was confirmed in the studies performed in Chapter 4), biofilm growth was neglected to simplify the model.

Physical parameters of the liquid and gas phases were adopted from the previous back-diffusion model for HFMs. Several model parameters were taken from experimental conditions (including biofilm thicknesses and bulk acetate concentrations, among others). Biofilm physical and kinetic parameters were adopted from literature.

Simulated DO concentrations at the surface of the membrane for MABRs were directly compared with experimental measurements for both steady and transient states.

2.3 REFERENCES

Ahmed, T., Semmens, M.J., 1992. The Use of Independently Sealed Microporous Hollow Fiber Membranes for Oxygenation of Water - Model Development. *J. Memb. Sci.* 69, 11–20.

Albizuri, J., Van Loosdrecht, M.C.M., Larrea, L., 2009. Extended mixed-culture biofilms (MCB) model to describe integrated fixed film/activated sludge (IFAS) process behaviour. *Water Sci. Technol.* 60, 3233–3241.

- APHA, 2005. Standard Methods for the Examination of Water and Wastewater, American Water Works Association/American Public Works Association/Water Environment Federation.
- Henze, M., Gujer, W., Mino, T., van Loosdrecht, M.C.M., 2000. Activated Sludge Models ASM1, ASM2, ASM2d and ASM3. IWA Publ. 121.
- Hondzo, M., Feyaerts, T., Donovan, R., O'Connor, B.L., 2005. Universal scaling of dissolved oxygen distribution at the sediment-water interface: A power law. *Limnol. Oceanogr.* 50, 1667–1676.
- Larrea, L., Irizar, I., Hildago, M.E., 2002. Improving the predictions of ASM2d through modelling in practice, in: *Water Sci. Technol.* pp. 199–208.
- Reichert, P., 1994. Aquasim - a Tool for Simulation and Data-Analysis of Aquatic Systems, *Water Sci. Technol.* 30(2), 21-30.
- Reichert, P., 1998. AQUASIM 2.0 - User Manual. Swiss Federal Institute for Environ. Sci. Technol. (EAWAG). Dübendorf, Switzerland.
- Rittmann, B.E., McCarty, P.L., 2001. Stoichiometry and bacterial energetics. In: *Environmental biotechnology: principles and applications.* McGraw-Hill International Editions, 126-164.
- USEPA, 1983. Methods for Chemical Analysis of Water and Wastes. *Environ. Prot.* 491.
- Wanner, O., Reichert, P., 1996. Mathematical modeling of mixed-culture biofilms. *Biotechnol. Bioeng.* 49, 172–184.

Chapter 3

Guidelines for the optimal design and operation of the hybrid membrane aerated biofilm reactor (HMABR) for nitrogen removal¹

¹ Part of this chapter has been published as:

Pérez-Calleja, P., Esteban-García, A.L., Tejero, I., Gabaldón, C., Larrea, L., 2014. *Guidelines for the optimal operation of the Hybrid Membrane Aerated Biofilm for nitrogen removal*. Book of Abstracts of the IWA 2ndh Specialized International Conference ecoSTP2014, EcoTechnologies for Wastewater Treatment: Technical, Environmental & Economic Challenges. Verona, Italy, 23-27 June. ISBN 978-8869250002, 185-188.

Pérez-Calleja, P., Esteban-García, A. L., Tejero, I., Aybar, M., Larrea, L., 2016. *Guidelines for the Energy Efficient Operation of the Hybrid Membrane Aerated Biofilm Process for Nitrogen Removal*. 13th IWA Leading Edge Conference on Water and Wastewater Technologies. Jerez de la Frontera, Spain, 13-16 June.

Pérez-Calleja, P., Esteban-García, A.L., Tejero, I., Aybar, M., Larrea, L., 2016. *Mathematical Model To Describe The Behaviour Of The Hybrid Membrane Aerated Biofilm Reactor (HMABR)*. 3rd IWA Specialized International Conference Ecotechnologies for Wastewater Treatment 2016 (ecoSTP16). Poster session 3315756. Cambridge, UK, 27-30 June.

Pérez-Calleja, P., Esteban-García, A.L., Tejero, I., Aybar, M., Larrea, L., 2017. *Model-based Study to Optimize the Hybrid Membrane Aerated Biofilm Reactor (HMABR) for Carbon and Nitrogen Removal*. 10th International Conference on Biofilm Reactors. Dublin, Ireland, 9-12 May.

OUTLINE

SUMMARY.....	81
3.1 INTRODUCTION.....	82
3.2 OBJECTIVES.....	86
3.3 MATERIALS AND METHODS.....	86
3.3.1 Experimental study.....	86
3.3.1.1 HMABR configuration.....	86
3.3.1.2 Feed wastewater.....	88
3.3.1.3 Operational conditions and criteria.....	88
3.3.1.4 Analytical methods.....	90
3.3.1.5 Mass balances in the HMABR.....	90
3.3.1.6 Nitrification and denitrification batch tests.....	92
3.3.2 Simulation study.....	92
3.3.2.1 HMABR mathematical model.....	92
3.3.2.2 HMABR model calibration.....	97
3.3.2.3 Systematic simulation studies for the optimization of the design and operation of the HMABR process.....	103
3.4 RESULTS AND DISCUSSION.....	107
3.4.1 Experimental results.....	107
3.4.1.1 Mixed Liquor Suspended Solids (MLSS) behavior.....	107
3.4.1.2 Removal of soluble Chemical Oxygen Demand (sCOD).....	108
3.4.1.3 Nitrogen removal.....	108
3.4.1.4 Nitrification and denitrification batch tests.....	114
3.4.2 Simulation results.....	115
3.4.2.1 HMABR model calibration.....	115
3.4.2.2 Systematic simulation studies.....	118
3.5 CONCLUSIONS.....	128

3.5.1	Experimental study	128
3.5.2	Simulation study.....	129
3.6	REFERENCES	130

SUMMARY

A new hybrid membrane aerated biofilm reactor (HMABR) has been developed to obtain a compact reactor for nitrogen removal and high oxygen transfer efficiencies. The HMABR aimed to achieve high nitrification rates taking place almost exclusively in the biofilm, and high denitrification rates occurring mostly in suspension. The first objective of this study was to establish the operational criteria that lead to the optimum performance of the HMABR process in an experimental study. Then, an HMABR mathematical model was developed and calibrated using the experimental results. The second objective was to establish the optimum design and operation conditions for the HMABR process (for treating urban raw wastewater) using systematic simulation studies with the calibrated model.

The experimental HMABR consisted of a bench-scale single reactor vessel (15 L) with a membrane module used for oxygen gas transfer and biofilm support. The bulk liquid had a mixed liquor suspended solids concentration typical of an activated sludge process. The HMABR was continuously fed with an influent mimicking a medium-high strength urban raw wastewater. Average nitrification rates of 3 gN/m²d were achieved. This result is better than those obtained in previous HMABR studies. Effluent residual NO₃-N concentration had a crucial role in maintaining the desired nitrifying and heterotrophic biomasses distribution.

Systematic simulations studies allowed to define some optimum design and operation parameters of the HMABR process for different membrane types and effluent requirements. Different combinations of membrane air pressures (MAP) and membrane areas allowed achieving the desired effluent ammonium concentration to maximize nitrification rates. Optimum MAPs for different operating temperatures were also determined. Combinations of HRTs and MLSS concentrations were obtained to satisfy TN effluent standards established in European legislation for different scenarios. Most favorable MLSS concentrations for different temperatures and for achieving the desired effluent NO₃-N concentrations were determined.

3.1 INTRODUCTION

The removal of total nitrogen (TN) has become an important challenge for many municipal and industrial wastewater treatment plants (WWTP) since there is an increasing concern about the eutrophication of the receiving water bodies that the excess of nitrogen could lead. This fact compels to find out cost-effective solutions to target this need, both for the design of new WWTPs and for retrofitting existing installations by profiting the available space. Taking into account the energy consumption, emissions and space occupation related to such upgrading of WWTPs, the search for more efficient treatment systems has become fundamental for the eco-sustainability of WWTPs. In this area, membrane aerated biofilm reactors (MABRs) are gaining in importance since they are able to achieve high oxygen transfer efficiencies and great energy savings.

The MABR is a reactor in which the biofilm is supported on and aerated/oxygenated by a gas-permeable membrane (Pankhania et al., 1999; Semmens et al., 2003; Esteban-García et al., 2012). Oxygen is able to diffuse straight to the biofilm growing on the other side of the membrane, in contact with the wastewater to be treated, while the substrates (nutrients and COD) are transferred from the bulk liquid to the biofilm. This approach offers significant advantages over conventional aeration methods, where frictional losses through the piping, low aqueous solubility of oxygen and backpressure required to blow bubbles demand large amounts of energy. In the MABR configuration all the oxygen supplied to the membranes is delivered by diffusion straight to the biofilm and without bubble formation. Moreover, the depth of the water is unimportant since air does not need to be compressed to overcome the hydrostatic pressure. These features can save up to 85% in energy costs compared to conventional activated sludge process (Aybar et al., 2014). The elimination of bubbling can also prevent the stripping of volatile organic compounds (VOCs), odors and greenhouse gases and avoid foam formation when surfactant products are present. Pressure drops across the membrane are low and it is possible to achieve high oxygen transfer and utilization efficiencies, up to 100% in some configurations (closed-end mode) (Brindle et al., 1998; Terada et al., 2003; Syron and Casey, 2008; Martin and Nerenberg, 2012).

MABR biofilms are counter-diffusional, meaning substrates are supplied from opposite sides of the biofilm (Nerenberg, 2016). The MABR also supports a unique counter-diffusive microbial community structure, allowing concurrent oxidation of chemical oxygen demand (COD), nitrification, and denitrification (Timberlake et al., 1988; Terada et al., 2003; Jácome et al., 2006; Matsumoto et al., 2007), therefore providing a smaller reactor footprint. Nitrifying bacteria reside near the

membrane surface where oxygen concentrations are greatest and result protected from biofilm erosion. Commonly oxygen is consumed within the biofilm, creating anoxic conditions suitable for denitrifying bacteria in the outer regions of the biofilm and bulk liquid (LaPara et al., 2006; Downing and Nerenberg, 2008) (Figure 3-1 a). Satisfactory results for nitrogen removal have been obtained in previous studies using synthetic wastewater (Osa et al., 1997; Semmens et al., 2003; Stricker et al., 2011). However, in these studies influent readily biodegradable COD (S_s) concentrations were typically high enough to achieve high denitrification and TN removal rates. Therefore, the MABR potential for application in real urban wastewater can be limited for achieving TN removal, because the lower S_s concentrations can hamper the growth of enough denitrifying biomass in the biofilm. Another limitation of MABRs is the control of the excessive biofilm thickness, which has been observed to be thicker than in conventional biofilms due to overgrowth of heterotrophs (Casey et al., 2000). Thick biofilms increase the mass transfer limitation and cause heterotrophic competition for oxygen and space within the biofilm resulting in decreased nitrification ability.

A hybrid or IFAS (integrated fixed biofilm activated sludge) process is defined as an activated sludge (AS) system that incorporates some form of technology (media, membrane) in the suspended growth reactor to enhance the level of treatment provided. The addition of the biofilm support media allows the reduction of the aerobic volume by compacting and increasing the amount of biomass concentration available for treatment. Very successful results, with high nitrification rates in the biofilm and satisfactory denitrification in suspended biomass, have been attained in full scale plants (Randall and Sen, 1996; Rutt et al., 2006) by maintaining low bulk biological oxygen demand (BOD) concentrations. Hybrid systems are typically installed as a retrofit solution for existing plants.

In this study an innovative integrated biological process was experimentally investigated in order to achieve nitrogen removal controlling at the same time the biofilm thickness, the hybrid MABR (HMABR) (Downing et al., 2007). The HMABR integrates a MABR process into a conventional completely mixed activated sludge reactor. The critical goal of the HMABR is to maintain nitrifying biomass on the membranes, and achieve denitrification via suspended growth in order to control heterotrophic attachment and avoid thick biofilms (Figure 3-1 b). Biodegradable soluble COD (sCOD) is expected to be oxidized mainly anoxically and in the bulk liquid while a nitrifying biofilm is established on the gas-permeable membranes.

Previous research showed that the HMABR was able to concurrently remove BOD and nitrate, maintaining a biofilm where nitrifying bacteria were predominant, while heterotrophic bacteria were mostly in the bulk liquid (Downing et al., 2008). In that study a HMABR was operated using synthetic wastewater with a low bulk suspended solids retention time (SRT) (with an average value of 2.5 days) in order to wash out suspended nitrifying biomass, obtaining a maximum mixed liquor suspended solids (MLSS) concentration of 120 mg/L and an average nitrification rate of 1 g/m²d. Denitrification performances up to 99% for influent BOD:N ratios of 11.5 were obtained. These results were very promising; however the proportion of readily biodegradable substrate (S_5) with respect to the BOD (100%) resulted in a much higher value than for a conventional urban raw wastewater (as acetate was used as BOD source). Besides, for BOD:N ratios lower than 5.5 (closer to the typical BOD:N ratio of an urban wastewater) incomplete denitrification occurred. These limitations may be overcome by developing a more efficient HMABR process for treating urban wastewater, maximizing both nitrification and denitrification rates. To this end, operating with MLSS concentrations closer to the typical values of activated sludge processes (3000-4000 mg MLSS/L) is proposed.

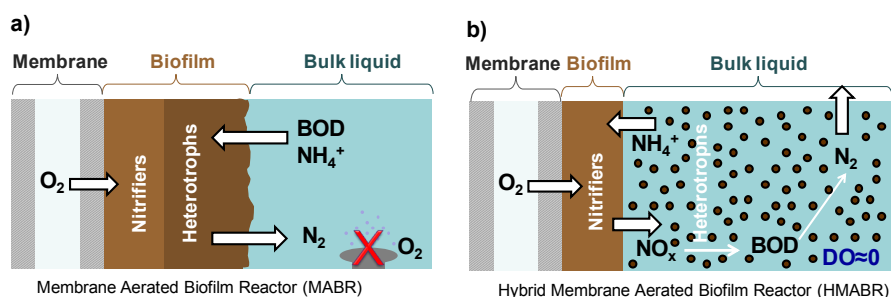


Figure 3-1 (a) Biofilm in a MABR with nitrifying and heterotrophic biomass, which can lead to substrate transfer limitations due to overgrowth of heterotrophs; (b) Biofilm in a HMABR, with nitrifying biomass in the biofilm, limiting heterotrophic attachment by maintaining high suspended solids and low bulk BOD concentrations.

In the present, the development of activated sludge models (Henze et al., 2000) allows the use of calibrated-validated models. Biofilm modelling has evolved significantly in the last few years (Wanner et al., 2006), but the application of these models for the optimization of the design and operation of a hybrid process is very limited since a calibrated model is required. Modeling hybrid processes introduces an additional complexity to activated sludge processes due to the interaction between biomass in suspended flocs and biofilms, and between the heterotrophic and nitrifying biomass (Albizuri et al., 2009).

Many models (such as ASM1 and ASM2d) assume that slowly biodegradable COD (sbCOD) is in particulate form (i.e., X_s). However, only a portion of sbCOD material is settleable. Consequently, to model the organics removal and the COD composition and load of streams passing through a wastewater treatment system, it is important to distinguish between the portions of the sbCOD that are soluble, colloidal and particulate.

Regarding the modelling of hybrid or IFAS processes, most authors assume that influent X_s is entirely adsorbed onto suspended flocs, and in addition, they do not consider the attachment of the flocs towards the biofilm, meaning that the nitrification rate in the biofilm will not be dependent on the applied X_s load in the influent wastewater (Albizuri et al., 2014). Other authors like Suzuki et al., (1999) obtained higher biofilm nitrification rates in the simulations than in the experimental tests. They attributed this to the fact that in the simulations the interaction of X_s with the biofilm was not being considered, however, it did occur in reality.

Albizuri et al., (2009) found that the description of nitrification and oxygen uptake rates in an IFAS Johannesburg process using the original mixed culture biofilm (MCB) model (Wanner and Reichert, 1996) and taking into account attachment and diffusion phenomena, could not reproduce their experimental results. For this reason, they proposed a new colloid model, the Extended MCB model, in which the colloids present in the influent wastewater interacted with both biofilm and suspended flocs through new attachment and detachment phenomena (Figure 3-2).

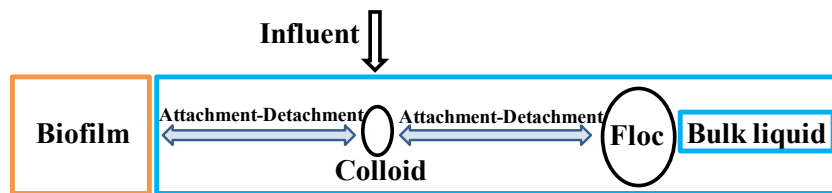


Figure 3-2 Diagram of different interactions between colloids, flocs and biofilm in the Extended MCB model. (Adapted from Albizuri et al., 2014).

The Extended MCB model described satisfactorily the experimental results obtained in IFAS and pure moving bed biofilm reactor (MBBR) pilot plants.

In this study, a new HMABR mathematical model was developed, by adapting the Extended MCB model (Albizuri et al., 2009), leading to the consideration of suspended flocs, colloids and biofilm (Figure 3-3).

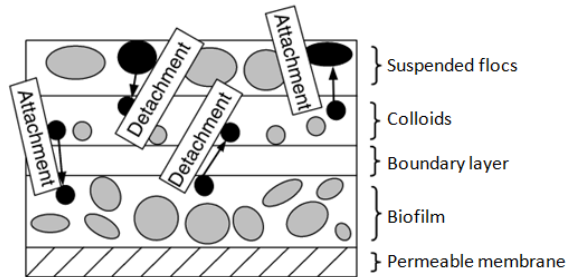


Figure 3-3 Conceptual structure of the HMABR model. (Adapted from Albizuri et al., 2009).

3.2 OBJECTIVES

In this research, the first objective was to experimentally define the criteria for the optimal operation of the HMABR, in order to achieve high nitrification rates taking place almost exclusively in the biofilm, and high denitrification rates, occurring mostly in suspension, as in continuous IFAS processes.

The second objective was to develop and calibrate a mathematical model able to reproduce the HMABR experimental results, and use it as a tool to establish the optimum design and operation conditions for the HMABR process treating urban wastewater.

3.3 MATERIALS AND METHODS

3.3.1 Experimental study

According to the first objective proposed in this study, a HMABR was constructed and operated to achieve TN removal. In this section, the bench-scale reactor, wastewater characteristics, operational conditions and criteria, analytical methods, mass balances and performed batch test essays in both, biofilm and suspended biomasses will be presented.

3.3.1.1 HMABR configuration

The hybrid reactor was located at the Environmental Engineering Laboratory of CEIT (University of Navarra). The bench-scale HMABR consisted of a 15 L PVC vessel with internal square section of 0.15 x 0.24 m² and height of 0.50 m, in which a single microporous polyethylene chlorinated flat membrane (type 203, size A4, KUBOTA) module was placed (Figure 3-4). As just one membrane module

was used, the total membrane specific area (MSA) per water volume was very low, resulting in $7.7 \text{ m}^2/\text{m}^3$. This commercial membrane module is typically used for wastewater microfiltration, in replacement for the usual sedimentation step. Thus, this membrane module was factory-hydrophilized for enhancing its filtration capacity. According to the instructions given by manufacturers KUBOTA, a reverse hydrophobication treatment was applied to the module before it was used as gas supplying membrane (since polymeric membranes are often hydrophobic in nature). Air was supplied to the membrane module by a pneumatic control panel at an inlet relative pressure of 0.07 atm. The membrane module was daily purged to expel water that may have accumulated inside the module by filtration or water vapour condensation.

Mixing was provided by a centralized axial mixer at the bottom of the reactor vessel. A settler of 22 L was located after the HMABR in order to recycle the activated sludge. It was equipped with some scrappers moved at very low revolutions to facilitate solids settling and prevent from sludge channelling. Between the HMABR and the settler, a small reservoir was placed, designed to strip N_2 gas from the effluent sludge by air bubbling, and avoid to the extent possible, sludge raising episodes in the settler. Sludge wastage was carried out from the mixed bulk liquid by an electrovalve which was opened every 20 minutes. The wastage flow rate (Q_w) was adjusted according to the desired MLSS concentrations.

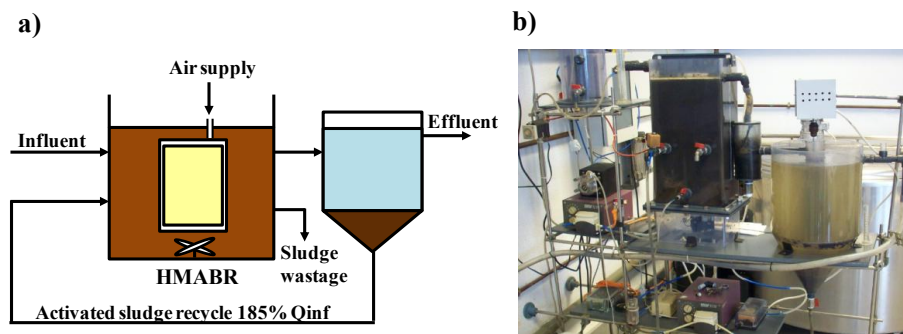


Figure 3-4 (a) Schematics of the HMABR and (b) an image of the experimental pilot plant.

3.3.1.2 Feed wastewater

In this research, it was tried to mimic a conventional medium-high strength urban raw wastewater. For that purpose, the feed water was prepared by mixing and diluting different portions of primary sludge, the supernatant resulting from its acid fermentation, and sludge return liquor from the municipal WWTP of Apraiz (North of Spain).

According to Tchobanoglous et al., (2014) typical values for medium-high strength untreated domestic wastewater are in the following ranges: TSS=210-400 mg/L, BOD₅=190-350 mg/L, COD=430-800 mg/L, and NH₄-N=25-45 mg/L. Primary sludge (with a MLSS concentration \approx 50000 mg/L) was used to reproduce a typical TSS concentration nearby 300-400 mg/L. A conventional raw wastewater can contain soluble COD concentrations (sCOD) of about 150-200 mg/L, from which it is estimated that around 35-40% can be readily biodegradable COD (S_s) (between 60-80 mg/L S_s) (Melcer et al., 2003). In this experiment, for the sCOD supply, the supernatant resulting from the primary sludge acid fermentation (produced during its anaerobic storage conditions), very rich in volatile fatty acids (VFA) (with sCOD concentrations \approx 6000 mg/L) was used. The proportion of S_s with respect to the sCOD in the supernatant was assumed to be greater than in a conventional urban raw wastewater, of around 60%.

In order to obtain S_s concentrations similar to the values of a conventional raw wastewater (of about 80 mg/L of S_s), the feed water was prepared at a sCOD concentration of approximately 130 mg/L. During the experimentation, due to biological degradation episodes inside the storage tank, an average influent sCOD value of 90 mg/L was obtained, resulting in a somewhat lower sCOD value than expected. An average influent total COD (tCOD) concentration of 610 mg/L was obtained. For the ammonium supply, sludge return liquor (with NH₄-N concentrations \approx 900 mg/L) was used, setting an influent ammonium concentration of around 35 mg NH₄-N/L, well within the typical values for medium-high strength urban raw wastewater. The prepared influent wastewater was stored in a mixed 500 L refrigerated tank.

3.3.1.3 Operational conditions and criteria

The HMABR was running over a period of 145 days. The operating conditions were set considering the following criteria.

The first criterion was to operate under non-limiting ammonium conditions (NH₄-N concentration above 2 mg/L) at any layer of the biofilm, to achieve high

nitrification rates. Therefore it was decided to maintain an effluent $\text{NH}_4\text{-N}$ concentration higher than 10 mg/L, since the gradient of ammonium that was taking place within the biofilm was unknown. Given this criterion and the influent $\text{NH}_4\text{-N}$ concentration of 35 mg/L, based on nitrification rates derived from previous HMABR studies (Downing and Nerenberg, 2007, Downing and Nerenberg, 2008), an influent flow rate (Q_{in}) of 1 L/h was adopted, resulting in an average HRT of 14 hours.

In order to maximize the HMABR nitrification and denitrification rates, another approach was to operate with MLSS concentrations in the order of magnitude typical of a conventional activated sludge process, of around 3000-4000 mg MLSS/L, for which the sludge wastage (Q_w) was adjusted. Higher MLSS and SRT allow the consumption by suspended flocs of S_s and X_s available for denitrification process. Low effluent S_s concentration will in turn maximize nitrification rates by preventing its diffusion towards the biofilm and the competence of nitrifying organisms with heterotrophs by available DO and space.

The last goal was to operate under non-limiting nitrate concentrations within the bulk liquid ($\text{NO}_3\text{-N}$ concentration above 5 mg/L), so that the majority of the S_s could be anoxically consumed in suspension. Due to the low specific membrane surface area per water volume used in the pilot HMABR ($7.7 \text{ m}^2/\text{m}^3$), nitrate production by the biofilm was not sufficient to provide the target bulk liquid nitrate concentration, so it was necessary to incorporate a continuous $\text{NO}_3\text{-N}$ dosage directly to the reactor. $\text{NO}_3\text{-N}$ dosage was supplied using a peristaltic pump at a constant flow rate of 1.7 L/d. Potassium nitrate (KNO_3) was used as $\text{NO}_3\text{-N}$ source in the dosage, and its concentration was varied depending on effluent nitrates concentrations values. A mean nitrate loading rate of 1.9 g $\text{NO}_3\text{-N}$ /d (79 mg $\text{NO}_3\text{-N}$ /L with respect to the influent flow rate) was added to the HMABR. In the case of a real plant, there would be enough membrane surface area for nitrification, so that the $\text{NO}_3\text{-N}$ dosage would not be required. Table 3-1 shows the established approximate values of various operational parameters.

Table 3-1 Operational conditions during the experimental campaign

Parameter	Symbol	Value	Units
Hydraulic retention time	HRT	14	h
Mixed liquor suspended solids	MLSS	3000	mg/L
Recycle rate	Q_R	185	Influent %
sCOD loading rate	-	0.15	Kg sCOD/m ³ d
NH ₄ -N loading rate	-	0.0075	Kg N/m ² d
Intra-membrane relative air pressure	MAP	7	kPa
Temperature	T	22	°C

3.3.1.4 Analytical methods

In order to characterize the biological behavior of the HMABR process, samples were taken twice or three times per week from the influent tank and from the HMABR reactor. The following parameters were analyzed according to the Standard Methods (APHA, 2005): total and soluble chemical oxygen demand (tCOD and sCOD), total and volatile suspended solids (TSS and VSS), ammonia nitrogen (NH₄-N) and nitrate nitrogen (NO₃-N). Daily measurements of pH, temperature and dissolved oxygen (DO) inside the HMABR were taken, using a glass electrode pH meter (CRISON Digilab - 517) and a portable DO meter (WTW OXI 340i) respectively. The details of the analytical methods are described in chapter 2.

3.3.1.5 Mass balances in the HMABR

A simplified mass balance where only dissolved compounds were considered was performed for the HMABR to assess the capacity of the system to remove the nitrogenous compounds.

In this system, nitrogen removal was calculated based on nitrification-denitrification processes (see Figure 3-5).

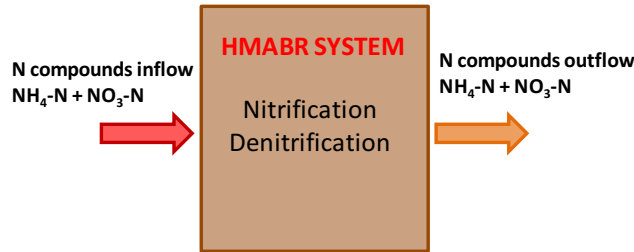


Figure 3-5 Nitrogen mass balance for this study.

The amount of nitrogen mass balance in the HMABR system in this study was presented as follows:

$$(NH_4 - N + NO_3 - N)_{in} = (NH_4 - N + NO_3 - N)_{eff} + N_{den} \quad \text{Eq. 3-1}$$

Where subindex *in* is influent, *eff* is effluent and *den* is denitrified.

In anoxic processes where denitrification occurs leading to heterotrophic growth and COD consumption, nitrogen assimilation due to bacterial growth was found to be in the same order as the hydrolysis of organic nitrogen (Albizuri et al., 2012). Thus, nitrogen assimilation in this case was considered negligible.

In the nitrification process, ammonium nitrogen was assumed to be converted to nitrates by nitrifying bacteria under aerobic conditions. Specific nitrification rate (SNR) per membrane surface area (g N/m²d) was calculated as follows:

$$SNR = \frac{Q_{in} \cdot (NH_4 - N_{in} - NH_4 - N_{eff})}{A_m} = \frac{Q_{in} \cdot (\Delta NH_4 - N)}{A_m} \quad \text{Eq. 3-2}$$

Where Q_{in} represented the influent flow rate (m³/d), $\Delta NH_4 - N$ corresponded to the removed ammonia concentration (g/m³) calculated as the difference between influent ammonia and effluent ammonia concentration, and A_m was the total membrane area (m²).

Denitrification rate (DNR) per reactor volume (gN/m³d) was obtained solving the following equation:

$$DNR = \frac{Q_{in} \cdot (\Delta NH_4 - N + NO_3 - N_{dos} - NO_3 - N_{eff})}{V_R} \quad \text{Eq. 3-3}$$

Where the denitrified nitrate concentration (g/m³), corresponded to the difference between the total available nitrates in the system and effluent nitrate concentrations ($NO_3 - N_{eff}$). The available nitrate concentrations in the reactor were

calculated based on the sum of nitrates produced as a result of nitrification process (ΔNH_4-N) and nitrates provided by dosing (NO_3-N_{dos}). V_R corresponded to the liquid volume of the HMABR reactor (m^3).

Nitrogen assimilation was found to account for less than 10% of the total nitrogen removed in the reactor.

3.3.1.6 Nitrification and denitrification batch tests

Nitrate production rate (NPR) and nitrate uptake rate (NUR) batch tests were carried out under no substrate and electron acceptor limiting conditions, in order to evaluate the activity of nitrifying and denitrifying biomass separately in both, biofilm and in suspended biomass. NPR and NUR batch tests allowed to estimate the relative abundance of each biomass in biofilm and suspended phases.

Further information regarding analytical methods of NPR and NUR batch tests is provided in chapter 2.

3.3.2 Simulation study

According to the second objective proposed in the present study, once the criteria for the optimum performance of the HMABR were established from the experimental study, a new HMABR mathematical model was developed. Then, the model was calibrated by matching the experimental results of the HMABR pilot plant, which referred to the general operation of the continuous plant (effluent NH_4-N , NO_3-N , COD, TSS concentrations, nitrification and denitrification rates) as well as to the batch test essays (nitrate production rate (NPR) and nitrate uptake rate (NUR) in biofilm and activated sludge). The calibrated model, able to reproduce the behavior of the HMABR, was used to establish optimum design and operation parameters for the HMABR process (for treating urban raw wastewater), by systematic simulation studies. Therefore, in this section, first the HMABR mathematical model, second the HMABR calibration methodology, and third, the simulation systematic studies carried out will be presented.

3.3.2.1 HMABR mathematical model

The HMABR mathematical model included three submodels: the biochemical model, the physic transport model, and the gas transfer model, which were implemented in AQUASIM 2.1 simulation platform (Reichert, 1994). The mentioned submodels will be described in this section, distinguishing the parameters which were adopted from the literature and the ones that were

obtained through the calibration process. Finally, the model implementation in AQUASIM simulation platform will be presented.

Biochemical model

Biochemical microbial kinetics and stoichiometries taking place both in the sludge and in the biofilm were based on Activated Sludge Model ASM2d (Henze et al., 2000). Therefore, substrate utilization and biomass synthesis by active bacterial cells in the biofilm and in suspended biomass were simulated with Monod kinetics. Each of these rate expressions included the product of several Monod terms and sometimes switching functions that depicted the simultaneous effects of electron donor, electron acceptor, and environmental conditions on the specific growth rate. Kinetic and stoichiometric parameters, as well as the matrixes of the process rate equations and stoichiometries of the ASM2d biochemical model were mostly adopted from the literature (Henze et al., 2000) and are summarized in Tables S-1, S-2, S-3 and S-4, of supplementary material section.

An extension of the ASM2d model proposed by Larrea et al., (2002), where the slowly biodegradable COD was divided into soluble (S_L) and particulate fractions (X_S) was considered.

In the same way as in Albizuri et al., (2009), the hypothesis of Ekama and Marais, (1979) was assumed, which stated that once X_S was attached to the enzymes present in the surface of heterotrophic bacteria in suspended flocs, it was hydrolyzed and consumed on the flocs itself, without releasing S_S to the bulk liquid. That is why a direct synthesis metabolism of X_S and S_L to heterotrophic bacteria (X_H) was adopted, maintaining in the kinetic expression the hydrolysis saturation coefficient. For S_L metabolism, a Monod expression was used. For X_S , an adsorption-hydrolysis kinetic was implemented (described in Table S-3 of supplementary material).

With respect to the wastewater characterization, soluble COD in ASM2d model was fractioned in readily biodegradable COD (S_S), slowly biodegradable COD (S_L), and in inert soluble COD (S_I). Particulate COD (pCOD), in ASM2d terms, was fractioned in heterotrophic bacteria (X_H), inert particulate COD (X_I) and slowly biodegradable COD (X_S). Each COD fraction, was associated with a nitrogen content ($i_{n,si}$ and $i_{n,xi}$), for which default values of the ASM2d model were adopted (Henze et al., 2000), except for the nitrogen content in X_S , ($i_{n,xs}$) in which a lower value (0.03 gN/gCOD) was adopted, according to Larrea et al., (2002). COD fraction values were mostly estimated from the experimentally prepared feed wastewater characterization, except the X_I/X_S fraction value, which was adjusted

during the calibration process in order to match the experimentally measured MLSS concentrations. Adopted COD fraction values will be explained in the model calibration section.

Physical transport model

For the physical transport model, the one-dimensional mixed culture biofilm (MCB) model (Wanner and Reichert, 1996) was used. Besides, an extension of the MCB model (Extended MCB model) developed at CEIT (Albizuri et al., 2009) was implemented.

The MCB model considers four essential elements in a biofilm process: the bulk liquid, the liquid diffusive layer at the biofilm surface, the biofilm, and the biofilm support media. The model is one dimensional in space, that means, only the space coordinate perpendicular to the support media is considered. In addition, it also considers the interactions between the different elements, including the attachment and diffusion of particulate components in the biofilm. Thus, the mass balance equations developed for each element allowed the simulation of biofilm thickness, spatial and temporal distribution of dissolved (S_i) and particulate (X_i) compounds within the biofilm, and the temporal distribution of S_i and X_i in the bulk liquid. The same kinetics and stoichiometric parameters of the ASM2d model were considered in the biofilm.

In the MCB model two groups of parameters can be differentiated: 1) the ones determining the behavior within the biofilm, and 2) the ones which determine the interaction of soluble and particulate components in the bulk liquid and in the biofilm. Regarding the parameters of the first group, a diffusion coefficient for all soluble components (D_{S_i}), densities of particulate components within the biofilm (ρ_{X_i}), a volumetric fraction of the biofilm (θ), and a biofilm diffusion coefficient for all the different particulate components (D_{X_i}) were selected. Concerning the parameters related with the interaction between the bulk liquid and the biofilm, in the present study a biofilm detachment coefficient ($K_{DE,B}$), which determined the biofilm thickness and the flux of detached particulate components from the biofilm to the bulk liquid, was adjusted. The liquid diffusive layer (LDL), which defined the penetration of soluble compounds towards the biofilm, was also taken as a fitting parameter.

As mentioned above, the Extended MCB model developed at CEIT (Albizuri et al., 2009) was also considered in the HMABR mathematical model. In the extended MCB model, colloids were incorporated in the state variables of particulate components, leading to three different states for such components: colloids ($X_{i,C}$), flocs ($X_{i,F}$) and biofilm. Colloid concentration was the result of the applied colloid

load by the influent, and the interaction with both, flocs through new attachment and detachment phenomena, and biofilm.

With respect to the interaction between colloids and flocs in the bulk liquid, in the Extended MCB model, attachment from colloids to suspended flocs was modelled as an adsorption process whereas the detachment from suspended flocs to colloids was simulated as a zero order process (Table S-5 supplementary material), considering that the detachment was only dependent on the external shear forces. Parameter values for colloids saturation (K_c), attachment to flocs ($K_{AT,F}$) and detachment from flocs ($K_{DE,F}$) were adopted according to Albizuri et al., (2009). Concerning the interaction between the colloids and the biofilm, an attachment coefficient of colloidal matter to the biofilm ($K_{AT,Bxc}$) was also adopted. The values of these parameters are summarized in Table S-6 of supplementary material.

Gas transfer model

In the HMABR model, a gas permeable membrane supplied oxygen at the biofilm base, while organic carbon and ammonia nitrogen were supplied from the bulk liquid. Oxygen flux (J_{O_2}) from the gas phase to the biofilm through the gas permeable membrane was given by the following equation:

$$J_{O_2} = AK_m \left(C_{O_2,g} / H_{O_2} - C_{O_2} \right) \quad \text{Eq. 3-4}$$

Where $C_{O_2,g}$ and C_{O_2} were the concentrations of oxygen in the air gas and biofilm phases respectively, K_m was the overall mass transfer coefficient in the membrane, A the membrane/biofilm surface and H_{O_2} the Henry coefficient for oxygen. A corresponded with the employed total membrane surface area (0.11 m²) and $C_{O_2,g}$ was calculated from the supplied average MAP of 7 kPa (where 21% of oxygen was considered). K_m value was adjusted in order to describe the observed nitrification rates in the biofilm.

The physical transport parameters adopted in the HMABR mathematical model are summarized in Table S-6 of supplementary material.

Model implementation in AQUASIM simulation platform

The HMABR mathematical model, which included the explained biochemical, physical transport, and gas transfer submodels was implemented in AQUASIM 2.1 simulation platform developed by EAWAG (Reichert, 1994). The steady-state mathematical model described a continuous-flow biofilm reactor.

The biofilm and the bulk liquid were modelled as a biofilm reactor compartment. The interior of the membrane was modelled as a completely mixed air filled compartment and the wall of the membrane permeable to oxygen as a diffusive link connected to the biofilm base. The inverse of H_{O_2} was specified in the diffusive link as a conversion factor for oxygen concentration in the air filled compartment.

The secondary settler was assumed to perform with a settling efficiency of 100%. Thus, the recirculation and wastage of suspended flocs were modelled as advective links from the bulk liquid compartment.

Once the HMABR model was implemented in AQUASIM, experimental HMABR operational conditions (Table 3-2) such as, reactor volume (V_R), biofilm area (A) influent flowrate (Q_{in}), wastage flow rate (Q_w), solids recirculation flow rate (Q_R), supplied membrane air pressure (MPA), and temperature (T) were defined, for which experimental average operational parameters values were considered.

Table 3-2 HMABR model operational parameters

Parameter	Symbol	Value	Units
Reactor volume	V	1.42×10^{-2}	m^3
Biofilm area	A	0.11	m^2
Influent flow rate	Q_{in}	2.5×10^{-2}	m^3/d
Recirculation flow rate	Q_R	4.4×10^{-2}	m^3/d
Wastage flow rate	Q_w	2×10^{-3}	m^3/d
Intra-membrane air pressure	MPA	7	kPa
Temperature	T	22	$^{\circ}C$

3.3.2.2 HMABR model calibration

The objective of this section was to obtain a HMABR mathematical model able to reproduce the experimental behavior of the HMABR technological process. For that purpose, first the HMABR mathematical model was developed (explained above). Then, the model parameters were selected according to literature and the model ability for reproducing the behavior of the HMABR process was evaluated. Finally the fitting parameters which were necessary to adjust in order to match the experimental results of the HMABR pilot plant, which referred to the general operation of the continuous plant, as well as batch test results (nitrate production rate (NPR) and nitrate uptake rate (NUR) in biofilm and activated sludge), were adopted. In this section, model parameters that were adopted together with the ones which were necessary to adjust (fitting parameters) will be explained, as well as the performed calibration methodology.

Parameters of the biochemical model

With respect to the biochemical model, kinetic and stoichiometry parameters, the process rate equations and stoichiometries for the ASM2d model were mostly adopted from literature (Henze et al., 2000), and are summarized in supplementary material (Tables S-1, S-2, S-3 and S-4 respectively).

According to the ASM2d extension proposed by Larrea et al., (2002), S_L was characterized by a high diffusion coefficient ($D_{S_L}=1.04 \cdot 10^{-4} \text{ m}^2/\text{d}$) equal to the readily biodegradable COD (S_S) (Perry and Green, 1999). For S_L metabolism, a Monod expression with a lower growth coefficient than for S_S ($\mu_{H,S_L}=3 \text{ d}^{-1}$) and with an equal saturation coefficient than for S_S ($K_{S_L}=4 \text{ g/m}^3$) was used. For X_S , an adsorption-hydrolysis kinetic with the same coefficient values as adopted by Henze et al., (2000) was considered ($\mu_{H,X_S}=3 \text{ d}^{-1}$ and $K_X=0.1 \text{ g/m}^3$).

As explained in materials and methods section of the experimental stage a conventional medium-high strength urban raw wastewater was tried to reproduce, by mixing different portions of primary sludge, the supernatant resulting from its acid fermentation, and sludge return liquor of an urban wastewater. These concentrated portions were diluted with tap water in order to get the desired TSS, $t\text{COD}$, $s\text{COD}$ and $\text{NH}_4\text{-N}$ concentrations. Influent soluble ($s\text{COD}$) and particulate ($p\text{COD}$) COD values were experimentally measured, and the fractionation of each according to the HMABR biochemical model is described below.

Soluble COD (sCOD)

sCOD was determined by filtering the samples through filters with a pore size of 0.45 μm . Influent sCOD resulted in an average value of 90 mg/L. sCOD in ASM2d terms was fractionated into readily biodegradable COD (S_S), slowly biodegradable COD (S_L), and in inert soluble COD (S_I).

Readily biodegradable soluble COD (S_S) fraction

Referring back to the preparation of feed wastewater in the present study, for the sCOD supply, the supernatant resulting from the primary sludge acid fermentation, very rich in VFAs, was used. That is why the proportion of S_S with respect to the sCOD was initially assumed to be greater than a conventional urban raw wastewater, of about 60%. However, an average influent sCOD value of 90 mg/L was obtained due biological degradation episodes occurred inside the storage tank. It was considered that most of the degraded sCOD in the storage tank corresponded to the S_S fraction. Therefore a slightly lower influent S_S proportion with respect to the sCOD was finally considered, of around 40%.

Inert soluble COD (S_I) fraction

Influent S_I fraction, was estimated by measuring the experimental effluent sCOD values, when the HMABR pilot plant was operating under stable conditions and no effluent residual $\text{NO}_3\text{-N}$ limitations, which allowed the biodegradable sCOD (S_S and S_L) to be entirely consumed in the HMABR. According to Melcer et al., (2003) for municipal wastewater treatments, it is usually reasonable to assume that there is no generation of S_I during the process. Average effluent sCOD concentrations resulted in pretty constant values, of around 36 mg/L, indicating that most of the biodegradable COD was removed in the reactor and that the resulting effluent sCOD concentrations were essentially inert. So it was assumed that 40% of the influent sCOD corresponded to the S_I fraction.

Slowly biodegradable soluble COD (S_L) fraction

S_L fraction was estimated by subtracting S_S and S_I fractions from the average measured influent sCOD concentration, resulting in a portion value of 20% relative to the sCOD.

Particulate COD (pCOD)

pCOD in the biochemical model was fractioned in: heterotrophic bacteria (X_H), inert particulate COD (X_I) and slowly biodegradable COD (X_S). Each influent particulate component (X_I) was in turn fractioned into 5% colloidal mater (X_{i_c}) and 95% flocs (X_{i_f}). pCOD concentration was calculated by subtracting the experimentally measured mean sCOD concentration (90 mg/L) from the average t COD concentration (590 mg/L), resulting in an average value of 500mg/L.

Fraction of heterotrophic bacteria (X_H)

X_H accounted for a 5% of pCOD, in accordance with the wastewater characterization proposed by Caminos (2010).

Inert (X_I) and slowly biodegradable (X_S) COD fractions

The remaining 95% of pCOD was fractioned in X_I and X_S . For systems treating raw municipal wastewater, X_S can range between 28-74% with respect to the t COD, and inert particulate material (X_I) between 8-39% (Roeleveld and Van Loosdrecht, 2002; Marquot et al., 2006). The X_I/X_H ratio was adjusted within the reported ranges, in order to match the experimental measured mixed liquor suspended solids (MLSS) concentrations.

The correlation between the fractionation of the experimental influent COD and the one adopted in the HMABR model is summarized in Figure 3-6 (fitting parameter values adopted for X_S and X_I will be further explained in model calibration results section).

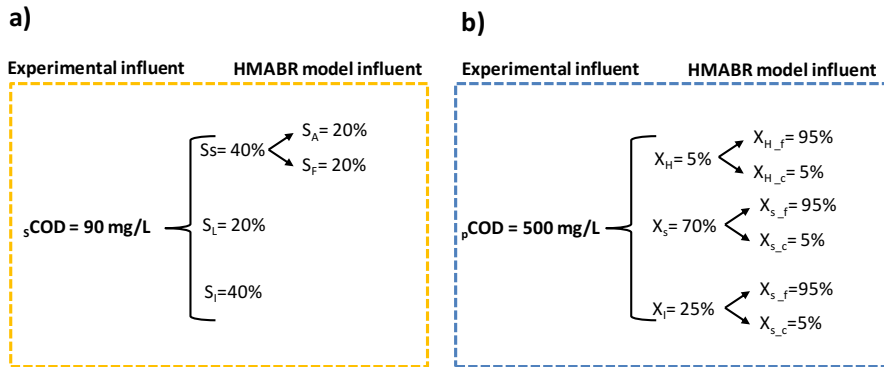


Figure 3-6 Fractionations of influent soluble COD (a) and particulate COD (b) in the HMABR model.

Parameters of the physical transport model

A diffusion coefficient (D_{Si}) for all soluble components of $2.10^{-4} \text{ m}^2/\text{d}$ (Wanner et al., 2006) was adopted. Besides, different densities (ρ) for particulate components within the biofilm were selected, considering a higher density value for nitrifying biomass (X_A) and a lower density value for X_H , X_i and X_s (Tackács et al., 2007). The density of the particulate components was fixed at $\rho_{X_A} = 400 \text{ KgCOD}/\text{m}^3$, $\rho_{X_H} = 150 \text{ KgCOD}/\text{m}^3$ and $\rho_{X_i-X_s} = 100 \text{ KgCOD}/\text{m}^3$ and the volumetric fraction of the biofilm (θ) at 0.8 (Wanner et al., 2006). For all the different particulate components ($X_{i,c}$ and $X_{i,f}$), a biofilm diffusion coefficient (D_X) of $1.10^{-9} \text{ m}^2/\text{d}$ (Wanner et al., 2006) was selected.

The parameter values concerning the interaction between colloids and flocs in the bulk liquid, and between colloids and the biofilm, that is, colloids saturation (K_C), attachment to flocs ($K_{AT,F}$), detachment from flocs ($K_{DE,F}$) and attachment of colloidal matter to the biofilm ($K_{AT,BXC}$), were adopted from Albizuri et al., (2009) (Table S-6 supplementary material).

Biofilm detachment coefficient ($K_{DE,B}$) was adjusted in order to obtain a biofilm thickness (L_F) in the range of 50 to 200 μm . These values are consistent with biofilm thicknesses reported by Boltz et al., (2009) for hybrid (IFAS) processes, who stated that lower biofilm thicknesses values were expected in IFAS processes compared with MBBR processes ($L_F = 600 \mu\text{m}$), due to the higher substrate demand by suspended biomass (maintaining lower soluble biodegradable COD concentrations in the bulk liquid).

LDL was adjusted in a range between 100 and 250 μm , in accordance with Wanner et al., (2006) and Boltz et al., (2009), who proposed LDL values between 100-200 and 50-120 μm respectively. Both stated that LDL value depended on the stirring in the reactor, acquiring lower values for higher stirring intensities. This parameter determined the soluble component fluxes towards the biofilm, and thus biofilm nitrification rates.

Parameters of the gas transfer model

The membrane oxygen mass transfer coefficient (K_m) was fitted so that nitrification rates observed in the biofilm could be reproduced. K_m values between 1 and 5 m/d were selected, being consistent with the values proposed by Li et al., (2010) for hydrophilic treated microporous polymeric membranes (as in the present experimentation), where the membrane pores can remain filled with the bulk water, resulting in lower K_m than for microporous hydrophobic membranes.

HMABR model calibration methodology

The calibration process consisted in an iterative step-wise procedure (Figure 3-7). First, initial values for the fitting parameters were selected, between the ranges reported by the literature described above. The next step was to carry out simulations and check them against the average behavior of the continuous operation of the HMABR. Then, fitting parameters were adjusted until the steady-state simulations matched experimental values (Loop 1). The steady state simulations provided the biomass concentration both in suspended flocs and biofilm of the HMABR process, and allowed the simulation of NPR and NUR batch tests. The results of batch tests simulations were checked against experimental batch tests results and the fitting parameters were adjusted until a satisfactory fitting was attained (Loop 2).

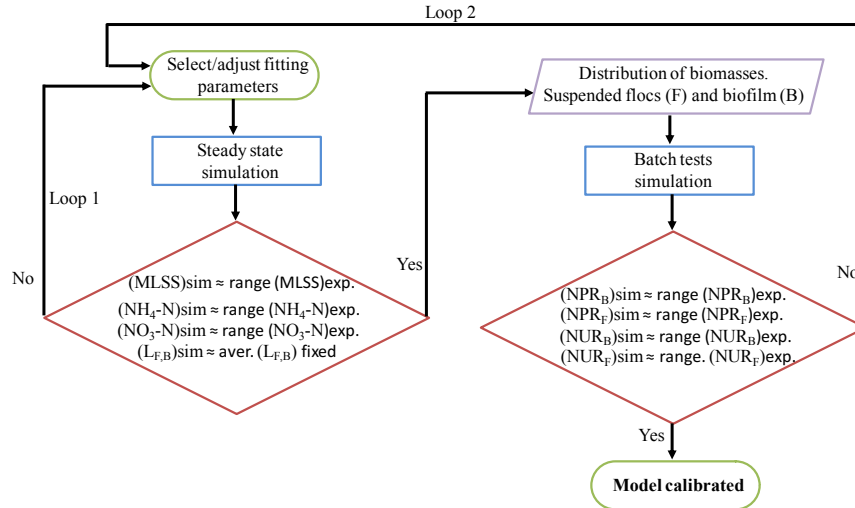


Figure 3-7 Flow chart of the iterative step-wise procedure for the HMABR mathematical model calibration.

With respect to the fitting parameters, first the X_i/X_s fraction was adjusted so that the experimental MLSS concentration of the continuous operation of the HMABR could be reproduced. Then, the membrane oxygen mass transfer coefficient K_m , was fitted in order to match effluent average ammonium concentration with the steady-state simulations results.

Biofilm detachment coefficient ($K_{DE,B}$) value was also adjusted so that the steady-state simulations of the HMABR could predict biofilm thicknesses (L_f) in the range of 100 to 250 μm , being these values consistent with the biofilm thicknesses reported for IFAS processes by Boltz et al., (2009). Biofilm thickness variation had a small effect in the effluent ammonium concentration in the steady-state simulation results, as ammonium concentration within the biofilm ($\text{NH}_4\text{-N}_{\text{biof}} > 15 \text{ mg/L}$) far exceeded the ammonium half saturation constant value for nitrifying organisms ($K_s=1 \text{ mg/L}$). However, biofilm detachment coefficient determined the particulate detachment flux from the biofilm to the suspended phase. Although $K_{DE,B}$ did not have a significant impact in reproducing MLSS concentration in the present HMABR process, it had a great effect in determining the concentration of nitrifying bacteria in suspended flocs, and thus in the reproducibility with the model of the experimental NPR batch tests in the suspended biomass.

LDL was adjusted in a range between 50 and 200 μm , in accordance with Wanner et al., (2006) and Boltz et al., (2009) in order to predict biofilm NPR and NUR observed during batch tests. The tested LDL value range during the calibration

process did not have a significant impact in the simulated steady-state nitrification behavior, as ammonium fully penetrated the biofilm in the continuous operation results. LDL had a slightly greater effect in the simulated NPR and NUR batch tests performed in the biofilm. As substrate concentrations decreased over time during batch tests essays, $\text{NH}_4\text{-N}$ and sCOD fluxes towards the biofilm were more affected by LDL thickness. Thus, LDL value was fitted so that NPR and NUR batch tests in the biofilm could be reproduced.

In Table 3-3 the experimental results which were intended to reproduce with each fitting parameter are represented.

Table 3-3 Summary of fitting parameters adopted during the HMABR model calibration process

Fitting parameter	Experimental result intended to reproduce
X_I/X_S	MLSS
K_m	$\text{NH}_4\text{-N}_{\text{eff}}$
K_{DE}	$L_F, \text{NPR}_{\text{SUSP.}}$
LDL	$\text{NPR}_{\text{BIOF}}, \text{NUR}_{\text{BIOF}}$

3.3.2.3 Systematic simulation studies for the optimization of the design and operation of the HMABR process

The optimization process was based on the analysis of several plots which contained curves that were obtained by connecting the points derived from an optimization systematic simulation study. Each optimization point was obtained by a step-wise iterative simulation procedure (Figure 3-8), in which the HMABR process design and operational parameters were adjusted (Figure 3-8, top part) in order to fulfill the constraints imposed in the steady-state simulation results (Figure 3-8, bottom part). In each optimization, a single design-operation parameter was determined, keeping the rest of the parameters with predefined constant values.

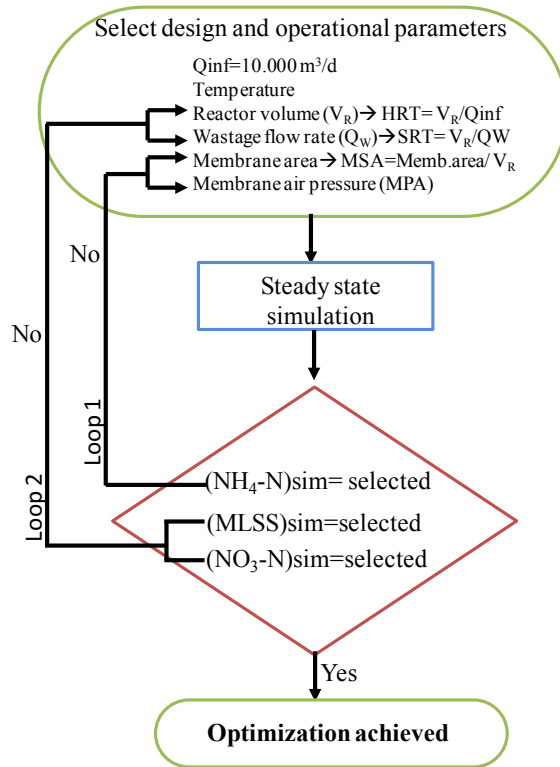


Figure 3-8 Schematics of the optimization process methodology during the systematic simulation studies.

The optimization process was made for treating 10000 m³/d of a conventional medium strength urban raw wastewater, fractioned in: 40 mg/L of NH₄-N (S_{NH_4}), 70 mg/L of S_s, 20 mg/L S_L, 350 mg/L X_S (340 mg/L X_{SF} and 10 mg/L X_{Sc}), 150 mg/L X_I (140 mg/L X_{IF} and 10 mg/L X_{IC}), and 5 mg/L X_H (2.5 mg/L X_{HF} and 2.5 mg/L X_{HC}).

In Figure 3-8, it can be noticed that in the most internal loop (Loop 1) in order to determine the required membrane air pressure (MAP) or membrane surface area, these should be adjusted so that the desired effluent ammonium concentration could be obtained: In this case, an effluent ammonium concentration value of around 4 mg/L was imposed as a constraint in order to prevent ammonium limiting conditions within the biofilm so high nitrification rates could be achieved. To that end, a biofilm thickness of 160 μm was adopted in all simulations (within the typical values for IFAS processes).

In the next loop (Loop 2), for determining the wastage flow rate (Q_w) or the reactor volume (V_R), these parameters were adjusted until the desired MLSS or

effluent nitrate concentrations were achieved, which were selected within a logical range of values.

Method to build design optimization plots at 12°C

A first plot which determined the required MAP according to the membrane area for achieving an effluent ammonium concentration of around 4 mg/L at 12 °C, was developed. Each point was calculated for MLSS concentrations of 2500, 3000, 4000, and 4500 mg/L and HRTs of 2, 2.5 and 3 hours. The following membrane area values were predefined in the simulations: 120000, 150000 and 180000 m². MAP and wastage flow rate (Q_w) were adjusted so that desired effluent ammonium ($\text{NH}_4\text{-N} \approx 4$ mg/L) and selected MLSS concentrations could be achieved.

The selected membrane material (microporous or oxygen permeable dense membranes) for the HMABR process, determines the operating pressure range in order to avoid air bubble formation at membrane surface. In this way, microporous hydrophobic membranes (i.e. polypropylene membranes), are restricted to operate at low gas pressures in order to avoid bubble formation at membrane surface. For instance, air bubbles at membrane pressures from 1 to 20 kPa have been observed for microporous membranes (Côté et al., 1988; Eguía 1991; Vidart 1992; Ahmed and Semmens, 1992). Oxygen permeable dense membranes (i.e. silicone membranes) due to their nonporous nature, have the advantage that they can be operated at much higher gas pressures, from 100 to 270 kPa without bubble formation (Weiss et al., 1998; Casey et al., 1999), increasing the concentration gradient and therefore the mass transfer rates.

Thus, the first design optimization plot also allowed determining the required membrane area according to the MAP restrictions associated with different available membrane types (microporous, dense, composite membranes). An intermediate membrane mass transfer coefficient for all the pressures was considered. Further research is needed to evaluate the effects of different membrane materials both on MAP and mass transfer coefficients.

A second plot to determine the process optimum design HRT for achieving the desired effluent nitrate and/or MLSS concentrations, at 12°C, was built. For this purpose, first a membrane material scenario was adopted. Dense membranes operated at an intermediate MAP of 40 kPa were selected. Then, the required membrane area for accomplishing with effluent ammonium criterion ($\text{NH}_4\text{-N}_{\text{eff}} \approx 4$ mg/L) was undertaken from previous plot (Figure 3-14). In this case, at 12°C, the required membrane area resulted in 150000 m². Each point of the figure was

obtained by predefining a HRT value (thus, the reactor volume, V_R) and adjusting the wastage flow rate (Q_W) until the desired MLSS concentrations were achieved. Effluent nitrate concentration was the result derived from such adjustment. Three HRT cases were predefined: 2, 2.5 and 3 hours. MLSS concentrations of 2500, 3000, 3500, 4000 and 4500 mg/L were selected. This MLSS range was adopted in order to promote an effective solids settling and to avoid solids overflowing the secondary settler.

Development method for operation optimization plots

First, a plot which determined the required MAPs at different operation temperatures of 12, 16 and 20°C, for achieving the target effluent ammonium criterion was developed. As in the previous case, a dense membrane operated at an intermediate MAP of 40 kPa was considered, for which at 12°C, the required membrane area for achieving the target effluent ammonium concentration resulted in 150000 m² (Figure 3-14). Each figure point was calculated for HRTs of 2, 2.5 and 3 hours and for MLSS concentrations of 2500, 3000, 4000, and 4500 mg/L. In each simulation, first the membrane area (150000 m²), the HRT (V_R), and temperature values were selected, then MAP and Q_W were adjusted so that effluent ammonium criterion and desired MLSS concentrations were fulfilled.

A second plot that allowed determining the optimum MLSS concentration to be maintained with respect to the operational temperature and the desired effluent nitrate concentrations was developed. In this case, a HMABR design scenario was predetermined, corresponding with an intermediate HRT of 2.5 hours and a dense membrane area of 150000 m² operated at a MAP of 40 kPa (accomplishing with effluent ammonium criterion at 12°C). Each figure point was obtained by predefining the temperature value, the membrane area (150000 m²), and the HRT (2.5 h), and adjusting the wastage Q_W and the MAP so that the desired MLSS and effluent ammonium concentrations were achieved. Temperature values of 12, 16, and 20°C were predefined for each optimization point.

The values of design and operation parameters varied during each optimization plot are summarized in Table 3-4.

Table 3-4 Summary of design and operation parameters values during the optimization plots

	HRT (h)	MLSS (mg/L)	T ^a (°C)	Membrane area (m ²)	MAP (kPa)
Design optimization					
<i>First plot</i>	2, 2.5, 3	2500-4500	12	120000,150000, 180000	8- 140 ^{adj.}
<i>Second plot</i>	2, 2.5, 3	2500-4500	12	150000	40
Operation optimization					
<i>First plot</i>	2, 2.5, 3	2500-4500	12, 16, 20	150000	1-40 ^{adj.}
<i>Second plot</i>	2.5	2500-4500	12,16,20	150000	1-40 ^{adj.}

^{adj.} Adjusted parameters

3.4 RESULTS AND DISCUSSION

In this section results derived from the HMABR experimental stage and mathematical modeling will be explained and analysed.

3.4.1 Experimental results

3.4.1.1 Mixed Liquor Suspended Solids (MLSS) behavior

Figure 3-9 shows that the MLSS concentrations achieved in the experimental HMABR were maintained, as intended, within the order of magnitude typical of a conventional activated sludge process, reaching an average value of 3200 mg/L. To this end, the sludge wastage flow rate was adjusted in 2 L/d corresponding to an average SRT of 8 days. This was a relatively high anoxic SRT, typical design SRT values for anoxic processes may range from 3 and 6 days (Tchobanoglous et al., 2014). Some variability in the MLSS concentration occurred during the HMABR operation, which remained in a range between 2000 and 4000 mg/L. On the one hand, this change was due to the fluctuation of the influent TSS concentration. On the other hand, the relatively low MLSS concentrations (of about 2000 mg/L) that were measured in the HMABR, resulted from sludge raising or solids flotation episodes that were produced in the settler as a consequence of nitrogen gas resulting from biological denitrification. The refloated solids in the settler were subsequently returned to the HAMBR.

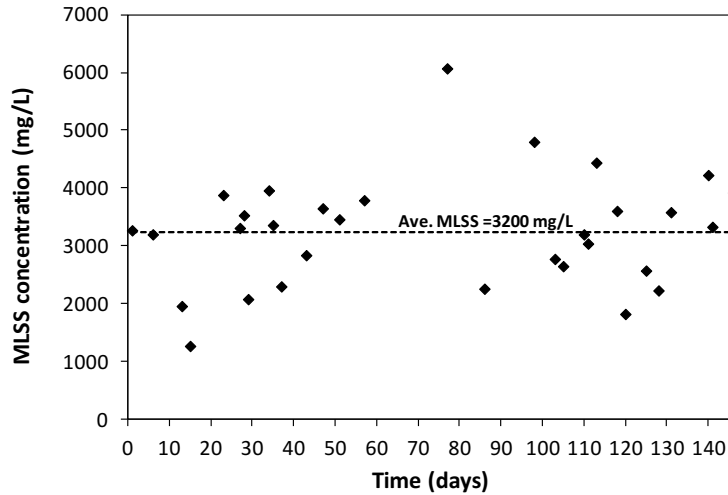


Figure 3-9 Evolution of MLSS concentration over time.

3.4.1.2 Removal of soluble Chemical Oxygen Demand (sCOD)

Regarding sCOD removal, it should be pointed out that although influent sCOD concentrations presented fairly marked variations (Figure 3-10), effluent sCOD concentrations resulted in pretty constant values. This fact indicated that mostly all biodegradable sCOD was removed in HMABR, resulting in an essentially inert effluent sCOD, of around 40 mg/L.

3.4.1.3 Nitrogen removal

Nitrification behavior

Concerning $\text{NH}_4\text{-N}$ removal, an average effluent $\text{NH}_4\text{-N}$ value of 22 ± 6 mg/L was obtained (Figure 3-11 a), which amply assured the non-limiting ammonium criterion for most operation days ($\text{NH}_4\text{-N}$ bulk liquid concentration > 10 mg/L). However, in Figure 3-11 a, it can be noticed that the ammonium removal and therefore nitrification rates experienced significant variations which will be discussed later.

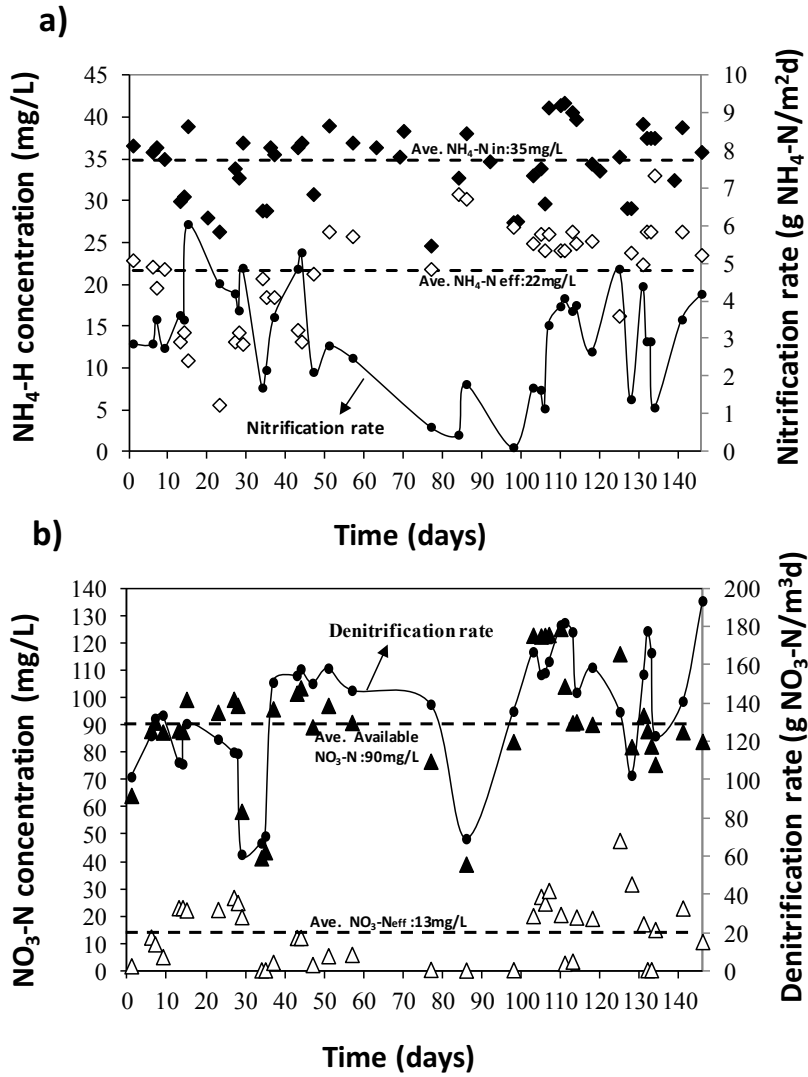


Figure 3-11 Performance of the HMABR over 145 days of operation. (a) Influent (closed diamonds, average black dashed line) and effluent (open diamonds, average gray dashed line) $\text{NH}_4\text{-N}$ concentrations and nitrification rates per unit of membrane area (closed circles with continuous line); (b) total available (closed triangles, average black dashed line) and effluent (open triangles, average gray dashed line) $\text{NO}_3\text{-N}$ concentrations, and volumetric denitrification rates (closed circles with continuous line).

Specific nitrification rates (SNR) per unit membrane surface area, were calculated based on the ratio between the removed ammonium loading (g/d) and the membrane area (Eq. 3-2). During the operation period high nitrification rates

were consistently achieved (except for days 77, 84 and 98 where nitrification rates $< 1 \text{ gN/m}^2\text{d}$ were obtained), attaining an average value of $3 \text{ gN/m}^2\text{d}$ (reaching a maximum value of $6 \text{ gN/m}^2\text{d}$). This average value was significantly higher than those obtained in previous HMABR investigations when air was supplied. Terada et al., (2006) operated a MABR as a sequencing batch reactor (SBR) where the nitrification occurred in the biofilm, while a bulk solution with suspended denitrifying-phosphate accumulating bacteria, was cycled between anaerobic/aerobic conditions, for simultaneous carbon, nitrogen, and phosphorus removal. In this study synthetic feed water was used, and the reactor was operated with MLSS concentrations of 2000 mg/L , obtaining an average nitrification rate of $0.96 \text{ gN/m}^2\text{d}$. Downing and Nerenberg, (2007) investigated a HMABR which was intended for nitrification in a membrane-aerated biofilm and denitrification in the bulk liquid. They operated the HMABR using synthetic wastewater with an average MLSS concentration of 200 mg/L , achieving a nitrification rate of $0.85 \text{ gN/m}^2\text{d}$. Downing and Nerenberg, (2008) achieved a slightly higher nitrification rate in their later HAMBR research, of $1 \text{ gN/m}^2\text{d}$. MLSS concentrations ranged from 50 to 250 mg/L , and effluent BOD was typically below the detection limit. Kunitz et al., (2016) reported the results of a 1-year study of a full-scale MABR which was installed in a side-stream at O'Brien Water Reclamation plant (Chicago, USA). The goal of this study was to evaluate the technology's ability to increase the existing aeration tank capacity by providing nitrification in a much smaller tank volume than the required by conventional activated sludge. The HMABR was operated with an average MLSS concentration of 2100 mg/L and effluent average $\text{NH}_4\text{-N}$ and filtered BOD concentrations of 6.6 and 3.6 mg/L respectively. In this case, a relatively high average nitrification rate of $1.6 \text{ gN/m}^2\text{d}$ was achieved.

Nitrification rates achieved in this study were also compared favorably to other technologies. A nitrifying activated sludge process can achieve volumetric nitrification rates of up to $100 \text{ gN/m}^3\text{d}$ (Tchobanoglous et al., 2014). The volumetric nitrification rate of the experimented HMABR ranged between 20 and $30 \text{ gN/m}^3\text{d}$. While the HMABR volumetric nitrification rates were considerably lower than a typical activated sludge process, the membrane specific surface area per reactor volume (or packing density) was only 7.7 m^{-1} , significantly lower than the 160 m^{-1} packing density achievable with rope-type IFAS systems (Sen et al., 2000). IFAS systems have achieved nitrification rates of 0.6 to $1 \text{ gN/m}^2\text{d}$ under aerobic bulk liquid conditions (Sen et al., 2000). MABRs (supplied with air) operating under TN removal conditions achieved nitrification rates ranging from 0.5 to $2.6 \text{ gN/m}^2\text{d}$ (Satoh et al., 2004; Terada et al., 2006; Jácome et al., 2006; Downing and Nerenberg, 2008).

The specific $\text{NH}_4\text{-N}$ removal rate per membrane area obtained in this study demonstrated that the present HMABR process had high nitrogen removal potential in a single reactor vessel.

Denitrification behavior

Denitrification rates also showed a significant variability (Figure 3-11 b). They were calculated based on the denitrified nitrate loading (g/d) and the liquid volume ratio (Eq. 3-3). Denitrification rate reached an average value of $136 \text{ gN/m}^3\text{d}$. This value corresponded with an average specific denitrification rate (SDNR) of 0.05 gN/gMLVSS/d . In a conventional post-anoxic process, SDNRs are found to reach values between 0.01 and $0.04 \text{ g N/g MLVSS/d}$ (Tchobanoglous et al., 2014). The high achieved denitrification rate in this study, as long as the system was operated under no $\text{NO}_3\text{-N}$ limiting conditions, was most likely due to the high anoxic SRT applied and to the removed biodegradable COD. DO concentration in the bulk liquid remained at 0 mg/L ; these anoxic conditions were probably due to the depletion of oxygen by the biofilm adhered onto the gas-permeable membrane, enhancing the denitrification process in suspension (avoiding denitrification process to be limited by the presence of DO). Therefore, almost all the readily biodegradable substrate was removed anoxically within the bulk liquid (primary denitrification). But as mentioned above, the availability of S_s , was not proved to be too high in this experiment. However, influent COD resulted in an average value of 600 mg/L , so it can be assumed that a great part of the denitrification was due to the anoxic degradation of slowly biodegradable COD (secondary denitrification). Furthermore, since the HMABR was operated with an average MLSS concentration of 3200 mg/L , the cell lysis due to endogenous respiration may have also played an important role in providing available biodegradable COD for the denitrification process (tertiary denitrification).

It should be taken into account that the potential denitrification capacity, essentially depended on the influent biodegradable COD concentration, whereas the denitrification rate, depended on the removed biodegradable COD concentration (or on the removed $\text{NO}_3\text{-N}$ concentration). In the same way, both (denitrification capacity and rates) depended on the effluent residual nitrate concentration, and on the heterotrophic denitrifying bacteria concentration, which were in turn related to the total MLSS of the HMABR.

As shown in Figure 3-11 b, the criterion of maintaining an effluent residual nitrate concentration above 5 mg/L was achieved on most days. Nevertheless, $\text{NO}_3\text{-N}$

concentrations above zero were found to have a large variability. To understand this variability it needs to be considered that $\text{NO}_3\text{-N}$ dosage was manually adjusted depending on denitrification rates that were observed, and aiming to comply with effluent residual nitrate concentration criterion. In cases when effluent $\text{NO}_3\text{-N}$ concentration values were greater than zero, was because the dosing provided a higher available $\text{NO}_3\text{-N}$ concentration than the system was able to denitrify, thereby preventing effluent $\text{NO}_3\text{-N}$ to be depleted.

In contrast, on certain days, effluent $\text{NO}_3\text{-N}$ concentrations reached values close to zero (Figure 3-11 b). This was attributed to specific episodes of higher influent sCOD and iCOD concentrations (Figure 3-10, days 77, 98, 107, 111, 113, 131 and 132) resulting in an increased denitrification capacity and thus in a greater $\text{NO}_3\text{-N}$ requirement. In other cases it was because of the lower input or availability of nitrates (sum of $\text{NO}_3\text{-N}$ produced in nitrification process and equivalent $\text{NO}_3\text{-N}$ provided by dosing) that took place in the system (Figure 5 b, closed triangles, days 34, 35 and 86), due to a decrease in nitrate dosage concentration, or due to the lower nitrate production rates during the nitrification process, resulting in a deficit of available nitrates to address the denitrification capacity.

Furthermore a correlation between the denitrification rates and MLSS concentrations was also observed, which in turn were associated with heterotrophic denitrifying biomass. This was reflected on days 13, 29, 86 and 128, when a drop of MLSS concentration occurred (Figure 3-9) due to sludge rising episodes produced in the settler, reducing the solids concentration that were recycled to the HMABR and resulting in decreased denitrification rates (Figure 3-11 b).

In a case of a real application, a dosage of $\text{NO}_3\text{-N}$ will not be possible, therefore design and operational parameters like HRT and SRT, should be adjusted so that the nitrates produced by nitrification of the influent ammonia will not be completely removed, ensuring a residual $\text{NO}_3\text{-N}$ concentration in the reactor. Thus, in case of a real application, HRT and SRT will decrease significantly so that the denitrification rate could be lower. This design optimization will be analyzed using the developed and calibrated HMABR mathematical model.

Correlation between nitrification rates and effluent $\text{NO}_3\text{-N}$ and sCOD concentrations

With respect to the performance of nitrification rates, it must be highlighted that this mainly depended on: effluent residual $\text{NH}_4\text{-N}$ concentration, delivered and available DO concentration for nitrification process, autotrophic nitrifying biomass concentration, and on the biofilm accessibility to the bulk liquid biodegradable sCOD.

In this experimentation, nitrification rates were not affected by effluent residual $\text{NH}_4\text{-N}$ concentration, as the established criteria of non bulk liquid ammonium limiting condition was always fulfilled.

Regarding the nitrification rates variability, it must be considered that they were completely correlated with effluent $\text{NO}_3\text{-N}$ and sCOD concentrations (Figure 3-12).

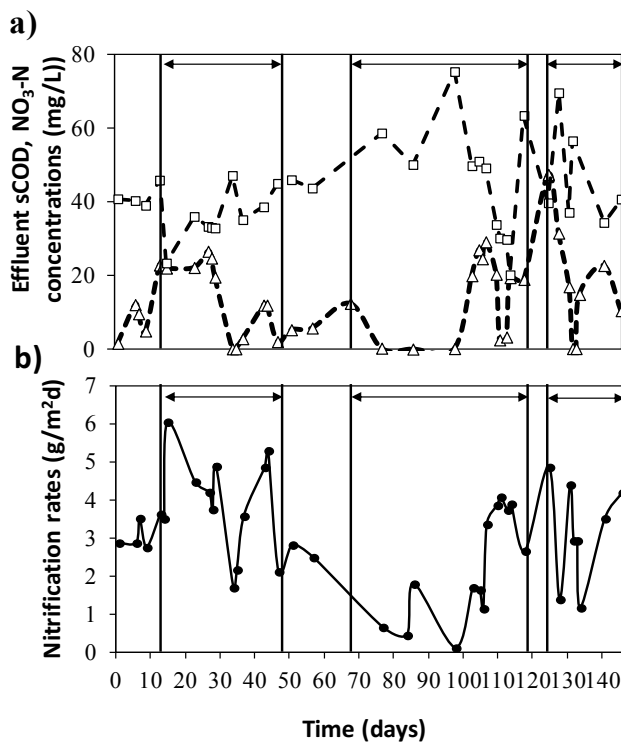


Figure 3-12 Relation between effluent $\text{NO}_3\text{-N}$ (open triangles) and sCOD (open squares) concentrations (a) and nitrification rates (black circles) (b).

Figure 3-12 shows a clear correlation between effluent $\text{NO}_3\text{-N}$ and sCOD concentrations, and nitrification rates. When effluent residual $\text{NO}_3\text{-N}$ concentrations decreased, effluent biodegradable sCOD concentrations increased, resulting in a decline of nitrification rates (Figure 3-12, days 34, 47, 77, 98, 118, 128 and 132). The same effect happened reversely, when effluent residual $\text{NO}_3\text{-N}$ concentrations were relatively high, a decrease in the available bulk liquid sCOD concentrations was observed, achieving higher nitrification rates (Figure 3-12, days 6, 15, 29, 43, 51, 103, 107, 110, 114, 125, 131 and 141).

Nitrates availability in the reactor allowed that almost all influent biodegradable sCOD was anoxically removed in the bulk liquid by heterotrophic denitrifying biomass. In this way, heterotrophic growth in the biofilm was limited, and so was the competence with autotrophic nitrifying biomass by the available DO and space within the biofilm.

On the contrary, when the bulk liquid presented nitrate limiting conditions, denitrifying biomass was not able to remove all influent biodegradable sCOD. Then, an increase in bulk liquid sCOD was produced, remaining accessible to the biofilm and consequently limiting nitrification rates.

3.4.1.4 Nitrification and denitrification batch tests

In this experimentation, NPR batch tests results showed that nitrification rate was nine times greater in the biofilm with respect to the suspended biomass (90% NPR in biofilm and 10% in suspended biomass). This is why it could be considered that as intended, practically all the nitrifying activity of the process took place in the biofilm. NPR batch tests in suspended biomass were performed under DO concentrations higher than 8 mg/L, while DO concentration in the bulk liquid during the HMABR experimentation was always lower than 0.2 mg/L, thus it can be assumed that nitrifying activity in suspended biomass during the experimental stage, was negligible. These results suggest that detected nitrifying activity in suspended biomass during batch tests, corresponded to the detached autotrophic nitrifying biomass from the biofilm.

NUR batch tests results indicated that denitrification rate was twenty times greater in suspended biomass than in the biofilm (95% NUR in suspended biomass and 5% in biofilm). So it can be assumed that the majority of the denitrification activity occurred in suspended biomass, which was one of the main goals of the present experimentation. Furthermore, it is worth noting that performed NUR batch tests in the biofilm, were carried out under not limiting bulk sCOD concentrations, and using N_2 gas for pressurizing the membrane and sparging the bulk liquid (in order to prevent any DO presence which could interfere in the

denitrification process). During the experimentation, the bulk liquid presented anoxic conditions, and sCOD was limiting in most cases (preventing its diffusion towards the biofilm). Besides the membrane was pressurized with air instead of N_2 gas. That is why in the real experimentation, denitrifying activity in the biofilm was expected to be much lower than the one detected by NUR batch tests.

3.4.2 Simulation results

3.4.2.1 HMABR model calibration

In this section, the adjusted values for the fitting parameters, which made possible to match the HMABR experimental results, will be presented. The predicted particulate and dissolved species distribution that took place within the biofilm will also be analysed.

Fitting parameters

With respect to the X_i/X_s ratio in the influent wastewater, it was adjusted to a value of 0.35, in order to match the experimental MLSS concentration. A membrane mass transfer coefficient (K_m) value of 3 m/d was able to reproduce the effluent ammonia concentration in the continuous operation of the HMABR process. Regarding the liquid diffusive layer (LDL), a value of 100 μm was considered the best in reproducing both, experimental continuous effluent ammonium concentration and biofilm NPR and NUR batch test results. Biofilm detachment coefficient ($K_{DE,B}$) was fitted to a value of 170 d^{-1} , which resulted in a 160 μm biofilm thickness, effectively reproducing the observed nitrification rates in the HMABR continuous operation and in the performed biofilm batch tests, as well as the NPR results in suspended biomass (as $K_{DE,B}$ determined the nitrifying suspended biomass concentration).

In Table 3-5 a summary of the adjusted fitting parameter values for the HMABR model calibration are presented.

Table 3-5 Adjusted values for the fitting parameters in the HMABR model

Fitting parameter	Adjusted value
X_i/X_S	0.35
K_m	3 m/d
K_{DE}	170 d ⁻¹
LDL	100 μ m

Therefore, the calibration of the HMABR model with the adjusted fitting parameters was able to match the experimental results with respect to bulk liquid $\text{NH}_4\text{-N}$, $\text{NO}_3\text{-N}$, sCOD and SSLM concentrations in the continuous HMABR operation, as well as NPR and NUR batch tests in suspension and in the biofilm (Table 3-6).

Table 3-6 Summary of experimental and model predicted continuous and batch test results of the HMABR

Continuous HMABR plant results	Symbol	Units	Experimental value	HMABR model value
Mixed liquor suspended solids concentration	MLSS	mg/L	3239±967	3200
Effluent ammonia concentration	$\text{NH}_4\text{-N}_{\text{eff}}$	mg/L	21.5±6.3	20
Effluent nitrate concentration	$\text{NO}_3\text{-N}_{\text{eff}}$	mg/L	14.4±11.5	13
Effluent soluble COD concentration	sCOD _{eff}	mg/L	43±12	42
Batch test results	Symbol	Units	Experimental Value	HMABR model value
Nitrate production rate in the biofilm	NPR_B	$\text{gN/m}^3\text{d}$	40.3	44.4
Nitrate production rate in suspended flocs	NPR_F	$\text{gN/m}^3\text{d}$	4.95	5.35
Nitrate uptake rate in the biofilm	NUR_B	$\text{gN/m}^3\text{d}$	23.6	25.12
Nitrate uptake rate in suspended flocs	NUR_F	$\text{gN/m}^3\text{d}$	704	756

It should be mentioned, that NUR batch test result in suspended biomass should had been higher than the obtained value if the essay had been carried out under non readily biodegradable substrate (S_s) limiting conditions. However, during NUR batch test essay in suspended flocs, important and fast acetate (S_s) degradation happened during the previous minutes prior to the start of the experiment. Thus NUR_F batch test essay was substantially carried out under slowly biodegradable COD (S_L and X_S) conditions (secondary denitrification), obtaining both, lower experimental and simulated NUR values. Despite this, experimental and model predicted NPR and NUR batch test results in the biofilm and in suspended flocs, confirmed that, as intended, most of the nitrification took place in the biofilm while the majority of the denitrification occurred in suspension. This can be validated when analyzing the model predicted steady-state biomasses concentrations in the biofilm and in suspension, resulting in an average nitrifying bacteria concentration (per bulk liquid volume) of 18 g/m^3 in the biofilm compared to 1.8 g/m^3 in suspension, and in a heterotrophic biomass concentration of 1082 g/m^3 in suspension in comparison with 9.8 g/m^3 predicted in the biofilm.

Predicted particulate and dissolved species concentration within the biofilm

Fixed densities of particulate components in the biofilm ($\rho_{XA}=400 \text{ KgCOD/m}^3$, $\rho_{XH}=150 \text{ KgCOD/m}^3$ and $\rho_{XI-XS}=100 \text{ KgCOD/m}^3$) together with the adopted volumetric water fraction (θ) of 0.8, led to an average total concentration of particulate components in the biofilm (X_{TOT}) of around 35000 g/m^3 , well within the typical ranges proposed by Maurer et al., (1999) and Boltz et al., (2009).

The fact of operating under non effluent $\text{NO}_3\text{-N}$ limiting conditions allowed all the readily biodegradable COD (S_s) to be consumed anoxically by suspended denitrifying heterotrophic organisms, limiting its diffusion towards the biofilm (Figure 3-13 b) and preventing nitrifying bacteria to be outcompeted by heterotrophic organisms (Figure 3-13 a).

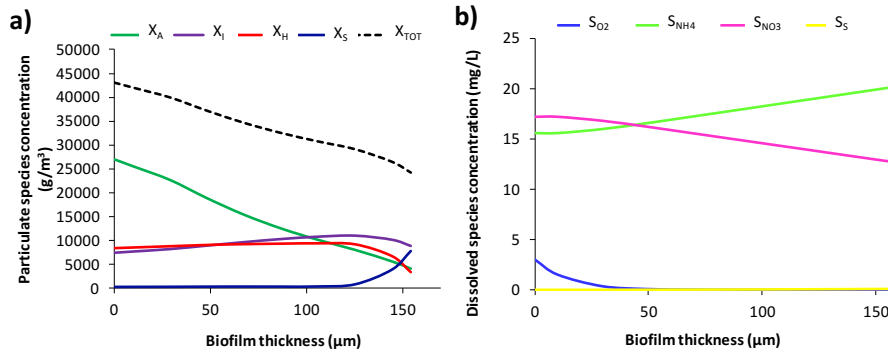


Figure 3-13 Model predicted particulate (a) and dissolved (b) species profiles within the biofilm.

As long as oxygen diffused through the biofilm and S_S did not fully penetrate into the biofilm depth (Figure 3-13 b), ammonium was oxidized in the deeper portions of the biofilm, dominated by autotrophic nitrifying biomass (Figure 3-13 a).

3.4.2.2 Systematic simulation studies

In this section results and discussion of the systematic simulation study which allowed defining some optimum design and operation parameters of the HMABR process, for different types of membrane scenarios and effluent requirements are presented. First, design optimization results for nitrification and denitrification at 12°C will be discussed. Then, the operation optimization results at different temperatures will be analyzed.

Design optimization plots at 12°C

Optimum nitrification

In Figure 3-14, as mentioned in materials and methods section, each point was calculated for different HRTs and MLSS concentrations. In order to fulfil the target effluent ammonium concentration around 4 mg/L, for membrane areas of 120000 m², 150000 m², and 180000 m², MAPs of 140, 40 and 8 kPa were required to supply respectively. Effluent ammonium criterion was accomplished for the selected HRTs and MLSS combinations within the following limits: HRT=2 h combined with MLSS from 3500 to 4500 mg/L, HRT=2.5 h combined with MLSS from 3000 to 4500 mg/L, and HRT=3 h, combined with MLSS ranging from 2500 to 4500 mg/L. In cases of HRT=2 h and MLSS < 3500mg/L, or HRT=2.5 h and MLSS <

3000 mg/L, effluent ammonium concentrations above 5 mg/L were obtained. These limits will be analysed below.

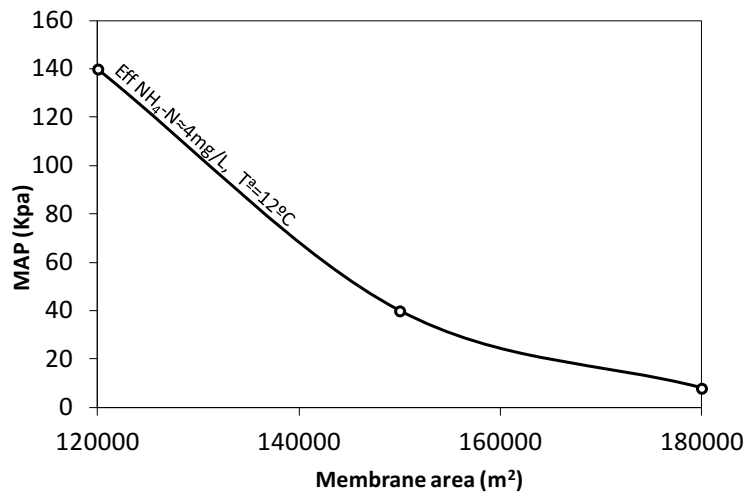


Figure 3-14 MAP required for different membrane areas in order to achieve effluent ammonium concentration of around 4 mg/L, at 12°C.

These results indicated that in most cases nitrification process was practically independent of the design HRTs and MLSS concentrations. To explain this, it must be underlined that in this simulation study, HRTs were varied by modifying the reactor volume, not the applied nitrogen loading (Kg N/d), thus, the removed nitrogen load (Kg N/d) remained the same, and HRTs only had an effect in MLSS concentrations. Nitrification process was practically independent of MLSS concentrations because the majority of nitrifying biomass (X_A) was retained in the biofilm (Table 3-7) and the resulting suspended X_A concentration was only caused by the accumulation of the detached biomass from the biofilm. Furthermore, the suspended X_A biomass was inactive due to the absence of DO in the bulk liquid. Therefore, in most cases (HRT: 2h with MLSS: 3500-4500 mg/L, HRT: 2.5h with MLSS: 3000-4500, HRT: 3h with MLSS: 2500-4500 mg/L), the total membrane areas and the supplied relative MAPs were the underlying design parameters influencing effluent ammonium concentrations.

Table 3-7 Example of obtained X_A concentrations in the biofilm and in suspension, for a membrane area of 150000 m², MLSS concentration of 3500 mg/L and HRT of 2, 2.5 and 3 hours

X_A (mg/L)	HRT (h)		
	2	2.5	3
Biofilm	335	293	242
Suspension	19.5	21	21.6

Similar isolines for achieving different effluent ammonium concentrations could be obtained. In case of a lower desired effluent ammonium concentration, ammonium isoline will be above the represented one in Figure 3-14, requiring higher MAPs for increasing nitrification capacities. However, if higher effluent ammonium concentrations want to be maintained, ammonium isolines below the represented one will be obtained.

The exceptions, in which effluent ammonium concentrations resulted in higher values than 5 mg/L, were attributed to a decrease in nitrification rates due to lower DO availability for nitrification process and/or lower nitrifying biomasses concentrations. Lower DO concentrations were caused by an increase in heterotrophic biomass (X_H) within the biofilm, which outcompeted nitrifying bacteria (X_A) by oxygen and space (impacting nitrification rates). The increase in heterotrophic biomass concentration within the biofilm was originated by a relatively high effluent residual S_S concentration (Table 3-8), which in the mentioned exceptions, was not completely consumed within the bulk liquid, thus, favouring its diffusion towards the biofilm.

Table 3-8 Comparison of two examples (membrane area = 150000 m² and HRT = 2.5 h) where target effluent ammonium concentration was and was not fulfilled

Effluent residual and biofilm biomasses concentrations (mg/L)	MLSS concentrations (mg/L)	
	3500	2500
Effluent NH ₄ -N	4.1	6
Effluent S_S	1.1	2.2
X_A Biofilm	293	239
X_H Biofilm	521	638

An analysis of the design depending on the different types of membranes scenarios and effluent ammonium requirement is presented next.

For a scenario in which membranes restricted to operate at relatively low gas pressures, like 8 kPa, are selected, higher membrane areas of 180000 m² were required for achieving the desired effluent ammonium concentration. On the contrary, if membranes that can be operated at much higher gas pressures, like 140 kPa without bubble formation, are selected, a slightly lower membrane area of 120000 m² could satisfy the predetermined effluent ammonium criterion. Nitrifying biomass concentration per biofilm volume remained practically unchanged for both membrane areas (Figures 3-15 a and 3-16 a). However, lower membrane areas also implied a lower overall nitrifying biomass concentration per reactor volume. Membranes operated at MAPs of 140 kPa, provided a higher DO availability within the biofilm, avoiding DO limitation at any biofilm layer (Figure 3-15 b). On the contrary, for membranes restricted to operate at lower MAPs (8 kPa), DO concentration became limiting for nitrifying bacteria located in the outer region of the biofilm (Figure 3-16 b). Thus, in case of dense membranes (140 kPa), slightly lower membrane areas were required, compensating the increased biofilm nitrification capacity by decreasing the amount of total nitrifying biomass in the reactor.

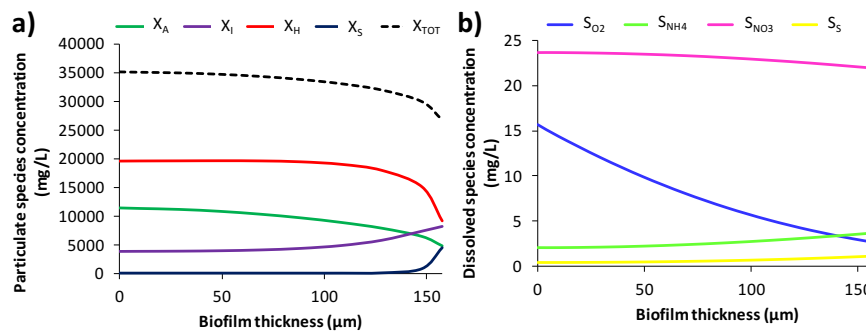


Figure 3-15 Particulate (a) and dissolved species (b) biofilm profiles for a membrane area of 120000 m² and a MAP of 140 kPa.

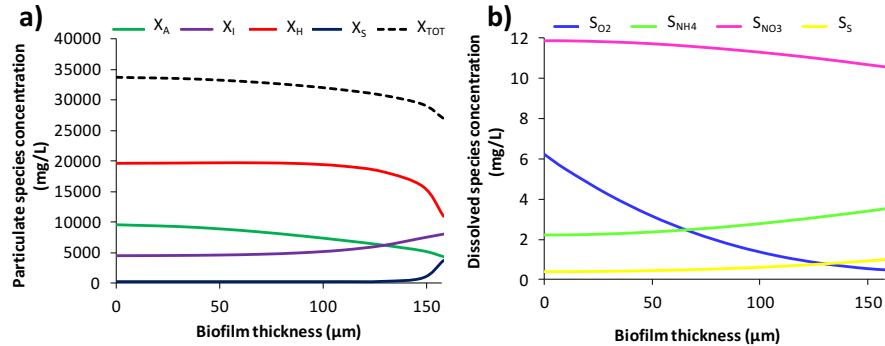


Figure 3-16 Particulate (a) and dissolved species (b) biofilm profiles for a membrane area of 180000 m² and a MAP of 8 kPa.

Optimum denitrification

As explained in materials and methods section, for optimum denitrification design, a membrane area of 150000 m² operated at an intermediate MAP of 40 kPa was selected as an example. As shown in Figure 3-17, any effluent nitrate concentration value could be obtained for different MLSS concentrations and HRTs combinations. This was because the total amount of suspended heterotrophic biomass (mass of X_H) remained almost unchanged for the different HRTs and MLSS combinations, resulting in similar denitrification capacities and effluent NO₃-N concentrations (Table 3-9).

Table 3-9 Examples of different HRTs and MLSS combinations that resulted in a similar effluent residual NO₃-N concentrations

	HRT= 2 h MLSS=4500 mg/L	HRT= 2.5 h MLSS=3500 mg/L	HRT=3 h MLSS=3000 mg/L
Suspended X_H concentration (g/m ³)	1500	1199	1001
Total mass of suspended X_H (Kg)	874.5	874	875
Effluent residual NO ₃ -N (g/m ³)	3 ± 0.5	3 ± 0.5	3 ± 0.5

As explained above, nitrification process was in most cases independent of HRTs and MLSS concentrations, thereby all the points represented in Figure 3-17 fulfilled the effluent ammonium criterion ($NH_4-N_{eff} \approx 4\text{mg/L}$).

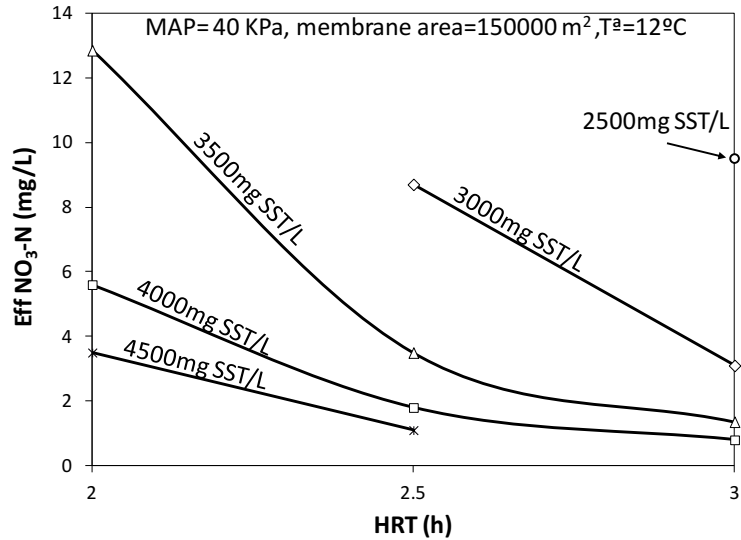


Figure 3-17 Design optimization plot that allows determining the HMABR process optimum design HRT to achieve the desired effluent nitrate and bulk MLSS concentrations, for a constant supplied MAP of 40 kPa and a membrane area of 150000 m².

For a typical MLSS concentration of 3500 mg/L, effluent NO₃-N concentrations around 12 mg/L can be obtained with a HRT of 2 hours. However, if lower effluent NO₃-N concentrations were desired (i.e. NO₃-N_{eff} ≈ 1.5 mg/L) a higher HRT value of 3 hours was required. This was because an increase in HRT (reactor volume) resulted in a higher total suspended X_H biomass and thus, in an increased denitrification capacity obtaining lower effluent NO₃-N concentrations (Table 3-10). For higher MLSS concentrations of 4500 mg/L, low effluent NO₃-N concentrations (around 3 mg/L) can be obtained with HRTs as low as 2 hours, as the attained suspended X_H biomass was sufficient to provide a high denitrification capacity. In case of operating with lower MLSS concentrations of 2500 mg/L, effluent NO₃-N concentration values around 10 mg/L were achieved for HRTs of 3 hours. In this case, the resulting relatively low suspended X_H biomass was not enough to provide higher denitrification capacity and thus, lower effluent NO₃-N concentrations.

Table 3-10 Example of the effect of HRTs in the resulting suspended X_H biomasses and effluent residual $\text{NO}_3\text{-N}$ concentrations. Data shown correspond with MLSS isoline of 3500 mg/L

	HRT= 2 h	HRT= 2.5 h	HRT=3 h
Suspended X_H concentration (g/m^3)	909	1199	1224
Total mass of suspended X_H (Kg)	529.9	874	1071
Effluent residual $\text{NO}_3\text{-N}$ concentration (g/m^3)	12.5	3.4	1.36

It needs to be emphasized that the solid retention times (SRTs) obtained for each HRT and MLSS combination were significantly low, ranging from 0.5 to 1 days (Table 3-11). The obtained low SRT values resulted from the high achieved suspended denitrification efficiencies, which were attributed to operate with very low bulk liquid DO concentrations (DO presence limits the denitrification process). This allowed practically all the S_5 to be anoxically consumed within the bulk liquid leading to the accumulation of X_5 in suspension (Table 3-12). In a conventional activated sludge (CAS) process, a significant portion of S_5 is removed aerobically during the nitrification step, so a higher portion of X_s is required for denitrification. In the HMABR process, as there is virtually no S_5 aerobic degradation, practically all the S_5 is available for denitrification, decreasing the consumption of X_s . Furthermore, as a result of the low SRTs obtained in the HMABR process, DO consumption due to X_H endogenous respiration is expected to be much lower compared with a CAS process. Then it can be confirmed, that the sludge resulting from the studied HMABR process was highly unstable. This is likely to lead to higher methane production during anaerobic digestion which is a useful renewable energy source.

Table 3-11 Summary of SRT values obtained for each HRT and MLSS combination represented in Figure 3-17

HRT (h)	MLSS concentrations (mg/L)				
	2500	3000	3500	4000	4500
2	-	-	SRT=0.5 d	SRT=0.6 d	SRT=0.7 d
2.5	-	SRT=0.6 d	SRT=0.7 d	SRT=0.8 d	SRT=0.9 d
3	SRT= 0.6 d	SRT=0.7 d	SRT=0.8 d	SRT=1 d	-

Table 3-12 Examples of obtained effluent X_s and S_s concentrations for MLSS isolate of 3500 mg/L

Effluent concentrations (mg/L)	HRTs (h)		
	2	2.5	3
Suspended X_s	1535	1185	995
Residual S_s	1.6	1.3	1.3

A design analysis for different effluent TN requirements according to European Directive 91/271/EEC for wastewater treatment is presented below.

For a scenario with agglomerations of 10000 - 100000 p.e., TN requirement for WWTPs discharging to sensitive areas is 15 mg/L, which means effluent nitrate concentrations of 6-7 mg/L, considering the TN as the sum of organic N (around 3-4 mg/L), NH_4 -N (4 mgN/L), and NO_3 -N. This effluent requirement can be accomplished for HRTs ranging from 2 to 3 hours, with approximate MLSS concentrations ranging from 3900 to 2700 mg/L. For agglomerations greater than 100000 p.e., required effluent TN concentration is 10 mg/L, which implies effluent nitrate concentrations of about 2-3 mg/L. Effluent nitrate standards for this scenario could be fulfilled with design HRTs from 2 to 3 hours, and MLSS concentrations from 4600 to 3400 mg/L.

Similar figures could be obtained for different MAPs and membrane areas according to the selected membrane scenario (dense or microporous).

Operation optimization plots

Optimum nitrification at 12, 16 and 20°C

For a design membrane area of 150000 m², Figure 3-18 shows that for increased temperature values lower MAPs were required for achieving the desired effluent ammonium concentration (MAPs of 40, 14, and 1 kPa for temperature values of 12, 16 and 20°C respectively). Temperature increase led to a greater biomass activity, thus to an increased nitrification capacity. Therefore in order to maintain equal nitrification rates (and effluent ammonium concentrations) the higher nitrifying biomass activity due to the temperature effect should be compensated by providing lower available DO concentrations within the biofilm. This was accomplished by reducing the supplied MAPs.

As explained in materials and methods section, each point of Figure 3-18 was calculated for different MLSS concentrations and HRTs, so as mentioned before,

nitrification process was practically independent of denitrification process (except for the cases explained above).

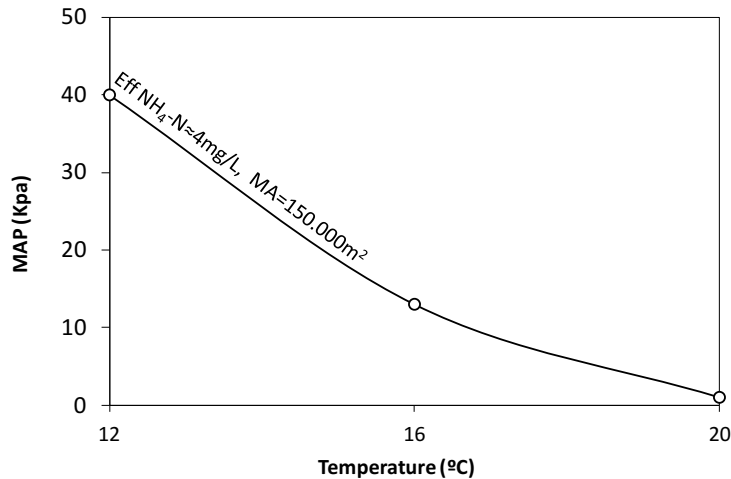


Figure 3-18 MAP required at different temperatures (12, 16 and 20°C) in order to accomplish with effluent ammonium concentration criterion ($\text{NH}_4\text{-N} \approx 4 \text{ mg/L}$), for a total membrane area of 150000 m^2 .

For the same membrane characteristics, similar ammonium isolines could be obtained for accomplishing with higher or lower effluent ammonium concentrations. In this way, for a determined temperature value different effluent ammonium and MAP combinations could be represented.

Optimum denitrification at 12, 16 and 20°C

For the selected HMABR design scenario (HRT 2.5 h and membrane area = 150000 m^2), Figure 3-19 shows that for increasing temperature values, lower curves were obtained. This was due to the greater X_H activity caused by temperature rise, which led to increased denitrification capacities and thus, to lower effluent nitrate concentrations. In the same way, higher MLSS concentrations provided lower effluent nitrate concentrations, as greater MLSS concentrations implied greater X_H biomass. As already discussed, in most cases, nitrification process was independent of MLSS concentrations, thereby all the points represented in Figure 3-19 accomplished with effluent ammonium criterion ($\text{NH}_{4\text{eff}} \approx 4 \text{ mg/L}$).

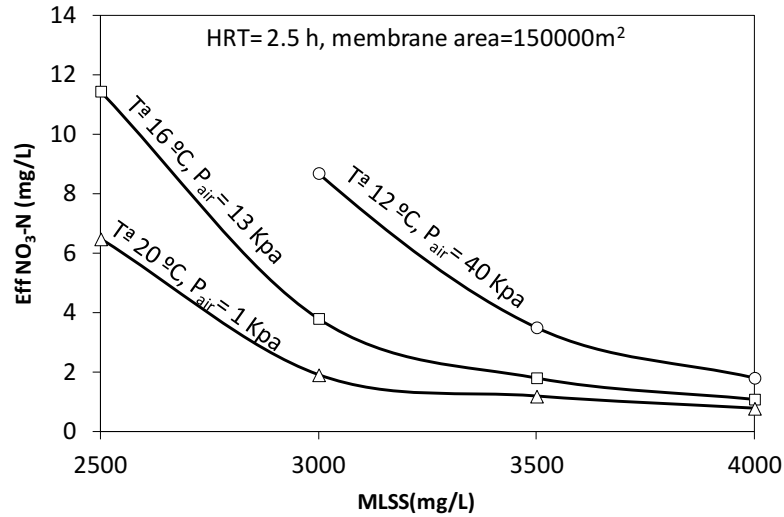


Figure 3-19 Operation optimization plots for determining the optimum MLSS concentration to be maintained depending on the temperature and the desired effluent NO₃-N concentrations for a total membrane area of 150000 m², and HRTs of 2.5 hours.

It is worth noting that for 16 and 20°C, when MLSS concentrations increased from 2500 to 3000 mg/L, sharp drops in effluent nitrate concentrations were produced. However, for higher MLSS concentrations of 3500 and 4000 mg/L, the decrease in effluent nitrate concentrations were less pronounced. This was attributed to: 1) lower variation in suspended X_H biomass for higher MLSS concentrations, which were rather reached by accumulation of inert particulate matter (X_I) (Table 3-13), and 2) the denitrification capacity became saturated due to the low residual nitrate concentrations. These facts made the effluent nitrate concentrations asymptotically approximate to zero as MLSS concentration increased.

Table 3-13 Example of variations in X_S and X_I concentrations for different MLSS at T_a=20°C

Suspended concentrations (mg/L)	MLSS concentrations (mg/L)			
	2500	3000	3500	4000
X _H	567	830	952	1040
X _I	744	975	1094	1270

According to the design analysis for different effluent TN requirements scenarios, Figure 3-19 allows determining optimum MLSS concentrations to be maintained for achieving the required effluent nitrate concentrations at different temperatures. As an example at 12°C, for an scenario with 10000-100000 p.e. in which effluent TN requirement is 15 mg/L (which implies nitrate concentrations of 6-7 mg/L) according to European Directive 91/271/EEC, effluent TN standards could be fulfilled operating with MLSS concentrations of around 3200 mg/L. For an scenario with agglomerations greater than 100000 p.e., which require more stringent effluent TN concentrations, of 10mg/L (implying nitrate concentrations of 2-3 mg/L), effluent standards could be satisfied operating with MLSS concentrations of 4000 mg/L.

3.5 CONCLUSIONS

3.5.1 Experimental study

In this experimentation, some relevant criteria for the optimal operation of a HMABR for biological total nitrogen removal were determined.

The fact of operating under non $\text{NO}_3\text{-N}$ limiting conditions in the bulk liquid had a crucial role in maintaining the desired biomasses distribution, preventing that biodegradable sCOD could penetrate and diffuse further into the biofilm, and consequently heterotrophic growth on it. NPR and NUR batch test results demonstrated that, as intended, most of the nitrifying biomass was in the biofilm (90%), while the majority of the denitrifying bacteria remained in suspension (95%).

The high achieved nitrification rates were due to 1) operating under non ammonium limiting conditions (bulk liquid $\text{NH}_4\text{-N}$ concentrations were significantly higher than the half saturation coefficient for ammonia, which also favored substrate diffusion into the biofilm), 2) supplying enough membrane air pressures to maintain high availability of DO concentrations in the biofilm, and 3) the majority of the biodegradable soluble COD was anoxically removed in the bulk liquid preventing its diffusion inside the biofilm and the inhibition of nitrifying biomass due to the lower availability of DO for nitrification process.

High denitrification rates were obtained due to operating with an anoxic SRT relatively high, and in most operating days, with non $\text{NO}_3\text{-N}$ limiting concentrations in the bulk liquid. On the other hand, in the present experimentation, the absence of DO in the bulk liquid enhanced the

denitrification process, allowing practically all biodegradable COD (S_s and X_s) to be consumed anoxically in the bulk liquid.

3.5.2 Simulation study

The developed HMABR mathematical model was able to match the experimental results with respect to bulk liquid $\text{NH}_4\text{-N}$, $\text{NO}_3\text{-N}$, sCOD and SSLM concentrations in the continuous HMABR operation, as well as NPR and NUR batch tests in suspension and in the biofilm.

Model predicted abundance, distribution and activities of nitrifying and heterotrophic populations. It showed that most nitrifying bacteria resided on the biofilm rather than in the mixed liquor, while the majority of denitrifying organisms remained in suspension.

The results of the systematic simulation studies, demonstrated that in the HMABR process, nitrification was in most cases decoupled from HRTs and MLSS concentrations, being the membrane areas and the supplied MAPs the underlying design parameters affecting effluent ammonium concentrations. This allowed the separate control and optimization of both nitrification and denitrification processes.

High nitrification rates were possible to obtain, as the membranes provided high DO concentrations in the biofilm internal layers available for nitrifying organisms.

The absence of DO in the bulk liquid allowed practically all the readily biodegradable substrate (S_s) to be consumed anoxically by suspended denitrifying organisms, enhancing the denitrification efficiency. Therefore high TN removal rates could be achieved with remarkably low HRTs (ranging from 2 to 3 hours) and SRTs (ranging from 0.5 to 1 d). The sludge resulting from the studied HMABR process presented a high X_s accumulation making the sludge substantially unstable. This will likely lead to high methane production during anaerobic digestion which is a useful renewable energy source.

Regarding nitrification process, different combinations of MAPs and membrane areas allowed achieving the desired effluent ammonium concentrations for preventing ammonium limiting conditions within the biofilm ($\text{NH}_{4\text{eff}} \approx 4$ mg/L). Optimum MAPs for different operating temperatures, in order to maintain the intended effluent ammonium concentration were determined.

With respect to denitrification process, the most favorable combinations of HRTs and MLSS concentrations were obtained, satisfying the TN effluent standards established in European legislation for different scenarios. Optimum MLSS

concentrations to be maintained depending on the temperature and the desired effluent NO₃-N concentrations were assessed.

3.6 REFERENCES

Ahmed, T., Semmens, M.J., 1992. The Use of Independently Sealed Microporous Hollow Fiber Membranes for Oxygenation of Water - Model Development. *J. Memb. Sci.* 69, 11–20.

Albizuri, J., Van Loosdrecht, M.C.M., Larrea, L., 2009. Extended mixed-culture biofilms (MCB) model to describe integrated fixed film/activated sludge (IFAS) process behaviour. *Water Sci. Technol.* 60, 3233–3241.

Albizuri, J., 2012. Modelado y simulación de comportamientos de procesos con lecho móvil para la eliminación de nutrientes de aguas residuales urbanas. Doctoral Thesis. Universidad de Navarra (TECNUN).

Albizuri, J., Grau, P., Christensson, M., Larrea, L., 2014. Validating the colloid model to optimise the design and operation of both moving-bed biofilm reactor and integrated fixed-film activated sludge systems. *Water Sci. Technol.* 69, 1552–1557.

APHA, 2005. Standard Methods for the Examination of Water and Wastewater, American Water Works Association/American Public Works Association/Water Environment Federation.

Aybar, M., Pizarro, G., Boltz, J.P., Downing, L., Nerenberg, R., 2014. Energy-efficient wastewater treatment via the air-based, hybrid membrane biofilm reactor (hybrid MfBR). *Water Sci. Technol.* 69, 1735–1741.

Boltz, J.P., Johnson, B.R., Daigger, G.T., Sandino, J., 2009. Modeling integrated fixed-film activated sludge and moving-bed biofilm reactor systems I: mathematical treatment and model development. *Water Environ. Res.* 81, 555–575.

Brindle, K., Stephenson, T., Semmens, M.J., 1998. Nitrification and oxygen utilisation in a membrane aeration bioreactor. *J. Memb. Sci.* 144, 197–209.

Caminos, M., 2010. Diseño óptimo de procesos biorreactor de membrana para eliminación de nutrientes de aguas residuales urbanas. Doctoral Thesis. (TECNUN)

Casey, E., Glennon, B., Hamer, G., 1999. Review of membrane aerated biofilm reactors, in: *Resources, Conservation and Recycling*. pp. 203–215.

- Casey, E., Glennon, B., Hamer, G., 2000. Biofilm development in a membrane-aerated biofilm reactor: Effect of flow velocity on performance. *Biotechnol. Bioeng.* 67, 476–486.
- Cote, P., Bersillon, J.L., Huyard, A., Faup, G., 1988. Bubble-Free Aeration Using Membranes - Process Analysis. *J. Water Pollut. Control Fed.* 60, 1986–1992.
- Downing, L.S., Nerenberg, R., 2007. Performance and microbial ecology of the hybrid membrane biofilm process for concurrent nitrification and denitrification of wastewater. *Water Sci. Technol.* 55(8-9), 355–362.
- Downing, L.S., Nerenberg, R., 2008. Total nitrogen removal in a hybrid, membrane-aerated activated sludge process. *Water Res.* 42, 3697–3708.
- Eguía, E., 1991. Desarrollo de la biopelícula en medio soporte permeable. Tesis doctoral. Universidad de Cantabria. Santander.
- Ekama, G.A., Marais, G.v.R., 1979. Dynamic Behaviour of the Activated Sludge Process. *Water Pollut. Control Fed.* 51, 534-556.
- Esteban-García, A.L., Díez, R., Rodríguez, L., Lobo, A., De Florio, L., Pérez, P., Tejero, I. 2012. Processes based on the growth of biofilms on gas permeable membranes: Biomembrane reactors. In *Innovative Technologies for Urban Wastewater Treatment Plants (2nd Edition)*, Editors Omil F. and Suárez S., Santiago de Compostela. ISBN: 9788469535141, 117-145.
- Henze, M., Gujer, W., Mino, T., van Loosdrecht, M.C.M., 2000. Activated Sludge Models ASM1, ASM2, ASM2d and ASM3. IWA Publ. 121.
- Jácome, A., Molina, J., Suárez, J., Tejero, I., 2006. Simultaneous Removal of Organic Matter and Nitrogen Compounds in Autoaerated Biofilms. *J. Environ. Eng.* 132, 1255–1263.
- Kunetz, T.E., Oskouie, A., Poonsapaya, A., Peeters, J., Adams, N., Long, Z., and Cote, P., 2016. Innovative Membrane-Aerated Biofilm Reactor Pilot Test to Achieve Low-Energy Nutrient Removal at the Chicago MWRD. WEFTEC 2016, New Orleans.
- LaPara, T.M., Cole, A.C., Shanahan, J.W., Semmens, M.J., 2006. The effects of organic carbon, ammoniacal-nitrogen, and oxygen partial pressure on the stratification of membrane-aerated biofilms. *J. Ind. Microbiol. Biotechnol.* 33, 315–323.
- Larrea, L., Irizar, I., Hildago, M.E., 2002. Improving the predictions of ASM2d through modelling in practice. *Water Sci. Technol.* 45, 199–208.

- Li, J., Zhu, L.P., Xu, Y.Y., Zhu, B.K., 2010. Oxygen transfer characteristics of hydrophilic treated polypropylene hollow fiber membranes for bubbleless aeration. *J. Memb. Sci.* 362, 47–57.
- Marquot, A., Stricker, A.E., Racault, Y., 2006. ASM1 dynamic calibration and long-term validation for an intermittently aerated WWTP, in: *Water Science and Technology*. pp. 247–256.
- Martin, K.J., Nerenberg, R., 2012. The membrane biofilm reactor (MBfR) for water and wastewater treatment: principles, applications, and recent developments. *Bioresour. Technol.* 122, 83–94.
- Matsumoto, S., Terada, A., Aoi, Y., Tsuneda, S., Alpkvist, E., Picioreanu, C., van Loosdrecht, M.C.M., 2007. Experimental and simulation analysis of community structure of nitrifying bacteria in a membrane-aerated biofilm. *Water Sci. Technol.* 55, 283–290.
- Maurer, M., Fux, C., Lange, D., Siegrist, H., 1999. Modelling denitrification in a moving bed of porous carriers from a low-loaded wastewater treatment plant, in: *Water Sci. Technol.* 39, 251–259.
- Melcer, H., Dold, P.L., Jones, R.M., Bye, C.M., Takacs, I., Stensel, H.D., Wilson, A.W., Sun, P., Bury, S., 2003. *Methods for wastewater characterisation in activated sludge modeling*. Water Environment Research Foundation (WERF), Alexandria, VA, USA.
- Nerenberg, R., 2016. The membrane-biofilm reactor (MBfR) as a counter-diffusional biofilm process. *Curr. Opin. Biotechnol.* 38, 131–136.
- Osa, J.J., Eguia, E., Vidart, T., Jacome, A., Lorda, I., Amieva, J.J., and Tejero, I. 1997. *Water treatment with biofilm membrane reactors*. International Conference on Advanced Wastewater Treatment Processes, Leeds University, UK.
- Pankhania, M., Brindle, K., Stephenson, T., 1999. Membrane aeration bioreactors for wastewater treatment: completely mixed and plug-flow operation. *Chem. Eng. J.* 73, 131–136.
- Perry, R.H., Green, D.W., 1999. *Perry's chemical engineer's handbook*. McGraw-Hill, New York, USA.
- Randall, C.W., Sen, D., 1996. Full-scale evaluation of an integrated fixed-film activated sludge (IFAS) process for enhanced nitrogen removal, in: *Water Sci. Technol.* 33, 155–162.

- Reichert, P., 1994. Aquasim - a Tool for Simulation and Data-Analysis of Aquatic Systems, *Water Sci. Technol.* 30, 21-30.
- Roeleveld, P.J., Van Loosdrecht, M.C.M., 2002. Experience with guidelines for wastewater characterisation in The Netherlands, in: *Water Science and Technology*. pp. 77–87.
- Rutt K., Seda J., Chandler H. J., 2006. Two year case study of integrated fixed film activated sludge at Broomfield, CO WWTP. *Proceedings WEFTEC 06*, Dallas, TX.
- Satoh, H., Ono, H., Rulin, B., Kamo, J., Okabe, S., Fukushi, K., 2004. Macroscale and microscale analyses of nitrification and denitrification in biofilms attached on membrane aerated biofilm reactors. *Water Res.* 38, 1633–1641.
- Semmens, M.J., Dahm, K., Shanahan, J., Christianson, A., 2003. COD and nitrogen removal by biofilms growing on gas permeable membranes. *Water Res.* 37, 4343–4350.
- Sen, D., Copithorn, R., Randall, C., Jones, R., Phago, D., Rusten, B., 2000. Investigation of hybrid systems for enhanced nutrient control: *Water Environment Research Foundation (WERF)*.
- Stricker, A.E., Lossing, H., Gibson, J.H., Hong, Y., Urbanic, J.C., 2011. Pilot scale testing of a new configuration of the membrane aerated biofilm reactor (MABR) to treat high-strength industrial sewage. *Water Environ. Res.* 83, 3–14.
- Suzuki, Y., Takahashi, M., Haesslein, M., Seyfried, C.F., 1999. Development of simulation model for a combined activated-sludge and biofilm process to remove nitrogen and phosphorus. *Water Environ. Res.* 71, 388–397.
- Syron, E., Casey, E., 2008. Membrane-aerated biofilms for high rate biotreatment: performance appraisal, engineering principles, scale-up, and development requirements. *Env. Sci. Technol.* 42, 1833–1844.
- Takács, I., Bye, C.M., Chapman, K., Dold, P.L., Fairlamb, P.M., Jones, R.M., 2007. A biofilm model for engineering design. *Water Sci. Technol.* 55, 329-336.
- Tchobanoglous, G., Burton, F.L., H.D., S., 2014. *Wastewater Engineering: Treatment and Reuse*, Metcalf and Eddy, 5th ed. McGraw-Hill, New York.
- Terada, A., Yamamoto, T., Igarashi, R., Tsuneda, S., Hirata, A., 2006. Feasibility of a membrane-aerated biofilm reactor to achieve controllable nitrification. *Biochem. Eng. J.* 28, 123–130.

Timberlake, D.L., Strand, S.E., Williamson, K.J., 1988. Combined aerobic heterotrophic oxidation, nitrification and denitrification in a permeable-support biofilm. *Water Res.* 22, 1513–1517.

Vidart, T.M., 1992. Biopelícula en medio soporte permeable con aportación de aire. Tesis doctoral. Universidad de Cantabria. Santander.

Wanner, O., Reichert, P., 1996. Mathematical modeling of mixed-culture biofilms. *Biotechnol. Bioeng.* 49, 172–184.

Wanner, O., Eberl, H., Morgenroth, E., Noguera, D., Picioreanu, C., Rittmann, B., van Loosdrecht, M.C.M., Wanner, O., 2006. Mathematical modeling of biofilms, Scientific and technical report series. IWA Publishing, London.

Weiss, P.T., Gulliver, J.S., Semmens, M.J., 1998. In-stream hollow-fiber membrane aeration. *Jour. Hydraul. Eng.* Vol. 124, 579–588.

Chapter 4

Periodic venting of MABR lumens allows high removal rates and high oxygen transfer efficiencies^{1,2}

¹ Part of this chapter has been published as:

Pérez-Calleja, P., Aybar, M., Picioreanu, C., Esteban-García, A.L., Nerenberg, R. 2015. *Effects of gas back-diffusion on Membrane-Aerated Biofilm Reactors (MABRs)*. Proceedings of the 3rd Water Research Conference, 11-14 January, 2015, Shenzhen, China.

Pérez-Calleja, P., Aybar, M., Picioreanu, C., Esteban-García, A.L., Nerenberg, R., 2015. *Membrane-Biofilm Reactors (MBfR) For Water Treatment: Overcoming Gas Back Diffusion Effects*. AEESP Research and Education Conference. Environmental Engineering and Science at the nexus. June 13-16, 2015, Yale University, Commons, New Haven.

Pérez-Calleja, P., Aybar, M., Picioreanu, C., Esteban-García, A.L., Nerenberg, R., 2015. *Enhanced Operation of Membrane-Biofilm Reactor (MBfR) for Waste Water Treatment by Mitigation of Gas Back-Diffusion Effect*. WEFTEC 2015, Chicago USA.

Aybar, M., **Pérez-Calleja, P.,** Picioreanu, C., Esteban-García, A.L., Nerenberg, R., 2016. *Enhancing Energy Efficiency of Membrane Aerated Biofilm Reactors (MABRs) by Managing of Gas Back-Diffusion*. 13th IWA Leading Edge Conference on Water and Wastewater Technologies, Jerez de la Frontera, Spain, June 13-16, 2016.

Pérez-Calleja, P., Aybar, M., Picioreanu, C., Esteban-García, A.L., Nerenberg, R., 2016. *Enhanced operation of Membrane Aerated Biofilm Reactors (MABRs) For Waste Water Treatment by Managing Gas Back-Diffusion*. 3rd IWA Specialized International Conference: Ecotechnologies for Wastewater Treatment 2016 (ecoSTP16). Invited platform presentation. Cambridge, UK, 27-30 June.

Pérez-Calleja, P., Aybar, M.; Picioreanu, C.; Esteban-García, A.L.; Nerenberg, R. 2017. *Periodic Venting of Membrane Aerated Biofilm Reactors (MABRs) Allows High Removal Rates and High Gas-Transfer Efficiencies*. 10th International Conference on Biofilm Reactors. Dublin, Ireland, 9-12 May.

Pérez-Calleja, P., Aybar, M., Picioreanu, C., Esteban-García, A.L., Martin, K.J., Nerenberg, R., 2017. *Periodic venting of MABR lumen allows high removal rates and high gas-transfer efficiencies*. Water Research. Accepted 20-05-2017.

² Part of this chapter was used for the discussion of the PhD Thesis:

Aybar, M., (2016). Mechanisms of gas transfer and biofilm development in membrane aerated biofilms, University of Notre Dame (U.S.).

OUTLINE

SUMMARY.....	139
4.1 INTRODUCTION.....	139
4.2 OBJECTIVES.....	141
4.3 MATERIALS AND METHODS.....	142
4.3.1 Experimental flow cell configuration.....	142
4.3.2 Synthetic medium for the MABRs.....	143
4.3.3 Analytical methods.....	144
4.3.4 DO measurements.....	144
4.3.5 Calculation of membrane mass transfer coefficient, K_m	145
4.3.6 Numerical model for gas back-diffusion.....	146
4.3.6.1 Flow and mass transport in the liquid.....	147
4.3.6.2 Flow and mass transport in the gas.....	148
4.4 RESULTS AND DISCUSSION.....	152
4.4.1 Determination of membrane mass transfer coefficient.....	152
4.4.2 Model evaluation.....	153
4.4.3 Model-based assessment of periodic venting.....	155
4.4.4 Experimental assessment of gas supply strategies on HFM with biofilm.....	160
4.5 CONCLUSIONS.....	165
4.6 REFERENCES.....	165

SUMMARY

The membrane-aerated biofilm reactor (MABR) is a novel treatment technology that employs gas-supplying membranes to deliver oxygen directly to a biofilm growing on the membrane surface. When operated with closed-end membranes, the MABR provides 100-percent oxygen transfer efficiencies (OTE), resulting in significant energy savings. However, closed-end MABRs are more sensitive to back-diffusion of inert gases, such as nitrogen. Back-diffusion reduces the average oxygen transfer rates (OTR), consequently decreasing the average contaminant removal fluxes (J). It was hypothesized that venting the membrane lumen periodically would increase the OTR and J. Using an experimental flow cell and mathematical modeling, this study showed that back-diffusion gas profiles developed over relatively long timescales. Thus, very short ventings could re-establish uniform gas profiles for relatively long time periods. Using modeling, the effect of the venting intervals (time between ventings) was systematically explored. At moderate venting intervals, of around 30 minutes, the venting significantly increased the average OTR and J without substantially impacting the OTEs. When the interval was short enough, in this case shorter than 20 minutes, the OTR was actually higher than for continuous open-end operation. Results of this study showed that periodic venting is a promising strategy to combine the advantages of open-end and closed end operation, maximizing both the OTR and OTE.

4.1 INTRODUCTION

Gas-transferring, hollow-fiber membranes (HFM) are commonly used to supply gases for environmental, industrial and medical applications. For example, bundles of HFMs have been used for oxygenation of rivers and water streams, for blood oxygenation, and for bioremediation of groundwater contaminants (Weiss et al., 1998; Roggy et al., 2002; Federspiel and Henchir, 2004). However, an emerging application is the membrane-biofilm reactor (MBfR), where HFMs supply gaseous substrates to a biofilm growing directly on the membrane's outer surface (Martin and Nerenberg, 2012; Nerenberg, 2016). When used to deliver air or oxygen, the process is often referred to as the membrane-aerated biofilm reactor (MABR). MABRs can simultaneously remove biological oxygen demand (BOD), nitrify, and denitrify (Timberlake et al., 1988; Hibiya et al., 2003; Terada et al., 2003; Semmens et al., 2003; Jácome et al., 2006; Matsumoto et al., 2007; Syron and Casey, 2008;

Downing and Nerenberg, 2008). Several commercial applications are in development, but very few full-scale applications exist.

MABRs can be operated with closed or open-ended HFMs. With closed-ended HFMs, all the oxygen supplied to the membranes is delivered to the biofilm, allowing 100% oxygen transfer efficiencies (OTEs) (Brindle et al., 1998; Pankhania et al., 1999; Hibiya et al., 2003; Terada et al., 2003; Syron and Casey, 2008; Martin and Nerenberg, 2012). This can save up to 85% in energy costs, compared to conventional activated sludge process (Aybar et al., 2014). However, closed-ended HFMs typically suffer from gas back-diffusion, where N_2 and other dissolved gases diffuse into the membrane lumen (Schaffer et al., 1960; Ahmed and Semmens, 1992a). With back-diffusion, the distal end of the membrane may be “deadened,” leading to lower average oxygen transfer rates (OTR) compared to open-end operation (Figure 4-1a). In this study, it was considered OTR to be synonymous with the oxygen flux, J_{O_2} , across the membrane.

With open-ended HFMs, the intra-membrane gas velocity is high throughout the membrane. With high velocities, advective mass transport in the lumen is much greater than the diffusive transfer across the membrane wall. This results in more uniform oxygen concentrations in the lumen, leading to high average OTRs (Figure 4-1b). However, a large amount of gas is lost from open end. Also, the high gas velocity leads to greater frictional pressure losses occurrence along the membrane, resulting in greater energy requirements and lower gas pressures at the distal end of the membrane. For the MABR, lower overall OTR translates into lower average substrate removal fluxes (J).

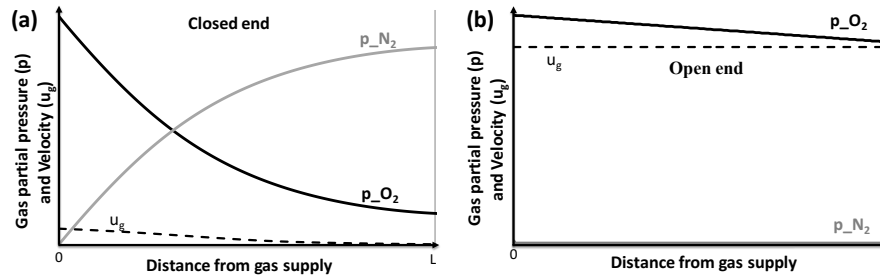


Figure 4-1 Schematic showing differences between hollow-fiber membranes at steady-state in: (a) closed-end operation, and (b) open-end operation. In this example, the membrane is pressurized with pure O₂ transferring to liquid containing dissolved N₂. Figures show typical oxygen and nitrogen partial pressures (pO₂ and pN₂) and gas velocities (u_g) along the membrane length. The open end membrane has higher pO₂ across the entire membrane, leading to higher gas transfer rates, but has low gas transfer efficiencies, as most of the gas is vented through the end.

Many researchers have explored ways to improve the OTR of HFMs (Weissman and Mockros, 1969; Tanishita et al., 1978; Côte et al., 1989; Ahmed and Semmens, 1992b; Matsuda et al., 1999; Ahmed et al., 2004). However, few studies have tried to concurrently improve the OTR and OTE. A novel approach may be periodically opening the membranes to vent back-diffusion gases. This will allow the back-diffusion gases to be vented to the atmosphere during the open phase, re-establishing the uniform almost constant gas pressure profile along the fiber length.

Previous research experimentally explored increasing the gas flow rates, or intermittent degassing processes (Li et al., 2010; Castagna et al., 2015). Fang et al., (2004) measured and modeled the gas composition inside a membrane, and gave modeled predictions of gas concentration profiles as a function of time applying when supplied with a pulsing strategy. However, they did not systematically explore the impacts of the pulsing frequency on the OTE and OTR, and their model was only applicable under conditions of liquid creeping flow.

4.2 OBJECTIVES

The objective of this study was to use experiments and modeling to systematically explore periodic venting of hollow-fiber membranes as a means to maximize the OTE and OTR of MABRs.

4.3 MATERIALS AND METHODS

The strategy followed in this study was to (1) experimentally study OTRs and OTEs for “clean” HFMs (i.e., without biofilm), for open end, closed end, and for periodic venting, (2) use mathematical modeling to expand the experimental findings and predict the effects of periodic venting for a clean HFM, and (3) experimentally assess the periodic venting strategy for an MABR (i.e., a HFM with biofilm). OTR was calculated as the oxygen flux difference between the inlet and the outlet which corresponds to the flux of oxygen transferred across the membrane surface. OTE was calculated as the flux difference divided by the inlet flux. OTE represents the percentage of the transferred oxygen flux with respect to the supplied oxygen. Fluxes were estimated according to equation (4-1).

4.3.1 Experimental flow cell configuration

An experimental flow cell with a single HFM was used to explore OTRs and gas back diffusion in clean HFMs, i.e., without biofilm. The flow cell consisted of square-section glass tube with 6-mm inside dimension, and 40-cm length. The flow cell had seven ports for dissolved oxygen (DO) measurements (Figure 4-2), separated 3.8 cm along the flow cell. Water was deoxygenated by nitrogen sparging and pumped through the flow cell using a peristaltic pump (Cole Palmer, Vernon Hills, IL, USA).

Tests were first carried out to determine the HFM’s mass transfer coefficient. To test the mathematical model, experiments were then performed with a range of water velocities, oxygen supply pressures, feed gases (air and pure oxygen), water flow directions (co-current or counter current with respect to the inlet gas supply), and transient shifts between open and closed ends.

The flow cell used a composite, microporous polyethylene membrane with a dense 1 μm polyurethane core (HFM200TL, Mitsubishi Rayon, Japan). The outer diameter was 280- μm and the wall thickness was 40- μm . A single membrane was located in the middle of the flow cell, supported at both ends by a gas-supplying manifold. The gas was supplied from one end at constant pressure, while a valve at the opposite end allowed open or closed operation of the membrane. Pure oxygen or air was supplied at 0.07 or 0.18 atm relative pressure. The influent flow rate ranged from 2 to 10 mL/min, resulting in a liquid velocity of 1 to 5 mm/s and a Reynolds number of 5 to 28, well within the laminar flow regime.

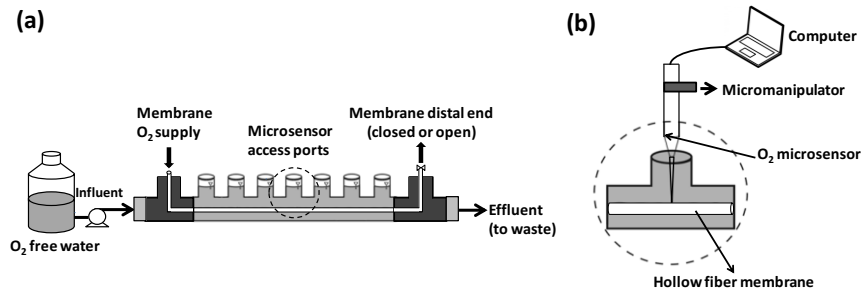


Figure 4-2 (a) Schematic of flow cell. Oxygen-free water from a reservoir was pumped into the square-section glass tube with a hollow-fiber membrane supplied with O₂ in the middle. (b) Detail of a flow-cell port used for DO measurement with a microsensor controlled by a micromanipulator.

Two separate reactors were used for the MABR tests, with the same configuration as described above. Reactor MABR-1 was operated with an open-ended membrane, while MABR-2 was initially operated with a closed end, but later was operated with periodic opening to vent lumen gases. De-oxygenated synthetic media (described below) was pumped through the flow cell. Each MABR had a recirculation pump and was connected to a purging reservoir, where the bulk liquid was sparged with N₂ to strip any residual DO from the reactor. Bulk liquid N₂ bubbles were vented in the reservoir before recycle line back to the flow-cell. This avoided any DO accumulation in the bulk liquid, which was a concern in the initial stages, prior to biofilm development. A magnetic stir bar kept the reservoir well-mixed with a high shear velocity, minimizing the attachment of biomass to the glass surface. An influent flow rate of 1 mL/min and a recirculation of 60 mL/min were provided to each MABR. Pure oxygen was supplied to the lumen of each at 0.05 atm relative pressure.

4.3.2 Synthetic medium for the MABRs

The synthetic wastewater for MABR-1 and MABR-2, was prepared from distilled water amended with 2.773 g Na₂HPO₄, 0.169 g KH₂PO₄, 0.410 g MgSO₄·7H₂O and 0.202 g (NH₄)₂SO₄ per liter, as well as a trace mineral and calcium iron solutions. Ca-Fe solution contained, per liter: 1 g CaCl₂·2H₂O and 1 g FeSO₄·7H₂O. The trace mineral solution contained, per liter: 100 mg ZnSO₄·7H₂O, 30 mg MnCl₂·H₂O, 300 mg H₃BO₃, 200 mg CoCl₂·6H₂O, 10mg CuCl₂·2H₂O, 10 mg NiCl₂·6H₂O, 30 mg Na₂MoO₄·2H₂O, and 30 mg Na₂SeO₃. Potassium acetate was added as a COD source to achieve 30 mgCOD/L. The synthetic wastewater was maintained anoxic by

sparging the medium with nitrogen gas and maintaining a positive pressure of nitrogen gas on the storage container. The pH was maintained at approximately 7, while the water temperature was 22 °C.

4.3.3 Analytical methods

Chemical oxygen demand (COD) was monitored in the influent and effluent of the MABR reactors using colorimetric methods (Hach, Loveland, CO, USA). A glass electrode pH meter was used to monitor pH.

For determining the biofilm thickness, a stereo-zoom light microscope was used (Cole-Palmer, Chicago, IL) equipped with a mounted digital camera (Cybershot DSC-F707, Sony) and a fiber-optic light source. The camera was fixed to the microscope with a 1× mounting adapter. Biofilm image acquisition was also performed in all seven flow-cell ports after four weeks of operation. Image processing for each measurement was followed by statistical evaluation of the results.

Further information regarding analytical methods is provided in chapter 2.

4.3.4 DO measurements

Clark-type oxygen microsensors (Unisense A/S, Denmark) with a 10 µm tip diameter were used to measure DO concentrations. The microelectrode movement was controlled with a micro-manipulator (Model MM33-2, Unisense A/S). The use of microsensors consists in an invasive method that can slightly affect the results. However, considering that the tip was only 10 µm diameter and was immersed in a much thicker boundary layer, the microsensors would be expected to have a minimal impact on the DO concentration. Hydrodynamic measurements made by Hondzo et al., (2005), using a similar DO microsensor diameters and Reynolds number as used in this study, concluded that the disturbance of the flow by microsensors stem was minimal.

Longitudinal profiles of DO at the HFM surface were collected from the seven ports once the system reached steady state, typically after two hours. For each port, transversal DO profiles were collected starting from the HFM surface, across the liquid diffusion layer (LDL), and into the bulk. The transversal DO measurements were collected at 20-µm intervals, typically reached a distance of around 1000 µm from the membrane surface. Profiles were collected at least in triplicate. For

transient conditions, DO was measured continuously at the membrane surface, for one of the intermediate ports, during the shift from open-end to closed-end operation. Longitudinal steady-state DO profiles were also taken in both MABRs after four weeks of operation.

4.3.5 Calculation of membrane mass transfer coefficient, K_m

The membrane mass transfer coefficient, K_m , was calculated from oxygen transfer tests in clean membranes. Measured transversal DO profiles in the diffusion-dominated liquid boundary layer were used, using the flux continuity condition. The oxygen flux across the HFM, $J_{O_2,m}$, is equal to the diffusion flux through the mass transfer boundary layer at the membrane surface, $J_{O_2,l}$, as follows:

$$J_{O_2,m} = K_m (C_{O_2,m(g)} - C_{O_2,m(l)}) = D_{O_2,l} \left. \frac{dC_{O_2,l}}{dr} \right|_{r=R_m} = J_{O_2,l} \quad \text{Eq. 4-1}$$

where $D_{O_2,l}$ is the diffusion coefficient in the liquid phase (water), $C_{O_2,l}$ is the measured oxygen concentration in water, $C_{O_2,m}$ is the oxygen concentration in the microporous membrane on (g) gas side and (l) liquid side, and R_m the outer radius of the membrane. Given the small membrane thickness relative to the HFM radius, the membrane was approximated as a planar surface. From Eq. 4-1 the oxygen mass transfer coefficient in the membrane is calculated as:

$$K_m = \frac{D_{O_2,l} \left(\frac{dC_{O_2,l}}{dr} \right)_{r=R_m}}{C_{O_2,m(g)} - C_{O_2,m(l)}} \quad \text{Eq. 4-2}$$

The oxygen diffusivity in water $D_{O_2,l}$ was obtained from the literature (Haynes et al., 2015). The oxygen concentration in the gas side of the microporous membrane, $C_{O_2,m(g)}$, is linked, by the ideal gas law, to the applied pressure and gas composition y_{O_2} (either O_2 or air, at the working temperature). When determining the K_m , the HFM was operated in open end mode to minimize concentration changes. Also, microsensor measurements were carried out at the first port of the flow cell (from the left side), where the gas concentration was essentially equal to the supply concentration, $C_{O_2,m(g)} = p y_{O_2, in} / (RT)$. The oxygen gas concentration in the membrane, where it contacts the liquid, is related to the DO concentration in the liquid by the partition equilibrium (Henry's law), such that $C_{O_2,m(l)} = (C_{O_2,l})_{r=R_m} / H_{O_2}$. Finally, microsensor measurements of concentration profiles of DO in water were used to determine the concentration gradient at the membrane surface, $(dC_{O_2,l}/dr)_{r=R_m}$ and

the concentration $(C_{O_2,l})_{r=Rm}$. As mentioned above, profiles were collected at least in triplicate, and the reported Km is the average of the replicates.

4.3.6 Numerical model for gas back-diffusion

A mathematical model for gas back-diffusion was developed, addressing both steady-state and transient conditions. The model included O₂ supply from the HFM lumen, and assumed that the bulk liquid was in equilibrium with 1 atm of N₂. The model was implemented with the finite-element simulation platform COMSOL Multiphysics (COMSOL 4.4, Comsol Inc., Burlington, MA, www.comsol.com).

The numerical model included fluid flow and mass transport of O₂ and N₂, both in the liquid surrounding the HFM and in the lumen gas (Figure 4-3). For the flow and mass transport in the liquid phase, a two-dimensional (2-D) axisymmetric geometry was set along the axis of the membrane lumen (direction x) with radial gradients along direction r. The 2-D model implies an annular cross-section for the flow, with size $L_f = 3.4$ mm (the radius of a circle with the same area as the square cross-section). This model was coupled with a one-dimensional (1-D) domain for gas flow and mass transport in the membrane lumen (assuming no radial gradients in the lumen).

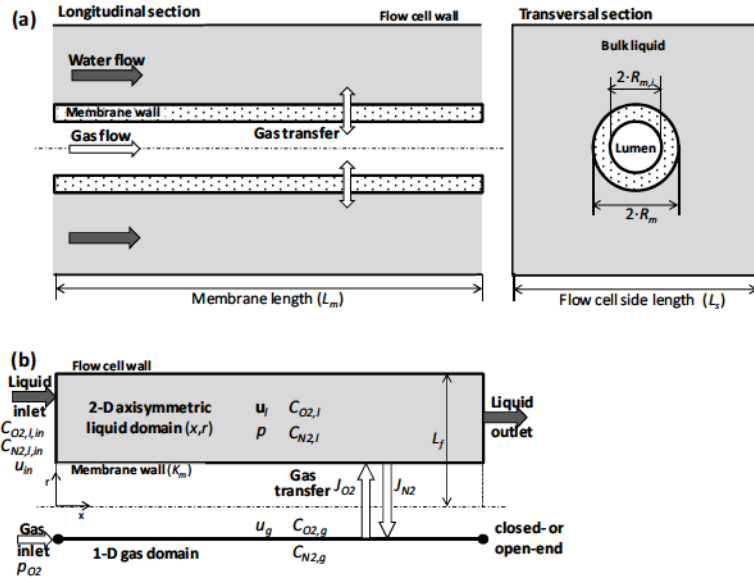


Figure 4-3 (a) Schematic representation (not at scale) of the experimental co-current aeration system with a single HFM inside a square-section flow cell filled with liquid. Water flows between the HFM and the flow cell wall, and the membrane is supplied with oxygen. (b) Model representation including a 2-D axisymmetric liquid domain connected via the membrane wall with a 1-D gas domain.

4.3.6.1 Flow and mass transport in the liquid

The liquid velocity distribution in the flow cell was determined by solution of the two-dimensional Navier-Stokes equations (4-3) and (4-4) in the 2-D axisymmetric domain:

$$\rho(\mathbf{u}_l \times \nabla) \mathbf{u}_l = \nabla \times \left[-p\mathbf{I} + \mu(\nabla \mathbf{u}_l + (\nabla \mathbf{u}_l)^T) \right], \quad \nabla \cdot \mathbf{u}_l = 0 \quad \text{Eq. 4-3, Eq. 4-4}$$

where \mathbf{u}_l is the water flow velocity, p is the pressure, ρ is the water density, μ is the liquid dynamic viscosity, and \mathbf{I} is the identity matrix. The water velocity was assumed to be zero at the membrane surface and at the flow cell wall (non-slip condition, $\mathbf{u}_l=0$). Laminar flow conditions were imposed, with average velocity u_{in} in the inlet and zero relative pressure in the outlet.

The mass transport of oxygen and nitrogen in the liquid flow results from convection-diffusion equations (4-5) and (4-6) solved for the dissolved O_2 and N_2 concentrations, $C_{O_2,l}$ and $C_{N_2,l}$:

$$\mathbf{u}_l \nabla C_{O_2,l} = D_{O_2,l} \nabla^2 C_{O_2,l}, \quad \mathbf{u}_l \nabla C_{N_2,l} = D_{N_2,l} \nabla^2 C_{N_2,l} \quad \text{Eq. 4-5, Eq. 4-6}$$

where $D_{O_2,l}$ and $D_{N_2,l}$ are the diffusion coefficients in the liquid. Constant dissolved O_2 and N_2 concentrations were imposed at the inlet boundary, $C_{O_2,l,in}$ and $C_{N_2,l,in}$. N_2 was present in the feed water at 18 mg/L, which corresponds to equilibrium with 1 atm of N_2 . Convection-only outlet boundary was assigned, ($\partial C_{O_2,l} / \partial x = \partial C_{N_2,l} / \partial x = 0$), while no-flux conditions were imposed at the flow cell wall ($\partial C_{O_2,l} / \partial y = \partial C_{N_2,l} / \partial y = 0$). On the membrane wall, flux continuity conditions were set:

$$J_{O_2} = K_m (C_{O_2,g} H_{O_2} - C_{O_2,l}), \quad J_{N_2} = K_m (C_{N_2,g} H_{N_2} - C_{N_2,l})$$

where H_{O_2} and H_{N_2} are the gas-liquid partition (Henry's) coefficients at 20 °C. It was assumed that the membrane, which was microporous, had the same selectivity for O_2 and N_2 (Ahmed and Semmens, 1992a), which translates to the same K_m .

4.3.6.2 Flow and mass transport in the gas

The mass balances for the gases in the membrane lumen were adapted from Ahmed and Semmens (1992a), who modeled steady-state O_2 and N_2 profiles in a closed-end HFM. Unlike the past model, this model includes transient behavior, and used computational fluid dynamics to determine dissolved gas concentrations in the fluid along the membrane length. Frictional gas pressure losses in the lumen were included, and the model allowed for transient conditions to be simulated, for example when switching from open-end to closed-end operation. Finally, the membrane mass transfer resistance (K_m) was considered explicitly. Note that only longitudinal gradients in gas concentrations (direction x) were considered in our model.

In both closed-end and open-end operation, the one-dimensional transient mass balances for O_2 (Eq. 4-7) and N_2 gas (Eq. 4-8) in the membrane lumen included transport by convection and diffusion, and transfer across the wall into or from the liquid phase. These equations allowed the concentrations $C_{O_2,g}(t, x)$ and $C_{N_2,g}(t, x)$ to be calculated.

$$\frac{\partial C_{O_2,g}}{\partial t} = \frac{\partial}{\partial x} \left(D_g \frac{\partial C_{O_2,g}}{\partial x} - u_g C_{O_2,g} \right) - \frac{2}{R_m} K_m (C_{O_2,g} H_{O_2} - C_{O_2,l}) \quad \text{Eq. 4-7}$$

$$\frac{\partial C_{N_2,g}}{\partial t} = \frac{\partial}{\partial x} \left(D_g \frac{\partial C_{N_2,g}}{\partial x} - u_g C_{N_2,g} \right) - \frac{2}{R_m} K_m (C_{N_2,g} H_{N_2} - C_{N_2,l}) \quad \text{Eq. 4-8}$$

In Eq.4-7 and 4-8, u_g is the gas velocity in the fiber, while $C_{O_2,l}$ and $C_{N_2,l}$ are the corresponding dissolved O_2 and N_2 concentrations, respectively, at position x . The same mass transfer coefficient through the membrane, K_m , and the same diffusion coefficient in the gas phase, D_g , was assumed for both gases.

The gas velocity in the lumen was calculated differently for close-end or open-end operation. In the closed-end operation, frictional losses were neglected due to the very low gas velocity in the lumen. For this case, the sum of gas concentrations at any point x is equal to that of the inlet: $C_{O_2,g} + C_{N_2,g} = C_{O_2,in} + C_{N_2,in} = \text{constant}$. In these conditions, the sum of Eq. 4-7 and 4-8 is equal to zero. Adding Eq. 4-7 and 4-8, and rearranging, results in:

$$\frac{du_g}{dx} = - \frac{2K_m (C_{O_2,g} H_{O_2} - C_{O_2,l} + C_{N_2,g} H_{N_2} - C_{N_2,l})}{R_m (C_{O_2,in} + C_{N_2,in})} \quad \text{Eq. 4-9}$$

which allows for calculation of the local gas velocity along the fiber, $u_g(x)$, resulting from the diffusion of gasses into or out of the membrane. At the sealed end, the gas velocity must be zero ($u_g=0$ at $x=L_m$). The inlet concentrations were calculated from the universal gas law, for example, $C_{O_2,g,in} = p y_{O_2,in} / (RT)$ with $y_{O_2,in}$ the oxygen fraction in the inlet gas (i.e., 1 for pure oxygen or 0.21 for air). In model simulations for the parametric study, only pure oxygen was used, i.e., $C_{N_2,g,in}=0$.

For the open-end HFM, the constant gas velocity u_g was calculated from the Hagen-Poiseuille relationship, which is valid for slightly compressible fluids (Federspiel et al., 1996):

$$u_g = \frac{R_{m,i}^2}{8\mu_g L_m} (p_{in} - p_{out})$$

where μ_g is the gas dynamic viscosity and $R_{m,i}$ is the internal fiber radius. The inlet pressure p_{in} was defined according to the measured value, while the outlet pressure p_{out} was set as atmospheric pressure.

The boundary conditions for equations 4-7 and 4-8 imply constant concentrations in the inlet $C_{O_2,g,in}$ and $C_{N_2,g,in}$ at $x=0$. At $x=L_m$, zero diffusion was assumed for the open-end case, while for the closed-end zero total flux was imposed, which in both cases leads to:

$$\frac{\partial C_{O_2,g}}{\partial x}(t, x = L_m) = 0, \quad \frac{\partial C_{N_2,g}}{\partial x}(t, x = L_m) = 0$$

Initial gas concentrations for the entire membrane were equal to the inlet concentrations.

Predicted DO concentrations at the surface of the fiber ($C_{O_2,l}$) were directly compared with experimental measurements for both steady and transient states. Several model parameters were taken from the experimental conditions, such as membrane thickness, average water velocity, membrane length and radius, dissolved nitrogen, dissolved oxygen in the influent water, and oxygen gas pressures in the membrane inlet and outlet. For the model application, parametric studies were used, where simulations were carried out for a range of values of a single parameter. These and other parameters obtained from literature are summarized in Table 4-1.

Table 4-1 Back-diffusion model parameters

Parameter	Symbol	Value	Units	Reference
<i>Physical parameters</i>				
Water density	ρ	1000	kg/m ³	(Haynes et al., 2015)
Water dynamic viscosity	μ	0.001	Pa·s	(Haynes et al., 2015)
Gas dynamic viscosity	μ_g	$1.8 \cdot 10^{-5}$	Pa·s	(Haynes et al., 2015)
O ₂ diffusion coefficient in water	$D_{O_2,l}$	$2 \cdot 10^{-9}$	m ² /s	(Haynes et al., 2015)
N ₂ diffusion coefficient in water	$D_{N_2,l}$	$1.7 \cdot 10^{-9}$	m ² /s	(Haynes et al., 2015)
O ₂ and N ₂ diffusivity in gas	D_g	$1.76 \cdot 10^{-5}$	m ² /s	(Haynes et al., 2015)
Henry coefficient for O ₂	H_{O_2}	0.0338	mol(aq.)/mol(g)	(Haynes et al., 2015)
Henry coefficient for N ₂	H_{N_2}	0.0156	mol(aq.)/mol(g)	(Haynes et al., 2015)

Parameter	Symbol	Value	Units	Reference
Ideal gas constant	R	$8.206 \cdot 10^{-5}$	$\text{m}^3 \cdot \text{atm} / (\text{mol} \cdot \text{K})$	-
<i>Membrane parameters</i>				
Mass transfer coefficient	K_m	$5.4 \cdot 10^{-5}$	m/s	Fitted to experiments
Length	L_m	0.32	m	Experimental
		2.5	m	Parametric study
Outer radius	R_m	140	μm	Mitsubishi Rayon
Inner radius	$R_{m,i}$	130	μm	Mitsubishi Rayon
<i>Operation conditions</i>				
Oxygen inlet liquid concentration	$C_{O_2,l,in}$	0	mol/m^3	Experimental
Nitrogen inlet liquid concentration	$C_{N_2,l,in}$	0.64	mol/m^3	Experimental
Oxygen inlet gas concentration	$C_{O_2,g,in}$	69.7	mol/m^3	Experimental
Nitrogen inlet gas concentration	$C_{N_2,g,in}$	0	mol/m^3	Experimental
Inlet gas pressure	p_{in}	1.07 and 1.18	atm	Experimental
		1.68	atm	Parametric study
Outlet gas pressure (for open-end)	p_{out}	1	atm	Experimental
Average liquid velocity	u_{in}	1 and 5	mm/s	Experimental
Venting interval	t_c	1, 2, 5, 10 and 30	min	Parametric study
Venting open-end duration	t_o	20	s	Parametric study
Temperature	T	293.15	K	Experimental

4.4 RESULTS AND DISCUSSION

4.4.1 Determination of membrane mass transfer coefficient

A typical plot of measured DO profiles, perpendicular to the membrane surface, is shown in Figure 4-4. From the slope of the measured DO concentration profile, the flux of oxygen was calculated with Eq. 4-1. Subsequently, the mass transfer coefficient K_m was calculated from Eq. 4-2. An average K_m value of 5.4×10^{-5} m/s was obtained. This value is consistent with previously determined oxygen mass transfer coefficients for the same membrane (Ahmed et al., 2004) who found $K_m = 5 \times 10^{-5}$ m/s. In this study, the mass transfer coefficients for N_2 and O_2 were assumed to be equal.

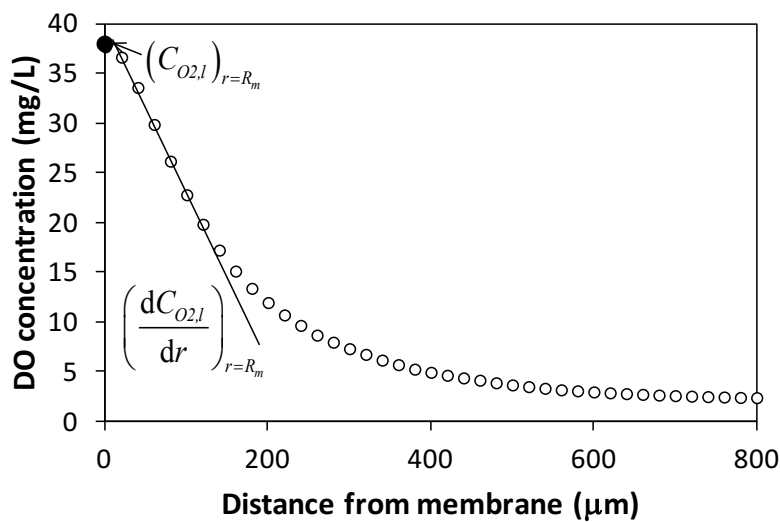


Figure 4-4 A representative profile of measured dissolved oxygen concentration through the mass transfer boundary layer in the liquid adjacent to the membrane. From this profile, the concentration and the normal gradient of concentration at the membrane surface ($d=0$ from membrane, which means $r=R_m$ in the numerical model) were extracted to calculate K_m .

4.4.2 Model evaluation

The back-diffusion model results were in good agreement with the measured values of DO along the membrane length, both for open- and closed-end operation, in steady state and transient conditions (Figure 4-5).

For closed ends using either air or pure O₂ supplied in co-current with the liquid flow ($u_{in}=5$ mm/s), the N₂ back-diffusion significantly reduced the concentrations of DO along the membrane length. The DO concentrations decreased from 35 mg/L to 5 mg/L when pure O₂ was supplied, and from 6 mg/L to 0.5 mg/L in case of air (Figure 4-5a). Accordingly, the steady state partial pressure of O₂ in the membrane lumen significantly decreased as O₂ was replaced by N₂ (Figure 4-5b). However, for the open-end operation, O₂ concentrations remained almost constant and at high values until the distal end of the membrane (Figure 4-5a). The open-end operation mode typically resulted in negligible back-diffusion effects. The partial pressure of O₂ in the gas decreased only slightly along the membrane because of the frictional pressure loss (Figure 4-5b).

The counter-current configuration showed lower DO concentrations towards the end of the membrane than the co-current configuration, in stationary conditions at an average water velocity of $u_{in}=1$ mm/s (Figure 4-5c). When water flows in the opposite direction of the supplied gas, i.e., in counter-current operation, O₂ transferred to the bulk liquid from the membrane does not accumulate downstream of the flow cell, thus decreasing DO concentrations in the liquid towards the closed end of the membrane. Therefore, the rest of the simulations considered only co-current operation. The partial pressure of O₂ in the counter-current operation decreases more than in the co-current because of the larger driving force for the trans-membrane transfer at the distal end, which is created by the oxygen-free influent water.

The model also accurately predicted the transient behavior of the DO concentration after suddenly closing the distal end of the membrane. The DO profile began with the steady state value in open-end operation, and progressively decreased towards the steady state value for the closed-end period. The experimental values and model predictions for the Port 4 are shown in Figure 4-5e. The time required to reach a steady O₂ profile in the lumen during the back-diffusion process was around 30 minutes.

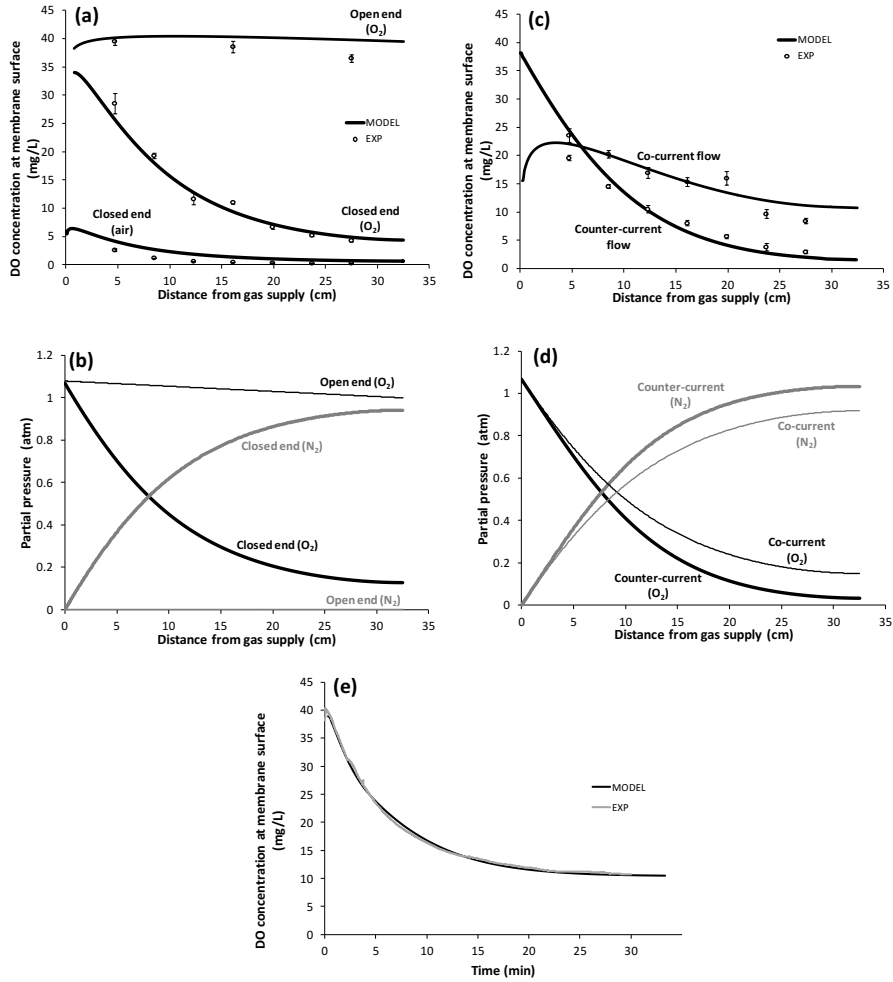


Figure 4-5 Experimental and model-simulated dissolved oxygen (DO) profiles at the membrane surface for the experimental HFM flow cell. Liquid and gas flows are co-current, unless indicated otherwise. (a) DO profiles for open and closed end operation modes using an inlet relative gas pressure of 0.18 atm and $u_{in}=5$ mm/s. DO profiles for air and oxygen as supply gases are shown for the closed end cases; (b) Simulations of partial pressures for O_2 and N_2 in the open-end and closed-end with pure O_2 supply; (c) DO profiles along the membrane length for closed-end mode in co- and counter-current flow configurations using pure oxygen at 0.07 atm and $u_{in}=1$ mm/s; (d) Simulations of partial pressures for O_2 and N_2 in the closed-end co- and counter-current operation with pure O_2 supply; (e) DO concentrations over time when transitioning from an open-end to a closed-end operation using pure O_2 at an inlet pressure of 0.18 atm. The microsensor measurement was performed at the membrane surface, for Port 4 at 16.1 cm from the inlet. Error bars in plots (a) and (c) are the standard deviation of triplicate measurements.

4.4.3 Model-based assessment of periodic venting

Closed-end HFMs initially have high gas transfer rates, as the membranes are filled with pure O₂. However, the rates quickly decrease as gas back-diffusion profiles develop. Numerical modeling was used to study the effects of periodically venting closed-end membranes, temporarily returning the membranes to the initial condition by venting the back-diffusion gases. The transitory gas dynamics of periodic venting were studied, and the impacts of different membrane opening intervals on OTRs and OTEs were explored.

Time-averaged O₂ partial pressures during three venting cycles were calculated from simulations with $R_m=140\ \mu\text{m}$, $K_m=5\times 10^{-5}\ \text{m/s}$, a longer membrane ($L_m=2.5\ \text{m}$) than in the experimental setup (closer to what might be used in a full-scale MABR) and an inlet gas pressure of $p_m=1.68\ \text{atm}$. Each cycle included a 30-minute closed period followed by a 20-second open (venting) period. This corresponds to a 30-minute “venting interval”. Figure 4-6 shows how, during the first cycle from $t=0$ to $t=30\ \text{min}$ (closed phase), a drop in the membrane-averaged O₂ partial pressure developed due to back-diffusion. Before the steady-state back-diffusion condition was fully obtained, the membrane was opened for 20 seconds, allowing the O₂ partial pressures along the membrane to recover their maximum value, which was slightly lower (1.54 atm) than the inlet gas pressure due to the pressure drop resulting from high gas velocities in open-end periods. The Hagen-Poiseuille relationship for slightly compressible fluids effectively predicted the observed flows for a broad range of pressures, ranging from 0.07 to 0.68 atm (Supplementary material, Figure S-7).

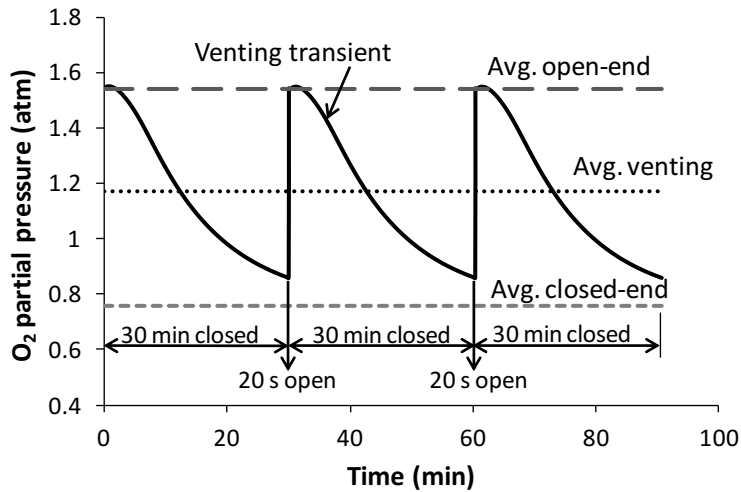


Figure 4-6 Simulated O_2 partial pressures in the lumen, averaged along the entire membrane length for different operation regimes: (i) transient (solid line) and time-averaged (dotted line) during three venting cycles, (ii) steady state closed end (short-dashed gray line), and (iii) steady state open end (long-dashed gray line).

This periodic venting provides high OTEs during most of the cycle duration, while maintaining higher time-averaged O_2 partial pressures than closed-end membranes. These results indicated that a 20-second open phase every 30 minutes was sufficient to allow oxygen pressure to recover its maximum value (1.54 atm) before the next closed phase. On the other hand, the membrane-averaged oxygen partial pressure dropped from 1.54 to 0.86 atm during the closed-end phase. On average, the membrane had a higher O_2 pressure than in the steady-state, closed-end operation. Therefore, it provided a greater OTR than the purely closed-end mode.

To evaluate how the duration of the closed-end/open-end cycles influenced the OTRs and OTEs, different venting intervals were simulated (i.e., time between openings) ranging from 1 to 30 minutes, with a constant venting (open end) duration of 20 seconds (Figure 4-7). The predicted average OTRs were 2 to 4 times higher than with permanently closed end. Furthermore, the OTE values (75-99%) were comparable to the closed end (100%), and dramatically higher than the open end mode (0.5%).

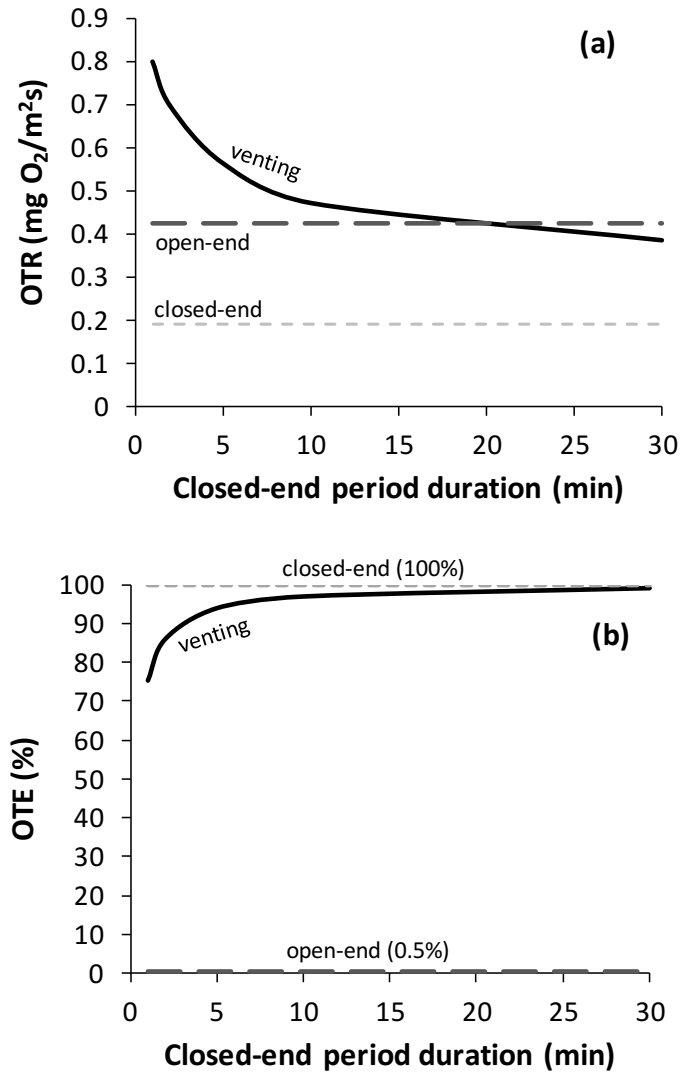


Figure 4-7 Comparison of simulated (a) oxygen transfer rates (OTR) and (b) oxygen transfer efficiencies (OTE) for open operation, closed operation, and intermittent opening. Venting mode was tested for venting intervals (time between ventings) ranging from 1 to 30 min, with 20 seconds open phases.

Interestingly, when the venting interval decreased below approximately 20 min, the OTR values were higher than for purely open-end operation, without significantly affecting the OTEs. This can be explained by the simulated O_2 pressure profiles along an HFM for open-end steady-state conditions, closed-end steady state conditions, and for the transition from open-end to closed-ended conditions (Figure 4-8). Profiles for the transition phase are presented at different times. For open-end operation, the O_2 pressure decrease is mainly due to frictional losses, whereas in closed-end operation the O_2 pressure drop is caused by back-diffusion. Furthermore, for the closed-end case, the O_2 concentration decreases from a constant initial value (equal to the inlet pressure of 1.68 atm), along the whole membrane until the steady state profile is reached. The shape of the transient profiles shows that, initially, N_2 back-diffusion only affects the initial portion of the HFM. This is where pure O_2 is supplied, and also where O_2 -free water enters the system, providing the maximum O_2 and N_2 concentration gradients. Then the N_2/O_2 gas mixture is transferred by advective flow towards the distal end of the membrane.

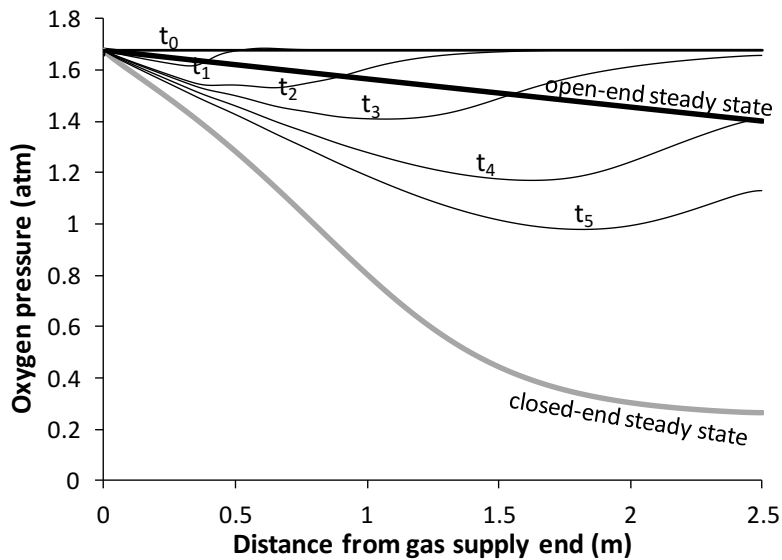


Figure 4-8 Oxygen partial pressure profiles along the membrane length for open-end (thick black line) and closed-end (thick gray line) steady state conditions, and time-averaged for transient conditions from open- to closed-end (thin black lines). The transient pressures are averages in time between the initial time and $t_1=2$ min, $t_2=5$ min, $t_3=10$ min, $t_4=20$ min, and $t_5=30$ min. Steady state conditions were essentially achieved after 60 minutes.

The time-dependent reduction in the O₂ pressure profiles occurs during the closed phase of a venting cycle. If the venting interval is smaller, the time- and length-averaged O₂ pressure concentrations increase, leading to higher OTRs. However, below a certain venting interval, the OTRs actually exceed those of the open-end configuration. This is caused by the pressure drop resulting from high gas velocities in open-end configuration. However, the pressure losses are negligible once the membrane is closed, thus allowing a higher total average pressure inside the membrane (see pressure profiles at times t_0 , t_1 , and t_2 in Figure 4-8).

The model results clearly indicated that periodic venting of closed-end operation can improve the gas transfer rates beyond those obtainable with conventional open-end operation, while maintaining high mass transfer efficiencies.

A simple calculation was made to compare different gas supply modes and show how the venting strategy could impact the MABR design, such as membrane area and required oxygen supply. Table 4-2 shows the OTRs, OTEs, required membrane areas, and O₂ supply needs using simulation results for the conditions in Figure 4-7. The membrane area was calculated for an arbitrary O₂ requirement. Oxygen supply requirements were determined by multiplying the OTE by the O₂ need. Finally, membrane areas and O₂ supply requirements for open-end and venting modes were normalized to the values for closed-end operation (first row in Table 4-2). Calculations indicated that the open-end operation requires only half of the membrane area of the closed-end operation. However, around 200 times more O₂ is required. With the intermittent venting of 20 seconds every 30 minutes, the required membrane area is the same as the open end, i.e., half of the area required for the closed-end operation. But O₂ requirement is essentially the same as the closed-end operation.

Table 4-2 Required membrane areas and oxygen fluxes for closed-end, open-end, and venting modes. Areas and fluxes are normalized by the closed-end value

Case	OTR ($\text{mg m}^{-2} \text{s}^{-1}$)	OTE (%)	Normalized required membrane area	Normalized O ₂ supply requirement
Closed end	0.19	100	1.0	1.0
Open end	0.42	0.47	0.5	213
Venting ($t_c=1$ min, $t_o=20$ s)	0.79	75.3	0.2	1.3
Venting ($t_c=30$ min, $t_o=20$ s)	0.38	98.9	0.5	1.0

4.4.4 Experimental assessment of gas supply strategies on HFM with biofilm

The periodic venting strategy was tested in a bench-scale MABR treating COD. Figure 4-9 shows the biofilm thicknesses and measured DO concentration profiles along the membrane surface in two MABRs that were run in parallel. MABR-1 was operated in open-end mode, and MABR-2 was operated in closed-end mode. Biofilm thickness images and measurements of DO profiles were taken after four weeks of operation.

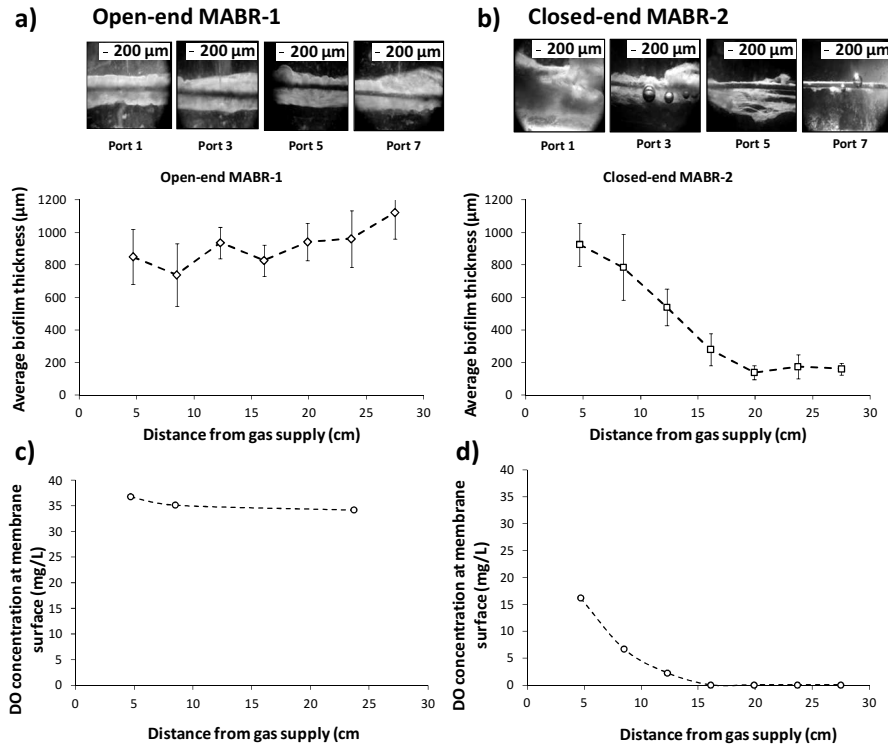


Figure 4-9 Biofilm thickness development along the membrane length in normally operated open-end MABR-1 (a) and closed-end MABR-2 (b). Experimental DO profiles at membrane surface for open-end MABR-1 (c) and closed-end MABR-2 (d). Port 1 is 4.7-cm from gas supply (left side), and Ports 3, 5, and 7 are at 7.6-cm increments from Port 1.

In MABR-1 (open end), a homogeneous biofilm grew through the fiber surface, with a similar thickness along the membrane length (Figure 4-9a). In MABR-2 (closed end), the biofilm was thick at the gas supply end, but was significantly reduced towards the sealed end of the membrane (Figure 4-9b). This can be explained by the measured DO profiles along the membrane (Figure 4-9 c and d). For MABR-1, the O_2 concentrations remained almost constant and at high values across the entire membrane (Figure 4-9c). This was because the high supply gas rate into the membrane resulted in negligible back-diffusion effects. The partial pressure of O_2 in the gas decreased only slightly along the membrane because of frictional pressure loss. N_2 back-diffusion was not significant in MABR-1, as inlet gas flow-rate was high enough to vent back-diffused N_2 to the atmosphere. However, for MABR-2, O_2 consumption and N_2 back-diffusion significantly reduced O_2

concentrations along the fiber length (Figure 4-9d) resulting in much lower OTRs and consequently lower overall COD removal fluxes (Figure 4-10).

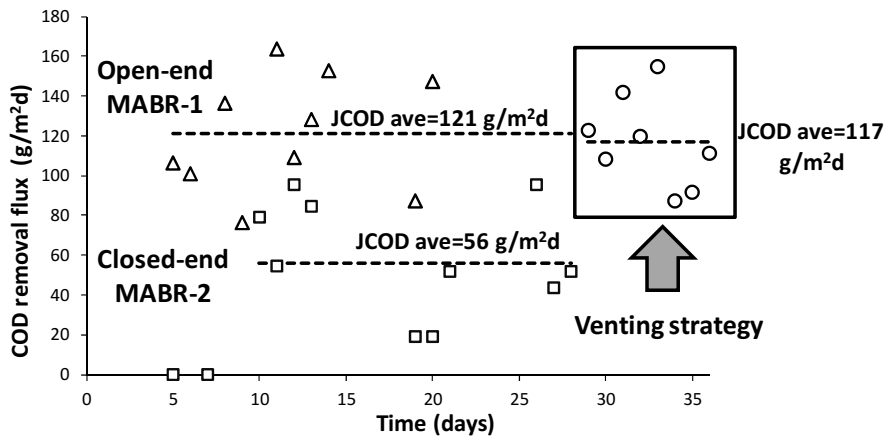


Figure 4-10 Experimentally observed COD removal fluxes in MABR-1 (triangles) and MABR-2 (squares) plotted against time. Circles enclosed in the black rectangle represent COD removal fluxes for the closed-end MABR-2 when a venting strategy of 20s open and 20 min closed was implemented.

The open-end MABR-1 had a higher average O_2 pressure than in the steady-state, closed-end MABR-2 (Figure 4-9 c and d). Therefore, it provided a greater OTRs and COD removal fluxes than the purely closed-end MABR-2 (Figure 4-10). The average COD removal flux for MABR-1 was double the value for MABR-2. In MABR-2, back-diffusion caused DO limitation in much of the membrane. This slowed the development of the biofilm, and consequently the increase in COD removal. Also, COD removal rates fluctuated considerably because this was a small reactor. As the biofilms grew, any biofilm detachment had a significant impact on the system. This would be more likely to average out in a larger system.

Note that the predicted OTR values for closed, open and venting strategies in a clean membrane were lower than those for MABRs. This was because the biofilm can eliminate the mass transfer resistance of the liquid concentration boundary layer (Semmens, 2008).

After four weeks of operation, MABR-2 was switched to periodic venting, which consisted of opening the membrane (venting) for 20 seconds every 20 minutes. Figure 4-10 shows the experimental COD removal fluxes that were obtained when periodic venting cycles were applied to MABR-2. Figure 4-11 shows the biofilm

thicknesses along the membrane length prior to venting, and after eight days of venting cycles.

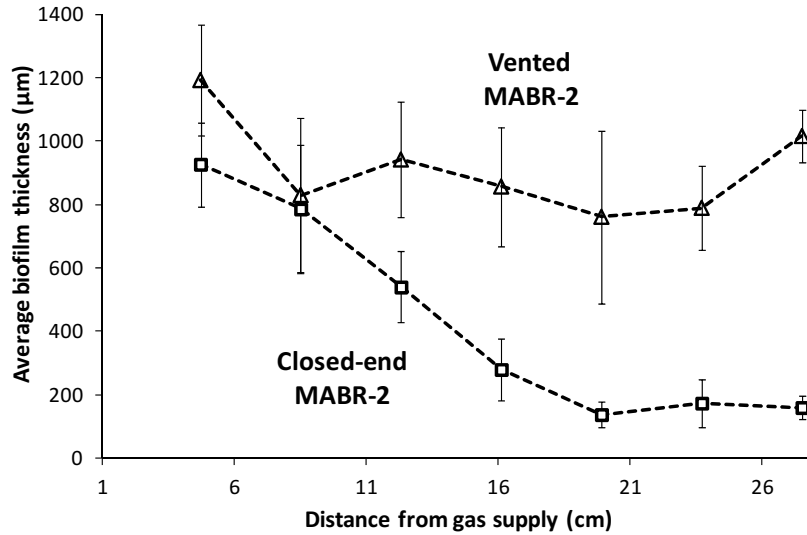


Figure 4-11 Biofilm thicknesses along the fiber length of MABR-2 just prior to initiating the venting cycles, and after eight days of periodic venting. Venting provides a much more uniform biofilm thickness.

The mathematical model predicted that greater average O_2 partial pressures, and consequently higher OTRs and removal fluxes, could be obtained by applying periodic venting to a closed-end MABR. The experimental COD removal fluxes are shown in Figure 4-10. The average COD removal flux became double that for the closed-end operation, increasing from $56 \text{ gCOD/m}^2\text{d}$ to $117 \text{ gCOD/m}^2\text{d}$. This value is very similar to the $121 \text{ gCOD/m}^2\text{d}$ obtained in MABR-1 (Figure 4-10). This was in part due to the more uniform biofilm thickness along the length of the fiber when periodic venting was implemented (Figure 4-11). Based on the measured gas flow rate through the membrane during the open cycles, OTEs of at least 97% were obtained when applying the periodic venting. In this research, the COD removal rates were greater than those obtained in some previous MABR studies. This was mainly because pure oxygen was used as the supplied gas. Also, acetate was used as organic carbon source. Acetate is readily biodegradable substrate, as opposed to more complex organics such as wastewater. Nevertheless, COD removal rates found in this study were similar than the ones obtained by Osa et al., (1997), Pankhania et al., (1999) and Brindle et al., (1999), who reported COD removal rate values in MABRs fed with pure O_2 of 180, 42.7, 62.6 $\text{gCOD/m}^2\text{d}$ respectively.

Experimental results verified that periodic venting of closed-end MABRs can lead to high OTRs and OTEs, improving the overall process performance and increasing the energy efficiency.

This work highlights the potential transient behavior of gas back-diffusion, and the potentially significant lag in reaching steady state operation after a perturbation. For example, changing the supply gas pressure, concentration of supply gas in the liquid phase, and concentration of back-diffusion gases in the liquid phase, among others. Following any of these changes, it may take a considerable amount of time to reach steady state.

The optimal venting interval (time between openings) and venting time (open period) depends on a variety of factors, including the membrane mass transfer coefficient, diameter, length, supply gas pressure and concentration, and dissolved gas concentrations in the liquid. For instance, larger membrane diameters will likely allow a greater venting interval, as there is greater gas storage in the membrane lumen relative to the gas transfer across the membrane. Larger HFM diameters, and longer membrane lengths, would require longer venting periods. When selective membranes are used, the relationship between the diffusion coefficients can also be important. Finally, the effect of liquid flow in a contactor, i.e., co-current, counter-current, or cross flow, can impact the gas transfer rates and the transition to steady-state conditions. Future research should explore the impact of the above factors in more detail.

Past research on MABRs has shown that water vapor can diffuse into the membrane and condense at the sealed end, plugging part of the membrane (Côte et al., 1988; Côte et al., 1989; Fang et al., 2004). However, it would take weeks or months for condensation to have an appreciable effect on the membrane behavior. In our closed-end experiments, the membranes were vented every two days, and no sign of condensate accumulation was observed during the ventings. Some MABRs are periodically vented to remove water condensation, but the frequency of venting is typically too low to obtain the gas transfer rate benefits. Based on our findings, it would be easy to increase the venting frequency to both remove condensate and obtain higher OTRs.

The above strategy was studied for O₂ supply to an MABR, but the periodic venting is also relevant to MABRs supplied with air, or MBfR applications with gases such as hydrogen gas (H₂) or methane (CH₄) (Martin and Nerenberg, 2012; Shi et al., 2013).

4.5 CONCLUSIONS

The periodic venting of lumen gases in a closed-end MABR can greatly improve the membrane's OTRs and contaminant removal fluxes, without significantly impacting the OTEs. This is due to the transient behavior of the lumen gas profiles when shifting from open-end to closed-end operation. When the venting interval is short enough, the OTR can be even higher than with continuous open-end operation. This novel gas supply strategy can greatly increase the capacity of MABRs, and decrease the capital and operating cost of new systems. Future research should address in more detail the range of factors that affect the selection of opening interval, the closed duration, and the impacts of these factors on the OTRs and OTEs.

4.6 REFERENCES

- Ahmed, T., Semmens, M.J., 1992a. The Use of Independently Sealed Microporous Hollow Fiber Membranes for Oxygenation of Water - Model Development. *J. Memb. Sci.* 69(1-2), 11-20.
- Ahmed, T., Semmens, M.J., 1992b. Use of Sealed End Hollow Fibers for Bubbleless Membrane Aeration - Experimental Studies. *J. Memb. Sci.* 69(1-2), 1-10.
- Ahmed, T., Semmens, M.J., Voss, M.A., 2004. Oxygen transfer characteristics of hollow-fiber, composite membranes. *Advan. Environ. Res.* 8, 637-646.
- Aybar, M., Pizarro, G., Boltz, J.P., Downing, L., Nerenberg, R., 2014. Energy-efficient wastewater treatment via the air-based, hybrid membrane biofilm reactor (hybrid MfBR). *Water Sci. Technol.* 69(8), 1735-1741.
- Brindle, K., Stephenson, T., Semmens, M.J., 1998. Nitrification and oxygen utilisation in a membrane aeration bioreactor. *J. Memb. Sci.* 144, 197-209.

- Brindle, K., Stephenson, T., Semmens, M.J., 1999. Pilot-plant treatment of a high-strength brewery wastewater using a membrane aeration bioreactor. *Water Environ. Res.* 71 (6), 1197–1204.
- Castagna, L., Zanella, A., Scaravilli, V., Magni, F., Deab, S.A.E., Introna, M., Mojoli, F., Grasselli, G., Pesenti, A., Patroniti, N., 2015. Effects on membrane lung gas exchange of an intermittent high gas flow recruitment maneuver: preliminary data in veno-venous ECMO patients. *J. Artif. Organs* 18(3), 213-219.
- Côte, P., Bersillon, J.L., Huyard, A., Faup, G., 1988. Bubble-Free Aeration Using Membranes - Process Analysis. *Journal Water Pollut. Control Fed.* 60(11), 1986-1992.
- Côte, P., Bersillon, J.L., Huyard, A., 1989. Bubble-Free Aeration Using Membranes - Mass-Transfer Analysis. *J. Memb. Sci.* 47(1-2), 91-106.
- Downing, L.S., Nerenberg, R., 2008. Total nitrogen removal in a hybrid, membrane-aerated activated sludge process. *Water Res.* 42(14), 3697-3708.
- Fang, Y., Clapp, L.W., Hozalski, R.M., Novak, P.J., Semmens, M.J., 2004. Membrane gas transfer under conditions of creeping flow: modeling gas composition effects. *Water Res.* 38(10), 2489-2498.
- Federspiel, W.J., Williams, J.L., Hattler, B.G., 1996. Gas flow dynamics in hollow-fiber membranes. *Aiche Journal* 42(7), 2094-2099.
- Federspiel, W.J., Henschir, K.A., 2004. *Encycl. Biomater. Biomed. Eng.* Marcel Dekker, Inc., Pittsburgh, PA.
- Haynes, W.M., Bruno, T.J., Lide, D.R. (Ed.), 2015. *CRC handbook of chemistry and physics* CRC. Press/Taylor and Francis, Boca Raton, FL. Online at <http://www.hbcnetbase.com/>
- Hibiya, K., Terada, A., Tsuneda, S., Hirata, A., 2003. Simultaneous nitrification and denitrification by controlling vertical and horizontal microenvironment in a membrane-aerated biofilm reactor. *J. Biotechnol.* 100(1), 23-32.
- Hondzo, M., Feyaerts, T., Donovan, R., and O'Connor, B.L. 2005. Universal scaling of dissolved oxygen distribution at the sediment-water interface: A power law. *Limnol. Oceanogr.* 50, 1667-1676.
- Jácome, A., Molina, J., Suárez, J., Tejero, I., 2006. Simultaneous Removal of Organic Matter and Nitrogen Compounds in Autoaerated Biofilms. *J. Environ. Eng.* 132(10), 1255-1263.

Li, J., Zhu, L.P., Xu, Y.Y., Zhu, B.K., 2010. Oxygen transfer characteristics of hydrophilic treated polypropylene hollow fiber membranes for bubbleless aeration. *J. Memb. Sci.* 362, 47-57.

Martin, K.J., Nerenberg, R., 2012. The membrane biofilm reactor (MBfR) for water and wastewater treatment: principles, applications, and recent developments. *Bioresour. Technol.* 122, 83-94.

Matsuda, N., Nakamura, M., Sakai, K., Kuwana, K., Tahara, K., 1999. Theoretical and experimental evaluation for blood pressure drop and oxygen transfer rate in outside blood flow membrane oxygenator. *J. Chem. Eng. Japan* 32(6), 752-759.

Matsumoto, S., Terada, A., Aoi, Y., Tsuneda, S., Alpkvist, E., Picioareanu, C., van Loosdrecht, M.C.M., 2007. Experimental and simulation analysis of community structure of nitrifying bacteria in a membrane-aerated biofilm. *Water Sci. Technol.* 55(8-9), 283-290.

Nerenberg, R., 2016. The membrane-biofilm reactor (MBfR) as a counter-diffusional biofilm process. *Curr. Opini. Biotechnol.* 38, 131-136.

Osa, J., Eguia, E., Vidart, T., Jácome, A., Lorda, I., Amieva, J., Tejero, I., 1997. Wastewater Treatment with biofilm Membrane Reactors. In *Conference on Advanced Wastewater Treatment Processes*; Leeds University: Leeds, UK, 1997.

Pankhania, M., Brindle, K., Stephenson, T., 1999. Membrane aeration bioreactors for wastewater treatment: completely mixed and plug-flow operation. *Chem. Eng. J.* 73(2), 131-136.

Roggy, D.K., Novak, P.J., Hozalski, R.M., Clapp, L.W., Semmens, M.J., 2002. Membrane gas transfer for groundwater remediation: Chemical and biological fouling. *Environ. Eng. Sci.* 19(6), 563-574.

Schaffer, R.B., Ludzack, F.J., Ettinger, M.B.C.F.p.d.S., 1960. Sewage Treatment by Oxygenation through Permeable Plastic Films. *Journal (Water Pollut. Control Fed.)* 32(9), 939-941.

Semmens, M.J., Dahm, K., Shanahan, J., Christianson, A., 2003. COD and nitrogen removal by biofilms growing on gas permeable membranes. *Water Res.* 37(18), 4343-4350.

Semmens, M.J., 2008. Alternative MBR configurations: using membranes for gas transfer. *Desalination* 231(1), 236-242.

Shi Y, Hu S, Lou J, Lu P, Keller J, Yuan Z (2103). Nitrogen removal from wastewater by coupling anammox and methane-dependent denitrification in a membrane biofilm reactor. *Environ. Sci. Technol.* 2013, 47:11577-11583.

Syron, E., Casey, E., 2008. Membrane-aerated biofilms for high rate biotreatment: performance appraisal, engineering principles, scale-up, and development requirements. *Environ. Sci. Technol.* 42(6), 1833-1844.

Tanishita, K., Nakano, K., Sakurai, Y., Hosokawa, T., Richardson, P.D., Galletti, P.M., 1978. Compact Oxygenator Design with Curved Tubes Wound in Weaving Patterns. *Trans. Am. Soc. Artif. Internal Organs* 24, 327-331.

Terada, A., Hibiya, K., Nagai, J., Tsuneda, S., Hirata, A., 2003. Nitrogen removal characteristics and biofilm analysis of a membrane-aerated biofilm reactor applicable to high-strength nitrogenous wastewater treatment. *Journal of Biosci. Bioeng.* 95(2), 170-178.

Timberlake, D.L., Strand, S.E., Williamson, K.J., 1988. Combined aerobic heterotrophic oxidation, nitrification and denitrification in a permeable-support biofilm. *Water Res.* 22(12), 1513-1517.

Weiss, P.T., Gulliver, J.S., Semmens, M.J., 1998. In-stream hollow-fiber membrane aeration. *J. Hydraul. Eng.* 124(6), 579-588.

Weissman, M.H., Mockros, L.F., 1969. Oxygen and Carbon Dioxide Transfer in Membrane Oxygenators. *Med. Biol. Eng.* 7(2), 169-184.

Chapter 5

Effect of biofilm development on gas dynamics in MABRs ¹

¹ Part of this chapter has been published as:

Pérez-Calleja, P., Aybar, M., Picioreanu, C., Esteban-García, A.L., Nerenberg, R., 2017. *Effect of Biofilm Development on Gas Back-Diffusion in Membrane Aerated Biofilm Reactors (MABRs)*. 24th Triennial Symposium on Advancements in Water & Wastewater. Borchardt Conference, Ann Arbor (U.S.), 21-22 February.

OUTLINE

SUMMARY.....	173
5.1 INTRODUCTION.....	173
5.2 OBJECTIVES	176
5.3 MATERIALS AND METHODS.....	176
5.3.1 Experimental flow cell configuration.....	177
5.3.2 Synthetic medium for the MABRs	177
5.3.3 Analytical methods	177
5.3.4 DO measurements at steady-state and transient conditions	178
5.3.5 Numerical model for gas back-diffusion in presence of a biofilm ..	178
5.3.5.1 General characteristics of the model	178
5.3.5.2 Mass transport and reaction in the biofilm	180
5.3.5.3 Model parameters and simulation scenarios	180
5.4 RESULTS AND DISCUSSION	184
5.4.1 Experimental results	184
5.4.1.1 Steady state DO profiles	184
5.4.1.2 Transient DO profiles	184
5.4.2 Simulation results	186
5.4.2.1 HFM vs MABR	186
5.4.2.2 Effect of biofilm activity and thickness in DO profiles of MABRs ...	189
5.4.2.3 Simulations of transient DO profiles in MABRs and HFM.	191
5.4.2.4 Optimization of the MABR operation	193
5.5 CONCLUSIONS.....	199
5.6 REFERENCES.....	200

SUMMARY

Back-diffusion of inert gases into the lumen of Membrane-Aerated Biofilm Reactor (MABR) membranes decreases overall gas transfer rates and contaminant removal fluxes. However, most back-diffusion studies have neglected the effects of biofilms growing on the membranes, even though they are an integral part of the process. In this Chapter, experiments and modeling were used to study the effect of aerobic, heterotrophic biofilms on back-diffusion in pure oxygen supplied MABRs. Gas back-diffusion profiles were found to be impacted by two phenomena. First, oxygen consumption within the biofilm affected oxygen transfer fluxes, which in turn affected the O_2 profiles along the membrane. Second, the biofilm acted as a diffusion barrier for N_2 diffusing into the membrane. This effect depended primarily on the biofilm thickness and the N_2 concentration in the lumen. The effects were significant for transient conditions. These results suggest that biofilm effects should be considered when using a venting approach to minimize the effects of gas back diffusion. It was also found that in closed-end air supplied membranes, not only back-diffusion of N_2 from the bulk liquid could result in a decreasing oxygen concentration profile along the fiber length, but also the accumulation of the N_2 gas present in the air gas supply. Venting strategies were specifically simulated for pure oxygen and air supplied MABRs, and demonstrated to have the potential of maximizing both, oxygen transfer capacities and oxygen transfer efficiencies. Applying the proper venting interval, it was found that average O_2 partial pressures inside the membrane lumen even higher than for open end operation modes could be achieved.

5.1 INTRODUCTION

The membrane-biofilm reactor (MBfR) is a treatment technology based on membranes that supply a gaseous substrate to a biofilm growing directly on the membrane surface (Nerenberg 2016). When used to deliver air or oxygen (O_2), it is referred to as the membrane-aerated biofilm reactor (MABR) (Semmens et al., 2003; Syron and Casey 2008; Martin and Nerenberg 2012; Nerenberg 2016).

MABRs typically use polymeric hollow-fiber membranes, which can be operated with open or closed ends. When the ends are closed, essentially 100% of the gas is utilized (Semmens et al., 2003; Syron and Casey, 2008; Martin and Nerenberg, 2012). This can save up to 85% in energy costs compared to bubbling aeration processes, where only 10-30% of the oxygen is typically transferred to the liquid

phase (Aybar et al. 2014). However, as demonstrated in Chapter 4, closed-end operation provides lower oxygen transfer rates (OTRs), due to oxygen depletion and back-diffusion of nitrogen gas (N_2), and other inert gases from the liquid into the membrane lumen. These gases are swept towards the end of the membrane, resulting in a “deadened” zone. Since only part of the membrane is fully active, the average removal fluxes across the whole membrane are lowered.

MABRs are also operated with open ended membranes. In this case, higher oxygen transfer efficiencies are obtained. However, this comes at the expense of higher energy consumption: as part of the gas is vented, a much smaller fraction of oxygen is utilized. This is shown schematically in Figure 5-1.

When an MABR membrane begins operation, it typically has uniform oxygen partial pressures along its length, providing uniformly high OTRs. However, the oxygen partial pressure quickly decreases due to biological consumption, friction losses (mainly in open-end operation, as gas velocity is much higher), and back-diffusion of other dissolved gases, such as N_2 (Schaffer et al., 1960, Ahmed and Semmens 1992) and CO_2 (Nemeth et al., 2016).

The transfer of O_2 , N_2 and other gases (like CO_2) between the membrane lumen and the biofilm/liquid phases is driven by the concentration gradients in the membrane, biofilm, and liquid diffusion layer. For O_2 transfer, the biofilm utilization of O_2 can have an impact on O_2 transfer rates. This in turn can affect O_2 profiles in the membrane.

Dissolved N_2 is typically present in waters, and can also be generated within denitrifying biofilms. Carbon dioxide (CO_2) is also present in water at low concentrations, but degradation of organic contaminants could generate significant concentration of CO_2 (Nemeth et al., 2016). For back-diffusion of N_2 from the bulk to the membrane lumen, the biofilm acts as a diffusion barrier. Thus, the biofilm behaves differently towards the diffusion of O_2 and N_2 . It can enhance O_2 diffusion, but it only hinders N_2 diffusion.

When a steady-state gas profile along the length of the membrane is reached, a significant portion of it is “deadened” by dilution with nitrogen, leading to lower overall OTRs (Figure 5-1 a).

In open-end configurations, the advective mass transport along the membrane typically is far greater than the diffusive mass transfer across the membrane wall. This results in more uniform oxygen partial pressures along the membrane and higher overall OTRs compared with closed-end systems. However, the OTEs

(oxygen transfer efficiencies) are lower, since a large amount of oxygen gas supplied to the membrane is lost from open end (Figure 5-1 b).

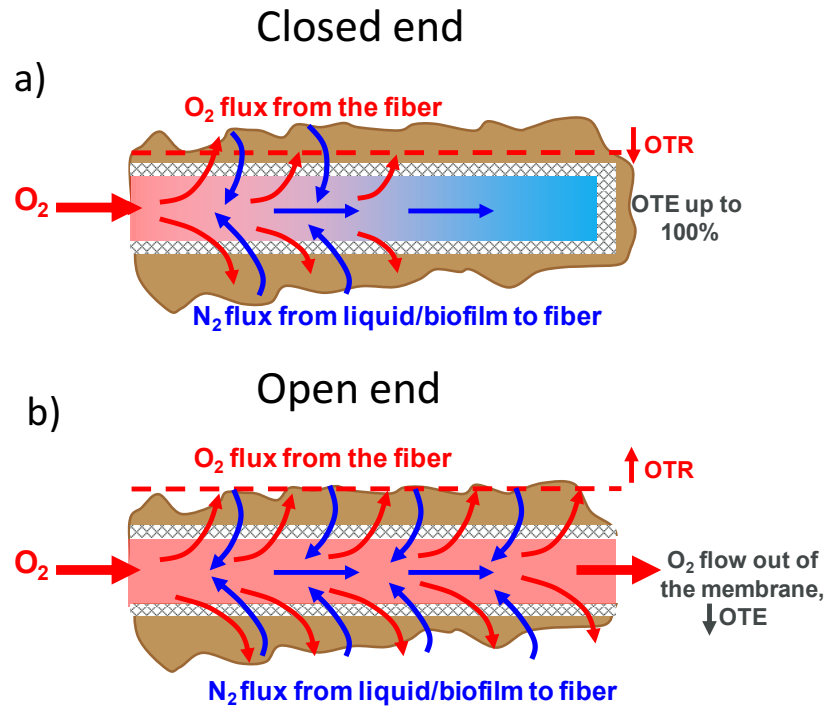


Figure 5-1: Schematic showing differences between hollow-fiber membranes with biofilm in: (a) closed-end operation, and (b) open-end operation.

While few past studies have explored gas-back-diffusion in clean membranes, there are no systematic studies of gas back-diffusion in membranes supporting a biofilm layer. This is especially complex, as gas back-diffusion affects biofilm activity, and biofilm activity influences gases profiles along the membranes.

Gilmore et al., (2009) proposed a simplified mechanistic model for oxygen transfer in MABRs. They also measured higher OTEs when an active biofilm was present compared with a clean membrane. However back-diffusion was not considered, the membrane was operated in open-end mode and only a single condition was investigated. Furthermore, no studies have explored the back-diffusion in MABRs for membranes supplied with air instead of pure gases.

It was hypothesized that back-diffusion behavior in membranes supporting biofilms (MABRs) may be significantly different from clean hollow-fiber membranes (HFM).

On the one hand, biofilm imposes a resistance for O_2 and N_2 to diffuse through the biofilm. On the other hand, the biofilm consumes O_2 , increasing gas transfer rates by lowering the O_2 concentration at the membrane surface. These phenomena may impact the steady-state O_2 concentration profiles along the membrane length, as well as the transient back-diffusion dynamics (i.e. the period while the membranes gases reaches steady state after opening or closing the membrane end).

Another hypothesis of the present study was that in closed-end air supplied membranes, not only back-diffusion of N_2 from the bulk liquid can dilute the oxygen concentration inside the membrane, but also the accumulation of the N_2 gas present in the air gas supply can result in a decreasing oxygen concentration profile along the membrane length. This effect could have a significant impact in MABRs that are operated in close-ended or periodically opened end modes in order to maintain a high total gas pressure inside the fibers. For instance, some MABR processes require that gas pressure exceeds the hydrostatic pressure of the water to avoid water leaks into the membranes, and in other cases high gas pressures may be wanted in order to achieve higher substrate removal rates.

5.2 OBJECTIVES

The main objective of this study was to explore the impact of biofilm on back-diffusion process in air and pure oxygen supplied MABRs, as a means to minimize the detrimental effects of gas back diffusion and maximize both OTEs and OTRs.

5.3 MATERIALS AND METHODS

Back-diffusion steady and transient behaviors were experimentally studied for a clean HFM and for a heterotrophic MABR by measuring the dissolved oxygen (DO) concentrations at the membrane surface with microsensors. A mathematical model was developed and then validated with the experimental data. Then, it was applied to expand the experimental findings and better understand the effect of the presence of a biofilm in back-diffusion process. The model was also used as a predictive tool to optimize MABRs operation by the implementation of periodic venting strategies.

5.3.1 Experimental flow cell configuration

Two experimental flow cells with a single membrane were used to explore gas back-diffusion in clean HFM and in MABR configurations. The same experimental set up as the one described in Chapter 4 was used (see Figure 4-2). In the same way, the flow cells had seven ports for DO microsensor measurements, located every 5 cm along the flow cells. Composite membranes (HFM200TL, Mitsubishi Rayon, Japan) had an outer diameter of 280 μm and a wall thickness of 40 μm . They were located in the middle of the flow cells, supported at both ends by a gas-supplying manifold. The gas was supplied from one end at constant pressure, while a valve at the opposite end allowed open or closed operation. Pure oxygen was supplied at 0.18 atm relative pressure. The influent flow in the HFM flow cell was 10 mL/min, resulting in a liquid velocity (u_{in}) of 5 mm/s and in a Reynolds number of 28. An influent flow rate of 1 mL/min and a recirculation flow rate of 60 mL/min were used for the MABR flow cell, providing a liquid velocity of 27 mm/s and a Reynolds number of 163. Liquid velocities in both flow cells were well within the laminar flow regime. For the MABR, synthetic media (described below) was previously deoxygenated and fed to the flow cell. The biofilm was grown under open end mode to maintain the same oxygen pressure in the membrane lumen and promote an evenly distributed biofilm thickness along the membrane length. Then, to evaluate back-diffusion steady and transient behaviors, the end of the membrane was closed and DO evolution was studied. Experimental DO measurements at the membrane surface were collected for the clean HFM and MABR for closed-end steady state and transient shifts between open and closed-end conditions and used to test the back-diffusion mathematical model.

5.3.2 Synthetic medium for the MABRs

The same synthetic medium as the one described in Chapter 4 (section 4.2.2) was used to feed the MABR. In the same way, potassium acetate was added as COD source to achieve around 30 mg COD/L.

5.3.3 Analytical methods

Chemical oxygen demand (COD) was monitored in the influent and effluent of the MABR reactors using colorimetric methods (Hach, Loveland, CO, USA). A glass electrode pH meter was used to monitor pH. Biofilm thickness was determined as

described in chapter 4, section 4.2.3. Further information regarding analytical methods is provided in chapter 2.

5.3.4 DO measurements at steady-state and transient conditions

Clark-type oxygen microsensors (Unisense A/S, Denmark) with a 10- μm tip diameter were used to measure DO concentrations at membrane surface. The microelectrode movement was controlled with a micro-manipulator (Model MM33-2, Unisense A/S).

Longitudinal steady-state DO profiles at the membrane surface were collected from the measurement ports in both, clean HFM and MABR (with a 180- μm biofilm thickness) flow cells. DO measurements were performed two hours after closing the end of the membrane in case of HFM and 5 hours after in case of MABR, to ensure back-diffusion steady-state was reached. For the MABR, DO steady-state profiles were measured for 180 μm biofilm thickness. DO measurements were collected at least in triplicate. For transient conditions, DO evolution in both flow cells was measured continuously at the membrane surface, for one of the intermediate ports, during the shift from open-end to closed-end operation in both clean HFM and MABR flow cells. The MABR transient measurements were made for a 700- μm biofilm thickness.

5.3.5 Numerical model for gas back-diffusion in presence of a biofilm

5.3.5.1 General characteristics of the model

A mathematical model for gas back-diffusion in MABRs was developed, addressing both steady-state and transient conditions. The model included pure oxygen or air supply from the membrane lumen, and assumed that the bulk liquid was in equilibrium with 1 atmosphere of N_2 gas. The model was implemented in the finite-element simulation platform COMSOL Multiphysics (COMSOL 4.4, Comsol Inc., Burlington, MA, www.comsol.com). The numerical model was based on the previously developed back-diffusion model for HFM (chapter 4, section 4.2.6). It included fluid flow and mass transport of dissolved oxygen, nitrogen and acetate in the liquid flow and inside the biofilm. Furthermore, the model included the biological consumption of oxygen and acetate inside the biofilm. A two-dimensional (2-D) axisymmetric geometry was set along the axis of the membrane lumen for liquid and biofilm domains (direction x) with radial gradients along

direction r . The 2-D model implied an annular cross-section for the flow, with size 3.4 mm (the radius of a circle with the same area as the square cross-section). This model was coupled with a one-dimensional (1-D) domain for gas flow and mass transport in the membrane lumen (assuming no radial gradients in the lumen) (Figure 5-2).

The description of the mathematical equations for flow and mass transport in the liquid and gas domains were undertaken from Chapter 4 (section 4.2.6).

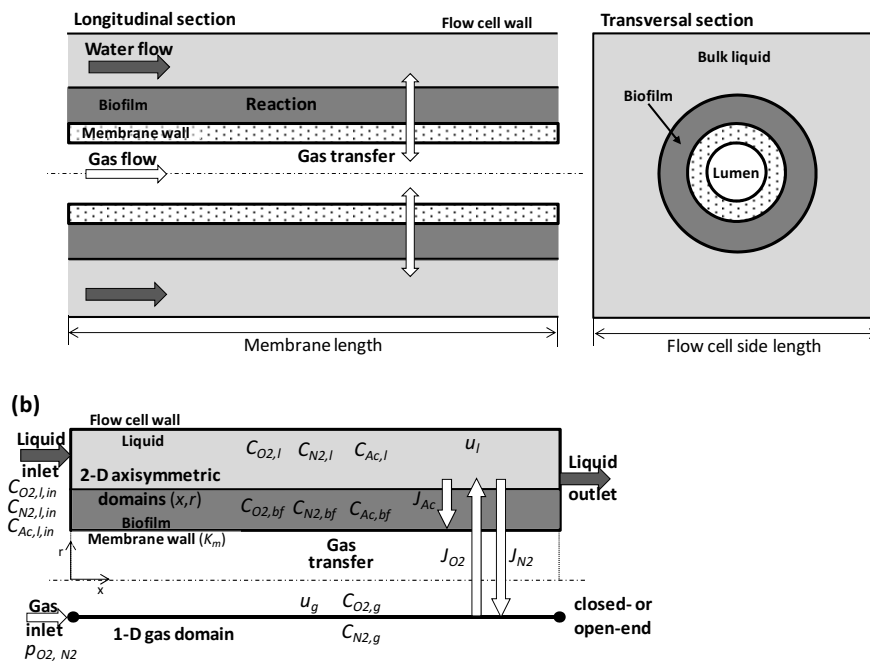


Figure 5-2: (a) Schematic representation (not at scale) of the experimental aeration system with a single HFM supporting a biofilm inside a square-section flow cell filled with liquid. (b) Model representation including a 2-D axisymmetric liquid domain connected via the membrane wall with a 1-D gas domain.

In Figure 5-2 a, water flows between the biofilm (in the MABR) or between the membrane (in the clean HFM) and the flow cell wall. The membrane can be supplied with different O_2 and N_2 partial pressures. In Figure 5-2 b, C_{O_2} , C_{N_2} and C_{Ac} represent oxygen, nitrogen and acetate concentrations in the liquid (l), biofilm (bf) or in the gas (g) phases; u_l and u_g refer to liquid and gas velocities and J to mass fluxes.

5.3.5.2 Mass transport and reaction in the biofilm

In the biofilm, dissolved species mass balance included diffusion and reaction, with an effective diffusivity assumed as 80% of that in the bulk liquid (Horn and Morgenroth, 2006). Biomass activity followed dual Monod kinetics (Rittmann and McCarty, 2001) as concentrations of oxygen and acetate (Ac) can be simultaneously limited in counter-diffusional biofilms. As the back-diffusion process time scale is in the order of seconds to minutes, biofilm growth was neglected to simplify the model.

The mass transport of oxygen, nitrogen and acetate in the biofilm were determined by Fick's law:

$$\nabla \cdot (-D_{O_2} \cdot f_{O_2} \nabla C_{O_2}) = 0 \quad \text{Eq. 5-1}$$

$$\nabla \cdot (-D_{N_2} \cdot f_{N_2} \nabla C_{N_2}) = 0 \quad \text{Eq. 5-2}$$

$$\nabla \cdot (-D_{Ac} \cdot f_{Ac} \nabla C_{Ac}) = 0 \quad \text{Eq. 5-3}$$

where D_{O_2} , D_{N_2} and D_{Ac} are the O_2 , N_2 and acetate diffusion coefficients in the liquid, C_{O_2} , C_{N_2} and C_{Ac} are the dissolved concentrations and f_{O_2} , f_{N_2} and f_{Ac} are the biofilm to water diffusion coefficient ratios. A condition of no flux was used for the flow in the glass cell wall.

Oxygen and acetate consumption rates are expressed as:

$$r_{O_2} = -X_a \cdot q_{max} \cdot \frac{C_{O_2}}{C_{O_2} + K_{O_2}} \cdot \frac{C_{Ac}}{C_{Ac} + K_{Ac}} \cdot \left(\frac{1-Y}{Y}\right) \quad \text{Eq. 5-4}$$

$$r_{Ac} = -X_a \cdot q_{max} \cdot \frac{C_{O_2}}{C_{O_2} + K_{O_2}} \cdot \frac{C_{Ac}}{C_{Ac} + K_{Ac}} \cdot \left(\frac{1}{Y}\right) \quad \text{Eq. 5-5}$$

where X_a is the biomass concentration, Y is the yield of biomass production per unit acetate utilized, q_{max} is maximum specific rate of substrate utilization for aerobic heterotrophs, and K_{O_2} and K_{Ac} are the half saturation concentrations for oxygen and acetate respectively. Nitrogen was assumed to be inert.

5.3.5.3 Model parameters and simulation scenarios

Simulated DO concentrations at the surface of the membrane for clean HFMs and MABRs were directly compared with experimental measurements for both steady and transient states. Several model parameters were taken from the experimental

conditions, such as membrane and biofilm thickness, average water velocity, membrane length and radius, dissolved nitrogen, dissolved oxygen in the influent water, bulk liquid acetate concentrations, and oxygen gas pressures in the membrane inlet and outlet. For the model application, parametric studies were used, where simulations were carried out for a range of values of a single parameter. These and other parameters obtained from literature are summarized in Table 5-1. Physical parameters of the liquid and gas phases and membrane parameters were adopted from the back-diffusion mathematical model for clean HFM developed in Chapter 4 (See Table 4-1).

Table 5-1. Biofilm back-diffusion model parameters

Parameter	Symbol	Value	Units	Reference
<i>Physical and kinetic parameters</i>				
Ac diffusion coefficient in water	$D_{Ac,l}$	$9.5 \cdot 10^{-10}$	m^2/s	Haynes et al., 2015)
Biofilm diffusivity correction factor	f	0.8	-	(Horn and Morgenroth, 2006)
Maximum specific utilization rate for heterotrophs	q_{max}	10	1/d	(Downing and Nerenberg, 2008)
Oxygen half saturation concentration	K_{O_2}	0.24	mg/L	(Downing and Nerenberg, 2008)
Acetate half saturation concentration	K_{Ac}	5	mg/L	(Downing and Nerenberg, 2008)
Heterotrophic yield	Y	0.4	gVSS/gBOD	(Downing and Nerenberg, 2008)
Biomass concentration	X_a	40	kg/m^3	(Rittman and McCarty, 2001)
<i>Operation conditions</i>				
Oxygen inlet liquid concentration	$C_{O_2,l,in}$	0	mg/L	Experimental
Nitrogen inlet liquid concentration	$C_{N_2,l,in}$	17.9	mg/L	Experimental
Acetate bulk liquid concentration	$C_{Ac,l}$	10 and 20	mg/L	Experimental
Oxygen inlet partial pressure	$P_{O_2,g,in}$	1.18 (pure O_2)	atm	Experimental
Nitrogen inlet partial pressure	$P_{N_2,g,in}$	0 (pure O_2)	atm	Experimental

Parameter	Symbol	Value	Units	Reference
Outlet gas pressure (for open-end)	p_{out}	1	atm	Experimental
Average liquid velocity	u_{in}	5 and 27	mm/s	Experimental
Membrane length	L_m	0.35	m	Experimental
Biofilm thickness	L_f	180 and 700	μm	Experimental
Temperature	T	293.15	K	Experimental
<i>Simulated DO steady and transient profiles in HFM and MABRS</i>				
Acetate bulk liquid concentration	$C_{Ac,l}$	20 and 320	mg/L	Parametric study
Biofilm thickness	L_f	300, 700, 1300	μm	Parametric study
Inlet gas pressure	$P_{g,in}$	1.05 (pure O ₂)	atm	Parametric study
Membrane length	L_m	0.35	m	Parametric study
Average liquid velocity	u_{in}	27	mm/s	Parametric study
<i>Simulated Venting strategies in O₂ and air supplied MABRS</i>				
Inlet gas pressure	$P_{g,in}$	1.05, 1.68 (O ₂) 1.68, 3 (air)	atm	Parametric study
Average liquid velocity	u_{in}	5	mm/s	Parametric study
Acetate bulk liquid concentration	$C_{Ac,l}$	20	mg/L	Parametric study
Biofilm thickness	L_f	700	μm	Parametric study
Venting interval	t_c	1, 2, 5, 10 and 30 (pure O ₂) 0.16, 1, 2, and 5 (air)	min	Parametric study
Venting open-end duration	t_o	20 (pure O ₂) 3 (air)	s	Parametric study
Membrane length	L_m	2.5	m	Parametric study

During the parametric study, back-diffusion steady state simulations were first performed for a closed-end HFM and a 700- μm biofilm MABR. Simulated conditions were: inlet pressure of pure oxygen at 1.05 atm, liquid velocity $u_{in}=27$ mm/s, membrane length $L_m=33.5$ cm, and bulk liquid Ac concentrations of 320 mg/L. Oxygen concentrations at membrane surface, N_2 and O_2 diffusive fluxes in and out of the membrane, gas velocity profiles and N_2 and O_2 partial pressures along the fiber lumen were analyzed.

Steady state and transient simulations were also carried out for MABRs (operated in closed-end modes) with different biofilm thicknesses of 300, 700 and 1300 μm , exposed to bulk liquid Ac concentrations of 20 and 320 mg/L. Pure oxygen at an inlet pressure of 1.05 atm, $u_{in}=27$ mm/s, and $L_m=33.5$ cm were considered. For back-diffusion transient studies, DO concentrations over time when transitioning from an open-end to a closed-end operation were simulated at membrane surface (at 16.1 cm from the inlet).

Venting intervals ranging from 1 to 30 min, with 20 seconds open phases, were simulated for a HFM and a 700- μm biofilm MABR fed with pure O_2 at inlet gas pressures of 1.68 atm, a $u_{in}=5$ mm/s, and $L_m=2.5$ m. Obtained average oxygen partial pressures in the membrane lumen and OTEs were compared for both, HFM and MABR, for three operation modes: open-end, closed-end, and venting mode.

Gas dynamic in an air supplied closed-end MABR (700 μm) was also analyzed using the mathematical model. In this case simulations at steady state for the MABR supplied with air at 1.68 atm, $u_{in}=5$ mm/s, $L_m=2.5$ m and bulk liquid Ac concentrations of 20 mg/L were performed. DO profiles at membrane surface, N_2 and O_2 diffusive fluxes and partial pressures of N_2 and O_2 along the membrane lumen were assessed. In order to evaluate how the duration of venting cycles affected the average partial pressures of oxygen, venting intervals ranging from 10 seconds to 5 minutes, with constant venting (open end) duration of 3 seconds were simulated. Simulations were performed at inlet air pressures $p_{in}=1.38$ and 3 atm. Average O_2 partial pressures were compared for open-end and venting modes.

5.4 RESULTS AND DISCUSSION

5.4.1 Experimental results

5.4.1.1 Steady state DO profiles

For both a clean membrane (HFM) and a membrane with a 180- μm thick biofilm (MABR), using pure O_2 supplied co-currently with the liquid flow, N_2 back-diffusion significantly reduced the experimentally measured DO concentrations along the membrane length (Figure 5-3 a). DO values decreased from approximately 35 mg/L at the beginning of the membrane to 0.5 and 5 mg/L for MABR and HFM respectively at the end of the membrane. For the MABR lower DO concentrations were observed from the middle of the membrane towards the end. In this case, as the biofilm consumed oxygen, higher oxygen fluxes and lower DO concentrations were expected at membrane surface.

5.4.1.2 Transient DO profiles

Figure 5-3 b shows the comparison of oxygen transient behavior between a clean and a membrane supporting a 700- μm biofilm layer. DO concentration decrease was significantly slower in the case of the membrane supporting a biofilm. The steady state DO concentration value in case of a membrane with biofilm took almost twice the time to develop in comparison with the clean membrane. For example, the decrease from 40 mg/L to 15 mg/L took around 12 min and 25 min for the clean membrane and the MABR respectively. This may be related with the diffusional resistance imposed by the biofilm thickness for N_2 to diffuse back into the membrane.

The back-diffusion model predicted values matched the experimental results in closed-end operation, for both, clean HFMs and MABRs, in steady-state and transient conditions (Figure 5- 3 a and b).

In order to understand and identify the processes involved in a biofilm supporting membrane, and to explain the differences observed in the experimental results when comparing the back-diffusion behavior with clean membranes, we used the developed mathematical model to explore the underlying mass transfer and biological consumption phenomena that affect back-diffusion process in MABRs.

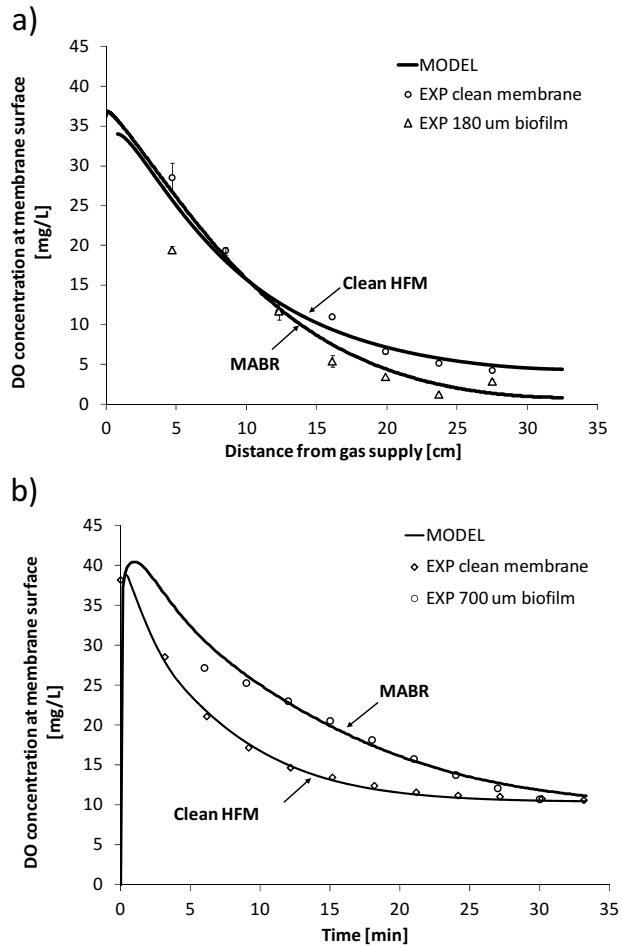


Figure 5-3 Experimental (open dots) and model-predicted (continuous line) dissolved oxygen (DO) profiles at membrane surface for a heterotrophic MABR and for a HFM flow cell. The membrane length is 0.35 m and is supplied with pure O_2 at an inlet pressure of 0.18 atm. (a) DO steady state profiles after closing the end of the membrane for a HFM flow cell without biofilm and for a 180- μ m biofilm MABR. Using a bulk liquid Ac concentration of 20 mg/L in case of the MABR. (b) DO concentrations over time at 0.16 m of the gas supply when transitioning from an open-end to a closed-end operation for a HFM with no biofilm and for a 700- μ m biofilm MABR, and a bulk liquid Ac concentration of 10 mg/L. Error bars in plot (a) are the standard deviation of triplicate measurements.

5.4.2 Simulation results

5.4.2.1 HFM vs MABR

The model was used to study and compare the steady-state DO profiles and gas dynamics in a clean membrane and in a membrane supporting a 700- μm biofilm layer, exposed to a bulk liquid Ac concentration of 320 mg/L (Figures 5-4 and 5-5). Both simulated scenarios considered the same operational conditions in terms of gas supply pressure (pure O_2 at 0.05 atm relative pressure), bulk liquid velocity ($u_{in}=27$ mm/s) and dissolved N_2 concentration in the water (8.7 mg/L) (Table 5-1).

As expected, a significantly lower DO concentration profile in the 700- μm biofilm MABR, compared with the clean HFM was observed (Figure 5-4 a). Oxygen concentration was indeed, limited in the second half of the membrane length. In this case, the driving force (concentration gradient) for oxygen transfer increased due to the oxygen consumption by the biofilm, which in this case, was not limited by electron donor (Ac concentration within the biofilm was always higher than 100 mg Ac/L) resulting in a greater overall oxygen diffusive flux from the membrane towards the biofilm (Figure 5-4 b, continuous black line). Consequently, oxygen supply flux from the inlet must compensate the increasing oxygen fluxes across the membrane wall, leading to a higher gas velocity profile in the lumen phase (Figure 5-5 a, continuous black line). Due to the higher gas velocity, more of the back-diffused N_2 is swept towards the end of the membrane increasing its relative abundance in that zone (Figure 5-5 b, continuous black line).

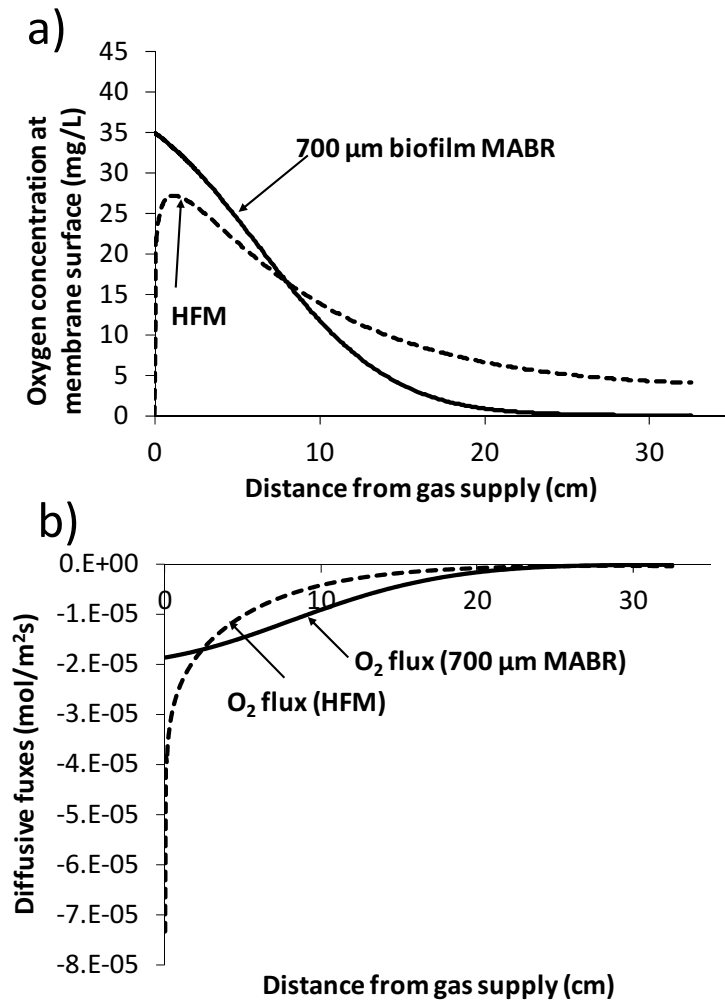


Figure 5-4 (a) Model-simulated DO profiles at membrane surface for a closed-end HFM without biofilm (dashed line), and a closed-end MABR with 700 μm biofilm (continuous black line). Using pure oxygen at an inlet relative pressure of 0.05 atm and $u_{\text{in}}=27$ mm/s for both HFM and MABR, and a bulk liquid A_c concentrations of 320 mg/L in the case of the MABR; (b) Diffusive fluxes of O_2 along the membrane in the HFM without biofilm (dashed lines) and in the 700- μm biofilm MABR (continuous line). Negative values mean diffusive fluxes outwards the membrane.

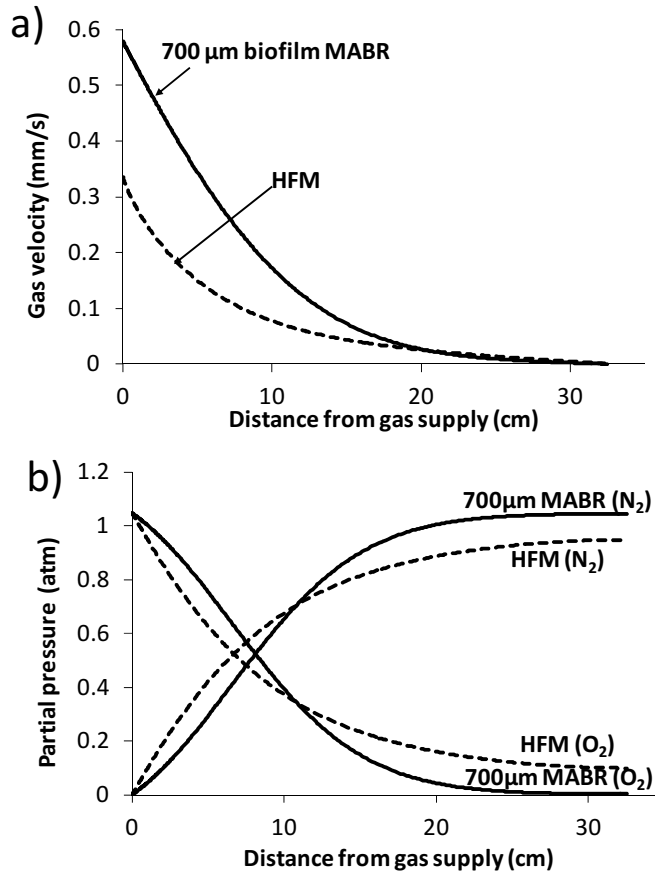


Figure 5-5 (a) Model-simulated gas velocity profiles inside the lumen gas for the closed-end HFM without biofilm (dashed line), and for the closed-end MABR (continuous black line); (b) Simulations of partial pressures for O₂ and N₂ in the closed-end HFM (dashed lines) and in the MABR (continuous line).

In addition, the presence of a biofilm located at the membrane surface, may help to resist the loss of gas to the bulk liquid, favoring N₂ accumulation inside the membrane lumen. The higher overall O₂ flux obtained in biofilm membranes due to oxygen consumption (Figure 5-4 b) led to a higher gas velocity profile and nitrogen accumulation in the membrane lumen, increasing the back-diffusion effect. In case of a HFM, lower gas velocity profile was developed (Figure 5-5 a, dashed line) as a result of the lower overall O₂ flux across the membrane wall. This promoted higher N₂ dilution along the fiber length, and thus lower N₂ accumulation towards the end of the membrane. This can be confirmed when partial pressures of O₂ and N₂ inside

the membrane lumen are analyzed (Figure 5-5 b), where higher partial pressures of N_2 occurred in about two thirds of the membrane length in case of the MABR.

5.4.2.2 Effect of biofilm activity and thickness in DO profiles of MABRs

The effect of different biofilm thicknesses (1300, 700 and 300 μm) and bulk liquid Ac concentrations (20 and 320 mg/L) in the steady-state DO profiles was also explored by model simulations (Figure 5-6 a and b). Biofilms exposed to Ac concentrations of 20 mg/L were Ac substrate limited towards the membrane-biofilm interface (Ac concentration < 5 mg/L), whereas biofilms exposed to bulk liquid Ac concentrations of 320 mg/L were not Ac substrate limited at any point in the biofilms (Ac concentrations > 100 mg/L).

Biofilm thicknesses had little effect in the steady-state DO profiles along the fiber for both cases. However, the effect was slightly higher in the case of acetate limited biofilms (Ac=20 mg/L) (Figure 5-6 a). Assuming the same intra-membrane O_2 pressure, the location of the active region in the biofilm is directly related to the biofilm thickness (due to the diffusional resistance for substrates to penetrate the biofilm). The thinner the biofilm, the more adjacent is the active region to the membrane-biofilm interface. This implied greater oxygen fluxes in thinner biofilms (due to O_2 consumption) and lower DO concentrations at membrane surface (Figure 5-6 a and b). In not substrate limited biofilms (Figure 5-6 b), Ac concentrations exceeded the value required for maximum biofilm activity in all biofilm thicknesses. This resulted in similar driving forces for oxygen to leave the fiber and in almost equal DO steady-state profiles along the membrane length for the studied biofilm thicknesses.

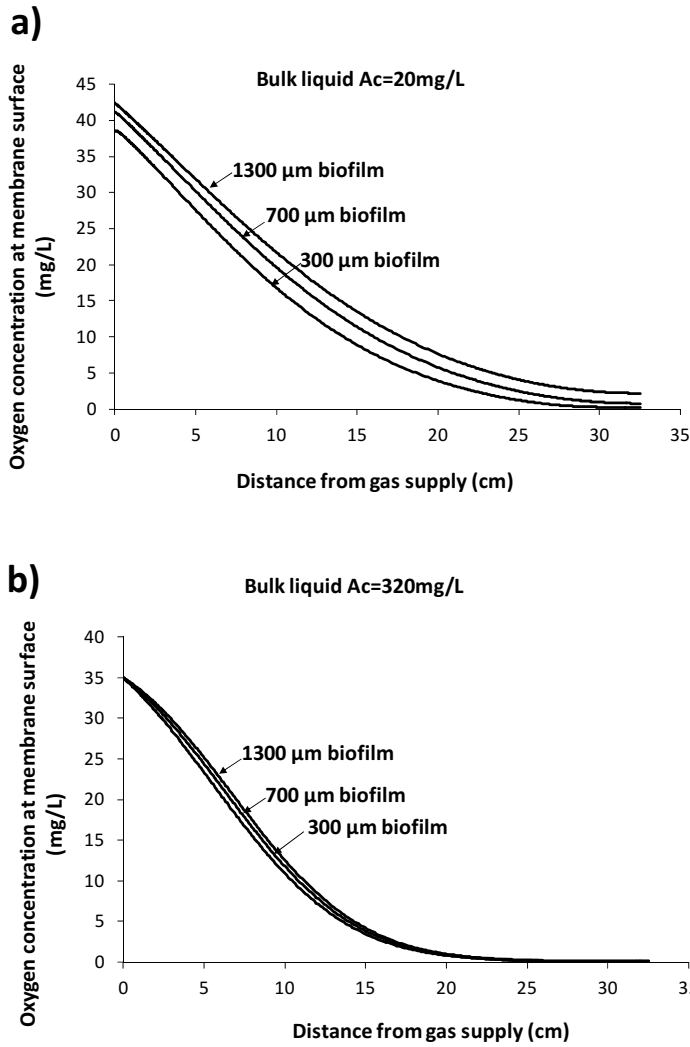


Figure 5-6 Model-simulated steady-state DO profiles for MABRs with biofilm thicknesses of 1300, 700 and 300 μm , for a bulk liquid A_c concentration of 20 mg/L (a), and 320 mg /L (b). Using pure oxygen at an inlet relative pressure of 0.05 atm and $u_{in}=27$ mm/s.

It should be highlighted that lower DO concentration profiles along the membrane length were obtained in biofilms exposed to higher bulk liquid Ac concentrations (Figure 5-6 b). In these cases, higher oxygen demand and consumption took place due to the increased biofilm activity.

5.4.2.3 Simulations of transient DO profiles in MABRs and HFM

The mathematical model was used to study and compare the transient DO concentrations between HFM and MABR at an inlet O_2 relative pressure of 0.05 atm and $u_{in}=27$ mm/s. Biofilm thicknesses of 300, 700 and 1300 μm and Ac bulk concentrations of 20 and 320 mg/L were modeled. Simulations considered 35 minutes of closed operation from the open condition.

Biofilm thickness had a significant effect in the transient DO behavior at membrane surface for both, Ac limited and not limited biofilms (Figure 5-7 a and b). This phenomenon can be attributed to the diffusional barrier imposed by the biofilm for N_2 to penetrate to the lumen of the membrane. In a clean membrane, DO concentration decreased at much higher velocity than in membranes with biofilm layers, being the back-diffusion transient behavior slower for increased biofilm thicknesses. Not Ac limited biofilms (Figure 5-7 b) presented a faster and sharper decrease in DO concentrations due to the higher oxygen demand at membrane surface, but still for a certain period (a minimum of 20 min in the example modeled) back-diffusion transient behavior resulted slower when comparing with clean membranes.

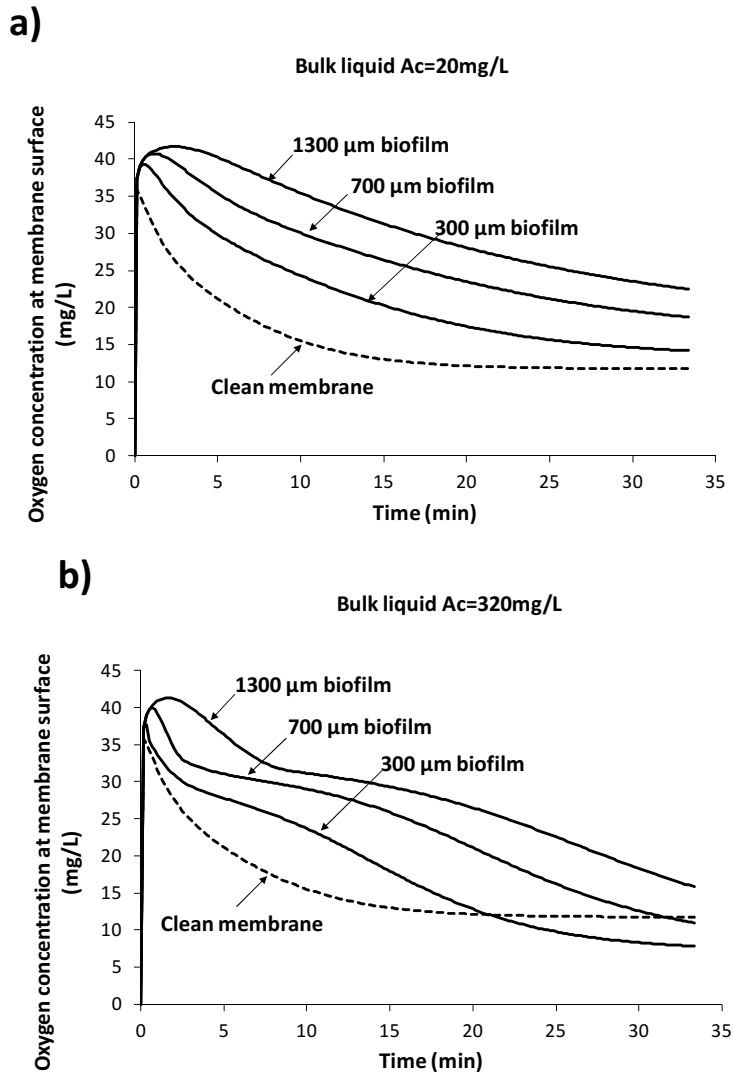


Figure 5-7 DO concentrations over time at 16.1 cm from gas supply when transitioning from an open-end to a closed-end operation for a HFM with no biofilm and MABRs with 1300, 700 and 300 μm biofilm thicknesses for a bulk liquid A_c concentration of (a) 20 mg/L and (b) 320 mg/L.

According to the steady-state and transient simulations it can be concluded that the overall effect of the biofilm in the N_2 gas back-diffusion into the membrane lumen can be separated into two phenomena. On the one side, the biofilm acts as a mass transfer resistance slowing down the diffusion of N_2 from the bulk liquid,

thus, the speed at which back-diffusion develops. On the other side, the oxygen consumption within the biofilm enhances overall fluxes and membrane lumen internal gas velocities, leading to higher N_2 accumulation towards the end of the membrane at an equilibrium state. This last phenomenon is more pronounced for higher biofilm activities. Considering these two effects, we can better use the model to minimize back-diffusion and optimize the operation of a MABR.

5.4.2.4 Optimization of the MABR operation

Oxygen supplied MABRs

As the presence of a biofilm in gas supplying membranes increased the time required for back-diffusion steady-state to develop, a venting strategy is an attractive way to maximize average partial pressures of O_2 (PO_{2ave}) in the lumen gas, and thus substrate removal fluxes, maintaining high OTEs of MABR reactors (as it was demonstrated in Chapter 4). It was expected that in comparison with clean membranes the presence of a biofilm might lead to a longer closed period duration during the venting strategy for achieving a certain PO_{2ave} value in the lumen gas, optimizing the operational OTEs.

The numerical model was used to study the differences between periodically venting the closed-end of a HFM (with no biofilm) and a 700- μm biofilm thickness MABR, exposed to a bulk Ac concentration of 20 mg/L. This bulk liquid Ac concentration was selected in order to simulate more realistic conditions of easily biodegradable bulk substrate concentrations that are found in conventional wastewater treatment processes, like AS or IFAS processes. In order to evaluate how the duration of the closed-end/open-end cycles affected the average partial pressures of oxygen and OTEs, different intervals between ventings ranging from 1 to 30 minutes, with a constant venting (open end) duration of 20 seconds were simulated. Simulations were performed for a longer membrane ($L_m=2.5$ m) than in the experimental set up (closer to what might be used in a full-scale MABR) and at an inlet oxygen pressure of $p_{in}=1.68$ atm.

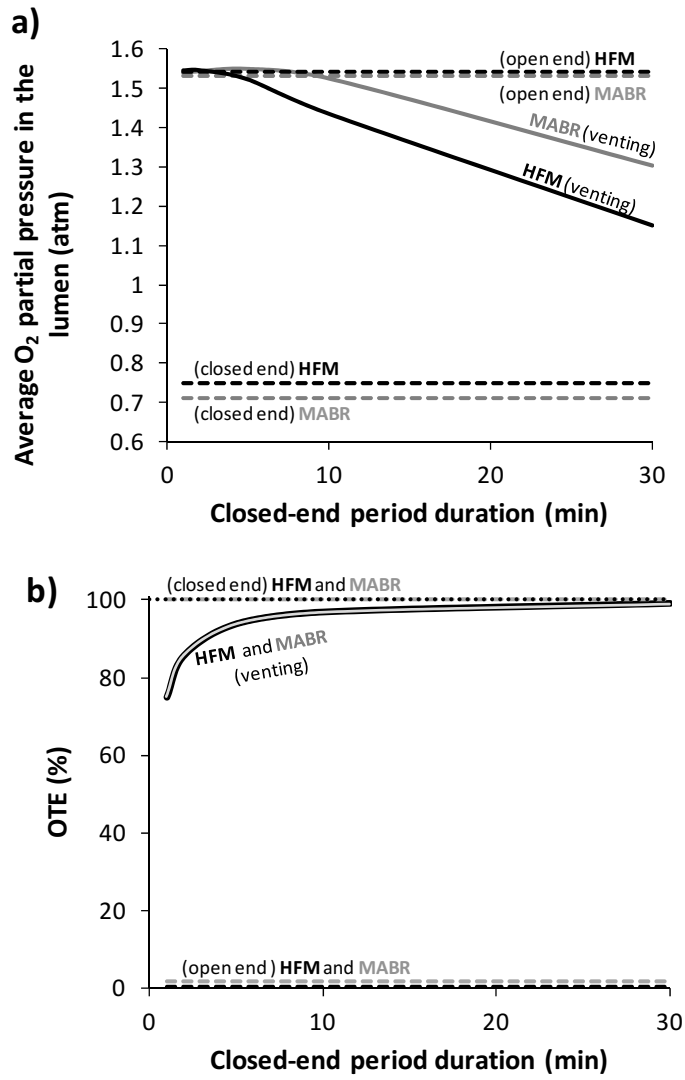


Figure 5-8 Comparison of simulated (a) average O_2 partial pressures (PO_{2ave}) and (b) oxygen transfer efficiencies (OTE) for open operation, closed operation, and intermittent opening modes in HFM and MABR supplied with pure oxygen at 1.68 atm pressure. Venting mode was tested for times between ventings ranging from 1 to 30 min, with 20 seconds open phases.

In comparison to only open or closed operation, venting mode benefited from high OTE values during most of the cycle duration (closed-end phase), while maintaining higher O₂ partial pressures than closed-end membranes at steady-state (Figure 5-8 a and b). In case of HFM and intervals between ventings below approximately 5 min, average O₂ partial pressures were very similar than for the open-end operation mode (around 1.5 atm) (Figure 5-8 a), but with a much higher oxygen transfer efficiency. OTE value ranged from 75 to 90%, in comparison with the dramatically lower OTE value of 0.5% obtained in the open-end mode (Figure 5-8 b). For the 700- μ m biofilm MABR, PO_{2ave} remained similar in open end and venting modes with closed-end period durations up to 10 min, which is twice the time than for HFMs (Figure 5-8 a). Moreover, oxygen partial pressures were even slightly higher in venting mode compared with open-end mode, increasing the achievable OTE values up to 97% in contrast to the significantly lower OTE value of 1.7% corresponding to the open-end mode (Figure 5-8 b). This unexpected higher PO_{2ave} when a venting mode is implemented can be explained by the effect of gas pressure drop in the lumen. In closed-end operation modes, the gas velocity inside the fiber is very low, and thus pressure losses are negligible compared to the open-end modes, which allows maintaining the inlet total gas pressure virtually constant along the length of the fiber. In contrast, in open-end the high gas velocities result in appreciable gas pressure losses, therefore diminishing the average O₂ partial pressure. For short intervals between ventings, the back-diffused N₂ lowers the average O₂ partial pressure in the same range (or even less) than it does the pressure losses resulting from high gas velocities in the open-end phase.

The average O₂ partial pressures in the lumen gas decreased continuously during the closed phase of a venting cycle due to N₂ back-diffusion. Therefore, if the time interval between open phases is smaller, higher average O₂ partial pressures are obtained. In the case of a 700- μ m biofilm MABR, the diffusional resistance imposed by the biofilm for N₂ to reach the lumen of the membrane, led to higher average O₂ partial pressures than the clean HFM for the same venting intervals. This favors the application of longer closed phases for achieving high average O₂ partial pressures, and thus high substrate removal capacities, which can be equal or even higher than the ones achieved in the open-end mode, but with a much higher OTE (similar to the ones obtained in closed-end mode).

Air supplied MABRs

In case of air supplied MABRs, N_2 accumulation inside the membrane lumen can be due to the N_2 coming from both the bulk liquid and the inlet air gas supply (which contains 79% partial pressure of N_2). N_2 diffuses back into the membrane when the bulk liquid or biofilm N_2 concentrations are higher than the ones in the membrane lumen. However, as air contains 79% of N_2 , if the inlet gas supply pressure is high enough, N_2 concentration inside the membrane can exceed the one in the bulk liquid or in the biofilm, and N_2 will not diffuse from the water or biofilm into the membrane lumen; instead the opposite will occur. Figure 5-9, represents a model simulated scenario of a 700- μm MABR supplied with air at 1.68 atm. N_2 concentration in the bulk liquid was in equilibrium with 1 atm N_2 , so a favorable gradient for N_2 to diffuse from the membrane lumen towards the biofilm or bulk liquid was expected. This was confirmed when looking into the resulting O_2 and N_2 diffusive fluxes out of the membrane (Figure 5-9 b continuous grey line).

In the simulated scenario, N_2 that accumulates inside the membrane lumen lowering O_2 partial pressures and DO concentrations along the membrane length (Figure 5-9 a) comes from the air supply, not from the bulk liquid. N_2 fluxes across the membrane wall were lower than O_2 fluxes at the beginning of the membrane, (where O_2 partial pressures were high) as Henry's or partition coefficient value for N_2 is half the value than for O_2 ($H_{N_2}=0.0156 \text{ mol(aq)}/\text{mol(g)}$, $H_{O_2}=0.0338 \text{ mol(aq)}/\text{mol(g)}$), resulting in lower concentration gradients (driving force for diffusion) and thus in lower N_2 fluxes out of the membrane. As a result of less N_2 diffusing out of the membrane (compared with O_2) and the permanent N_2 supply from the feed air gas, the relative abundance of N_2 increased inside the membrane lumen (Figure 5-9 c) resulting in a decreased DO concentration profile along the membrane length (Figure 5-9 a). Due to the increase in N_2 partial pressures, N_2 flux out the membrane increased accordingly along the membrane length consequently with the higher developed N_2 concentration gradients.

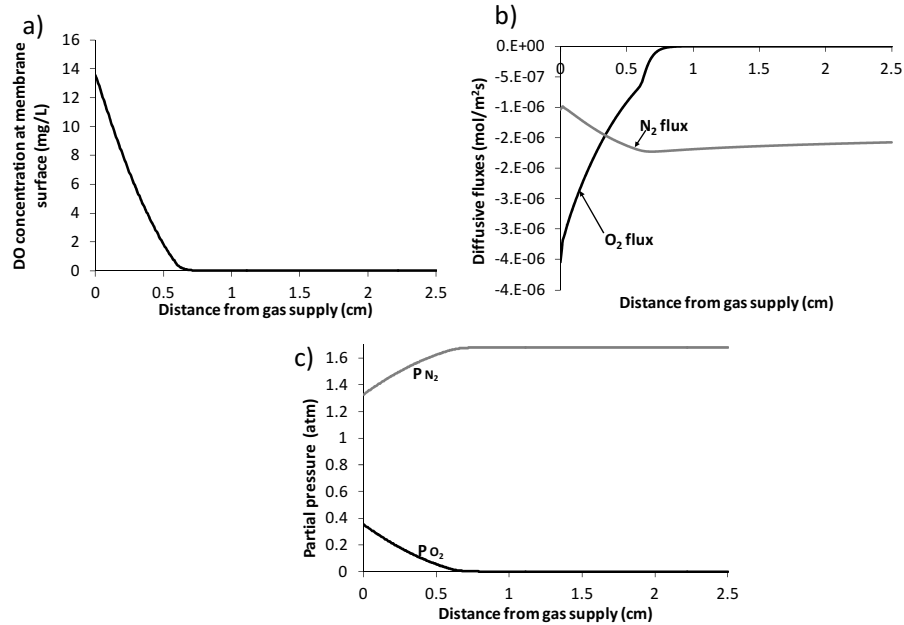


Figure 5-9 (a) Model-simulated DO profiles at membrane surface for a closed-end air supplied 700- μm MABR (bulk liquid Ac concentrations of 20 mg/L; length=2.5 m). Using air at an inlet relative pressure of 1.68 atm and $u_{in}=5$ mm/s; (b) Diffusive fluxes of N_2 and O_2 out of the membrane (negative values); (c) Simulations of partial pressures for O_2 and N_2 along the membrane lumen.

With the aim of improving O_2 average partial pressures and therefore OTRs and removal efficiencies of air supplied MABRs, the effect of periodically venting the closed-end was evaluated with the numerical model. The influence of the time between ventings (in a range from 1 to 5 minutes) was studied, considering a constant venting (open end) duration of 3 seconds. Simulations were performed for an air supplied 700- μm biofilm MABR, a length of $L_m=2.5$ m and inlet air pressures of $p_{in}=1.38$ and 3 atm (Figure 5-10), exposed to bulk Ac concentration of 20 mg/L. Average O_2 partial pressures and OTRs were compared for open-end and venting modes.

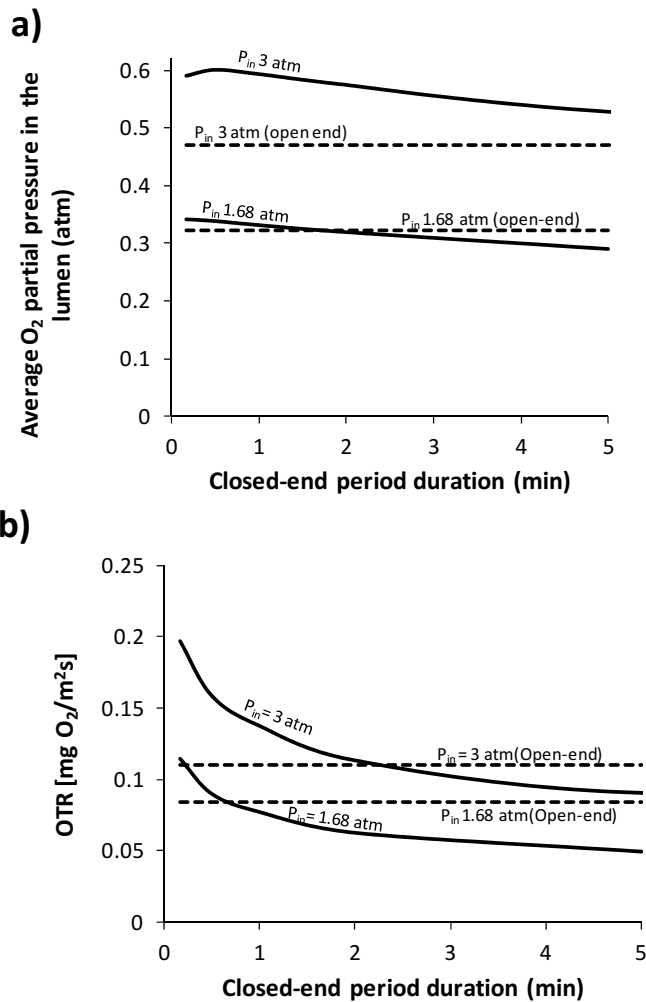


Figure 5-10 Comparison of simulated (a) average O₂ partial pressures inside the membrane lumen and oxygen transfer rates (b) for a 700-µm biofilm air supplied MABR operated in open-end mode (dashed lines) and venting mode (continuous black line). Using air at an inlet relative pressure $p_{in} = 1.68$ and 3 atm. Venting mode was tested for time between ventings ranging from 10 s to 5 min, with 3 s open phases.

When the interval between ventings increased, average O₂ partial pressures in the lumen gas and OTRs decreased, due to the accumulation of N₂. In MABRs supplied with 1.68 atm of air pressure, for intervals below approximately 1 min, the average partial pressure of oxygen slightly exceeded the value obtained in open-end configuration. As explained above, this effect was caused by the pressure drop

resulting from high gas velocities in open-end configurations. Pressure losses in closed-end MABRs are negligible, allowing a higher total average pressure inside the membrane. Below a certain venting interval, the MABR benefitted from the higher average oxygen partial pressure resulting from the closed-end phase. Moreover for inlet gas pressures of 3 atm, almost a 30% increase in average partial pressures of O_2 and 60% increase in OTRs compared with the open-end mode were achieved, increasing the oxygen transfer and substrate removal capacities. For the simulated venting intervals, OTEs ranging from 76% (interval between ventings of 10 seconds) to 99% (interval of 5 minutes) were obtained.

5.5 CONCLUSIONS

In this work, the effects of the biofilm growing on the membranes of MABRs on gas dynamics have been explored.

On the one hand, the presence of a non substrate limited biofilm on a HFM, increased the back-diffusion effect at steady state in comparison with a clean HFM, due to oxygen consumption by the biofilm, which led to higher overall oxygen fluxes and gas velocities in the lumen gas. Higher gas velocities in closed-end membranes resulted in more N_2 pushed and accumulated towards the end of the membrane, increasing the back-diffusion effect. In the same way, higher biofilm activity resulted in lower DO concentration profiles along the membrane length.

On the other hand, the presence of a biofilm increased the time required to reach the back-diffusion steady-state, due to the diffusional resistance imposed by the biofilm for N_2 to enter the lumen of the membrane. This favors the possibility of periodically venting the lumen gases of closed-end MABRs, so that higher average O_2 partial pressures inside the lumen gas and substrate removal capacities could be reached, while benefitting from high OTEs of closed-end systems.

In air supplied MABRs, not only back-diffusion of N_2 , but also the accumulation of the N_2 present in the inlet gas supply can result in a decreasing oxygen concentration profile along the membrane length. Venting strategies can overcome this problem.

Applying appropriate intervals between ventings to each case, O_2 average partial pressures in the membrane lumen and OTRs equal or even higher than the open-end operation mode can be obtained, but with much higher OTE values (ranging from 75 to 99%). The membrane lumen can benefit from the higher average

oxygen partial pressures resulting from the early stage of the closed-end phase, where back-diffused N_2 is not enough to exceed the decrease in oxygen partial pressures caused by open-end pressure losses.

An important consideration is that model predictions made in this study were specific to the configuration and conditions of the experiments and simulated scenarios. The trends of oxygen transfer efficiencies and partial pressures obtained for clean HFM and MABRs could be extrapolated to other conditions, as the physical phenomena are similar. However, specific values should be taken into account applied to the scale and conditions of every case.

5.6 REFERENCES

- Ahmed, T., Semmens, M.J., 1992. The Use of Independently Sealed Microporous Hollow Fiber Membranes for Oxygenation of Water - Model Development. *J. Memb. Sci.* 69, 11–20.
- Aybar, M., Pizarro, G., Boltz, J.P., Downing, L., Nerenberg, R., 2014. Energy-efficient wastewater treatment via the air-based, hybrid membrane biofilm reactor (hybrid MfBR). *Water Sci. Technol.* 69, 1735–1741.
- Downing, L.S., Nerenberg, R., 2008. Total nitrogen removal in a hybrid, membrane-aerated activated sludge process. *Water Res.* 42, 3697–3708.
- Gilmore, K.R., Little, J.C., Smets, B.F., Love, N.G., 2009. Oxygen Transfer Model for a Flow-Through Hollow-Fiber Membrane Biofilm Reactor. *J. Environ. Eng.* 135, 806–814.
- Haynes, W.M., Bruno, T.J., Lide, D.R. (Ed.), 2015. *CRC handbook of chemistry and physics*. CRC. Press/Taylor and Francis, Boca Raton, FL. Online at <http://www.hbcpnetbase.com/>
- Horn, H., Morgenroth, E., 2006. Transport of oxygen, sodium chloride, and sodium nitrate in biofilms. *Chem. Eng. Sci.* 61, 1347–1356.
- Martin, K.J., Nerenberg, R., 2012. The membrane biofilm reactor (MBfR) for water and wastewater treatment: principles, applications, and recent developments. *Bioresour. Technol.* 122, 83–94.
- Nemeth, A., Picard, C., Vale, P., Syron, E., 2016. Variation in off gas composition changing effluent conditions in Membrane Aerated Biofilm Reactor. 13th IWA

Leading Edge Conference on Water and Wastewater Technologies. 13-16 June 2016, Jerez de la Frontera, Spain.

Nerenberg, R., 2016. The membrane-biofilm reactor (MBfR) as a counter-diffusional biofilm process. *Curr. Opin. Biotechnol.* 38, 131–136.

Rittmann, B.E., McCarty, P.L., 2001. *Environmental Biotechnology: Principles and Applications*. New York: McGraw-Hill.

Schaffer, R.B., Ludzack, F.J., Ettinger, M.B.C.F. publication date S., 1960. Sewage Treatment by Oxygenation through Permeable Plastic Films. *J. (Water Pollut. Control Fed.* 32, 939–941.

Semmens, M.J., Dahm, K., Shanahan, J., Christianson, A., 2003. COD and nitrogen removal by biofilms growing on gas permeable membranes. *Water Res.* 37, 4343–4350.

Syron, E., Casey, E., 2008. Membrane-aerated biofilms for high rate biotreatment: performance appraisal, engineering principles, scale-up, and development requirements. *Env. Sci .Technol.* 42, 1833–1844.

Conclusiones y recomendaciones

Los resultados obtenidos tras la operación experimental y simulaciones matemáticas de los RBSOM, ponen de manifiesto que 1) los RBSOM combinados con fangos activos convencionales tienen aplicaciones potenciales para la eliminación de nutrientes en aguas residuales de forma compacta y con una alta eficiencia energética, y 2) la ventilación periódica del lumen de las membranas de los RBSOM es una estrategia prometedora que permite combinar las ventajas de los modos de operación basados en mantener abiertos o cerrados los extremos de las membranas, maximizando tanto las tasas de transferencia de oxígeno (OTRs) como las eficiencias de transferencia de oxígeno (OTEs). Las principales conclusiones que sustentan estos hallazgos se presentan a continuación, estructuradas de acuerdo a los principales objetivos de la presente Tesis Doctoral.

Resultados de la investigación

1. Evaluación del rendimiento del RBSOM híbrido (RBSOMH). Definición experimental de los criterios para la óptima operación del RBSOMH y distribución de biomasas. Desarrollar y validar un modelo matemático del proceso. Emplear estudios sistemáticos de simulaciones con el fin de establecer los parámetros óptimos de diseño y operación del proceso RBSOMH para el tratamiento de agua residual urbana bruta.

Se desarrolló y operó un nuevo RBSOMH a escala de bancada. Se empleó un módulo de membrana plana para la transferencia de oxígeno y como soporte de la biopelícula. Las concentraciones de SSLM se mantuvieron dentro del orden de magnitud típico de los procesos convencionales de fangos activos. El RBSOMH se alimentó con un agua afluyente tratando de reproducir un agua residual urbana de media-alta carga, para lo que se emplearon materias concentradas procedentes de una EDAR.

La configuración propuesta mostró un buen potencial para la eliminación de NT mediante nitrificación y desnitrificación simultáneas. Se alcanzó una tasa de nitrificación media de 3 gN/m²d. Este resultado es mejor que las tasas de nitrificación observadas en estudios previos de RBSOMH suministrados con aire y en procesos IFAS.

Se encontró que la presencia en el efluente de concentraciones de N-NO₃ residual tuvo un papel muy importante en el logro de la distribución de biomasa nitrificante y desnitrificante deseada, impidiendo que la DQO soluble biodegradable penetrara en la biopelícula, y limitando en consecuencia el crecimiento heterotrófico sobre la misma. Los resultados referentes a los ensayos de TPN y TCN demostraron que la mayor parte de la biomasa nitrificante estuvo en la biopelícula (90%), mientras que la mayoría de las bacterias desnitrificantes permanecieron en suspensión (95%).

Las elevadas tasas de nitrificación obtenidas se debieron a 1) la operación bajo condiciones no limitantes de amonio, 2) el suministro suficiente de presión de aire a la membrana, lo que permitió mantener una elevada disponibilidad de oxígeno disuelto (OD) en la biopelícula y 3) la mayoría de la DQO soluble biodegradable se eliminó anóxicamente en el seno del líquido, impidiendo su difusión hacia la biopelícula y la inhibición de bacterias nitrificantes debido a la competencia con la biomasa heterótrofa por el oxígeno y espacio disponible. También se obtuvieron tasas altas de desnitrificación (con un valor promedio de 136 gN/m³d) debido a que se operó con un TRS anóxico relativamente elevado (8 d) y con concentraciones no limitantes de N-NO₃ en el seno del líquido. Además, la ausencia de OD en el seno del líquido favoreció al proceso de desnitrificación, permitiendo que prácticamente toda la DQO biodegradable se consumiera anóxicamente en el seno del líquido.

Los resultados de los estudios sistemáticos de simulaciones para tratar agua residual urbana bruta, demostraron que en el proceso RBSOMH la nitrificación estuvo en la mayoría de los casos desacoplada de los TRH y de las concentraciones de SSLM (y por lo tanto de la desnitrificación). Las áreas de membrana empleadas y las presiones de aire intra-membrana (PAM) suministradas fueron los parámetros fundamentales de diseño que afectaron a las concentraciones de amonio en el efluente. Esto posibilitó el control y optimización de forma separada de los procesos de nitrificación y desnitrificación.

Durante los estudios sistemáticos de simulaciones se obtuvieron tasas de nitrificación muy eficientes, ya que las membranas proporcionaron concentraciones de OD elevadas en las capas internas de la biopelícula quedando disponibles para los organismos nitrificantes. La ausencia de OD en el seno del líquido permitió que prácticamente todo el sustrato rápidamente biodegradable se consumiera anóxicamente mediante la biomasa desnitrificante en suspensión, aumentando por tanto la eficiencia del proceso de desnitrificación. De este modo, se pudieron obtener tasas de eliminación de NT elevadas con TRHs y TRSs

notablemente bajos (TRHs entre 2-3 h, y TRSs entre 0.5 y 1 d). Los fangos resultantes de las configuraciones de RBSOMH simuladas presentaron una alta acumulación de DQO lentamente biodegradable, lo cual es beneficioso para generar altas producciones de metano mediante digestión anaerobia.

Con respecto al proceso de nitrificación, se obtuvieron diferentes combinaciones de PAM y áreas de membrana (a 12 °C) que permitieron alcanzar la concentración de amonio en el fluente requerida para evitar condiciones de amonio limitantes en la biopelícula ($N-NH_{4\text{eff}} \approx 4$ mg/L). Se determinaron las PAM óptimas a diferentes temperaturas de operación con el fin de mantener la concentración de amonio en el efluente deseada.

Con respecto al proceso de desnitrificación, se obtuvieron las combinaciones de TRH y concentraciones de SSLM más favorables que permitieron cumplir con los estándares de NT en el efluente establecidos por la normativa Europea para diferentes escenarios. También se determinaron las concentraciones de SSLM óptimas para diferentes temperaturas en función de las concentraciones de $N-NO_3$ deseadas en el efluente.

2. Estudiar sistemáticamente el efecto de retrodifusión en membranas de fibra hueca mediante experimentación y simulaciones matemáticas. Explorar estrategias de suministro de gas con el fin de maximizar las OTEs y OTRs de los RBSOM.

Se empleó una celda de flujo experimental provista de una única membrana de fibra hueca (MFH) para explorar las OTRs y el proceso de retrodifusión de gases en MFH limpias (sin biopelícula). Se utilizaron microsensores de oxígeno para medir los perfiles longitudinales de OD en la superficie de la membrana, una vez que el sistema alcanzó el estado estacionario. Para condiciones transitorias el OD se midió continuamente en la superficie de la membrana durante la transición desde el modo de operación con extremo abierto a cerrado.

Se desarrolló un modelo matemático de retrodifusión de gases en MFHs, considerando tanto condiciones en estado estacionario como transitorias.

El modelo matemático de retrodifusión de gases fue capaz de predecir adecuadamente los valores experimentales de OD medidos a lo largo de la membrana, tanto para condiciones de extremo abierto como cerrado, en estado estacionario y en condiciones transitorias.

Para membranas con extremos cerrados, el efecto de retrodifusión de gases redujo significativamente las concentraciones de OD a lo largo de la membrana. Sin embargo, para la operación con extremos abiertos, las concentraciones de O₂ se mantuvieron casi constantes y con valores elevados hasta el extremo final de la membrana. Los efectos de retrodifusión en los modos de operación con extremo abierto fueron típicamente insignificantes. Se descubrió que el tiempo requerido para alcanzar una concentración de OD estable dentro del lumen de la membrana durante el proceso de retrodifusión, fue de aproximadamente 30 minutos. Por ello se pensó que la ventilación periódica del lumen de las MFHs, devolviendo temporalmente a las membranas a sus perfiles iniciales y uniformes de concentración de OD mediante la ventilación de los gases retrodifundidos, podría maximizar tanto las OTRs como las OTEs. Se exploraron con el modelo las dinámicas transitorias de los gases aplicando ventilaciones periódicas, así como el impacto de los intervalos de ventilación sobre las OTRs y OTEs.

Con intervalos de ventilación moderados, de aproximadamente 30 minutos, la ventilación de gases aumentó considerablemente las OTRs promedio sin prácticamente afectar las OTEs. Cuando el intervalo de ventilación fue lo suficientemente corto, en este caso menor a 20 minutos, se obtuvieron valores de OTR promedio incluso mayores que para membranas operadas con el extremo abierto. Se aplicó experimentalmente una estrategia de ventilación periódica a un RBSOM operado con extremo cerrado, resultando en grandes incrementos de las OTRs y tasas de remoción de sustrato (alcanzando valores de remoción similares a los obtenidos en modos de operación con extremo abierto) y obteniendo valores de OTEs superiores al 97% (el valor de OTE obtenido en el modo de operación con extremo abierto fue del 0.5%).

Los resultados de este estudio mostraron que la ventilación periódica de gases es una estrategia prometedora para combinar las ventajas de los modos de operación con extremo de las membranas abierto y cerrado, capaz de maximizar tanto las OTRs como las OTEs.

3. Explorar el impacto de las biopelículas en la dinámica de gases en RBSOMs suministrados con oxígeno puro y con aire, con el fin de mejorar las estrategias de suministro de gas para mitigar los efectos perjudiciales de la retrodifusión de gases.

Los fenómenos de retrodifusión de gases en membranas con biopelícula son especialmente complejos, ya que la retrodifusión de gases afecta a la actividad de la biopelícula y la actividad de la biopelícula afecta a su vez a los perfiles de gases desarrollados a lo largo de la membrana. Se estudió experimentalmente el comportamiento de la retrodifusión de gases en estado estacionario y en condiciones transitorias en una MFH limpia y en un RBSOM heterotrófico, midiendo las concentraciones de OD en la superficie de la membrana con microsensores. Se desarrolló un modelo matemático de retrodifusión en el que se incorporó la biopelícula. Este modelo se utilizó para explorar los fenómenos principales de transferencia de masa y consumo de oxígeno que afectan al proceso de retrodifusión en los RBSOMs. El modelo de retrodifusión también se empleó como herramienta predictiva con el fin de optimizar la operación de los RBSOMs suministrados con oxígeno puro y con aire mediante la implementación de estrategias de ventilación periódicas. El modelo de retrodifusión desarrollado fue capaz de reproducir satisfactoriamente los resultados experimentales, tanto para MFHs como para RBSOMs, en estado estacionario y en condiciones transitorias.

Los resultados de este estudio mostraron por un lado que, la presencia de una biopelícula no limitada por sustrato en una MFH, aumentó el efecto de retrodifusión en estado estacionario en comparación con MFH sin biopelículas, debido al consumo de oxígeno por la biopelícula. Este hecho condujo a mayores flujos globales de oxígeno y velocidades en el lumen de la membrana. Las velocidades de gas más altas en membranas con extremo cerrado resultaron en más N_2 arrastrado y acumulado hacia el extremo final de la membrana, donde aumentó su abundancia relativa, y por tanto el efecto de retrodifusión.

Por otro lado, se observó que la presencia de biopelículas aumentó el tiempo necesario para que el proceso de retrodifusión alcanzase el estado estacionario. Esto se debió a la resistencia difusional impuesta por la propia biopelícula para que el nitrógeno difundiese hacia lumen de la membrana. Este hecho favorece la posibilidad de ventilar periódicamente los gases de los RBSOM operados con extremo cerrado, de manera que se puedan obtener mayores presiones parciales promedio de O_2 y capacidades de remoción, beneficiándose al mismo tiempo de las elevadas OTEs de los sistemas con extremo cerrado.

Se descubrió que en los RBSOM suministrados con aire, no solo la retrodifusión de N_2 , sino que la acumulación del N_2 presente en el aire suministrado podía resultar en un perfil decreciente de OD a lo largo de la membrana.

Aplicando los intervalos de ventilación apropiados a cada caso, se pudieron obtener valores promedios de presiones parciales de O_2 y OTRs en el interior de la membrana iguales o incluso mayores que en el modo de operación abierto, pero con valores de OTE mucho más altos (entre el 75 y el 99%, en comparación con los valores de OTE obtenidos en modos de operación con extremos abiertos, de 0.5-1.7%). En estos casos, el lumen de la membrana se benefició de las mayores presiones parciales promedio de O_2 resultantes de los estados iniciales de la fase cerrada, donde el N_2 retrodifundido no fue suficiente para superar la disminución en las presiones parciales de oxígeno originadas por las pérdidas de fricción en los sistemas con extremo abierto.

Recomendaciones para futuras investigaciones

Con base en los principales resultados obtenidos en este trabajo, surge un potencial de investigación en el campo de los sistemas RBSOM. En concreto, se recomiendan las siguientes investigaciones:

- Parte de los resultados de este estudio sugieren que el RBSOM híbrido podría superar las limitaciones de transferencia de masa asociadas a biopelículas espesas debido al crecimiento excesivo de organismos heterotróficos. Esto se consiguió manteniendo una adecuada distribución de biomasa (bacterias nitrificantes en la biopelícula y organismos desnitrificantes en suspensión). Considerando que el crecimiento excesivo de biopelículas sigue siendo un problema en aplicaciones de RBSOM, la configuración híbrida podría ser una opción interesante para paliar esta limitación. Sin embargo, son necesarios estudios más profundos sobre los métodos para el control de la biopelícula, tales como cizalladura mecánica, burbujeo de gases o agentes químicos. Estos estudios deben además abordar las propiedades mecánicas de la biopelícula.
- El control de la biomasa en biopelículas multiespecie presenta dificultades adicionales. El efecto del desprendimiento de la biopelícula sobre la estructura de la comunidad microbiana tiene gran importancia en los RBSOM con biopelículas multiespecie, y debe ser estudiado con mayor profundidad.

- Es necesario abordar los tiempos de puesta en marcha y procesos de inoculación en RBSOM con biopelículas de crecimiento lento o multiespecie, de modo que se pueda lograr la ecología apropiada de forma rápida y consistente.
- Se precisa estudiar en más detalle las tasas de remoción de los RBSOM y nuevas aplicaciones, tales como procesos basados en metano para eliminar contaminantes específicos.
- En cuanto a la rentabilidad, los costos de las membranas y duración de las mismas son las mayores preocupaciones. Es por tanto necesario encontrar materiales de membrana y diseños óptimos para aplicaciones específicas.
- Desde el punto de vista de aplicación de los RBSOM a escala real, se deben considerar todos los aspectos de diseño del proceso. Por ejemplo, se deben estudiar las características de los sólidos de los procesos RBSOM y RBSOM híbridos. También es necesario ampliar el conocimiento sobre el potencial de los efluentes tratados con RBSOMs para ensuciar membranas de filtración, esto es importante cuando se requiere de un paso de filtración post-anóxico.

En conclusión, los resultados obtenidos en este trabajo evidencian que el RBSOM puede llegar a ser una opción energéticamente eficiente y rentable para el tratamiento de aguas residuales.

Conclusions and recommendations

Findings obtained, after the experimental and simulation studies of MABRs evidenced that 1) MABRs combined with conventional activated sludge have potential applications for compact energy-efficient wastewater nutrient removal, and 2) periodic venting applied to the lumen of MABRs is a promising strategy to combine the advantages of open-end and closed-end operation modes, maximizing both oxygen transfer rates (OTRs) and oxygen transfer efficiencies (OTEs). The main results that support them are presented below, structured according to the main objectives of this Doctoral Thesis.

Research Findings

1. Performance evaluation of a hybrid MABR (HMABR). Experimental definition of the criteria for the optimal HMABR operation and biomasses distribution. Development and validation of a simulation model of the process. Establish the optimum design and operation conditions of the HMABR process for treating urban raw wastewater through systematic simulation studies.

A new HMABR was developed and operated at bench-scale. A flat membrane module was used for oxygen transfer and biofilm support. Bulk liquid MLSS concentrations were maintained in the order of magnitude typical of a conventional activated sludge process. The HMABR was continuously fed with an influent mimicking medium-high strength urban wastewater, for what concentrated matters proceeding from a real WWTP were used.

The configuration showed good potential for TN removal through simultaneous nitrification and denitrification. An average nitrification rate of 3 g/m²d was achieved, which is higher than those observed in previous air supplied HMABRs and IFAS processes.

It was found that maintaining an effluent residual NO₃-N concentration had a crucial role in achieving the desired nitrifying and heterotrophic biomasses distribution, preventing that biodegradable sCOD could penetrate into the biofilm and consequently limiting heterotrophic growth on it. NPR and NUR batch test

results demonstrated that most of denitrifying biomass was in the biofilm (90%), while the majority of denitrifying organisms remained in suspension (95%).

The high achieved nitrification rates were due to 1) operating under non ammonium limiting conditions, 2) supplying enough membrane air pressures to maintain high availability of dissolved oxygen (DO) concentrations in the biofilm and 3) the majority of biodegradable sCOD was anoxically removed in the bulk liquid preventing its diffusion inside the biofilm and the inhibition of nitrifying bacteria due to the competence with heterotrophs for oxygen and space. High denitrification rates were obtained (with an average value of $136 \text{ gN/m}^3\text{d}$) due to operating with an anoxic SRT relatively high (8 d) and with non $\text{NO}_3\text{-N}$ limiting concentrations in the bulk liquid. Besides, the absence of DO in the bulk liquid enhanced the denitrification process, allowing practically all the biodegradable COD to be anoxically consumed in the bulk liquid.

The results of the systematic simulation studies for treating urban raw wastewater, demonstrated that in the HMABR process, nitrification was in most cases decoupled from HRTs and MLSS concentrations (and therefore from denitrification process). The membrane areas and the supplied membrane air pressures (MAPs) were the underlying design parameters affecting effluent ammonium concentrations. This allowed the separate control and optimization of both nitrification and denitrification processes.

During systematic simulation studies highly efficient nitrification rates were possible to obtain, as the membranes provided high DO concentrations in the biofilm internal layers available for nitrifying organisms. The absence of DO in the bulk liquid allowed practically all the readily biodegradable substrate to be consumed anoxically by suspended denitrifying organisms, enhancing the denitrification efficiency. Therefore high TN removal rates could be obtained with remarkably low HRTs (ranging from 2 to 3 hours) and SRTs (ranging from 0.5 to 1 d). The sludge resulting from the simulated HMABR configurations presented high slowly biodegradable COD accumulation, which could lead to high methane production during anaerobic digestion process.

Regarding nitrification process, different combinations of MAPs and membrane areas (at 12°C) allowed to achieve the desired effluent ammonium concentration for preventing ammonium limiting conditions within the biofilm ($\text{NH}_{4\text{eff}} \approx 4 \text{ mg/L}$). Optimum MAPs for different operating temperatures, in order to maintain the intended effluent ammonium concentration were determined.

With respect to denitrification process, the most favorable combinations of HRTs and MLSS concentrations were obtained, satisfying the TN effluent standards established in European legislation for different scenarios. Optimum MLSS concentrations to be maintained depending on the temperature and the desired effluent $\text{NO}_3\text{-N}$ concentrations were assessed.

2. Systematically study the back-diffusion effect in hollow-fiber membranes through experimentation and modeling. Explore gas supply strategies as a means to maximize OTEs and OTRs of MABRs.

An experimental flow cell with a single hollow fiber membrane (HFM) was used to explore OTRs and gas back diffusion in clean HFMs (without biofilm). Oxygen microsensors were used to measure longitudinal profiles of DO at the HFM surface once the system reached the steady state. For transient conditions DO was measured continuously at membrane surface during the shift from open-end to closed-end operation.

A mathematical model for gas back diffusion in a HFM was developed, addressing both steady-state and transient conditions.

The back-diffusion mathematical model was in good agreement with the measured values of DO along the membrane length, both for open-end and closed-end operation, in steady-state and transient conditions.

For closed-end mode, N_2 back diffusion significantly reduced the DO concentrations along the membrane length. On the contrary, for the open-end operation O_2 concentrations remained almost constant and at high values until the distal end of the membrane. The open-end operation mode typically resulted in negligible back-diffusion effects. It was found that the time required to reach a steady O_2 profile in the lumen during back-diffusion process was around 30 minutes in the studied system. It was hypothesized that periodically venting the membrane lumen of HFMs, temporarily returning the membranes to their initial uniform DO concentration profiles by venting the back-diffusion gases, would maximize both OTRs and OTEs. The transitory gas dynamics of periodic venting were studied with the model, and the impacts of different membrane opening intervals on OTRs and OTEs were explored.

At moderate intervals between ventings, of around 30 minutes, the venting significantly increased the average OTRs without substantially affecting the OTEs. When the interval was short enough, in this case shorter than 20 minutes, the OTR was actually higher than for continuous open-end operation. A periodic

venting strategy was experimentally assessed for a closed-end MABR greatly increasing OTRs and removal fluxes (reaching similar values to the ones obtained in open-end operation mode) and achieving OTEs higher than 97% (obtained OTE value in open-end operation mode was 0.5%).

Results of this study showed that periodic venting is a promising strategy to combine the advantages of open-end and closed-end operation, maximizing both the OTRs and OTEs.

3. Explore the impact of biofilms on gas dynamics in pure oxygen and air supplied MABRs, in order to improve gas supply strategies to mitigate gas back-diffusion detrimental effects.

Gas back-diffusion phenomena in membranes supporting biofilms is specially complex, as gas back-diffusion affects biofilm activity and biofilm activity impacts gases profiles along the membranes. Back-diffusion steady and transient behavior was experimentally studied for a clean HFM and for a heterotrophic MABR, measuring DO concentrations at membrane surface with microsensors. A back-diffusion mathematical model with the incorporation of biofilm domain was developed. The model was used to explore the underlying mass transfer and biological consumption phenomena that affect back-diffusion process in MABRs. The back-diffusion model was also used as a predictive tool to optimize oxygen and air supplied MABRs operation by the implementation of periodic venting strategies. The developed back-diffusion model predicted values matched the experimental results, for both, HFMs and MABRs, in steady-state and transient conditions.

Results of this study showed on the one hand, that the presence of a non-substrate limited biofilm on a HFM, increased the back-diffusion effect at steady state in comparison with clean HFMs. This is a consequence of oxygen consumption by the biofilm, that led to higher overall oxygen fluxes and gas velocities in the lumen gas. Higher gas velocities in closed-end membranes resulted in more N₂ pushed and accumulated towards the end of the membrane, increasing its relative abundance, and thus back-diffusion effect.

On the other hand, the presence of a biofilm increased the time required to reach the back-diffusion steady-state. This was due to the diffusional resistance imposed by the biofilm for N₂ to enter the lumen of the membrane. This favours the possibility of periodically venting the lumen gases of closed-end MABRs, so

higher average O_2 partial pressures inside the membrane lumen and substrate removal capacities could be reached, while benefitting from high OTEs of closed-end systems.

It was found that in air supplied MABRs, not only back-diffusion of N_2 , but also the accumulation of the N_2 present in the inlet gas supply could result in a decreasing oxygen concentration profile along the membrane length.

Applying appropriate venting intervals to each case, high O_2 average partial pressures in the membrane lumen and OTRs equal or even higher than the open-end operation mode could be obtained, but with much higher OTE values (ranging from 75 to 99% for venting strategies in comparison with 0.5-1.7% values obtained in open-end operation modes). In these cases, the membrane lumen benefits from the higher average oxygen partial pressure resulting from the early stage of the closed-end phase, where back-diffused N_2 is not enough to exceed the decrease in oxygen partial pressures caused by pressure losses in open-end systems.

Recommendations for further research

Based on the main results obtained from this work, there exists a significant research potential in the field of MABR systems. Specifically, the following studies are recommended:

- Part of the results of this study suggested that the hybrid MABR could avoid mass transfer limitations associated with thick biofilms due to the overgrowth of heterotrophs. This was achieved by maintaining the proper distribution of biomasses (nitrifying bacteria in the biofilm and denitrifying organisms in suspension). Considering that thick biofilms are still a concern in MABR applications, hybrid MABR could be an interesting option to overcome this limitation. However, more thorough studies should address improved methods of biofilm management such as mechanical shear, gas sparging or chemical agents. These studies should also address biofilm mechanical properties.
- Biomass control in multispecies biofilms presents additional challenges. The effect of biofilm detachment on microbial community structure is a topic that has great relevance for multispecies MABRs and should be studied in greater depth.
- It is necessary to address start-up times and enrichment processes for slow growing or multispecies MABRs, so that the proper ecology could be achieved quickly and consistently.
- MABR removal fluxes and new applications, such as methane-based processes to remove novel contaminants, need to be researched.
- As for cost-effectiveness, membranes capital costs and life expectancy are the largest concerns. It is necessary to find ideal membrane material and design for specific applications.
- From MABR scale-up point of view, all aspects of process design should be considered. For example, research is needed to determine the settling characteristics of MABR or HMABR solids. The potential of MABR treated effluents to foul membrane filters should also be studied, this is important when post-anoxic filtration step is required.

To conclude, the results obtained in this work evidenced that the MABR may become in an energy-efficient and cost-effective option for wastewater treatment.

Supplementary material¹

¹ Information contained in this supplementary material section refers to Chapter 3 and Chapter 4.

OUTLINE

Table/Figure	Title	Page
S-1	Kinetic parameters used in the HMABR mathematical model	222
S-2	Stoichiometric coefficients used in the HMABR mathematical model	223
S-3	Matrixes of the process rate equations for the HMABR mathematical model	224
S-4	Stoichiometric matrix of the HMABR mathematical model	225
S-5	Kinetics of the interaction between suspended flocs and colloids	227
S-6	Physical and fitting parameters of the HMABR mathematical model	227
S-7	The Hagen-Poiseuille relationship for slightly compressible fluids and observed flows for a broad range of pressures	228

Table S-1 Kinetic parameters used in the HMABR mathematical model

	Symbol	Description	Value (20°C)	Reference
Hydrolysis of X_S	K_h	Hydrolysis rate constant	3 d^{-1}	Henze et al., (2000)
	Θ_{v_h}	Arrhenius coefficient for K_h	1.041	Henze et al., (2000)
	η_{NO_3}	Anoxic hydrolysis reduction factor	0.6	Henze et al., (2000)
	η_{fe}	Anaerobic hydrolysis reduction factor	0.2	Larrea et al., (2002)
	K_{NO_2}	Saturation/Inhibition coefficient for S_{NO_2}	0.2 g/m^3	Henze et al., (2000)
	K_{NO_3}	Saturation/Inhibition coefficient for S_{NO_3}	0.5 g/m^3	Henze et al., (2000)
	K_X	Saturation coefficient for X_S	0.1 g/m^3	Henze et al., (2000)
	K_{SL}	Saturation coefficient for S_L	4 g/m^3	Larrea et al., (2002)
Heterotrophic biomass: X_H	μ_h	Maximum growth rate of X_H	6 d^{-1}	Henze et al., (2000)
	Θ_{μ_h}	Arrhenius coefficient for μ_h	1.072	Henze et al., (2000)
	q_{fe}	Maximum rate for fermentation	3 d^{-1}	Henze et al., (2000)
	$\Theta_{q_{fe}}$	Arrhenius coefficient for q_{fe}	1.072	Henze et al., (2000)
	η_{NO_3}	Reduction factor for denitrification	0.8	Henze et al., (2000)
	b_H	Rate constant for lysis and decay of X_H	0.4 d^{-1}	Henze et al., (2000)
	Θ_{b_H}	Arrhenius coefficient for b_H	1.072	Henze et al., (2000)
	K_{O_2}	Saturation/Inhibition coefficient for S_{O_2}	0.2 g/m^3	Henze et al., (2000)
	K_{NO_3}	Saturation/Inhibition coefficient for S_{NO_3}	0.5 g/m^3	Henze et al., (2000)
	K_A	Saturation/Inhibition coefficient for S_A	4 g/m^3	Henze et al., (2000)
	K_F	Saturation/Inhibition coefficient for S_F	4 g/m^3	Henze et al., (2000)
	K_{NH_4}	Saturation/Inhibition coefficient for S_{NH_4}	0.05	Henze et al., (2000)
Nitrifying biomass: X_A	μ_A	Maximum growth rate of X_A	1 d^{-1}	Henze et al., (2000)
	Θ_{μ_A}	Arrhenius coefficient for μ_A	1.111	Henze et al., (2000)
	b_A	Decay rate of X_A	0.15 d^{-1}	Henze et al., (2000)
	Θ_{b_A}	Arrhenius coefficient for b_A	1.116	Henze et al., (2000)
	K_{O_2}	Saturation coefficient for S_{O_2}	0.5 g/m^3	Henze et al., (2000)
	K_{NH_4}	Saturation coefficient for S_{NH_4}	1 g/m^3	Henze et al., (2000)

Table S-2 Stoichiometric parameters used in the HMABR mathematical model

Symbol	Description	Value	Reference
Y_H	Yield coefficient for X_H	0.625 g X_H /gCOD	Henze et al., (2000)
Y_{PAO}	Yield coefficient for X_{PAO}	0.625 g X_{PAO} /g X_{PHA}	Henze et al., (2000)
Y_{PO4}	PP requirements per stored PHA	0.4 gP/gCOD	Henze et al., (2000)
Y_{PHA}	X_{PHA} required per stored X_{PP}	0.2 gDQO/gP	Henze et al., (2000)
Y_A	Yield coefficient for X_A	0.24 g X_A /gN	Henze et al., (2000)
f_{XI}	Fraction of inert generated in lysis	0.1 g X_i /g X_{BM}	Henze et al., (2000)
i_{NSI}	Nitrogen content of S_I	0.01 gN/gCOD	Henze et al (2000)
i_{NSS}	Nitrogen content of S_S	0.03 gN/gCOD	Henze et al., (2000)
i_{NSL}	Nnitrogen content of S_L	0.03gN/gCOD	Larrea et al., (2002)
i_{NXI}	Nitrogen content of X_I	0.02 gN/gCOD	Henze et al., (2000)
i_{NXS}	Nitrogen content of X_S	0.03 gN/gCOD	Larrea et al., (2002)
i_{NBM}	Nitrogen content of biomass	0.07 gN/gCOD	Henze et al., (2000)

Table S-3 Matrixes of the process rate equations for the HMABR mathematical model

Process	Kinetics
Hydrolysis Processes	
Aerobic hydrolysis of X_S	$K_{H,XS} \cdot \frac{S_{O_2}}{K_{O_2} + S_{O_2}} \cdot \frac{X_S/X_H}{K_X + X_S/X_H} \cdot X_H$
Anoxic Hydrolysis of X_S	$K_{H,XS} \cdot \eta_{NO_3,XS} \cdot \frac{K_{O_2}}{K_{O_2} + S_{O_2}} \cdot \frac{S_{NO_3}}{K_{NO_3} + S_{NO_3}} \cdot \frac{X_S/X_H}{K_X + X_S/X_H} \cdot X_H$
Aerobic hydrolysis of S_L	$K_{H,SL} \cdot \frac{S_{O_2}}{K_{O_2} + S_{O_2}} \cdot \frac{S_L}{K_{SL} + S_L} \cdot X_H$
Anoxic hydrolysis of S_L	$K_{H,SL} \cdot \eta_{NO_3,SL} \cdot \frac{K_{O_2}}{K_{O_2} + S_{O_2}} \cdot \frac{S_{NO_3}}{K_{NO_3} + S_{NO_3}} \cdot \frac{S_L}{K_{SL} + S_L} \cdot X_H$
Heterotrophic biomass: X_H	
Growth on fermentable substrates, S_F	$\mu_H \frac{S_{O_2}}{K_{O_2} + S_{O_2}} \cdot \frac{S_F}{K_F + S_F} \cdot \frac{S_F}{S_F + S_A} \cdot X_H$
Growth on fermentation products, S_A	$\mu_H \frac{S_{O_2}}{K_{O_2} + S_{O_2}} \cdot \frac{S_A}{K_A + S_A} \cdot \frac{S_A}{S_A + S_F} \cdot X_H$
Anoxic growth on fermentable substrates, S_F	$\mu_H \cdot \eta_{NO_3} \cdot \frac{K_{O_2}}{K_{O_2} + S_{O_2}} \cdot \frac{S_{NO_3}}{K_{NO_3} + S_{NO_3}} \cdot \frac{S_F}{K_F + S_F} \cdot \frac{S_F}{S_A + S_F} \cdot X_H$
Anoxic growth on fermentable substrates, S_A	$\mu_H \cdot \eta_{NO_3} \cdot \frac{K_{O_2}}{K_{O_2} + S_{O_2}} \cdot \frac{S_{NO_3}}{K_{NO_3} + S_{NO_3}} \cdot \frac{S_A}{K_A + S_A} \cdot \frac{S_A}{S_A + S_F} \cdot X_H$
Fermentation	$q_{fe} \cdot \frac{K_{O_2}}{K_{O_2} + S_{O_2}} \cdot \frac{S_{NO_3}}{K_{NO_3} + S_{NO_3}} \cdot \frac{S_F}{K_F + S_F} \cdot X_H$
Lysis of X_H	$b_H \cdot X_H$
Nitrifying biomass: X_A	
Aerobic growth of X_A	$\mu_A \frac{S_{O_2}}{K_{O_2} + S_{O_2}} \cdot \frac{S_{NH_4}}{K_{NH_4} + S_{NH_4}} \cdot X_H$
Lysis of X_A	$b_A \cdot X_A$

Table S-4 Stoichiometric matrix of the HMABR mathematical model

Process	S_S mgCOD/L	S_{NH4} mgN/L	S_{O2} mgO ₂ /L	S_{NO3} mgN/L	S_L mgCOD/L	X_H mgCOD/L	X_A mgCOD/L	X_S mgCOD/L	X_I mgCOD/L
Heterotrophic biomass: X_H									
Aerobic growth of X_H	$-\frac{1}{Y_H}$	$-i_{N,XH}$	$-\frac{1-Y_H}{Y_H}$			1			
Anoxic growth of X_H	$-\frac{1}{Y_H}$	$-i_{N,XH}$		$-\frac{1-Y_H}{2.86 \cdot Y_H}$		1			
Direct aerobic metabolism of X_S		$\left(\frac{i_{N, XS}}{Y_H}\right) - i_{N, XH}$	$-\frac{1-Y_H}{Y_H}$			1		$-\frac{1}{Y_H}$	
Direct anoxic metabolism of X_S		$\left(\frac{i_{N, XS}}{Y_H}\right) - i_{N, XH}$		$-\frac{1-Y_H}{2.86 \cdot Y_H}$		1		$-\frac{1}{Y_H}$	
Direct aerobic metabolism of S_L		$\left(\frac{i_{N, SL}}{Y_H}\right) - i_{N, XH}$	$-\frac{1-Y_H}{Y_H}$			1		$-\frac{1}{Y_H}$	
Direct anoxic metabolism of S_L		$\left(\frac{i_{N, SL}}{Y_H}\right) - i_{N, XH}$		$-\frac{1-Y_H}{2.86 \cdot Y_H}$		1		$-\frac{1}{Y_H}$	
Lysis of X_H		$i_{N,XH} - f_{XI} \cdot i_{N,XI}$ $-(1-f_{XI}) \cdot i_{N,XS}$				-1		$1-f_{XI}$	f_{XI}

Process	S_S mgCOD/L	S_{NH4} mgN/L	S_{O2} mgO2/L	S_{NO3} mgN/L	S_L mgCOD/L	X_H mgCOD/L	X_A mgCOD/L	X_S mgCOD/L	X_I mgCOD/L
Nitrifying biomass: X_A									
Aerobic growth of X_A		$-i_{N,XA} - \frac{1}{Y_A}$	$-\frac{4.57 - Y_A}{Y_A}$	$\frac{1}{Y_A}$			1		
Lysis of X_A		$i_{N,XA} - f_{XI} \cdot i_{N,XI}$ $-((1 - f_{XI}) \cdot i_{N,XS})$					-1	$1 - f_{XI}$	f_{XI}
X_H	Heterotrophic biomass					$i_{N,XA}$	N content in X_A (gN/gCOD)		
X_A	Nitrifying biomass					$i_{N,XH}$	N content in X_H (gN/gCOD)		
X_S	Particulate slowly biodegradable COD					$i_{N,XS}$	N content in X_S (gN/gCOD)		
X_I	Inert particulate material					$i_{N,SL}$	N content in S_L (gN/gCOD)		
Y_H	Yield coefficient for X_H (gCOO/gN)					$i_{N,XI}$	N content in X_I (gN/gCOD)		
Y_A	Yield coefficient for X_A (gCOD/gN)					f_{XI}	Fraction of inert COD generated in biomass lysis (gCOD/gCOD)		

Table S-5 Kinetics of the interaction between suspended flocs and colloids (Albizuri et al., 2009)

Process	Kinetics
Attachment from colloids to flocs	$K_{AT,F} \cdot \frac{X_{i,C}}{K_C \cdot X_{i,F} + X_{i,C}} \cdot X_{i,F}$
Detachment from flocs to colloids	$K_{DE,F}$

$X_{i,C}/X_{i,F}$: concentration of particulate component in colloidal form and in suspended flocs, respectively

Table S-6 Physical and fitting parameters of the HMABR mathematical model

Parameter	Symbol	Value	Units	Reference
<i>Physical parameters</i>				
Diffusion coefficient of soluble components	D_{Si}	$2 \cdot 10^{-4}$	m^2/d	Wanner et al., (2006)
Diffusion coefficient of particulate components	D_{Xi}	1×10^{-9}	m^2/d	Wanner et al., (2006)
Biofilm liquid volumetric fraction	θ	0.8	-	Wanner et al., (2006)
Attachment coefficient of particulate components to the biofilm	$K_{AT,BXi}$	1000	m/d	Albizuri et al., (2009)
Attachment coefficient from colloid to flocs	$K_{AT,F}$	5	d^{-1}	Albizuri et al., (2009)
Detachment coefficient from flocs to colloids	$K_{DET,F}$	5	d^{-1}	Albizuri et al., (2009)
Colloids saturation coefficient	K_C	0.05	$gX_{i,C}/gX_{i,F}$	Albizuri et al., (2009)
Henry's law for oxygen	H_{O_2}	0.0338	$mol(aq.)/mol(g)$	CRC handbook

Parameter	Symbol	Value	Units	Reference
Inert to particulate slowly biodegradable COD ratio	X_I/X_S	0.35	-	This study
Biofilm detachment coefficient	$K_{DE,B}$	170	d^{-1}	This study
Membrane mass transfer coefficient for O_2	K_m	3	m/d	This study
Liquid diffusive layer	L_L	100	μm	This study

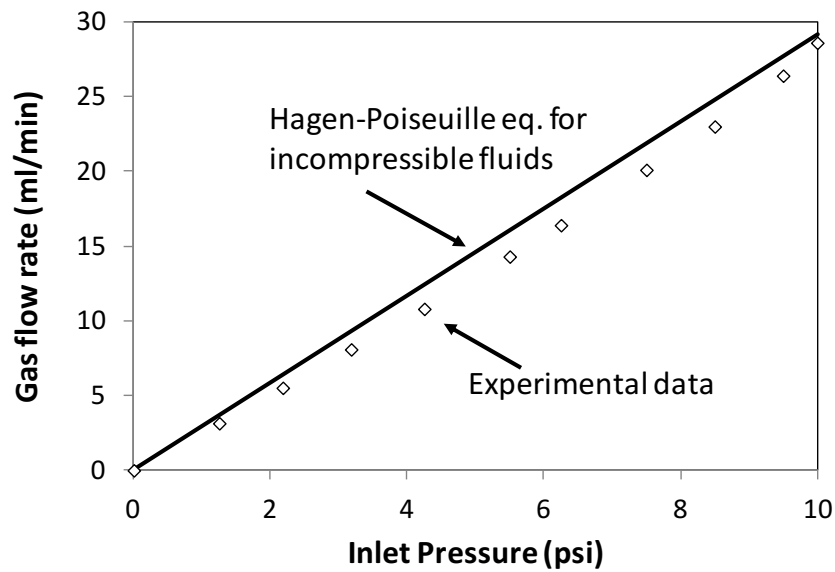


Figure S-7 The Hagen-Poiseuille relationship for slightly compressible fluids and observed flows for a broad range of pressures, ranging from 0.07 (1 psi) to 0.68 (10 psi) atm.

REFERENCES

Albizuri, J., Van Loosdrecht, M.C.M., Larrea, L., 2009. Extended mixed-culture biofilms (MCB) model to describe integrated fixed film/activated sludge (IFAS) process behaviour. *Water Sci. Technol.* 60, 3233–3241.

Haynes, W.M., Bruno, T.J., Lide, D.R. (Ed.), 2015. *CRC handbook of chemistry and physics* CRC.

Henze, M., Gujer, W., Mino, T., van Loosdrecht, M.C.M., 2000. *Activated Sludge Models ASM1, ASM2, ASM2d and ASM3*. IWA Publ. 121.

Larrea, L., Irizar, I., Hildago, M.E., 2002. Improving the predictions of ASM2d through modelling in practice. *Water Sci. Technol.* 45, 199–208.

Wanner, O., Eberl, H., Morgenroth, E., Noguera, D., Picioreanu, C., Rittmann, B., van Loosdrecht, M.C.M., Wanner, O., 2006. *Mathematical modeling of biofilms*, Scientific and technical report series.

